NEURON GUIDANCE BY BIOMIMETIC TOPOGRAPHICAL CUES

By Jan M. Bruder

Sc.B., Brown University, 2003

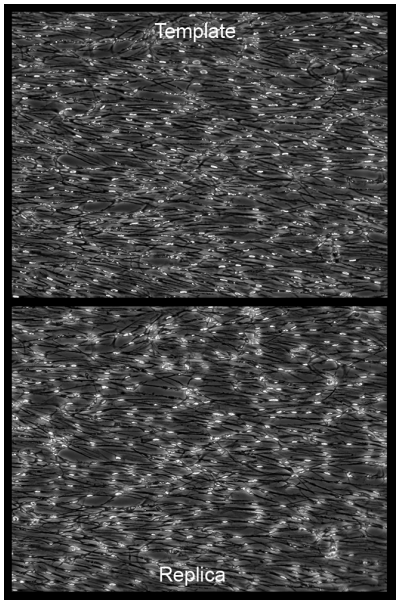

Submitted in partial fulfillment of the requirements for the degree of

Doctor of Philosophy

in the Division of Biology and Medicine at Brown University

Providence, Rhode Island

May 2008

© Copyright 2008 by Jan M. Bruder

This dissertation by Jan M. Bruder is accepted in its present form

by the Division of Biology and Medicine as satisfying the

dissertation requirement for the degree of Doctor of Philosophy.

Date_____ _____

Diane Hoffman-Kim, Ph.D., Advisor

Recommended to the Graduate Council

Date_____ _____

Michael J. Lysaght, Ph.D., Reader

Date_____ _____

Edith Mathiowitz, Ph.D., Reader

Date_____ _____

Jeffrey Morgan, Ph.D., Reader

Date_____ _____

Helen Buettner, Ph.D.,
External Reader

Approved by the Graduate Council

Date_____ _____

Sheila Bonde, Dean of the Graduate School

CURRICULUM VITAE FOR
JAN MARKUS BRUDER

DATE AND PLACE OF BIRTH

February 14th, 1980, Iserlohn, Germany

EDUCATION

Expected	Brown University, Providence, RI
May 2008	**Ph.D. in Medical Science**
	Artificial Organs, Biomaterials, and Cellular Technology Program
	Advisor: Professor Diane Hoffman-Kim
	Title of Dissertation: *Neuron Guidance by Biomimetic Topographic Cues*
May 2003	Brown University, Providence, RI
	Sc.B. in Biology with Honors / Biotechnology Focus
	Advisor: Professor Michael J. Lysaght
	Title of Thesis: *Encapsulated Cell Therapy for Removal of Uremic Toxins*
June 1999	Burggymnasium Altena, Germany (High School)
	German Baccalaureate (Abitur), Valedictorian

Refereed Journal Articles

1. **Bruder, J.**, Lee, A.P. & Hoffman-Kim, D. Biomimetic materials replicating Schwann cell topography enhance neuronal adhesion and neurite alignment in vitro. *Journal of Biomaterials Science, Polymer Edition* 18, 967-982 (2007).
2. **Bruder, J.**M., Monu, N.C., Harrison, M.W. & Hoffman-Kim, D. Fabrication of polymeric replicas of cell surfaces with nanoscale resolution. *Langmuir* 22, 8266-8270 (2006).
3. Campaner, A.B., Ferreira, L.M., Gragnani, A., **Bruder, J.**M., Cusick, J.L. & Morgan, J.R. Upregulation of TGF-beta1 expression may be necessary but is not sufficient for excessive scarring. *The Journal of investigative dermatology* 126, 1168-1176 (2006).
4. Goldner, J.S., **Bruder, J.**M., Li, G., Gazzola, D. & Hoffman-Kim, D. Neurite bridging across micropatterned grooves. *Biomaterials* 27, 460-472 (2006).
5. O'Loughlin, J.A., **Bruder, J.**M. & Lysaght, M.J. Oral administration of biochemically active microcapsules to treat uremia: new insights into an old approach. *Journal of Biomaterials Science, Polymer Edition* 15, 1447-1461 (2004).
6. O'Loughlin, J.A., **Bruder, J.** & Lysaght, M.J. Degradation of low molecular weight uremic solutes by oral delivery of encapsulated enzymes. *ASAIO Journal* 50, 253-260 (2004).
7. O'Loughlin, J.A., **Bruder, J.**M. & Lysaght, M.J. Degradation of uremic toxins with free and encapsulated enzymes. *ASAIO Journal* 49, 208 (2003).
8. O'Loughlin, J.A., **Bruder, J.**M. & Lysaght, M.J. In Vivo and in Vitro Degradation of Urea and Uric Acid by Encapsulated Genetically Modified Microorganisms. *Tissue Engineering* 10, 1446-1455 (2004).

Patents

1. **Bruder J.** & Hoffman-Kim, D. *Topographic Templating of Polymeric Materials Using Cellular Morphology*. WO/2007/021,590
2. Lysaght M.J., **Bruder, J.M.** & Jill, A.O.L. *Systems and methods related to degradation of uremic toxins*. US Patent 7,198,785 - currently licensed.

Abstracts

1. **Bruder, J.**, Lee, A.P., & Hoffman-Kim, D. Substrate-bound Biochemical and Biomimetic Cell-shaped Topographical Cues Direct Neuronal Growth. *Annual Northeast Bioengineering Conference,* Providence, RI, April 2008
2. Lee, A.P., Palley, J., **Bruder, J.** & Hoffman-Kim, D. Competing Cues Influence Dorsal Root Ganglia Growth. *Annual Meeting of the Biomedical Engineering Society,* Hollywood, CA, September 2007
3. Gourd, C., Rollo, J., **Bruder, J.** & Hoffman-Kim, D. Neurite Outgrowth on Aligned Glial Cell Topographies. *Annual Meeting of the Biomedical Engineering Society,* Hollywood, CA, September 2007
4. **Bruder, J.**, Santos, M.A. & Hoffman-Kim, D. Neurite Growth in Biomimetic Guidance Channels Containing Schwann Cell Topography. *Annual Meeting of the Biomedical Engineering Society,* Hollywood, CA, September 2007
5. Hoffman-Kim, D., Monu, N.C. & **Bruder, J.** Fabrication of polymeric replicas of cell surfaces with nanoscale resolution. *Regenerate World Congress,* Pittsburgh, PA, April 2006

6. Hoffman-Kim, D., Monu, N.C. & **Bruder, J.** Fabrication of polymeric replicas of cell surfaces with nanoscale resolution. *Annual Meeting of the Society for Biomaterials,* Pittsburgh, PA, April 2006

7. **Bruder, J.**, Santos, M.A. & Hoffman-Kim, D. Nerve guidance channels composed of novel biomimetic nanoscale materials. *Annual Meeting of the Biomedical Engineering Society,* Chicago, IL, October 2006

8. **Bruder, J.**, Monu, N.C., Harrison, M.W. & Hoffman-Kim, D. Neuronal growth on nanopatterned biomimetic materials. *Annual Meeting of the Biomedical Engineering Society,* Chicago, IL, October 2006

9. Bremus-Koebberling, E.A., **Bruder, J.** & Hoffman-Kim, D. Neuron-material interactions on surfaces with complex topographies. *Regenerate World Congress,* Pittsburgh, PA, April 2006

10. Campaner, A.B. et al. Upregulation of TGF-ß1 Expression May Be Necessary But Is Not Sufficient For Excessive Scarring. *Plastic Surgery,* Chicago, IL, September 24-28, 2005

11. **Bruder, J.**, Goldner, J.S. & Santos, M.A. Cellular extensions bridge across micropatterned grooves. *Annual Meeting of the Biomedical Engineering Society,* Baltimore, MD, September 28 - October 1, 2005

12. **Bruder, J.**, Goldner, J.S. & Hoffman-Kim, D. Formation of neurite bridges on micropatterned substrates. *Annual Meeting of the Biomedical Engineering Society,* Baltimore, MD, September 28 - October 1, 2005

13. Yu, P., Goldner, J.S., **Bruder, J.** & Hoffman-Kim, D. Micron-scale topography supports neurite bridging. *International Society of Biological Engineering Conference on Bioengineering and Nanotechnology,* Singapore, September 2004

14. O'Loughlin, J.A., **Bruder, J.** & Lysaght, M.J. Biochemically active microcapsules which enable the gut to do the work of the kidney. *27th meeting of the International Society of Blood Purification,* London, UK, September 2004

15. O'Loughlin, J.A., **Bruder, J.** & Lysaght, M.J. In vivo evaluation of microencapsulated enzymes for the enteral removal of non-protein nitrogen (NPN) compounds in experimental uremia. *31st meeting of the European Society of Artificial Organs,* Warsaw, Poland, 2004

16. Goldner, J.S., **Bruder, J.**, Li, G., Gazzola, D. & Hoffman-Kim, D. Neurite bridging across micropatterned grooves. *Nanotech 2004 Montreux,* November 14-18, 2004

17. Goldner, J.S., **Bruder, J.**, Li, G., Gazzola, D. & Hoffman-Kim, D. Effects of groove dimensions on neurite bridging across micropatterned grooves. *Annual Meeting of the Biomedical Engineering Society,* Philadelphia, PA, October 13-16, 2004

18. Goldner, J.S., **Bruder, J.**, Gazzola, D. & Hoffman-Kim, D. Neurite bridging across micropatterned grooves. *Annual Meeting of the Biomedical Engineering Society,* Philadelphia, PA, October 13-16, 2004

19. **Bruder, J.**, Livi, L., C., S. & Hoffman-Kim, D. Gene expression of neurons in three-dimensional collagen matrix. *Society for Biomaterials Meeting-- Biomaterials in Regenerative Medicine: The Advent of Combination Products,* Philadelphia, PA, October 16-18, 2004

20. O'Loughlin, J.A., **Bruder, J.** & Lysaght, M.J. Microencapsulated enzymes for enteral removal of uremic toxins. *26th meeting of the International Society of Blood Purification,* Uncasville, CT, 2003

21. Lysaght, M.J., **Bruder, J.** & O'Loughlin, J.A. Development of orally administered microcapsules for removal of uremic toxins. *World Congress of Nephrology,* Berlin, Germany, June 8-12, 2003

22. **Bruder, J.**, O'Loughlin, J.A. & Lysaght, M.J. Encapsulated Cell Therapy for Removal of Uremic Toxins. *ET 2003: Engineering Tissues - 7th Annual Hilton Head Workshop & Annual ET Workshop*, Sea Pines Plantation, Hilton Head, SC, February 26 - March 2, 2003

Journal Articles in Preparation

1. O'Brien, T.M., Keefe, D.F., **Bruder, J.M.,** Hoffman-Kim, D., Laidlaw, D.H. 3D Visualization and Analysis of Neuron and Glial Cell Alignment from Confocal Microscopy Images.
2. **Bruder, J.M.**, Lee, A.P., Hoffman-Kim, D. Cellular Alignment on Substrates Combining Biochemical and Biomimetic Cell-shaped Cues.
3. Morales, A., **Bruder, J.M.**, Lysaght, M.J. Demographic Scope and Economic Magnitude of Contemporary Organ Replacement Therapies.

RELATED / OTHER WORK EXPERIENCE

2007	Collaboration with Computer Science Department, Brown University, to develop novel quantitative 3D analysis software for volumetric assessment of cellular growth and alignment
2006-2007	Collaboration with Dr. Thomas Webster, Brown University, characterizing neuronal responses to novel polymer/carbon-nanotube composite materials
2005-2006	Collaboration with Dr. Elke Bremus Koebberling, Fraunhofer Institute for Laser Technology, quantifying cellular responses to complex laser-ablated topographies in polymer surfaces.

2003	Rotation with Dr. Jeffrey Morgan, Brown University, in-vivo analysis of the effects of TGF-beta on scar and kieloid formation in skin wound models

HONORS AND AWARDS

Fellowships

2007	Brain Science Program Susan and Robert Kaplan Summer Graduate Fellowship
2004	Divisional Summer Fellowship
2003	Graduate School Fellowship, Semester I, II, & summer
2001	Burroughs-Wellcome Brain Science Research Fellowship

Other Awards

2008	Sigma-Xi Scientific Honor Society – Full Member
2005	First Recipient of Brown University Award for Technological Innovation
2003	Honors in Biology, Brown University
2003	Sigma Xi Scientific Honor Society – Student Member
1999	Karl-von-Frisch Prize in Biology (German National Award for Outstanding Scholarship)

TEACHING EXPERIENCE

Mentoring Honors Theses in Biology and Bioengineering

Mentored eight undergraduate students and one High School student in the theories and practices of primary research work.

The objective of these relationships is to give students a taste and working knowledge of what it means to be a scientist in theory and at the bench – everything one needs to know in order to conduct experimental research in a laboratory setting. My role was to communicate the theoretical background and motivation of our research area, incite enthusiasm for the work, and teach the craft of science on a technical level. This includes learning how to brainstorm approaches, experimental design, statistics and data analysis, problem-solving approaches, ethical considerations in science, and how to present research orally and/or in writing.

Over the last five years, my mentees and I published 3 research articles and presented 22 abstracts at professional meetings. Seven of the undergraduates I have advised have or will finish their degrees with Honors based on their work with me.

2006-2008	Andrea P. Lee*	Thesis Title: *Competing Biochemical And Topographical Guidance Cues*
2007	Jennifer Pallay*	

2003-2007	Michael A. Santos*	Thesis Title: *Nerve Growth on Biomimetic Nerve Guidance Channels*
2006-2007	Johnathon Rollo*	Thesis Title: *Neurite Alignment in Response to Cellular Topography*
2005-2006	Nicolas Monu*	Thesis Title: *Micropatterned Cell Templates for Neural Growth*
2005-2006	Caitlin Elgarten*	Thesis Title: *The Synergistic Effects of Topographical and Substrate-Bound Cues on Neuron Adhesion, Migration, and Growth*
2004-2005	Nhu-An Le	Project Title: *Micro-scale Protein Deposition with Ink-jet Technology*
2004	Thomas Murphy (High School Student)	Project Title: *Micro-scale Protein Deposition with ink-jet technology*
2003-2004	Joshua S. Goldner*	Thesis Title: *Future Directions of Neurite Bridging Research: Micro-stamped Protein Patterning*

(= degrees with Honors)*

Teaching Assistant

As a teaching assistant over six semesters, I have taken on many facets of teaching duties. I designed and graded exams, final projects, and homework assignments. I have planned, led,

and taught bi-weekly discussion sections dealing with the wider implications of biotechnology on society in terms of its ethical issues, its economical development and outlook, its scientific mode of progress, and the difficulties of governing and regulating a rapidly expanding field such as pharmaceutical or medical device industry. While closely working with a faculty member, I have designed lecture slides, built extensive web pages, organized networking events, built interactive networking sites into course pages, and fostered the contact of "course alumni" after the course had finished.

The Courses I accompanied as a TA were:

Biotechnology and Management

Professor M. Lysaght and Professor B. Bready

TA during: 2005, 2007, 2008

Description: An examination of the pharmaceutical, biotechnology, and medical product industries: what they are, how they function, whence they originate, and various perspectives on why some succeed and others fail. Pathways from lab-bench to marketplace are described as are the pervasive influences of the FDA, patent office, and courts. Extensive reading; emphasis on oral presentation. Primarily intended for students planning a career in biomedical industry. Class size: ~20 students.

Biotechnology in Medicine

Professor B. Zielinski and Professor M. Lysaght

TA during: 2007

Description: Introduces undergraduates to the main technological advances currently dominating the practice of medicine. Provides an overview of the objectives, techniques, and problems related to the application of biomedical technology to the diagnosis and treatment of disease and the contemporary health care industry. Topics include: pharmaceutical development and formulation; organ replacement by prosthesis and transplantation; medical imaging; tissue engineering, therapeutic cloning, regenerative medicine; stem cells; societal, economic, and ethical issues. Class size: ~110 students.

Organ Replacement

Professor M. Lysaght

TA during: 2005, 2006

Description: Organ replacement provides the foundation for contemporary substitutive medicine. Surveys the physiologic rationale and quantitative features of existing therapies (cardiac, renal, musculoskeletal), emerging technologies (regenerative medicine, tissue engineering, and stem cells). Interdisciplinary approach; suitable for students focused in biology or engineering. Class size: ~90 students.

Teaching Certificates – Formal Pedagogical Training

Expected 2008 Teaching Certificate Program III – Professional Developmental Seminar for Advanced Graduate Students

Expected 2008	Teaching Certificate Program II – The Classroom Tools Seminar
2007	Teaching Certificate Program I – The Sheridan Teaching Seminar
2007-present	Sheridan Center Teaching Fellow and Presentation Consultant

SERVICE TO THE UNIVERSITY

2007	**University Search Committee for the Dean of Student Life,** Member
2001-present	**Brown Outdoor Leadership Program,** Leader and Website Coordinator

SERVICE TO THE SCIENTIFIC COMMUNITY

2007	***Journal of Biomedical Biomaterials Research A,*** Reviewer

MEMBERSHIP IN PROFESSIONAL SOCIETIES

2006	Tissue Engineering and Regenerative Medicine International Society
2004-present	Biomedical Engineering Society
2004	Society for Biomaterials

SELECTED TECHNICAL AND SPECIALIZED SKILLS

Imaging

- Operation of

  Multi-channel (5D) time-lapse microscopy of live cells, Scanning Electron Microscope (SEM), Transmission Electron Microscope (TEM), Confocal Laser Microscope, White Light Interference Microscope (WIM), Atomic Force Microscope (AFM), IR interferometer

- Sample preparation for SEM, thick sectioning

Certifications

- Laser Operation
- Clean Room Operation (mask aligner, spinner, Dektak Profilometer)

Software

- Microscopy:

  Leica Imaging Suite, Improvision Openlab (with Automations), Improvision Volocity LE, Zeiss Axiovert Suite

- Image Analysis / 3D Reconstruction:

  NIH ImageJ, Indiana Center for Biological Microscopy: Voxx 2 Volume Renderer, Osirix 3D Renderer, Scientific use of Adobe Photoshop image processing,

Exposure to Matlab image processing

- Digital Design:

  Autodesk AutoCAD for creation of lithography masks

- Data Analysis / Statistics:

  Kovach Oriana Circular Statistics Software, SigmaPlot Graphing Software, SPSS Statistical Software

- General:

  Image editing / compositing in Adobe Photoshop, Corel Draw, Office Suite: Microsoft Powerpoint, Word, Excel, Outlook on Mac and PC, Thompson Endnote reference manager, Web page creation with Photoshop, Adobe Dreamweaver, Computer operation and networking administration on Mac and PC, Basic computer programming: Introductory exposure to C, Computer Hardware Troubleshooting

Processes / Techniques

Photolithography, soft lithography, micro-contact printing of proteins, replica molding at sub-micron level, live cell encapsulation, surgical technique in animals (bowel resection, carotid artery repair, thyroidectomy, cell sourcing operations), basic animal handling, multi-label immunostaining, ELISA, western blotting, data analysis of Affymetrix Gene Chips (MAS 4/5), electrophoresis, cell culture of mammalian cells, including human cell lines, minipreps, SDS-PAGE, restriction enzyme processing, transfection

LANGUAGE SKILLS

Fluent in English and German

4 years of Latin study

2 years of French study

Table of Contents

ABSTRACT **1**

SUMMARY **3**

Background 3

Neurite Bridging 4

Fabrication of Biomimetic Replicas 5

Cellular Response to Biomimetic Replicas 6

Conflicting Cues 6

Appendix 8

CHAPTER 1 ..... **9**

BACKGROUND AND RATIONALE 9

Topography and Contact Guidance 10

Topographically Biomimetic Substrates 12

Artificial Nerve Guidance Channels 13

Conflicting Cues – Recombining Topography and Biochemical Substrate-Bound Cues 15

References 17

CHAPTER 2 ..... **23**

NEURITE BRIDGING ACROSS MICROPATTERNED GROOVES 23

Abstract *24*

Introduction *25*

Materials and Methods *28*

Substrate Production 28

Pattern Design and Printing 28

Photolithography 28

Preparation of Poly(dimethyl siloxane) (PDMS) Substrates 28

Cell Culture 29

Dorsal Root Ganglion (DRG) Culture 30
Hippocampal Neuron Culture 30
Schwann Cell Culture 30
B104 Cell Culture 31
Fixing and Immunostaining 31
Analysis *32*
Microscopy 32
Confocal Microscopy 32
Phase Contrast and Epifluorescence Microscopy 33
Scanning Electron Microscopy 33
Quantification and Statistical Analysis 33
Time-lapse Microscopy 34
Results and Discussion *34*
Micropatterned Substrates 34
Bridges Across Micropatterned Grooves 35
Conditions for Neurite Bridges 36
Bridging and Alignment 38
Dynamics of Bridge Formation 40
Conclusions *42*
Acknowledgments *44*
Figures *45*
Supplemental Data *57*
References *59*
CHAPTER 3 64
FABRICATION OF POLYMERIC REPLICAS OF CELL SURFACES WITH NANOSCALE RESOLUTION 64
Abstract *65*
Introduction *66*
Materials and Methods *67*
Microcontact Printing 67

Cell Culture 68
Substrate Preparation 69
Analysis 70
Results and Discussion *71*
Conclusion *74*
Acknowledgements *75*
Figures *76*
Supporting Information Available *81*
References *83*
CHAPTER 4 85
BIOMIMETIC MATERIALS REPLICATING SCHWANN CELL TOPOGRAPHY ENHANCE NEURONAL ADHESION AND NEURITE ALIGNMENT IN VITRO 85
Abstract *86*
Introduction *87*
Materials and Methods *88*
Cell Culture 88
Substrate Preparation 89
White Light Interferometry 90
Study Parameters 91
LN Adsorption Study 91
Adhesion Study 91
Alignment Study 92
Cell Processing and Immunocytochemistry 92
Microscopy 93
Image Analysis 94
Statistical Analysis 95
Results *95*
Discussion *98*
Acknowledgements *101*

Figures *102*

References *111*

CHAPTER 5 ..... **113**

CELLULAR ALIGNMENT ON SUBSTRATES COMBINING BIOCHEMICAL AND BIOMIMETIC CELL-SHAPED CUES 113

Abstract *114*

Introduction *115*

Methods *117*

Cell Culture 117

Substrate Preparation 118

Protein Coating 119

Experimental Setup 120

Fixing and Immunostaining 120

Microscopy 121

Image Analysis 122

Statistical Analysis 122

Results *123*

Generation of Substrates 123

DRG Alignment: Orientation 123

DRG Alignment: Strength 125

SC-Alignment: Orientation 126

SC-Alignment: Strength 127

Discussion 128

Conclusion *135*

Acknowledgement *135*

Figures *136*

References *147*

CHAPTER 6 ..... **152**

CONCLUSIONS AND FUTURE DIRECTIONS 152

Neurite Bridging (Chapter 2) 152
Fabrication of Biomimetic Materials (Chapter 3) 156
Cellular Response to Biomimetic Substrates (Chapter 4) 158
Conflicting Cues (Chapter 5) 160
References 164

FINAL THOUGHTS 166

APPENDIX 167

APPENDIX A 168
NEURITE BRIDGING BEYOND DORSAL ROOT GANGLIA 168
Introduction 168
Methods 169
Cell Culture 171
Results 171
Conclusion 176
APPENDIX B 177
NEURONAL BRIDGING EXERTS TENSION 177
Introduction and Rationale 177
Methods 177
Results 177
Figures 178
APPENDIX C 180
EXTRACELLULAR PROTEIN PATTERNS INFLUENCE FREQUENCY OF NEURITE BRIDGE FORMATION 180
Introduction and Rationale 180
Methods 181
Results 183
Conclusion 183
Figures 184
References 187
APPENDIX D 188

BIOMIMETIC MATERIALS REPLICATING SCHWANN CELL TOPOGRAPHY ENHANCE NEURONAL ADHESION AND NEURITE ALIGNMENT IN VITRO - ADDENDUM 188
Introduction and Rationale 188
Methods 188
Results 188
Conclusion 188
Figures 189
APPENDIX E 194
NERVE GUIDANCE CHANNELS FEATURING CELLULAR TOPOGRAPHY ON THEIR LUMINAL SURFACES ENHANCE NERVE REGENERATION IN VITRO 194
Introduction and Rationale 194
Methods 196
Results 197
References 204
APPENDIX F 205
SCHWANN CELLS AND DORSAL ROOT GANGLIA ON POLYCARBONATE URETHANE-CARBON-NANOTUBE COMPOSITES 205
Introduction and Rationale 205
Methods 206
Results 207
Conclusions 207
Figures 208
APPENDIX G 215
PROTOCOLS AND DESIGNS 215
Protocols for Cell Media 216
Protocol for Cell Thawing 218
Protocol For Cell Splitting 221
Protocol for Paraformaldehyde Fixation 223
Protocol for Dissection and Culture of Dorsal Root Ganglia (DRG) Neurons 224
Protocol for Hoechst 33342 Live DNA staining 231

Protocol for Alexa Fluor 488 Phalloidin (Actin Stain) *233*

Protocol for Dapi Staining *235*

Protocol for Immunostaining *237*

Procedure for Microstamping *242*

Procedure for Schwann Cell Seeding And Alignment *246*

Procedure for Cell Fixation of Cell Templates *249*

Protocol for Osmium-thiocarbohydrazide-Osmium SEM Preparation *251*

Protocol for Preparing PDMS Polymer *253*

Protocol For Replica Molding *256*

Procedure for Timelapse Microscopy *259*

Protocol for Image Analysis of Nuclear Cell Alignment *265*

Protocol for Handling and Compiling Confocal Images *271*

Protocol for Use of Matlab Program to Measure Pixel Alignment *272*

Program 1: 275

Program 2 276

Automations for Improvision Openlab Software *278*

Protocol for Microfabrication/Soft Lithography *282*

AutoCAD Designs for Photolithography *296*

Abstract

My graduate work examined the reaction of neuronal cells to the shape of their extra-cellular environment. Over the last century, many studies have confirmed that external topography has a profound influence on cellular behavior. Using geometric, rectangular repeating grooves with size ranges in the tens of micrometers, we were the first to describe "cellular bridging" in which a variety of anchorage-dependent cell types including primary rat and human cell cultures as well as a variety of immortal rat, mouse, and human cell lines extended from one plateau to an adjacent plateau of a multiple grooved substrate without underlying support. Extending our research to more complex shapes, we developed a platform technology based on a two-stage replica molding approach that is capable of reproducing adherent cellular shapes at a macro-, micro-, and nano-scale in various polymeric substrates and thus create cell-shaped polymeric surfaces. This allowed us to separate the presentation of cellular shape from cellular biochemistry and characterize cellular behavior in response to cellular shape in the absence of other heterogeneous cellular cues that are inherent to cell-cell interactions in co-cultures. Utilizing these novel materials, we were able to show that cellular topography is capable of enhancing adhesion, motility, and alignment in the absence of other directional cues. Pilot experiments with nerve guidance channels incorporating cell-shaped biomimetic topography showed increased cellular migration and outgrowth from dorsal root ganglion explants on surfaces with aligned biomimetic topography when compared to topographically homogeneous controls. The results of this research inform efforts at the basic science level by enabling the deconstruction of cellular environments

beyond previous capabilities and quantifying the contribution of cellular and extra-cellular matrix shape to cellular behavior. These results also open new avenues to controlling cellular response to implant surfaces. Currently, these techniques and approaches are continued and expanded by my colleagues to encompass different organ systems such as the vascular system and the control of differentiation of stem cells by cellular topography.

Summary

Background

Injuries of the nervous system are very common, with a prevalence of 1.1 million patients in the US per year. Damage to the central nervous system (CNS) remains permanent, as the CNS environment is non-permissive to neuronal growth on a biochemical and structural level (scarring).The peripheral nervous system (PNS) retains the ability to regenerate to a degree, and this ability is due to its permissive extracellular environment. PNS regeneration is vastly mediated via Schwann cells (SCs), glial cells that migrate into a site of injury, clear debris, and act as pathfinders for regenerating axons. To date, it is unclear which properties of SCs have the largest impact on fostering nerve growth; however, it is likely that several factors (biochemical and mechanical) act in concert. To optimize nerve injury treatment regimes, two fundamental issues have to be addressed: 1) To quantitatively understand neural and glial cell behavior to external stimuli on a cellular level, and 2) to design novel approaches and materials to control neural and glial cells in vivo or for de-novo tissue engineering.

The ultimate goal of my efforts is to isolate and quantify the contributions of biochemical and mechanical aspects of SCs to regenerating axons, and my dissertation work focuses on the impact of substrate topography on neuronal growth. The results of this research open new avenues into basic research applications exploring cellular responses to cell-shaped environments and inform efforts to optimize implant materials at an applied level.

Better materials can bridge larger defects in PNS injuries than previously possible and can contribute to overcoming the mechanical and biochemical obstacles encountered in the CNS.

Neurite Bridging

Most research on the effect of topography on neuronal cell behavior has been conducted on substrates with geometric surface shapes, often repeating grooves. Cells align to a direction parallel with linear surface discontinuities, according to a phenomenon called "contact guidance", first described as early as 1945. We characterized a behavior we termed "cellular bridging" that conflicts with the tenets of contact guidance. We observed that a small subset of neurons on a substrate with repeating grooves (of 50 um depth, 30-300 um width, and 50 um – 1 mm pitch) extend from one plateau to an adjacent plateau without underlying support. This behavior is novel in several points. First, not all cells in a given sample align to substrate features; some cells appear to respond in ways that counter what one would expect were contact guidance the only mechanism governing cellular orientation on these substrates. Second, neuronal cells generate enough tension to cause them to (partially) detach from their substrates, an unusual occurrence for substrate-dependent cells. Third, the tension generated was considerable, as qualitative observations noted deformations of the substrate in some instances. Overall, bridging frequency was dependent on the substrate dimensions and cell density. Highest numbers of bridges were observed with groove widths of 30 um, groove depth of 50 um, and plateau width of 200 um at a cell density of 125,000 cells/cm^2. The immediate impact of

these studies is to optimize design of porous biomaterials, as pore parameters can be tailored to promote bridging behavior.

These finding were published in Biomaterials (27):3 460, 2006. – 11 citations to date.

Fabrication of Biomimetic Replicas

Cells in vivo are surrounded by extracellular matrix and other cells. Topography is one of the major mediators of cellular behaviors including orientation, attachment, motility, and differentiation. Studies to date have assessed cellular behavior to either geometric or completely random topography at various defined size ranges, but have not characterized cellular response to the much more complex mix of micro- and nano-scale features of cell surfaces which are neither random nor entirely ordered. We have developed a double replica molding process that can accurately reproduce the full gamut of adherent cellular shapes down to the nanoscale. The process is not dependent on the polymer or cell type used, and was demonstrated using poly-(dimethyl siloxane) (PDMS) and polyurethane replicating SCs and smooth muscle cells. Reproduction accuracy was assessed via Scanning Electron Microscopy, White Light Interference Microscopy, and Atomic Force Microscopy and indicated accuracy in the tens of nanometer range. These novel materials allow characterization of cell response to topographies that mimic the natural cellular environment much more closely than previous studies. This technique also allows generating implant materials that topographically mimic the permissive environment of a regenerating peripheral nerve.

These findings were published in Langmuir (22): 20 8266, 2006 – 2 citations to date.

Cellular Response to Biomimetic Replicas

Using novel biomimetic PDMS substrates replicating the shapes of aligned SCs, we were able to assess neuronal response to SC shapes in the absence of directional biochemical cues. This enabled us to quantify the potential contribution of cellular topography to regenerative responses in the peripheral nervous system. Results showed that SC-shaped surfaces enhanced adhesion, motility, and alignment of dorsal root ganglion cultures (DRGs). Cellular alignment was assessed via analysis of nuclear orientation and via custom-written software analyzing fluorescently labeled neuronal projections. Alignment was dependent on cell density, with densities above 13,160 cells/cm^2 resulting in significant alignment after 5 days of culture. Unpublished results indicate that both DRGs and SCs are aligned by SC topography, either indented or protruding. These findings can aid the design of novel biomaterials for nerve implants.

These findings were published in Journal of Biomaterials Science, Polymer Edition (18):8, 967-82, 2007 – no citations to date.

Conflicting Cues

Our novel biomimetic materials allowed us to investigate the hierarchy of cell shaped topography and protein cues and to look for possible synergistic interactions. By combining micro-contact printing (uCP) of laminin stripes (with 50 um width and pitch) with aligned SC-shaped topography, we assembled 5 different conditions: 1) flat substrates with a full laminin coat, 2) flat substrates with uCP laminin stripes, 3) biomimetic substrates with aligned SC-shapes and a full laminin coat (topography only),

4) biomimetic substrates with uCP stripes aligned in parallel to the direction of topography (parallel cues), and biomimetic substrates with uCP laminin stripes oriented orthogonally to the orientation of the topography (orthogonal cues).

Analysis of nuclear alignment of DRGs grown on the various experimental setups after 5 days of culture revealed the following hierarchy of cues in terms of strength of alignment (highest to lowest): 1) parallel cues, 2) protein cue, 3) orthogonal cue, 4) topography-only, and 5) flat fully coated control. On samples with orthogonal cues, DRG alignment was in the direction of the protein cue after 5 days. On all other conditions, DRG alignment was parallel to the direction of the cue(s) as expected.

Since SCs act as "pathfinders" for axonal tips during regeneration, assessment of SC behavior can aid the understanding and control of cellular behavior in a site of injury. Thus, we also examined SC alignment to the same cues as described above in a follow-up study, measuring nuclear alignment daily over 5 days. Alignment direction was parallel to the cues presented, except for the orthogonal cue setup, where we observed a transient turning response. The mechanisms underlying this turning response are not clear at this point. Strength of alignment over five days indicated a possible delayed sensitivity to topographic cues: alignment to topographic cues on day 1 was low, and surged on day 2; whereas alignment on orthogonal cues showed the inverse trend. In general, the hierarchy of cues was (highest to lowest alignment) 1) parallel cues, 2) protein cue, 3) topography-only, 4) orthogonal cues, and 5) flat fully coated control. We did not observe any synergistic or additive interactions for the different cues for neither DRGs nor SCs;

however, the cells clearly were capable of integrating both cues simultaneously, as shown by the reduced alignment on orthogonal cue conditions.

Understanding the individual contributions of topographical and biochemical cues can help decipher the underlying cellular machinery that integrates these cues. A better understanding of the interplay between different cues can also help streamline biomaterials for regenerative and de-novo tissue engineering approaches.

These findings are part of a manuscript for publication.

Appendix

The appendix contains a number of materials that did not merit more extensive write up due to pilot status or represent data that was not included in an initial publication in order to keep the published material focused. Some materials included here also represent contributions to colleagues' projects, as I completed a rotation inside the DHK lab before settling on topography as a focus and continued to contribute to those projects throughout my time in the lab. Lastly, the appendix contains a selection of essential protocols that I include for two reasons: Some protocols, such as cell media recipes, are intended to be a handy reference for future DHK lab generations; other protocols, such as the matlab protocol or the Openlab automations are research tools that I developed and thus represent a substantial portion of the body of work I completed as part of my duties as a graduate student.

Chapter 1

Background and Rationale

Traumatic injuries to the nervous system are among the most debilitating and untreatable injuries commonly encountered today. The prevalence of spinal cord injuries in the US in 2006 was 253,000 with an incidence of 11,000 new cases per year. Lifetime medical costs for these injuries vary widely depending on the severity and location of damage, but commonly cited figures are $2.9 million for a patient injured at age 25, and $1.7 million for a patient injured at age 50[1]. Peripheral nerve injuries are prevalent in approximately 3% of all trauma patients in the US, setting the incidence at roughly 900,000 cases per year[2]. These figures exemplify the strong need for treatment of both central as well as peripheral nerve injuries, as they present a burden not only to patients and their families, but to the healthcare system as a whole.

By combining innovative material engineering with insights into novel cellular behaviors, my research furthers the mechanistic understanding of neuronal growth during regeneration and informs efforts to develop treatment strategies both at the basic science and at the applied science levels. With this knowledge I am working towards implementing enhanced biomaterials for the design of implants and de-novo tissue engineering approaches to overcome obstacles in neural regeneration that have defied medical treatment so far.

After injury or degeneration, nerve cells must navigate complex environments in order to reconnect to their proper targets or bridge dysfunctional areas. During this process, regenerating cells integrate a variety of soluble, substrate-bound, and topographical cues [3-9], the sum of which can foster or prevent regeneration. Central nervous system (CNS) environments discourage nerve regeneration on a variety of chemical and mechanical levels [10-13], while peripheral nervous system (PNS) environments enable regrowth to a degree [14-16]. For a more thorough review, see reference [17]. The long term goal of my studies is to decipher the contribution of topography to net cell growth decisions relative to other cues and to utilize these results as a prerequisite to design improved materials to enhance nerve regeneration in areas of injury.

Topography and Contact Guidance

For decades it has been known that neurons are highly dynamic cells[18, 19] which react to varying topographies at the micro- and nanoscale with changes in adhesion, migration, and alignment [8]. Early on in cellular research, observations showed that cells are capable of following small grooves during growth, migration, and extension [20-25]. Later, this phenomenon was extended to include any kind of linear discontinuity in a substrate (grooves, cliffs, ridges, angles, arcs) [26-33] and summarized under the term "contact guidance." Contact guidance is the behavior of a cell that initially encounters a linear substrate disturbance, then aligns to it, and travels or extends parallel along its length. The strength of cellular alignment was shown to be dependent on the cell type, as well as

the substrate dimensions, i.e. groove width, plateau width, groove depth, edge fidelity and angle, etc. [30, 34-40].

Contact guidance is hypothesized to be one of the major mechanical guidance mechanisms in vivo, both during development and after injury. Although theories abound, the exact cellular mechanism of contact guidance remains unclear. It is likely that contact guidance involves not only direct mechanical restriction of cytoskeletal dynamics but also involves downstream regulatory pathways via cytoskeletal-associated proteins[41-43]. Recent studies suggest that topography-induced changes in cellular shape are directly translated into alterations in nuclear shape which in turn are linked to changes in gene expression[44, 45].

While contact guidance has been observed in many different in vitro systems, it appears that not all cells of a given population are guided by substrate discontinuities to the same extent. I have come to observe a phenomenon I will refer to as "cellular bridging", in which a subset of any given cell population seeded on a substrate (with geometric rectangular grooves in the size range of several tens of micrometers) extends cellular processes from one plateau to an adjacent plateau without underlying support[26]. These findings appear to contradict the principles of "contact guidance", may represent a separate class of cellular reactions to topography, and suggest that cellular response to topographical cues can be more complex than previously anticipated. I have also gathered pilot data that suggests that bridging frequency correlates with certain aspects of the biochemical environment of a cell population (see appendix for pilot data). Unraveling

these complexities may help to further elucidate fundamental mechanisms of cellular interactions with their environment and help to optimize biomaterials for implants.

Topographically Biomimetic Substrates

Cellular behavior in vivo is influenced by cellular topography and biochemical factors, but so far it has been difficult to separate these factors experimentally. After restorable injuries in the peripheral nervous system, Schwann cells migrate along any remaining fragments of basal lamina, align to each other and surrounding cues, and act as "pathfinders" for the regenerating axonal tips [16, 46]. To this end, they present a combination of substrate-bound cues such as laminin, as well as other biochemical factors, while at the same time presenting an aligned topography to the regenerating neurons. Aligned SCs in culture have been shown to align DRG neurons parallel to their orientation[47, 48], but so far it has been unclear whether the effect of SCs on neurons is predominantly mediated via biochemical cues, topography, or both.

Cellular response to geometrical shapes has been described on substrates with a wide variety of shapes and sizes, ranging from the nano- to the macroscale [8, 36, 49-54]. Other studies have described the effects of random topography created by polymer demixing, surface etching, and nano-fabrication techniques [36, 52, 55, 56]. However, in vivo environments present topography to cells in a rich mix of size ranges and complex contours, simultaneously confronting resident cells with shapes arising from extra-cellular matrix (ECM) as well as other cells [57]. This natural topography is neither ordered nor entirely random, and thus has proven difficult to replicate up to this point.

Past studies have created replicas of ECM reaching nanoscale resolution,[58] as well as impression (indented) replicas of living cells [59, 60] but have stopped short of assessing cellular growth on substrates that mimic cellular shape. My research is the first to address the effect of cell-shaped topography on cellular growth, particularly neuronal growth. To this end, I have developed transparent, biocompatible, biomimetic, polymeric substrates that replicate the surface shapes of SCs at the macro-, micro-, and nanoscale[61] (details described in chapter 2). Assessment of neuronal response to these materials in vitro showed significant enhancement of important regenerative characteristics such as adhesion, migration, and alignment[62] (details in Chapter 3).

Artificial Nerve Guidance Channels

Based on the encouraging in vitro results of neuronal response to our topographically biomimetic substrates, the experimental focus of my efforts shifted towards determining the feasibility of incorporating cell-shaped topography into current tissue engineering and implant technology. More specifically, I have developed a process to fabricate nerve guidance channels that replicate complex cellular shapes on their luminal surfaces, and I have quantitatively assessed the influence of cellular shape on cellular outgrowth and migration in a nerve guidance channel setting.

For peripheral nerve repair, autografts have been the gold standard for the past few decades. However, sourcing of these tissues creates additional morbidity and secondary impairment to patients already dealing with neurological damage. Artificial grafts could

eliminate the need for graft sourcing and allow for greater control of mechanical properties, such as length, diameter, wall thickness, permeability, degradability, and interior surface morphology [63-65]. In addition, artificial grafts can be tailored from the onset to incorporate drug delivery systems for temporally and spatially succinct delivery of diffusible as well as substrate-bound cues[66].

Before building a graft that incorporates a variety of different cues, it is important to understand the contribution of single guidance cues, in this case topography. Previous studies employing geometrical topographies on the luminal surface of guidance channels have shown the potential benefit of these surface morphologies[50, 55, 63-65]. Employing SC-shaped biomimetic patterning that mimics the natural environment of a regenerating nerve is the logical next step in developing an optimal artificial nerve guidance channel both for nerve repair and for de-novo tissue engineering. A number of studies have shown that macro-topography, such as the bending of a surface at the sub-millimeter and millimeter level can have profound effects on cellular behavior [49]. It is thus important to test the effect of cellular topography in combination with the macro-topography presented in the inside of a nerve guidance channel. The findings of this approach work towards untangling the combined effects of biomimetic macro-, micro-, and nanotopography on cells in culture.

Once deciphered, topography as a regenerative enhancement becomes one part in a modular approach to artificial nerve graft design. Other “modules” such as surface chemistry treatments or drug delivery can then be easily combined to form an “ideal”

nerve graft. An ideal artificial nerve graft will be biodegradable to avoid secondary impairment on newly formed nervous tissues during removal. However, since our initial in vitro studies were focused on the effect of surface morphology, we chose a polymer that is non-biodegradable in order to minimize surface degradation during the course of the experiments. Poly-(dimethyl-siloxane) (PDMS) is flexible, elastic, gas-permeable, transparent, biocompatible, and non-degrading, making it a good material for in vitro evaluation of cell fitness in an artificial nerve guidance channel (NGC) with SC-shaped topography. Other biodegradable polymers can and will have to be adapted for this replica molding approach in working towards an in vivo model.

Conflicting Cues – Recombining Topography and Biochemical Substrate-Bound Cues

The in vivo environment presents a multitude of simultaneous (soluble, substrate-bound, topographical, electrical) cues to growing neurons during development, stasis, and after injury. Understanding the interplay of these factors necessitates the careful deconstruction of very complex systems. Once the individual contributions of each group of cues is better understood, we can make informed decisions to custom-tailor new materials and devices to optimize clinical outcomes, both in de novo tissue engineering as well as in clinical repair and recovery. Topography has been identified as one major factor capable of governing and influencing cell behavior. Our research exploits a new technique to isolate and systematically study the effects of cellular topography in vitro, and enables us to carefully probe possible synergistic and antagonistic behaviors of biomimetic topography and substrate-bound cues for the first time.

The relative hierarchy of geometric topography and chemical cues depends largely on the size of the topographical features a cell encounters [67, 68]. To date, no studies have examined the relative contributions of *cellular* topography and chemical cues in situations where the two cues conflict with each other. Contact guidance is likely mediated through cellular pathways other than chemical guidance; though all of these mechanisms ultimately converge on the cytoskeleton to affect net growth[7, 43, 45, 69]. Identifying the hierarchy of these pathways provides a base for untangling the interaction points of these chemical / biomechanical systems.

References

1. NSCISC (National Spinal Cord Statistics Center (NSCISC), June 2006).

2. CDC (Center for Disease Control / National Center for Injury Prevention and Control, June 2006).

3. Tessier-Lavigne, M. & Goodman, C.S. The molecular biology of axon guidance. Science 274, 1123-1133 (1996).

4. Dickson, B.J. Molecular mechanisms of axon guidance. Science 298, 1959-1964 (2002).

5. Huber, A.B., Kolodkin, A.L., Ginty, D.D. & Cloutier, J.F. Signaling at the growth cone: ligand-receptor complexes and the control of axon growth and guidance. Annual review of neuroscience 26, 509-563 (2003).

6. Chilton, J.K. Molecular mechanisms of axon guidance. Dev Biol 292, 13-24 (2006).

7. Raivich, G. & Makwana, M. The making of successful axonal regeneration: genes, molecules and signal transduction pathways. Brain research reviews 53, 287-311 (2007).

8. Curtis, A.S., Dalby, M. & Gadegaard, N. Cell signaling arising from nanotopography: implications for nanomedical devices. Nanomedicine (London, England) 1, 67-72 (2006).

9. Song, H. & Poo, M. The cell biology of neuronal navigation. Nature cell biology 3, E81-88 (2001).

10. Schwab, M.E. & Thoenen, H. Dissociated neurons regenerate into sciatic but not optic nerve explants in culture irrespective of neurotrophic factors. J Neurosci 5, 2415-2423 (1985).

11. Caroni, P., Savio, T. & Schwab, M.E. Central nervous system regeneration: oligodendrocytes and myelin as non-permissive substrates for neurite growth. Progress in brain research 78, 363-370 (1988).

12. Schwab, M.E. Experimental aspects of spinal cord regeneration. Current opinion in neurology and neurosurgery 6, 549-553 (1993).

13. Yiu, G. & He, Z. Glial inhibition of CNS axon regeneration. Nature reviews 7, 617-627 (2006).

14. Aguayo, A.J., David, S. & Bray, G.M. Influences of the glial environment on the elongation of axons after injury: transplantation studies in adult rodents. The Journal of experimental biology 95, 231-240 (1981).

15. Bunge, R.P. The role of the Schwann cell in trophic support and regeneration. Journal of neurology 242, S19-21 (1994).

16. Chen, Z.L., Yu, W.M. & Strickland, S. Peripheral regeneration. Annual review of neuroscience 30, 209-233 (2007).

17. Fawcett, J.W. & Keynes, R.J. Peripheral nerve regeneration. Annual review of neuroscience 13, 43-60 (1990).

18. Zito, K. & Svoboda, K. Activity-dependent synaptogenesis in the adult Mammalian cortex. Neuron 35, 1015-1017 (2002).

19. Ridley, A.J. et al. Cell migration: integrating signals from front to back. Science 302, 1704-1709 (2003).

20. Clark, P., Connolly, P., Curtis, A.S., Dow, J.A. & Wilkinson, C.D. Topographical control of cell behaviour. I. Simple step cues. Development 99, 439-448 (1987).

21. Brunette, D.M. Fibroblasts on micromachined substrata orient hierarchically to grooves of different dimensions. Exp Cell Res 164, 11-26 (1986).

22. Ohara, P.T. & Buck, R.C. Contact guidance in vitro. A light, transmission, and scanning electron microscopic study. Exp Cell Res 121, 235-249 (1979).

23. Ebendal, T. The relative roles of contact inhibition and contact guidance in orientation of axons extending on aligned collagen fibrils in vitro. Exp Cell Res 98, 159-169 (1976).

24. Dunn, G.A. & Heath, J.P. A new hypothesis of contact guidance in tissue cells. Exp Cell Res 101, 1-14 (1976).

25. Weiss, P. Experiments on cell and axon orientation in vitro: the role of colloidal exudates in tissue organization. J Exp Zool 100, 353-386 (1945).

26. Goldner, J.S., Bruder, J.M., Li, G., Gazzola, D. & Hoffman-Kim, D. Neurite bridging across micropatterned grooves. Biomaterials 27, 460-472 (2006).

27. Schmalenberg, K.E. & Uhrich, K.E. Micropatterned polymer substrates control alignment of proliferating Schwann cells to direct neuronal regeneration. Biomaterials 26, 1423-1430 (2005).

28. Stepien, E., Stanisz, J. & Korohoda, W. Contact guidance of chick embryo neurons on single scratches in glass and on underlying aligned human skin fibroblasts. Cell biology international 23, 105-116 (1999).

29. Curtis, A.S. & Wilkinson, C.D. Reactions of cells to topography. Journal of biomaterials science 9, 1313-1329 (1998).

30. Rajnicek, A., Britland, S. & McCaig, C. Contact guidance of CNS neurites on grooved quartz: influence of groove dimensions, neuronal age and cell type. J Cell Sci 110 (Pt 23), 2905-2913 (1997).

31. Nagata, I., Kawana, A. & Nakatsuji, N. Perpendicular contact guidance of CNS neuroblasts on artificial microstructures. Development 117, 401-408 (1993).

32. Clark, P., Connolly, P., Curtis, A.S., Dow, J.A. & Wilkinson, C.D. Topographical control of cell behaviour: II. Multiple grooved substrata. Development 108, 635-644 (1990).

33. Yoshinari, M., Matsuzaka, K., Inoue, T., Oda, Y. & Shimono, M. Effects of multigrooved surfaces on fibroblast behavior. Journal of biomedical materials research 65, 359-368 (2003).

34. Dalby, M.J., Riehle, M.O., Yarwood, S.J., Wilkinson, C.D. & Curtis, A.S. Nucleus alignment and cell signaling in fibroblasts: response to a micro-grooved topography. Exp Cell Res 284, 274-282 (2003).

35. Dalby, M.J. et al. Fibroblast reaction to island topography: changes in cytoskeleton and morphology with time. Biomaterials 24, 927-935 (2003).

36. Dalby, M.J., Riehle, M.O., Johnstone, H.J., Affrossman, S. & Curtis, A.S. Polymer-demixed nanotopography: control of fibroblast spreading and proliferation. Tissue engineering 8, 1099-1108 (2002).

37. Curtis, A. & Wilkinson, C. Topographical control of cells. Biomaterials 18, 1573-1583 (1997).

38. Wojciak-Stothard, B., Madeja, Z., Korohoda, W., Curtis, A. & Wilkinson, C. Activation of macrophage-like cells by multiple grooved substrata. Topographical control of cell behaviour. Cell biology international 19, 485-490 (1995).

39. Wojciak-Stothard, B. et al. Role of the cytoskeleton in the reaction of fibroblasts to multiple grooved substrata. Cell motility and the cytoskeleton 31, 147-158 (1995).

40. Clark, P., Connolly, P., Curtis, A.S., Dow, J.A. & Wilkinson, C.D. Cell guidance by ultrafine topography in vitro. J Cell Sci 99 (Pt 1), 73-77 (1991).

41. Rajnicek, A. & McCaig, C. Guidance of CNS growth cones by substratum grooves and ridges: effects of inhibitors of the cytoskeleton, calcium channels and signal transduction pathways. J Cell Sci 110 (Pt 23), 2915-2924 (1997).

42. Letourneau, P.C. The cytoskeleton in nerve growth cone motility and axonal pathfinding. Perspectives on developmental neurobiology 4, 111-123 (1996).

43. Gallo, G. & Letourneau, P.C. Regulation of growth cone actin filaments by guidance cues. Journal of neurobiology 58, 92-102 (2004).

44. Dalby, M.J. et al. Nanomechanotransduction and Interphase Nuclear Organization influence on genomic control. J Cell Biochem (2007).

45. Dalby, M.J. Topographically induced direct cell mechanotransduction. Medical engineering & physics 27, 730-742 (2005).

46. Bray, G.M., Rasminsky, M. & Aguayo, A.J. Interactions between axons and their sheath cells. Annual review of neuroscience 4, 127-162 (1981).

47. Thompson, D.M. & Buettner, H.M. Neurite outgrowth is directed by schwann cell alignment in the absence of other guidance cues. Annals of biomedical engineering 34, 161-168 (2006).

48. Thompson, D.M. & Buettner, H.M. Oriented Schwann cell monolayers for directed neurite outgrowth. Annals of biomedical engineering 32, 1120-1130 (2004).

49. Smeal, R.M., Rabbitt, R., Biran, R. & Tresco, P.A. Substrate curvature influences the direction of nerve outgrowth. Annals of biomedical engineering 33, 376-382 (2005).

50. Berry, C.C., Dalby, M.J., McCloy, D. & Affrossman, S. The fibroblast response to tubes exhibiting internal nanotopography. Biomaterials 26, 4985-4992 (2005).

51. Dalby, M.J. et al. Increasing fibroblast response to materials using nanotopography: morphological and genetic measurements of cell response to 13-nm-high polymer demixed islands. Exp Cell Res 276, 1-9 (2002).

52. Dalby, M.J., Marshall, G.E., Johnstone, H.J., Affrossman, S. & Riehle, M.O. Interactions of human blood and tissue cell types with 95-nm-high nanotopography. IEEE transactions on nanobioscience 1, 18-23 (2002).

53. Flemming, R.G., Murphy, C.J., Abrams, G.A., Goodman, S.L. & Nealey, P.F. Effects of synthetic micro- and nano-structured surfaces on cell behavior. Biomaterials 20, 573-588 (1999).

54. Curtis, A. & Wilkinson, C. New depths in cell behaviour: reactions of cells to nanotopography. Biochemical Society symposium 65, 15-26 (1999).

55. Guenard, V., Valentini, R.F. & Aebischer, P. Influence of surface texture of polymeric sheets on peripheral nerve regeneration in a two-compartment guidance system. Biomaterials 12, 259-263 (1991).

56. Webster, T.J., Ergun, C., Doremus, R.H., Siegel, R.W. & Bizios, R. Enhanced osteoclast-like cell functions on nanophase ceramics. *Biomaterials* **22**, 1327-1333 (2001).

57. Even-Ram, S. & Yamada, K.M. Cell migration in 3D matrix. *Current opinion in cell biology* **17**, 524-532 (2005).

58. Sims, P.A. & Albrecht, R.M. Corrosion Casting in the Reproduction of the Microsurface Topography of Fibrillar Collagen. Microsc Microanal 5, 99-105 (1999).

59. Muys, J.J., Alkaisi, M.M. & Evans, J.J. Cellular replication and atomic force microscope imaging using a UV-Bioimprint technique. Nanomedicine 2, 169-176 (2006).

60. Muys, J.J. et al. Cellular transfer and AFM imaging of cancer cells using Bioimprint. Journal of nanobiotechnology 4, 1 (2006).

61. Bruder, J.M., Monu, N.C., Harrison, M.W. & Hoffman-Kim, D. Fabrication of polymeric replicas of cell surfaces with nanoscale resolution. Langmuir 22, 8266-8270 (2006).

62. Bruder, J.M., Lee, A.P. & Hoffman-Kim, D. Biomimetic materials replicating Schwann cell topography enhance neuronal adhesion and neurite alignment in vitro. Journal of biomaterials science 18, 967-982 (2007).

63. Huang, Y.C. & Huang, Y.Y. Biomaterials and strategies for nerve regeneration. Artificial organs 30, 514-522 (2006).

64. Belkas, J.S., Shoichet, M.S. & Midha, R. Peripheral nerve regeneration through guidance tubes. Neurological research 26, 151-160 (2004).

65. Kim, S.M., Lee, S.K. & Lee, J.H. Peripheral nerve regeneration using a three dimensionally cultured schwann cell conduit. The Journal of craniofacial surgery 18, 475-488 (2007).

66. Pfister, L.A., Papaloizos, M., Merkle, H.P. & Gander, B. Nerve conduits and growth factor delivery in peripheral nerve repair. J Peripher Nerv Syst 12, 65-82

(2007).

67. Britland, S. et al. Morphogenetic guidance cues can interact synergistically and hierarchically in steering nerve cell growth. Exp Biol Online 1 (1996).

68. Britland, S. et al. Synergistic and hierarchical adhesive and topographic guidance of BHK cells. Exp Cell Res 228, 313-325 (1996).

69. Guan, K.L. & Rao, Y. Signalling mechanisms mediating neuronal responses to guidance cues. Nature reviews 4, 941-956 (2003).

Chapter 2

Neurite Bridging Across Micropatterned Grooves

Joshua S. Goldner[a], Jan M. Bruder[a], Grace Li, Daniele Gazzola, and Diane Hoffman-Kim

[a]These two authors contributed equally to this work.

The following chapter was published in *Biomaterials* 27:3:460-472 (January 2006).

Abstract

After injury, regenerating axons must navigate complex, three-dimensional (3D) microenvironments. Topographic guidance of neurite outgrowth has been demonstrated in vitro with culture substrates that contain micropatterned features on the nanometer-micron scale. In this study we report the ability of microfabricated biomaterials to support neurite extension across micropatterned grooves with feature sizes on the order of tens of microns, sizes relevant to the design of biomaterials and tissue engineering scaffolds. Neonatal rat dorsal root ganglion (DRG) neurons were cultured on grooved substrates of poly(dimethyl siloxane) coated with poly-l-lysine and laminin. Here we describe an unusual capability of a subpopulation of DRG neurons to extend neurites that spanned across the grooves, with no underlying solid support. Multiple parameters influenced the formation of bridging neurites, with the highest numbers of bridges observed under the following experimental conditions: cell density of 125,000 cells per sample, groove depth of 50 μm, groove width of 30 μm, and plateau width of 200 μm. Bridges were formed as neurites extended from a neuron in a groove, contacted adjacent plateaus, pulled the neuron up to become suspended over the groove, and the soma translocated to the plateau. These studies are of interest to understanding cytoskeletal dynamics and designing biomaterials for 3D axon guidance.

Introduction

Traumatic injury to the spinal cord can result in significant reduction of function and multiple complications in victims of such injuries. After injury, neurons do not spontaneously regenerate their axons, largely due to the inhibitory post-lesion environment that impedes regrowth on multiple levels. Myelin-associated molecules act to block axon growth (1-3) and the formation of an astrocytic glial scar also acts as a barrier for regeneration (4-6). In the past few decades, advances in our comprehension of nerve regeneration have confronted previous beliefs that CNS neurons were inherently incapable of regrowth. In the 1980s Aguayo and colleagues provided injured neurons in the brain and spinal cord with peripheral nerve grafts, and demonstrated that CNS neurons retain the capacity for regrowth when provided with an appropriate, permissive environment (7, 8).

After nerve injury, successful nerve regeneration requires the coordinated presentation of multiple permissive signals, many of which have been incorporated into biomaterial platforms designed to promote regrowth. Candidate axon guidance cues include diffusible factors such as neurotrophins (9), substrate-bound factors such as extracellular matrix and cell adhesion molecules (10), and electrical gradients (11). A number of studies have drawn attention to the fact that interactions with the three-dimensional extracellular microenvironment influence neuronal growth, mediating functions such as adhesion, migration, and neurite extension (12-15). Thus, topography has been added to the list of factors that can influence nerve growth and regeneration.

Cellular abilities to respond to topographical features in their environments have been known for a number of years (16-18). Surface features can direct cellular functions such as activation, orientation, and migration (17). The observation that fibroblasts modulate their orientation and morphology in response to surface topographies gave rise to the principle of contact guidance (19, 20). The term “contact guidance” typically refers to the phenomenon where a cell encounters a geometrical feature (for example, a step) and is both inhibited from crossing over it and polarized along the length axis of the feature. The contact guidance phenomenon has been described in particular in regard to the response of cells to repeating grooved topography over a wide range of feature dimensions (21-31).

Neurite extension both during development and after an injury requires mechanical interactions between growth cone and substrate. Neurons have the capacity to respond to topographical features in their microenvironments, and they have been shown to adhere, migrate, and orient their axons to navigate surface features such as grooves in substrates (23, 32-35). For the past few decades, micropatterned substrates have been used as tools to study and direct neurite outgrowth. Initially, proteins were patterned using simple techniques that allowed the investigation of guidance effects, but lacked reproducibility and precision on the cellular level, at the physiologically relevant micron scale. With the implementation of microlithography adapted from the microelectronics industry (36, 37), topographically patterned features can be transferred to polymers for use as cell culture substrates (22, 38). This versatile technology facilitates the precise and reproducible control of adhesive and topographical substrate features. Subsequently, topographic

guidance of neurite outgrowth has been explored *in vitro* with culture substrates that contain well-defined micropatterned features on the nanometer-micron scale (25, 33, 35, 39, 40).

In this study we employed photolithographic techniques to create poly(dimethyl siloxane) (PDMS) grooved substrates with feature sizes in the range of tens to hundreds of microns. This scale is larger than that previously investigated in the context of directing neurite outgrowth. It is important to examine these features because they are critical for the design of biomaterial scaffolds and porous matrices for neural tissue engineering for spinal cord repair. Postnatal rat dorsal root ganglion (DRG) neurons were cultured on laminin-coated micropatterned substrates, and neurite outgrowth was evaluated after 24 hours in culture. Here we describe an unusual neurite extension phenomenon that to our knowledge has not been reported previously. DRG neurons extended neurites that spanned across grooves of widths up to 200μm. The neurite bridges were as long as 495μm and were characterized by a lack of solid substrate to support the bridge region. Time-lapse microscopy analysis of bridge formation suggests that neurites can adhere to plateaus and pull a neuron into a suspended bridge position. We discuss the implications of these observations both for understanding the fundamental mechanisms of neurite outgrowth and for the design of future biomaterials that can promote directed axon growth.

Materials and Methods

Substrate Production

Pattern Design and Printing

Patterns for photolithography were designed with AutoCAD LT 2004 (Autodesk) and printed on high resolution transparent film at 10,000 dpi (CAD/Art Services, Inc.). At this resolution, features with sizes of 3µm were reliably reproducible.

Photolithography

Standard photolithography techniques were used to pattern substrates. Si wafers (Silicon Sense Inc.) were coated with a layer of negative tone Nano SU-8 50 photoresist (MicroChem) by spin coating with a CEE100 spinner (Brewer Scientific) in a two stage process: 1) spinning at 500rpm for 10sec with a ramp of 100rpm/sec, and 2) spinning at 2000rpm for 30sec with a ramp of 300rpm/sec. Wafers were baked at 65°C for 6min, 95°C for 20min, and slowly cooled to 22°C. Photoresist was polymerized by UV exposure through the pattern film with a Karl Suss mask aligner (MJB3 UV300) at 5.3 mW/cm2 for 1.1 min. Wafers were baked at 65°C for 2min, 95°C for 5min, and slowly cooled. Non-crosslinked photoresist was dissolved with SU-8 Developer (MicroChem), and wafers were rinsed with isopropanol and dried under nitrogen.

Preparation of Poly(dimethyl siloxane) (PDMS) Substrates

Tridecafluoro-1,1,2,2-tetrahydrooctyl-1-trichlorosilane (silane, United Chemical Technology) was deposited under vacuum onto the micropatterned wafers to prevent

adhesion of the photoresist to the PDMS during casting. Sylgard 184 PDMS elastomer base (Dow Corning) was mixed with Sylgard 184 PDMS curing agent at a 10:1 wt/wt ratio, degassed, poured onto a micropatterned wafer to a thickness of 1-2 mm, degassed, cured at 95°C for 45 min, and peeled off the wafers to generate substrates of 1cm x 1cm x 1-2mm for cell culture. Substrates were post-baked at 95°C for 45 min to ensure completion of the curing reaction.

All coating and cell culture reagents were from Invitrogen Life Technologies unless otherwise indicated. PDMS substrates were plasma activated at 10.5 W for 60 sec with a plasma cleaner/sterilizer (PDC – 32 G, Med RF level, Harrick), sterilized by immersion in 70% ethanol, and rinsed with sterile dH2O. Substrates were coated with 100 µg/ml poly-L-lysine (PLL, 70-150 kDa, Sigma) for one hour, rinsed with dH2O, coated with 50 µg/ml mouse laminin in Hanks' Balanced Salt Solution without calcium or magnesium (HBSS-CMF) for one hour, and rinsed with dH2O before plating.

Cell Culture

Cells were cultured as detailed below for each cell type. All cultures were incubated at 37°C and 5% CO2 in a humidified environment. For culture on micropatterned substrates, cells were initially plated at specified densities onto substrates in 100µl of appropriate plating medium. After cells adhered to substrates for 3 h, 3 ml of appropriate culture media were added.

Dorsal Root Ganglion (DRG) Culture

DRG were dissected from the spinal columns of postnatal (P0-P4) rat pups and cleaned of axons, blood, and connective tissue. DRG were incubated in 0.05% trypsin-EDTA in HBSS-CMF at 37˚C for 60 min and dissociated by trituration. Cells were plated at specified densities (see Results and Discussion) onto substrates in serum-containing base medium: Dulbecco's Modified Eagle's Medium (DMEM), 10% fetal bovine serum, 4mM L-glutamine, penicillin (100U/ml)/streptomycin (100µg/ml) and 50ng/ml nerve growth factor (NGF). After cells adhered to substrates, additional serum-containing media was added.

Hippocampal Neuron Culture

Hippocampi from embryonic day 18 (E18) rat pups were dissected on ice in HBSS-CMF, 1% HEPES buffer (1M) and penicillin (100U/mL)/ streptomycin (100µg/ml). Hippocampi were incubated in 0.05% trypsin-EDTA at 37ºC for 15 min and dissociated by trituration. Cells were plated onto micropatterned substrates at 50,000 cells/cm2 in Earle's Modified Eagle's Medium, 1mM pyruvic acid, 0.6% glucose and 10% horse serum. After cells adhered to substrates, neurobasal media with 0.25% Glutamax and 2% B27 supplement was added.

Schwann Cell Culture

Schwann cells were obtained from adult rat sciatic nerve using methods described by Morrissey et al.(41). Briefly, sciatic nerve from an adult rat was harvested and cleaned of epineurium, blood vessels and connective tissue. The sciatic nerve was cut into 1mm2

explant pieces that were cultured in DMEM with 10% FBS on tissue culture plastic dishes. Media was changed every 3 days, and explants were transferred to fresh dishes every 7 days for 6 weeks to allow for fibroblast migration out of the explants. Once fibroblast migration was complete, explants were digested with 0.3% trypsin-EDTA, 0.1% collagenase IV and 0.1% hyaluronidase at 37ºC for 1h, and dissociated by trituration. Dissociated Schwann cells were cultured on dishes coated with 100 ug/mL PLL in DMEM supplemented with 10%FBS, 1% L-glutamine, 2 uM forskolin, 10 ug/mL bovine pituitary extract and penicillin (100U/mL)/ streptomycin (100 ug/ml) (Schwann cell media). Cells at passage 20-25 were cultured on micropatterned substrates at 50,000 cells/cm^2 in Schwann cell media.

B104 Cell Culture

Rat neuroblastoma B104 cells were cultured on micropatterned substrates at 50,000 cells/cm^2 in DMEM with 10% FBS, 4mM L-glutamine, and penicillin (100 U/ml)/streptomycin (100 ug/ml).

Fixing and Immunostaining

Samples were fixed with 1% paraformaldehyde (Sigma), 2% sucrose (CalBiochem), in 0.1 M phosphate buffered saline, pH 7.4 (PBS) for 15 min at room temperature, then rinsed with PBS. Nonspecific staining was blocked by incubating for 1 h at room temperature with 10% goat serum, 1% bovine serum albumin (Sigma), in PBS (blocking buffer) with the addition of 0.1% Triton X-100 (VWR) for permeabilization. Samples were incubated overnight at 4°C with primary antibody diluted in blocking buffer, rinsed

in PBS, incubated for 1 h at room temperature with appropriate Cy3-conjugated secondary antibody (Jackson Laboratories) diluted 1:200 in blocking buffer, rinsed in PBS, and viewed under fluorescence microscopy. Primary antibodes included a polyclonal rabbit antibody directed against laminin (1:500, Biomedical Technologies Inc.), a mouse monoclonal antibody MAB079 directed against S-100 protein (1:200, Chemicon), and a mouse monoclonal antibody RT97 (1:200), that was directed against the phosphorylated epitopes of neurofilament, developed by Dr. John Wood, and obtained from the Developmental Studies Hybridoma Bank (developed under the auspices of NICHD and maintained by the University of Iowa). For controls, samples were processed without incubation with primary antibody.

Analysis

Microscopy

Confocal Microscopy

Samples coated with PLL and laminin were processed for laminin immunocytochemistry as in 2.3, sectioned, and examined under confocal microscopy. Immunostained samples were embedded in Tissue-Tek OCT resin (Sakura Finetek), sections were cut at 30µm thickness with a Leica CM 1510-3 cryostat, and sections were mounted on superfrost microscope slides (VWR) for examination on a spectral confocal microscope (Leica TCS SP2 AOBS). Slides were viewed with a 63x oil immersion lens and z-plane slices of 1.11µm per slice were obtained per section. Stacks of multiple z-planes were assembled using Voxx 2.0 software (University of Indiana).

Phase Contrast and Epifluorescence Microscopy

Samples plated with cells were examined on a Nikon Eclipse TE2000-S microscope, equipped with phase-contrast and epifluorescence optics with appropriate filter cubes. Images were captured using a Hamamatsu Orca-ER camera and Orbit shutter controller (Improvision), outputting to OpenLab v4.0.2 (Improvision) running on Mac OS v10.3.

Scanning Electron Microscopy

For examination under scanning electron microscopy (SEM), samples were fixed in paraformaldehyde as described above, fixed further in Karnovsky's fixative for 3h, rinsed in 0.1M cacodylate buffer, and postfixed in 1% OsO4 in 0.1M cacodylate buffer for 1h. Samples were incubated as follows: dH2O, 1% thiocarbohydrazide in dH2O for 30min, dH2O, 0.5% OsO4 in dH2O for 30min, and graded ethanols to 100% ethanol. After air drying and gold-platinum coating, samples were examined with a Hitachi S-2700 scanning electron microscope using an acceleration voltage of 3kV. Image contrast was corrected to improve visibility of the neurites, using the Adobe Photoshop CS level function.

Quantification and Statistical Analysis

Numbers of bridging cellular extensions were observed under phase-contrast optics at 200x magnification and counted for each sample, with the examiner blinded to the experimental conditions. Bridges were counted in unfixed samples to eliminate the possibility of disruption of bridges by the fixation process. Ten grooves were analyzed

for each sample. These representative areas were selected to be at least 500μm from the sample edges to avoid edge effects of cell plating.

To evaluate the significance of substrate and cell conditions on neurite bridging, one-way analysis of variance was performed for each group (cell density, groove width, and plateau width) in the between-subject design (ANOVA). Post-hoc multiple comparison analysis was done using Tukey's test. SPSS 11.5 software was used, and significance levels were taken to be p=0.05.

Time-lapse Microscopy

For time-lapse microscopy, cells plated on substrates were cultured at 37°C and 5% CO2 in an incubation chamber with a heater and a carbon dioxide enrichment accessory (Solent Scientific). Images were collected with the Nikon microscope and Orca ER camera system described above. Using custom-designed Openlab 4.0.2 automations, images were recorded every 5 min between 3-24 h post-plating. At each time point, 20 focal planes were recorded with 5 μm spacing between planes. Images were analyzed using Volocity 3.1 (Improvision).

Results and Discussion

Micropatterned Substrates

Micropatterned PDMS substrates contained repeating rectangular groove – plateau patterns with varied groove width (w_g), varied plateau width (w_p), and a constant groove

depth (d_g) of 50µm (Fig. 1a-c). Substrates were coated with laminin, an extracellular matrix glycoprotein that is expressed ubiquitously along pathways in the developing nervous system (42), that accelerates regeneration after injury (43-45), and that promotes neurite outgrowth *in vitro* (42). Confocal microscopy confirmed that both groove and plateau regions were coated with laminin (Fig. 1d), and these substrates were used for experiments in order to vary a single feature – surface topography – in the context of a growth-promoting molecular microenvironment.

Bridges Across Micropatterned Grooves

Topographical surface features of substrates can influence nerve function and in particular, show a robust impact on neurite outgrowth. There is a large body of evidence that demonstrates contact guidance of neurites along grooved topographical features at the nanometer - single micron scale. In the present study, we report that accompanying their ability to align to grooves and plateaus, postnatal rat DRG neurons have an additional capacity for a distinctly different response; neurons can extend neurites that form "bridges" spanning from one plateau to an adjacent plateau across relatively wide micropatterned grooves, with w_g on the order of tens of microns.

A "bridge" was defined as a cellular process that crossed a groove to extend between two adjacent plateaus (Fig. 2; Fig. 3a,c,d; Fig. 4). In some cases, cellular processes extended between a groove wall or floor and another groove wall or a plateau (Fig. 3b); however, for the quantification portion of this study, we excluded these types of extensions from being counted as neurite bridges (see below). Bridging extensions were immunopositive

for neurofilament, confirming that they were neurites (Fig. 4). Bridges exhibited diverse morphologies, as demonstrated under both phase-contrast microscopy and SEM. In some cases a bridge was composed of a single neurite (Figs. 2, 3d, 4) or multiple neurites, while in other instances, cell somata as well as neurites were components of the bridge (Fig. 3a). Bridges extended at various angles, with observed lengths up to 495µm.

Conditions for Neurite Bridges

In the present study, DRG neurons exhibited neurite bridges on micropatterned substrates with the following features: d_g of 50µm, w_g of 30-100µm, and w_p of 30-1000µm. Multiple parameters correlated with the numbers of neurite bridges. For the purpose of quantifying numbers of neurite bridges and correlating these numbers with substrate parameters, we applied a narrow definition of "neurite bridge" as a cellular process that extended between two adjacent plateaus and exhibited a morphology of the types shown in Fig. 2b. To facilitate the quantification experiments, we excluded from this counting any bridges that contained suspended somata, since they were more difficult to distinguish as individual bridges.

Cell density significantly influenced the numbers of neurite bridges ($p<0.001$, ANOVA). Minimal bridging was observed at 12,500 cells/cm^2, perhaps because the frequency of cell-cell interactions was too low to permit bridging or because, as the sample with the lowest cell density, it had fewer neurons from which to extend neurite bridges. Numbers of neurite bridges increased as cell concentration increased from 12,500 to 125,000, with highest numbers of neurite bridges observed at 125,000 cells/cm^2 (Fig. 5a). When

normalized to cell concentration, numbers of neurite bridges per cell were highest for 62,500 and 125,000 cells/cm^2. Multiple comparison tests showed that seeding the substrate with 12,500 cells resulted in a significantly different number of neurite bridges from all other cell concentrations tested. Seeding the substrate with 62,500 cells resulted in a significantly different number of neurite bridges than seeding with 12,500 and 125,000 cells. These results are consistent with the notion that at the higher cell concentrations tested, cell-cell interactions within grooves or on plateaus predominate over cell-cell interactions that result in bridging between plateaus.

Groove width also significantly affected neurite bridges ($p < 0.005$, ANOVA). Numbers of neurite bridges were highest at the lowest w_g tested: 30µm (Fig. 5b). Above w_g of 100µm, very few neurite bridges were observed, suggesting that beyond this threshold, the grooves were too wide for neurite bridging to occur at 24h. A few atypical neurite bridges that were loosely attached to two plateaus were seen on substrates with 160 µm grooves and one neurite bridge has been observed spanning a groove of 200 µm. Post hoc multiple comparison tests showed that the number of neurite bridges found on the 30µm grooved substrates differed significantly from those on the 200 µm and 1000 µm grooves, but not significantly from those on the 60 µm, 130 µm, or 160 µm grooves.

Further, we tested the effects of plateau width on neurite bridges, and found that plateau width affected neurite bridges significantly ($p < 0.001$, ANOVA). The optimal w_p was 200 µm, with fewer neurite bridges observed from cells cultured on both narrower and wider plateaus (Fig. 5c). The numbers of neurite bridges on 200 µm plateau and on 1000

μm plateau substrates were significantly different from the numbers of neurite bridges on substrates with narrower (30 μm and 60 μm) plateaus.

A subpopulation of DRG exhibited neurite bridges on the grooved substrates, corresponding to approximately 1-3% of the total cell population. DRG contain multiple cell types, including neurons, fibroblasts, and glial cells. It is likely that the non-neuronal cells produced growth-promoting factors such as trophic factors and extracellular matrix molecules that contributed to the *in vitro* environment that was permissive for neurite extension. In addition, DRG neurons are comprised of several sensory neuron subpopulations that have been identified on the basis of anatomical, cytochemical, trophic, electrophysiological, and functional criteria (46-49). Further studies will be needed to determine which subtype(s) of DRG neurons extend neurite bridges.

Preliminary studies in our laboratory have revealed effects of these topographically micropatterned substrates on process extension from other cell types. Bridging cellular extensions have been observed from cultures of embryonic rat hippocampal neurons (Fig. 6a-c), of adult rat Schwann cells (Fig. 6d-f), and of rat B104 neuroblastoma cells (Fig. 7a-b). It will be interesting in future work to investigate the range of cell types that exhibit the capacity to bridge micropatterned grooves with their cellular extensions.

Bridging and Alignment

In these experiments the majority of DRG extended neurites parallel / aligning to the groove pattern, and a subset of DRG extended neurites perpendicular to / bridging the

groove pattern. In previous studies, aligning and bridging neurites have been observed in response to grooved surfaces patterned at the nanometer – single micron scale. CNS neuroblasts have been reported to migrate and orient their neurites both parallel and perpendicular to the axis of grooves with d_g on the order of 0.5μm and w_g of 1μm (39). No bridging was observed at $w_g > 4$μm. Embryonic rat hippocampal neurites have been shown to grow both parallel to grooves with d_g of 1μm and w_g of 4μm, and perpendicular to grooves with d_g of 130nm and w_g of 1μm (50). The hippocampal neurites extended out of grooves and onto plateaus when d_g was 3.16μm, and neurites were predicted to be unable to extend out of the grooves at $d_g \geq 4.7$μm. The reported abilities of groove depth and groove width to constrain neurite extension out of grooves and onto adjacent plateaus contrast directly with the results of the present study, in which bridging neurites spanned grooves up to 100μm wide and 50μm deep. It is likely that the more narrow plateaus of the previous studies (1-8μm vs. 30-1000μm in the present study) provided a smaller surface area that was also more constraining and less favorable for neurite bridging.

Our observations of decreased bridging and corresponding increased alignment of neurites on substrates with more narrow plateaus agree with the results of Miller et al. (51), in which postnatal rat DRG neurons aligned with 10μm plateaus more strongly than with 20μm plateaus. This phenomenon has been described as a “flow effect” by which more narrow plateaus function to keep neurites aligned with the plateau-groove axis. Neurites in their study were also more likely to prefer laminin-coated grooves than uncoated plateaus, which may explain the lack of bridging neurites in their work, in contrast to the observations of the present study.

Dynamics of Bridge Formation

An unusual and surprising characteristic of the bridges observed in this study was that they had no underlying solid support; they spanned adjacent plateaus immersed in liquid media. Observation of neurons with SEM provided initial insight into a potential mechanism by which the bridges could form. In some instances neurites were observed extending between a cell soma on the floor of a groove and the groove wall (Fig. 7a,b). In the region of the cell where the neurites emerged from the cell soma, part of the soma was lifted off the substrate. We hypothesized that this lifting was an early event in the formation of a bridge, and we carried out studies using time-lapse microscopy in order to characterize the dynamics of bridge formation.

We observed DRG neurons cultured on micropatterned substrates during the period of 3-24 h after plating, and analyzed the formation of 11 bridges. Cultures were highly dynamic, with cell migration and process extension and retraction throughout the time of observation (see movies in Supplemental Data). When a bridge was observed, its presence was preceded by the series of events depicted in Fig. 8a. At time t1, a cell that has adhered to the floor of a groove extends neurites on the groove floor. At t2, the neurites extend partway up the groove walls, then extend higher toward the adjacent plateaus during t3-t4. As the neurites extend higher, the cell body detaches from the groove floor and rises toward the level of the plateaus. At t5, the cell body and neurites are suspended over the groove, bridging across the two adjacent plateaus. The cell body then translocates to one of the adjacent plateaus where it is shown at t6.

Representative images of this process are shown for two cultures in Fig. 8 with views at the focus plane of the plateau (8b-d, 8h-j) and at the focus plane of the groove (8e-g). In the first case (8b-g), at 6h 10min, neurites from a cell on the groove floor extended toward the groove wall with lengths of 17 – 32 µm (arrows in 8e), and the cell was out of focus at the level of the plateau (8b). At 10h 45min, neurites moved toward the top of the plateau while contacting the groove wall, and the soma began to lift off of the groove floor. At this point the soma and neurites were out of focus in both the groove floor and plateau focus planes (arrow heads in 8c and 8f). The neuron slowly rose upward until the soma was suspended by four neurites at the level of the plateau after 23h 40min (arrows in 8d). The lengths of the neurite regions that were suspended over the groove were 34 – 93 µm. The neuron was suspended in media as illustrated by the lack of neurites on the groove floor (8g). The images at these three time points approximate the conditions at t1, t3, and t5 as depicted in Fig. 8a.

In the second case (8h-j), at 11h two neurons and their extended neurites were present on the groove floor and therefore out of focus at the focus plane of the plateau (8h). The neurons rose upwards until they were suspended by three neurites at the level of the plateau after 19h 30min (8i). The lengths of the neurite regions that were suspended over the groove were between 24µm and at least 244µm (the attachment point for the longest neurite was out of the field of view by 19h 30min). The somata then translocated to the right onto the adjacent plateau, as clearly visible at 21h 10min (8j). At this point a neurite extended between the somata on one plateau and the surface of the adjacent plateau, with

a suspended neurite bridge spanning the groove between the two plateaus (neurite out of the field of view of 8j). The images at these three time points approximate the conditions at t2, t5, and t6 as depicted in Fig. 8a.

We hypothesize that bridging occurs when neurons exert forces on each other that can override the effects of substrate features on neurite alignment, as has been suggested previously in studies of the effects of micro-topography on fibroblasts (33). As fibroblasts respond to topography, the actin cytoskeleton has been shown to be important (21); however, in the case of neurite guidance by topographical features, treatment with actin and tubulin inhibitors did not disrupt the neurite preference for grooves. In contrast, calcium influx by voltage-dependent calcium channels and protein kinase C have been suggested to be involved in neurite guidance in response to grooved topography (52). Physical tension has also been shown to influence neurite extension, as demonstrated by Chada et al. (53). Further studies including pharmacological experiments will be needed to elucidate the cytoskeletal mechanisms that underlie the bridging phenomenon observed in the present study.

Conclusions

A major finding of this study is that postnatal rat DRG neurons exhibit complex interactions with micropatterned substrates that contain topographical features of dimensions from tens to hundreds of microns. When cultured on micropatterned substrates, a population of neurons demonstrated a unique growth pattern, with neurites bridging across grooves between adjacent plateaus. The dynamic growth of these neurites

-- pulling a neuron 50 μm above its initial adhesion point to suspend it between grooves in the absence of underlying solid support -- is particularly interesting in the context of understanding the intracellular mechanisms that mediate neurite extension and axon guidance.

Efforts to promote nerve regeneration must consider that axons attempting to regrow after an injury navigate a complex, three-dimensional matrix of molecules and cells. A more rigorous comprehension of how neurons respond to three-dimensional topographical cues is critical as scientists apply microfabrication technologies such as those used in the present study, in efforts to guide axons. Significantly, strategies for axon guidance that employ grooved substrates to align and direct neurons and glial cells must take into account the results demonstrated here: that neurons and glia have the capacity to grow counter to the intended direction of growth. The results from this study can influence the design of future tissue engineering scaffolds that tailor topographical features (i.e. pores) to optimize cell-scaffold interactions, in order to incorporate and sustain cells to support nerve regeneration.

Acknowledgments

The authors thank Michael Angelo Santos and Leigh Needleman for assistance with cell cultures and Pearl Yu for assistance with manuscript preparation. This work was funded by grants from NSF (REU fellowship to J.S.G.) and the Whitaker Foundation.

Figures

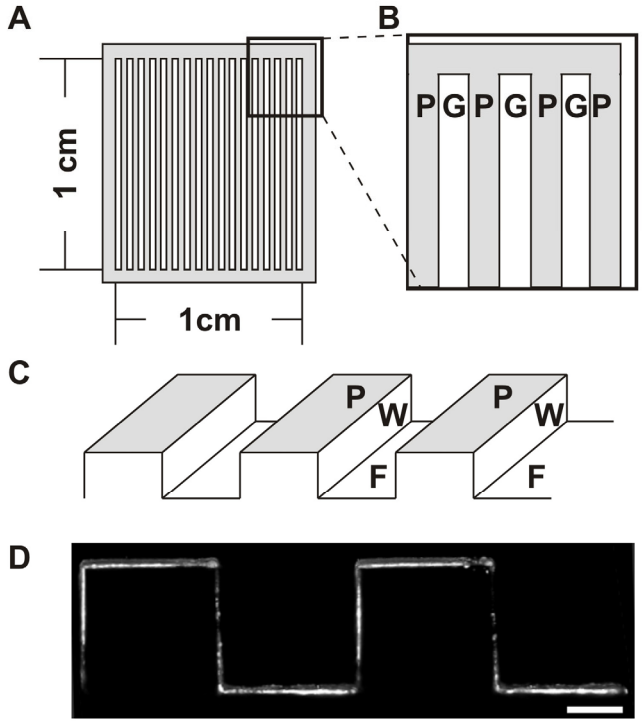

Figure 1. Experimental design

A. Top view cartoon of micropatterned PDMS substrate with repeating groove pattern; overall surface area for cell seeding is $1cm^2$.

B. Close-up top view cartoon of micropatterned PDMS substrate showing alternating topographical features: grooves (white) and plateaus (shaded). Widths of grooves and plateaus were varied in these experiments.

C. Three-dimensional view cartoon of micropatterned PDMS substrate.

D. Confocal z-stack of a 30μm section of micropatterned PDMS with w_g of 60μm and w_p of 60μm. Substrate was coated with PLL and laminin, and stained for anti-laminin immunofluorescence. Twenty-five planes of 1.11μm per plane were combined into a single stack. Scale bar, 25μm.

P, plateau; G, groove; W, groove wall; F, groove floor.

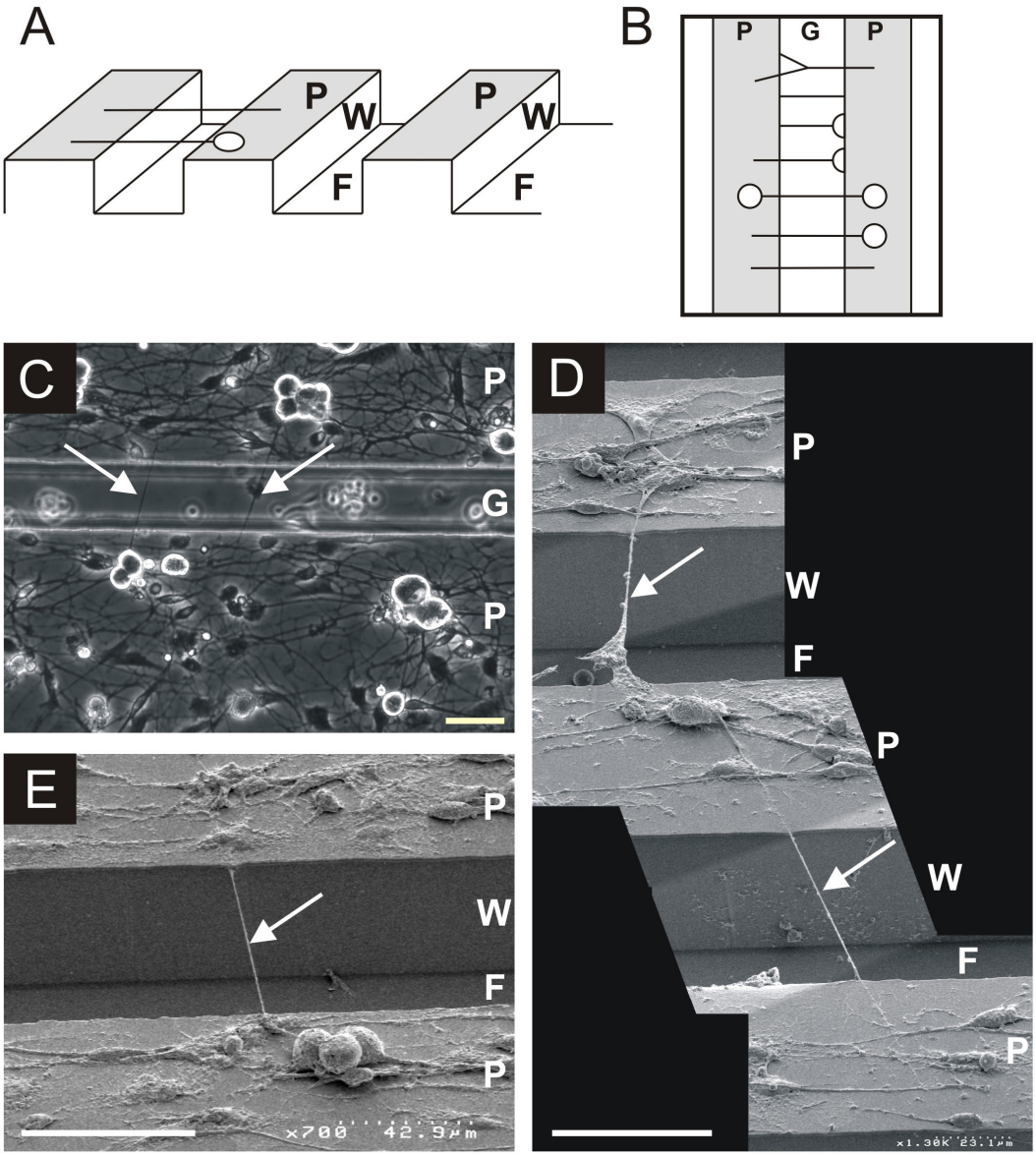

Figure 2. DRG bridges on micropatterned substrates

A. Three-dimensional view cartoon of micropatterned PDMS substrate depicting two typical neurites spanning across the groove on the left. Circles represent somata and lines represent neurites.

B. Top view cartoon of micropatterned PDMS with various configurations of bridging neurites, including those with one, two, or no soma visible on adjacent plateaus, and those with single or branching neurites. Circles represent somata and lines represent neurites.

C. Phase contrast photomicrograph of DRG after 24h culture on laminin-coated, micropatterned PDMS substrate with cell density of 125,000 cells/cm2, wg of 50µm and wp of 1mm. Two bridging

neurites are shown (arrows); each connects between a soma on a plateau and the surface of the respective adjacent plateau, spanning across the groove.

D. Scanning electron micrograph of DRG after 24h culture on laminin-coated, micropatterned PDMS substrate with cell density of 125,000 cells/cm2, wg of 50μm and wp of 70μm. Two bridging neurites are shown (arrows); each connects between a soma on the upper plateau and the surface of the respective adjacent plateau, spanning across the groove. The bridging neurites do not interact with the groove wall or groove floor. The upper bridging neurite was originally attached to its lower plateau at two points; the left attachment region broke during processing. Multiple images were assembled with the Photomerge function in Adobe Photoshop.

E. Scanning electron micrograph of DRG after 24h culture on laminin-coated, micropatterned PDMS substrate with cell density of 125,000 cells/cm2, wg of 50μm and wp of 70μm. A neurite (arrow) bridges between two adjacent plateaus without interacting with the groove wall or groove floor.

P, plateau; G, groove; W, groove wall; F, groove floor. Scale bars, 50μm.

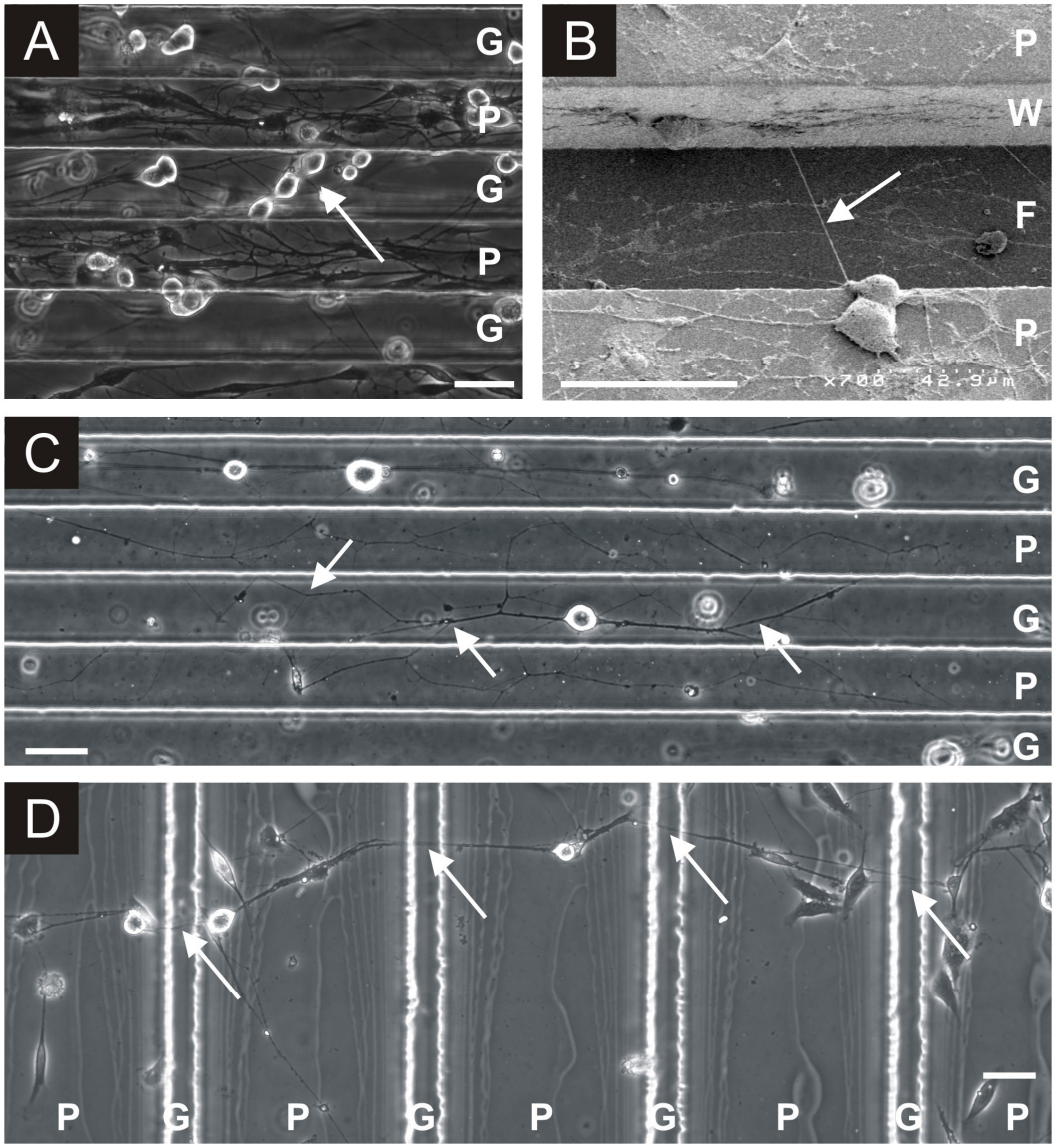

Figure 3. Varied morphologies of DRG on micropatterned substrates

A. Phase contrast photomicrograph of DRG after 24h culture on laminin-coated, micropatterned PDMS substrate with cell density of 125,000 cells/cm^2, w_g of 50µm and w_p of 70µm. An extensive network of neurites, including 3 somata that contact each other (arrow), is visible between two plateaus.

B. Scanning electron micrograph of DRG after 24h culture on laminin-coated, micropatterned PDMS substrate with cell density of 125,000 cells/cm^2, w_g of 50µm and w_p of 70µm. Arrow shows a neurite extending between a cell on the edge of the bottom plateau and a cell at mid-level of the groove wall.

C. Phase contrast photomicrograph of DRG after 24h culture on laminin-coated, micropatterned PDMS substrate with cell density of 12,500 cells/cm^2, w_g of 50μm and w_p of 70μm. Arrows show multiple bridging neurites from a single neuron suspended over a groove.

D. Phase contrast photomicrograph of DRG after 3d culture on laminin-coated, micropatterned PDMS substrate with cell density of 12,500 cells/cm^2, w_g of 30μm and w_p of 200μm. Arrows show neurites bridging across 4 grooves.

P, plateau; G, groove. Scale bars, 50μm.

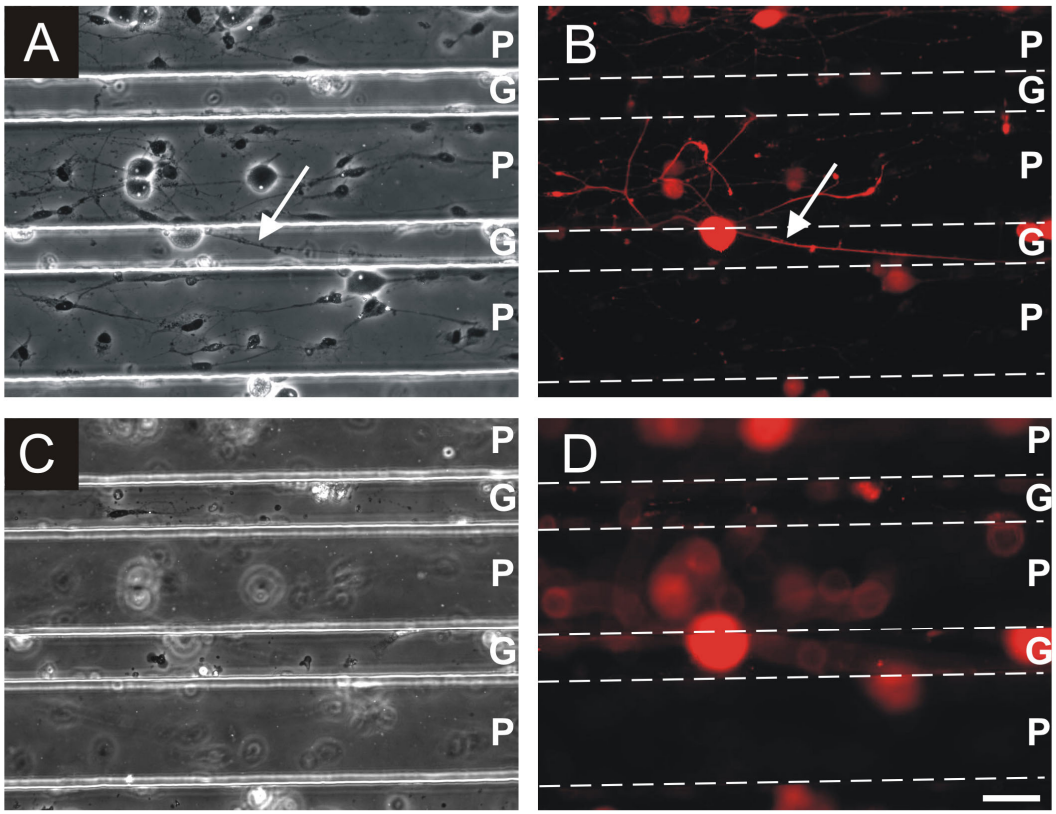

Figure 4. DRG bridges are neurofilament-positive

Phase contrast (A,C) and epifluorescent (B,D) micrographs of DRG after 24h culture on laminin-coated, micropatterned PDMS substrate with cell density of 125,000 cells/cm^2, w_g of 50μm and w_p of 100μm. All four images are of the same portion of the substrate. Immunofluorescent staining for neurofilament (B,D) shows a bridging neurite (arrow) visible in the plane of focus of the plateau (A,B), with no visible neurites in the plane of focus of the groove (C,D). The bridging neurite connects between a soma on one plateau and the ridge of the adjacent plateau, spanning across one groove. Dashed lines were added over the position of the groove walls in epifluorescent images to indicate the micropatterned features. P, plateau; G, groove. Scale bar, 50μm.

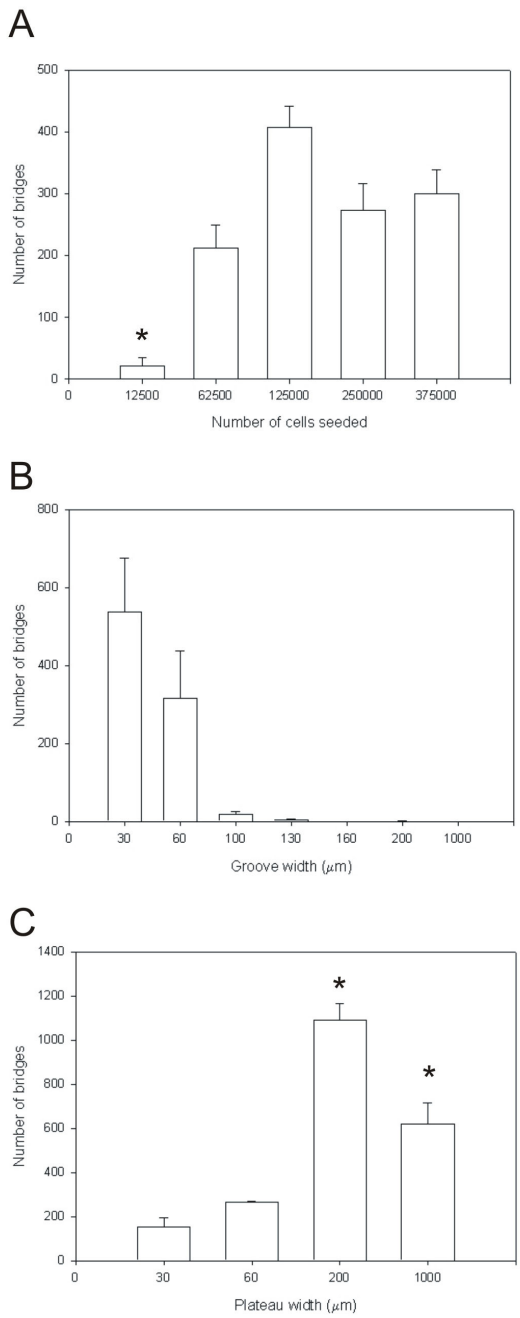

Figure 5. Bar graphs quantifying bridging.

A. Number of neurite bridges as a function of cell density
Mean number of neurite bridges per ten grooves[+] is shown for 5 cell densities tested. Substrate dimensions were d_g of 50μm, w_g of 50μm and w_p of 70μm. The asterisk denotes the number of cells seeded that resulted in a significantly different number of neurite bridges when compared to

all other cell densities tested. Seeding 125,000 cells resulted in the highest number of neurite bridges. (n=3; Error bars are SEM.)

[+]The mean number of neurite bridges in ten grooves for 375,000 cells was calculated from three samples. For one of these three, a projected value of neurite bridges in ten grooves was used, since only six grooves could be counted due to an optical obstruction of a section of the PDMS substrate.

B. Number of neurite bridges as a function of groove width
Mean number of neurite bridges per ten grooves on substrates with varying groove widths. Experimental conditions were cell density of 125,000 cells per sample, d_g of 50µm, and w_p of 100µm. Grooves of 30µm width resulted in significantly different numbers of neurite bridges than substrates with 200µm and 1000µm widths. (n=4 for w_g=30, 60; n=3 for w_g=200, 1000; n=2 for w_g=100, 130, 160; Error bars are SEM.)

C. Number of neurite bridges as a function of plateau width
Mean number of neurite bridges per ten grooves on substrates with varying plateau widths. Experimental conditions were cell density of 125,000 cells per sample, d_g of 50µm, and w_g of 50µm. Asterisks indicate the plateau widths that showed significantly different numbers of neurite bridges with respect to all other plateau widths tested. Highest number of neurite bridges was observed on substrates with plateau widths of 200µm. (n=3; Error bars are SEM.)

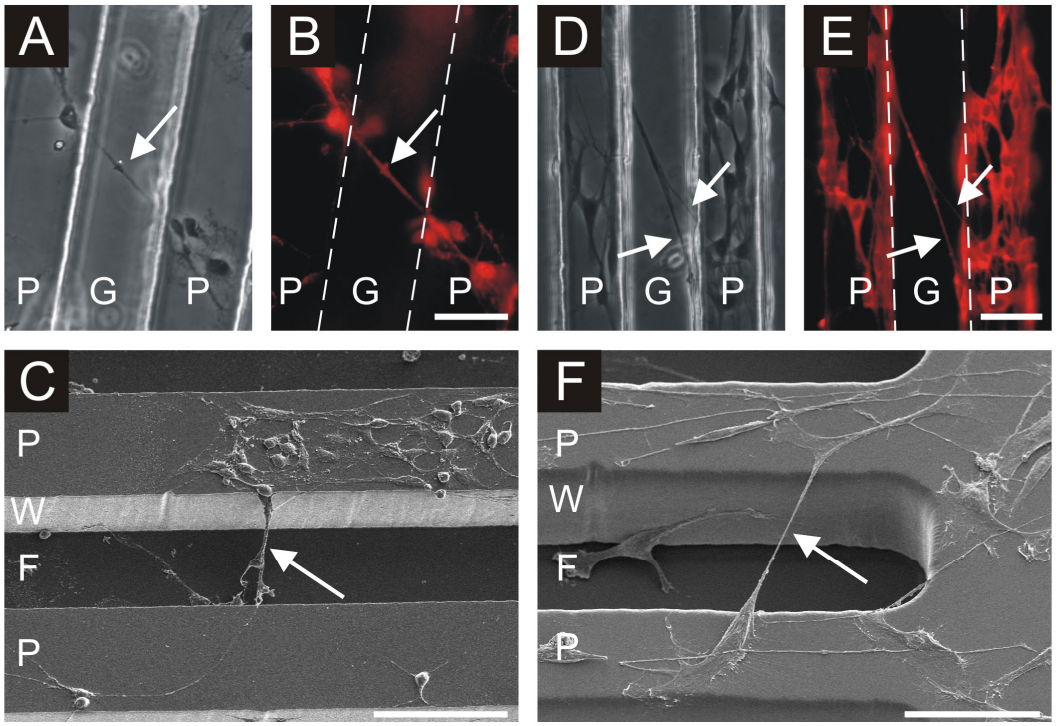

Figure 6. Hippocampal neurons and Schwann cells extend bridges on micropatterned substrates

A-B. Phase contrast (A) and corresponding epifluorescent (B) photomicrographs of hippocampal neurons after 72h culture on PLL-coated, micropatterned PDMS substrate with cell density of 50,000 cells/cm^2, w_g of 60μm and w_p of 60μm. Immunofluorescent staining for neurofilament shows a bridge that spans across the groove to connect two somata on adjacent plateaus. Dashed lines were added over the position of the groove walls in epifluorescent images to indicate the micropatterned features. Scale bar, 50μm.

C. Scanning electron micrograph of hippocampal neurons after 72h culture on PLL-coated, micropatterned PDMS substrate with cell density of 50,000 cells/cm^2, w_g of 60μm and w_p of 60μm. Arrow shows a bridge that connects between a soma on the top plateau and a soma on the lower plateau (lower left corner of image). Scale bar, 66.7μm.

D-E. Phase contrast (D) and epifluorescent (E) photomicrographs of Schwann cells after 24h culture on PLL-coated, micropatterned PDMS substrate with cell density of 50,000 cells/cm^2, w_g of 60μm and w_p of 60μm. Immunofluorescent staining for S100 protein shows Schwann cell processes (arrows) that connect between cells on the left plateau and cells on the right plateau, spanning across the groove in the form of a single process over the left groove region and two distinct processes over the right groove region. Dashed lines were added over the position of the groove walls in epifluorescent images to indicate the micropatterned features. Scale bar, 50μm.

F. Scanning electron micrograph of Schwann cell culture after 24h culture on PLL-coated, micropatterned PDMS substrate with cell density of 50,000 cells/cm^2, w_g of 60μm and w_p of 60μm. Arrow shows a bridge spanning across a groove to connect cellular regions on adjacent plateaus. Scale bar, 60μm.

(P) plateau; (W) groove wall; (F) groove floor.

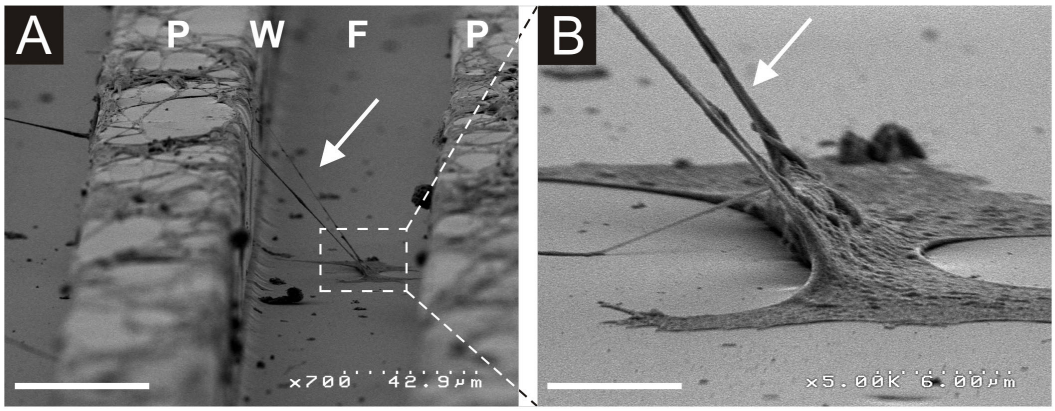

Figure 7. Neuroblastoma bridges

A-B. Scanning electron micrographs of B104 rat neuroblastoma cells after 24h culture on PLL-coated, micropatterned PDMS substrate with cell density of 50,000 cells/cm2, wg of 60µm and wp of 60µm. A. Arrow shows two neurites connecting a cell on the groove floor to the top edge of the groove wall. Scale bar, 42.9µm. B. Close-up view of cell in panel A, showing two neurites directed upwards with part of the soma rising off the groove floor, and one smaller neurite directed downwards and adhering to the groove floor. Scale bar, 6µm.

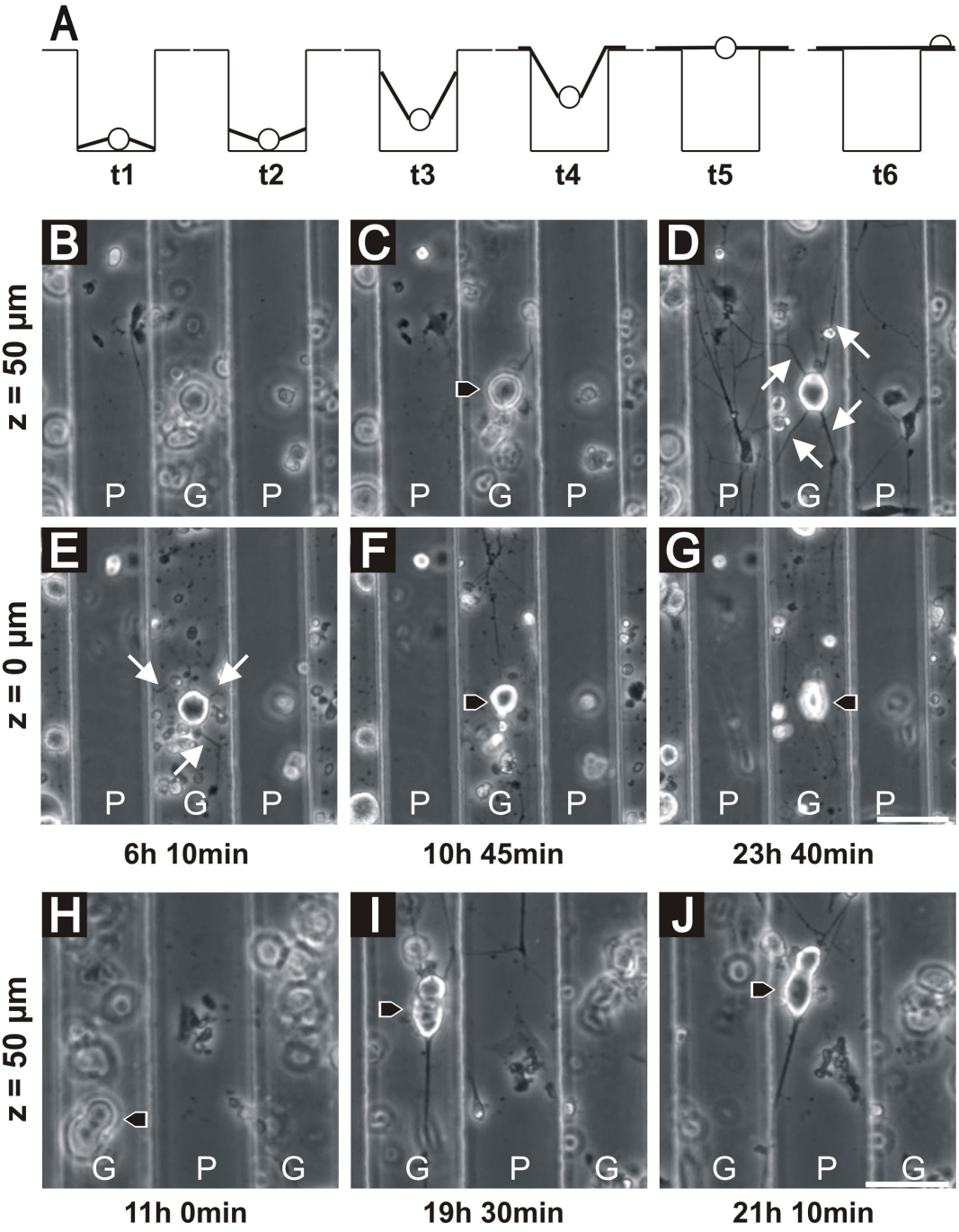

Figure 8. Dynamics of bridge formation

A. Cartoon depicts representative cell growth on a micropatterned substrate over time. The substrate is shown from the side, looking down the length of a groove at a cell extending processes. From time t1 to time t5, the processes extend up the groove walls to the plateau surfaces, and the cell body moves from its initial position, adhered to the groove floor, to become

suspended over the groove, with processes bridging between adjacent plateaus. From time t5 to time t6, the cell body moves laterally to adhere to the adjacent plateau.

B-J. Phase contrast micrographs obtained by time-lapse microscopy showing the dynamics of bridge formation from DRG cultured on laminin-coated, micropatterned PDMS substrate with cell density of 100,000 cells/cm2, wg of 60µm and wp of 60µm. The events underlying bridge formation from two distinct neurons are shown (B-G and H-J).
For the first neuron, micrographs of a single substrate region of 207µm width by 207µm length are shown at the planes of focus of the plateau (B-D; z=50µm) and of the groove floor (E-G; z=0µm), at three time points during 6-24h after plating. Note that at 6 h 10 min the soma and neurites were in focus on the groove floor (E) but not at the level of the plateau (B). This time point corresponds to t1 (A). At 10 h 45 min, the soma and neurites were visible but out of focus when viewed at the plateau level (C) and at the floor level (F), corresponding to t3 (A). At 23 h 40 min, the soma and neurites were in focus at the plateau (D) and not at the groove (G), corresponding to t5 (A).
For the second neuron, micrographs of a single substrate region of 207µm width by 207µm length are shown at the plane of focus of the plateau (H-J; z=50µm), at three time points during 11-22h after plating. Note that at 11h the soma and neurite were on the groove floor and therefore out of focus at the level of the plateau (H), corresponding to t2 (A). At 19h 30min, the soma and neurite were in focus over the groove, at the plane of focus of the plateau (I), corresponding to t5 (A). By 21h 10min, the soma and neurite were visible and in focus on the plateau (J), corresponding to t6(A).
White arrows, neurites; black arrowheads, somata; P, plateau; G, groove. Scale bars, 50µm.

Supplemental Data

Figures S1 and S2 contain two movies of sequential phase contrast micrographs obtained by timelapse microscopy showing the dynamics of bridge formation from DRG cultured on laminin coated, micropatterned PDMS substrate with cell density of 100,000 cells/cm^2, w_g of 60µm and w_p of 60µm. Movies of a single substrate region of 225µm width by 229µm length are shown at the planes of focus of the groove floor (S1) and of the plateau (S2) over 248 time points, five minutes apart, starting 3 hours after plating. The frame rate of the movie is 6 frames/sec, corresponding to 30 minutes of elapsed real time per second of movie. The neuron of interest is the neuron present in Fig. 8b-g.

Figure S1 shows the neuron of interest on the groove floor, at the center of the field of view, surrounded by smaller cells and cellular material from the dissection. As the time elapsed, the neuron of interest extended neurites along the groove floor, contacting the groove walls and a second neuron (outside of this field of view). The portions of the neurites closest to the groove walls were the first cellular regions to leave the focal plane, followed by the soma (starting around 19s).

Figure S2 shows the neuron of interest at the plane of focus of the plateau. Initially this neuron was out of focus below the field of view (but in focus on the groove floor as seen in S1). Three cells were initially visible on the plateaus. At 15s, neurites from the groove extended onto the plateau to the left, contacting the cells already present. At 21s, neurites from the groove extended onto the plateau to the right. Between 25 and 30s, distal

portions of neurite close to the groove walls came into focus, followed by proximal neurite portions and soma (32s).

References

1. Schwab ME, Thoenen H. Dissociated neurons regenerate into sciatic but not optic nerve explants in culture irrespective of neurotrophic factors. Journal of Neuroscience 1985;5(9):2415-23.

2. Caroni P, Schwab ME. Two membrane protein fractions from rat central myelin with inhibitory properties for neurite growth and fibroblast spreading. J Cell Biol 1988;106(4):1281-8.

3. Schwab ME, Kapfhammer JP, Bandtlow CE. Inhibotors of neurite outgrowth. Annu Rev Neurosci 1993;16:565-595.

4. McKeon RJ, Schreiber RC, Rudge JS, Silver J. Reduction of neurite outgrowth in a model of glial scarring following CNS injury is correlated with the expression of inhibitory molecules on reactive astrocytes. Journal of Neuroscience 1991;11(11):3398-411.

5. Fawcett JW, Asher RA. The glial scar and central nervous system repair. Brain Res Bull 1999;49(6):377-91.

6. Reier PJ, Houle JD. The glial scar: its bearing on axonal elongation and transplantation approaches to CNS repair. Adv Neurol 1988;47:87-138.

7. Aguayo AJ, David S, Bray GM. Influences of the glial environment on the elongation of axons after injury: transplantation studies in adult rodents. J Exp Biol 1981;95:231-240.

8. Bray GM, Vidal-Sanz M, Aguayo AJ. Regeneration of axons from the central nervous system of adult rats. Prog Brain Res 1987;71:373-9.

9. Richardson PM. Neurotrophic factors in regeneration. Curr Opin Neurobiol 1991;1(3):401-406.

10. Hynes RO, Lander AD. Contact and adhesive specificities in the associations, migrations, and targeting of cells and axons. Cell 1992;68(2):303-322.

11. McCaig CD, Rajnicek AM. Electrical fields, nerve growth and nerve regeneration. Exp Physiol 1991;76:473-494.

12. Newgreen DF. Physical influences on neural crest migration in avian embryos: contact guidance and spatial restriction. Dev Biol 1989;131:136-148.

13. Nagata I, Nakatsuji N. Rodent CNS neuroblasts exhibit both perpendicular and parallel contact guidance on the aligned parallel neurite bundle. Development 1991;112:581-590.

14. Ebendal T, Jacobson CO. Tissue explants affecting extension and orientation of axons in cultured chick embryo ganglia. Exp Cell Res 1977;105(2):379-87.

15. Lofberg J, Ebendal T. Substrate topography and shape of motile cells. Experientia 1980;36(5):508-10.

16. Ito Y. Surface micropatterning to regulate cell functions. Biomaterials 1999;20:2333-2342.

17. Curtis A, Wilkinson C. Topographical control of cells. Biomaterials 1997;18:1573-1583.

18. Curtis ASG, Varde M. Control of cell behavior: topographical factors. J Natl Cancer Res Inst 1964;33:15-26.

19. Dunn GA, Heath JP. A new hypothesis of contact guidance in tissue cells. Exp Cell Res 1976;101:1-14.

20. Ohara PT, Buck RC. Contact guidance in vitro. A light, transmission, and scanning electron microscopic study. Exp Cell Res 1979;121:235-249.

21. Wojciak-Stothard B, Curtis ASG, Monaghan W, McGrath M, Sommer I, Wilkinson CDW. Role of the cytoskeleton in the reaction of fibroblasts to multiple grooved substrata. Cell Motil Cytoskeleton 1995;31:147-158.

22. Flemming RG, Murphy CJ, Abrams GA, Goodman SL, Nealy PF. Effects of synthetic micro- and nano-structured surfaces on cell behavior. Biomaterials 1999;20:573-588.

23. Clark P, Connolly P, Curtis ASG, Dow JAT, Wilkinson CDW. Topographical control of cell behaviour I. Simple step cues. Development 1987;99:439-448.

24. Bruinink A, Wintermantel E. Grooves affect primary bone marrow but not osteoblastic MC3T3-E1 cell cultures. Biomaterials 2001;22:2465-2473.

25. Clark P, Connolly P, Curtis ASG, Dow JAT, Wilkinson CDW. Cell guidance by ultrafine topography in vitro. J Cell Sci 1991;99:73-77.

26. Wojciak-Stothard B, Madeja Z, Korohoda W, Curtis A, Wilkinson C. Activation of macrophage-like cells by multiple grooved substrata. Topographical control of cell behaviour. Cell Biol Int 1995;19(485).

27. Webster TJ, Ergun C, Doremus RH, Siegel RW, Bizios R. Enhanced osteoclast-like cell functions on nanophase ceramics. Biomaterials 2001;22:1327-1333.

28. Eisenbarth E, Meyle J, Nachtigall W, Breme J. Influence of the surface structure of titanium materials on the adhesion of fibroblasts. Biomaterials 1996;17:1399-1403.

29. Eriksson C, Lausmaa J, Nygren H. Interactions between human whole blood and modified Ti-O2-surfaces: influence of surface topography and oxide thickness on leukocyte adhesion and activation. Biomaterials 2001;22:1987-1996.

30. Dalby MJ, Kayser MV, Bonfield W, Di Silvio L. Initial interaction of osteoblasts to an optimised HAPEXTM topography. Biomaterials 2002;23:681-690.

31. Curtis ASG, Casey B, Gallagher JO, Pasqui D, Wood MA, Wilkinson CDW. Substratum nanotopgraphy and the adhesion of biological cells. Are symmetry or regularity of nanotopography important? Biophys Chem 2001;94:275-283.

32. Miller CA, Shanks H, Witt A, Rutkowski G, Mallapragada SK. Oriented schwann cell growth on micropatterned biodegradable polymer substrates. Biomaterials 2001;22:1263-1269.

33. Clark P, Connolly P, Curtis ASG, Dow JAT, Wilkinson CDW. Topographical control of cell behaviour: II. multiple grooved substrata. Development 1990;108:635-644.

34. Brunette DM. Fibroblasts on micromachined substrata orient hierarchically to grooves of different dimensions. Exp Cell Res 1986;164:11.

35. Hirono T, Torimitsu K, Kawana A, Fukuda J. Recognition of artificial microstructures by sensory nerve fibers in culture. Brain Res 1988;446:189-194.

36. Folch A, Toner M. Microengineering of cellular interactions. Annu Rev Biomed Eng 2000;2:227-56.

37. Connolly P. Bioelectronic interfacing: micro- and nanofabrication techniques for generating predetermined molecular arrays. Trends Biotechnol 1994;12(4):123-7.

38. Wilkinson CDW, Curtis ASG, Crossan J. Nanofabrication in cellular engineering. J Vac Sci Technol B 1998;16:3132-3136.

39. Nagata I, Kawana A, Nakatsuji N. Perpendicular contact guidance of CNS neuroblasts on artificial microstructures. Development 1993;117:401-408.

40. Rajnicek A, Britland S, McCaig C. Contact guidance of CNS neurites on grooved quartz: influence of groove dimensions, neuronal age and cell type. J Cell Sci 1997;110 (Pt 23):2905-13.

41. Morrissey TK, Kleitman N, Bunge RP. Isolation and functional characterization of Schwann cells derived from adult peripheral nerve. Journal of Neuroscience 1991;11(8):2433-2442.

42. Luckenbill-Edds L. Laminin and the mechanism of neuronal outgrowth. Brain Res Brain Res Rev 1997;23(1-2):1-27.

43. Madison RD, da Silva C, Dikkes P, Sidman RL, Chiu TH. Peripheral nerve regeneration with entubulation repair: comparison of biodegradeable nerve guides versus polyethylene tubes and the effects of a laminin-containing gel. Exp Neurol 1987;95(2):378-90.

44. Martini R. Expression and functional roles of neural cell surface molecules and extracellular matrix components during development and regeneration of peripheral nerves. J Neurocytol 1994;23(1):1-28.

45. Grimpe B, Dong S, Doller C, Temple K, Malouf AT, Silver J. The critical role of basement membrane-independent laminin gamma 1 chain during axon regeneration in the CNS. J Neurosci 2002;22(8):3144-60.

46. Perl ER. Function of dorsal root ganglion neurons: an overview. New York: Oxford UP; 1992.

47. McMahon S, Armanini M, Ling L, Phillips H. Expression and coexpression of Trk receptors in subpopulations of adult primary sensory neurons projecting to identified peripheral targets. Neuron 1994;12:1161-1171.

48. Gilabert R, McNaugthon P. Enrichment of the fraction of nociceptive neurons in cultures of primary sensory neurons. J Neurosci Methods 1997;71:191-198.

49. Baudet C, Mikarls A, Westphal H, Johansen J, Johansen T, Ernfors P. Positive and negative interactions of GDNF, NTN, ART in developing sensory neuron subpopulations, and their collaboration with neurotrophin. Development 2000;127:4335-4344.

50. Rajnicek AM, Britland S, McCaig CD. Contact guidance of CNS neurites on grooved quartz: influence of groove dimensions, neuronal age and cell type. J Cell Sci 1997;110:2905-2913.

51. Miller C, Jeftinija S, Mallapragada S. Synergistic effects of physical and chemical guidance cues on neurite alignment and outgrowth on biodegradable polymer substrates. Tissue Engineering 2002;8(3):367-378.

52. Rajnicek AM, McCaig CD. Guidance of CNS growth cones by substratum grooves and ridges: effects of inhibitors of the cytoskeleton, calcium channels and signal transduction pathways. J Cell Sci 1997;110:2915-2924.

53. Chada S, Lamoureux P, Buxbaum RE, Heidemann SR. Cytomechanics of neurite outgrowth from chick brain neurons. J Cell Sci 1997;110:1179-1186.

Chapter 3

Fabrication of Polymeric Replicas of Cell Surfaces with Nanoscale Resolution

Jan M. Bruder, Nicholas C. Monu, Michael W. Harrison, and Diane Hoffman-Kim

The following chapter was published in *Langmuir* 22 (20), 8266 -8270, 2006.

Abstract

We report an approach for fabricating biomimetic surface replicas of cells with nanoscale resolution. Fixed cells serve as a template for a two-stage replica molding process. Cast from the template, the impression replica contains a reproduction of cellular topographical features indented into its surface, and cast from the impression replica, the relief replica contains a copy of these features protruding from its surface. Various polymers and cells can be utilized, and scanning electron microscopy, atomic force microscopy, and white light interferometry analyses confirm replication of nanoscale features. These replicas are useful for investigating cellular function and for biomimetic tissue engineering.

Introduction

Advances in tissue engineering, prosthetics, and regenerative medicine require the development of biomaterials that promote specific cellular responses[1]. Current research is directed toward generating substrates and scaffolds that influence cell adhesion, growth, and organization[2-5]. For example, cells may be recruited to an implanted material in order to improve its physical integration into a surgical site[6], to improve its biocompatibility, as for the patency of a vascular graft [7], or to attract and direct other cell types, as for nerve regeneration[8, 9].

Cells normally reside and interact in local environments with distinct and organized micro- and nano-topography, provided in part by the cells that surround them. Cells respond to topographical features[10, 11], and these features can influence many important cellular functions[11-14]. Previous studies suggest that material substrates with nanometer- and micron-scale surface features can increase cell adhesion, migration, and process extension, as compared to substrates with smooth surfaces[4, 15-17].

Therefore, topography has been incorporated into material surfaces with the goal of tailoring cell function. Earlier studies have utilized substrates with surface features that contain either regular, ordered topography, i.e. repeating grooved features [18, 19], or disordered, random topography[7, 20, 21]. In some cases, substrates have been developed to replicate the geometry of components of the extracellular matrix [22-25]. Substrates have typically included either features that are on the order of tens of microns in size, i.e. the size of a cell, or features that are sub-micron in size, i.e. the size of cellular features such

as cellular processes. However, none of these materials that aim to tailor cell function has replicated the complex mixture of micro- and nanotopography that cells encounter *in vivo*, in which the local cellular environment is much richer in its mixture of sizes, shapes, and organization.

In this work we employed cultured cells as templates to impart the morphology of the cells to a material substrate. A variety of methods have been used in previous studies to incorporate topographical features into materials, including conventional "top-down" techniques such as photo- and scanning beam lithography, as well as "bottom-up" techniques such as nanoimprint lithography, step-and-flash lithography, replica molding, and solvent-assisted micromolding[26]. A recent study reported the transfer of features from unfixed cells to poly(dimethylsiloxane) for the purpose of imaging and analysis[27]. Here we report a replica molding approach using fixed cells and elastomeric polymers that is more reproducible and versatile in its applicability to multiple cell types and materials. This approach is novel in its generation of two distinct and corresponding impression and relief replicas that incorporate the external morphology of the cell templates and that can be employed to investigate the growth and differentiation of cells *in vitro* and *in vivo*.

Materials and Methods

Microcontact Printing

Poly (dimethyl siloxane) (PDMS, Dow Corning) stamps with repeating grooves and plateaus were fabricated as described by Goldner et al.[19] The pattern was designed in

AutoCAD LT 2004 (Autodesk), printed at 10,000 dpi onto a mylar mask, and transferred via photolithography onto a Si wafer spin-coated with a 50µm layer of negative tone Nano SU-8 50 photoresist (Microtech). The resulting micropatterned wafer contained repeating grooves with 60µm groove width, 60µm plateau width, and 50µm groove depth. Sylgard 184 PDMS elastomer base was mixed with Sylgard 184 PDMS curing agent (10:1 wt/wt), degassed, poured onto the micropatterned wafer to a thickness of 1-2 mm, cured at 95°C for 1h, and removed to produce stamps of 1cm x 1cm x 1-2mm for microcontact printing (µCP).

All coating and cell culture reagents were from Invitrogen Life Technologies unless otherwise indicated. Stamps were submerged in 10% sodium dodecyl sulfate (Sigma) in dH_20, rinsed in dH_20, and incubated with 50µg/ml mouse laminin (LN) in Hanks' balanced salt solution without calcium or magnesium (HBSS-CMF) for 1h. Glass coverslips were plasma activated with a plasma cleaner/sterilizer (PDC – 32 G, Med RF level, Harrick), and incubated in contact with stamps overnight.

Cell Culture

Schwann cells (SC) were obtained from adult rat sciatic nerves using a modification of the method of Morrissey et al.[19, 27] Dissociated SC were cultured on tissue culture plastic dishes coated with 100µg/mL poly-L-lysine (PLL) in Dulbecco's Modified Eagle's Medium (DMEM) with 10% Fetal Bovine Serum (FBS), 4mM L-glutamine, 100U/ml penicillin, and 100µg/ml streptomycin (base media) supplemented with 2µM forskolin and 10µg/mL bovine pituitary extract (SC media). In later experiments SC were obtained

via a generous gift of Dr. Mary Bunge (University of Miami). Cultures of aligned SC were prepared by a modification of the technique of Thompson and Buettner[29]. SC were cultured on LN-micropatterned coverslips at 30,000 cells/ml in SC media for 3-7 days to reach the desired level of cell density.

Embryonic rat aortic smooth muscle cells (SMC) were obtained from American Type Culture Collection (CRL-1444). SMC were cultured on flasks coated with 100µg/ml PLL in base medium supplemented with 4mM L-glutamine at 37°C and 5% CO_2. SMC were rinsed with HBSS-CMF, treated with 0.25% trypsin-EDTA for 10 minutes to detach cells, resuspended in media, and plated on glass slides coated with 100µg/ml PLL.

DRG were obtained from the spinal columns of postnatal (P0-P4) rat pups according to Goldner et al.[19]. Cells were cultured in base medium with 50ng/ml nerve growth factor.

Cell cultures were fixed with 2% paraformaldehyde (Sigma), 4% sucrose (CalBiochem), in 0.1M phosphate buffered saline pH 7.4 (PBS) for 15 min at room temperature, and rinsed with PBS. Immunocytochemistry was performed according to Goldner et al.[19] using the primary mouse monoclonal antibody RT97 directed against the phosphorylated epitopes of neurofilament (developed by Dr. John Wood and obtained from the Developmental Studies Hybridoma Bank), and a Cy3-conjugated goat anti-mouse secondary antibody (Jackson Laboratories).

Substrate Preparation

Reagents for cell template preparation were from Electron Microscopy Sciences. For preparation of the cell template, samples were incubated in Karnovsky's fixative

overnight, rinsed with 0.1M cacodylate buffer, incubated in 1% OsO_4 in 0.1M cacodylate buffer for 1h, rinsed with dH_2O, incubated in 1% thiocarbohydrazide in dH_2O for 30min, incubated in 0.5% OsO_4 in dH_2O for 30min, dehydrated with graded ethanols to 100% ethanol, air-dried, and sputter-coated with gold-palladium. For replica molding with PDMS, Sylgard 184 elastomer base was mixed with Sylgard 184 curing agent (10:1 wt/wt) and applied to the template to form a layer of 1-3mm thickness. The solution was heated to 95ºC for 1h, and the resulting polymer film was removed. For replica molding with polyurethane (PU), a 7.5% weight/volume solution of PC-3585A Carbothane (Thermedics Polymer Products) in chloroform (Sigma) was heated to 65ºC until clear, and entrapped air bubbles were removed by bath-sonication. The polymer mixture was applied to the template to form a layer of 1-1.5mm thickness. Following solvent evaporation, the resulting polymer film was removed. The fixed cells were used as a template to generate the impression replica, and the impression replica was used without any additional processing as a template to generate the relief replica.

Analysis

Substrates were examined with a Hitachi S-2700 scanning electron microscope using an acceleration voltage of 8kV; with a Zygo New View 6000 3D profiler to generate white light interferometry (WIM) profiles of the surface features; and with a DI 3100 atomic force microscope (AFM, Veeco Instruments) with a silicon tip (100nm diameter; resonant frequency of 378 kHz; Mikro Masch) used in tapping mode with a scan rate of 1Hz.

Results and Discussion

Here we describe the generation of biomimetic polymer materials with surfaces that contain replicas of cellular topography. Two distinct types of materials were produced: the impression replica contained indented topographical features and the relief replica contained protruding topographical features. Because of our laboratory's interest in axon guidance and nerve regeneration, pre-aligned Schwann cells were used as the source of cellular topography for the initial experiments, in order to mimic the organization of Schwann cells that promote regeneration after nerve injury. However, there is no limit to the type of cell that can be employed.

The impression replica was prepared in a four-stage process, and the relief replica was prepared in a five-stage process, requiring one additional step beyond the preparation of the impression replica. As depicted in Figure 1, the stages included (1) Photolithographic production of a polymeric stamp for micro-contact printing (μCP); (2) μCP of a micropatterned laminin-striped glass coverslip; (3) Cell culture to generate a cell template containing fixed, aligned SC; (4) Fabrication of the impression replica with indented topographical features; and (5) Fabrication of the relief replica with protruding topographical features. The first three stages of the fabrication process were performed to align the SC; when using other cell types for applications where alignment is not desired, the cell template can be prepared simply by fixing the cultured cells (see below). Use of a strong fixation procedure, similar to that required for SEM, preserved the cell morphology and allowed the cells to act as a template. To generate the impression replica, which contains a replica of cellular topographical features indented into its

surface, a solution containing the desired polymer was applied to the fixed cell sample. Once the solution had polymerized or phase separated, the impression replica was removed. A similar procedure was used to generate the relief replica, which contains a replica of cellular topographical features protruding from its surface. A solution containing the desired polymer was applied to the patterned surface of the impression replica, thus using the impression replica as a template. Once the solution had polymerized or phase separated, the relief replica was removed. Of note, the cell template, the impression replica and the relief replica could all be re-used as templates for subsequent experiments.

Examination of corresponding regions of the cell template (Figure 2A-C), the impression replica (Figure 2D-F), and the relief replica (Figure 2G-I) under SEM demonstrated that multiple features could be replicated from the cell template, including: cell organization and alignment (Figure 2A, D, G), cell morphology (Figure 2A-I), and sub-cellular features (Figure 2C, F, I). At 1800x magnification (Figure 2C, F, I), the detailed morphological features of somata and cell extensions were visible and reproduced clearly in both replicas. Inherent to the replica process, the impression replica contains features that are mirrored with respect to both the cell template and the relief replica, since the impression replica was cast from the cell template and subsequently functioned as the template for the relief replica.

Polymeric materials with surface replicas of nanoscale features can be achieved with this technique. Comparison of surface features between corresponding regions of the cell

template (Figure 3A-C), the impression replica (Figure 3D-F), and the relief replica (Figure 3G-I) with WIM analysis confirmed that feature geometry and dimensions were reproduced by the replica processing. The shapes, lengths, widths, and heights (or depths for the impression replica) of the cell somata were reproduced with this fabrication method, as measured and shown in the WIM oblique images (Figure 3A, D, G) and overhead images (Figure 3B, E, H). Shapes and x- and z-dimensions of cell extensions were replicated accurately to within 5-10 nm, as demonstrated by the corresponding surface profiles (Figure 3C, F, I) measured along the lines overlaid on the top views of Figures 3B, E, and H. The corresponding surface profiles are presented on a single graph for closer examination of feature replication in Supplemental Materials.

Various polymers can be employed using this approach to generate a wide range of material properties. For example, SC cell templates containing cellular processes of approximately 100nm in width were replicated in polyurethane (PU) (Figure 4A,B). Polymers that are useful for this technique are flowable in the liquid phase, capable of conversion to a rubbery or gelled solid upon curing or phase separation, detachable from a cell template, and capable of maintaining the cell-templated dimensions and geometry upon detachment from the cell template.

There is no limit to the type of cell whose topographical features can be replicated with this technique. In addition to SC, smooth muscle cells have served as cell templates (Figure 4C), with their features replicated in the impression replica (Figure 4D) and the relief replica (Figure 4E). In general, adherent cells can be utilized with the procedure

described here, and cells that are cultured in suspension require just one additional step of immobilization on a solid material in order to function as a template. Future exploration of the use of critical point drying in conjunction with this technique may further enhance the preservation of cellular features in the generation of the initial cell template.

The materials generated with this technique are biocompatible and support the growth of cells. DRG neurons grew on LN-coated PDMS impression replicas and extended neurites that aligned along features that replicated SC topography (Figure 5).

Previous studies have shown that cells react to microscale and nanoscale surface features, where the features are either geometrically patterned or randomly ordered[4, 30, 31]. The availability of two distinct types of surface replicas with indented cellular features - the impression replica, and protruding cellular features - the relief replica, paves the way for a systematic investigation into the effects of cellular topography on cellular functions such as adhesion, orientation, activation, extension, and migration.

Conclusion

We have developed transparent, topographically biomimetic replicas of mammalian cellular surfaces containing combinations of micron-scale and nanoscale features. With the incorporation of cellular topography onto surfaces, the roles of biomaterials can be expanded from providing simple mechanical support to providing critical cues for the study of cellular function. By combining materials that are biomimetic in cellular

topography with technologies to modify bulk material properties, surface chemistry, and controlled release of diffusible factors, tailored biomaterial systems can be developed toward the ultimate goal of directing cells to form functional tissues.

Acknowledgements

The authors thank Caitlin Elgarten and Vivian Fong for assistance with cell cultures and substrate production, Elke Bremus-Koebberling and Almut Kuhnen for initial WIM studies, Vinay Gill and Julie Waters for assistance with the WIM and AFM, and Tayhas Palmore and Dan Jay for helpful discussion of the manuscript. This work was funded by a grant from The Whitaker Foundation and a Seed Funding Award from Brown University.

Figures

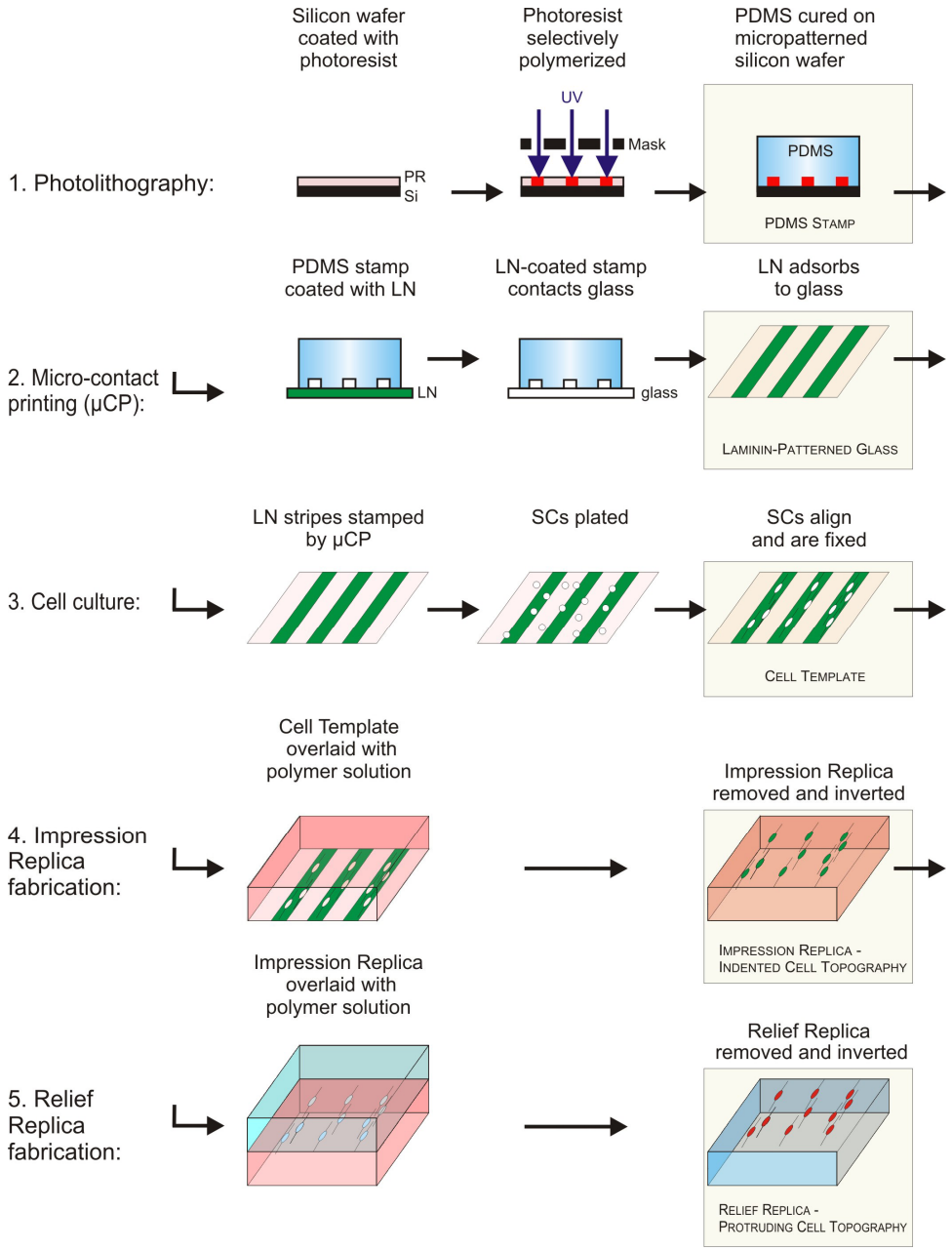

Figure 1. Overview of the technique, highlighting the 5 main steps:

(1) Production of a polymeric stamp for μCP; (2) μCP of laminin stripes onto glass coverslips; (3) Cell culture; (4) Fabrication of the impression replica with indented topographical features; and (5) Fabrication of the relief replica with protruding topographical features. Technique can begin with step 4 using fixed cells, if no alignment of cells is desired.

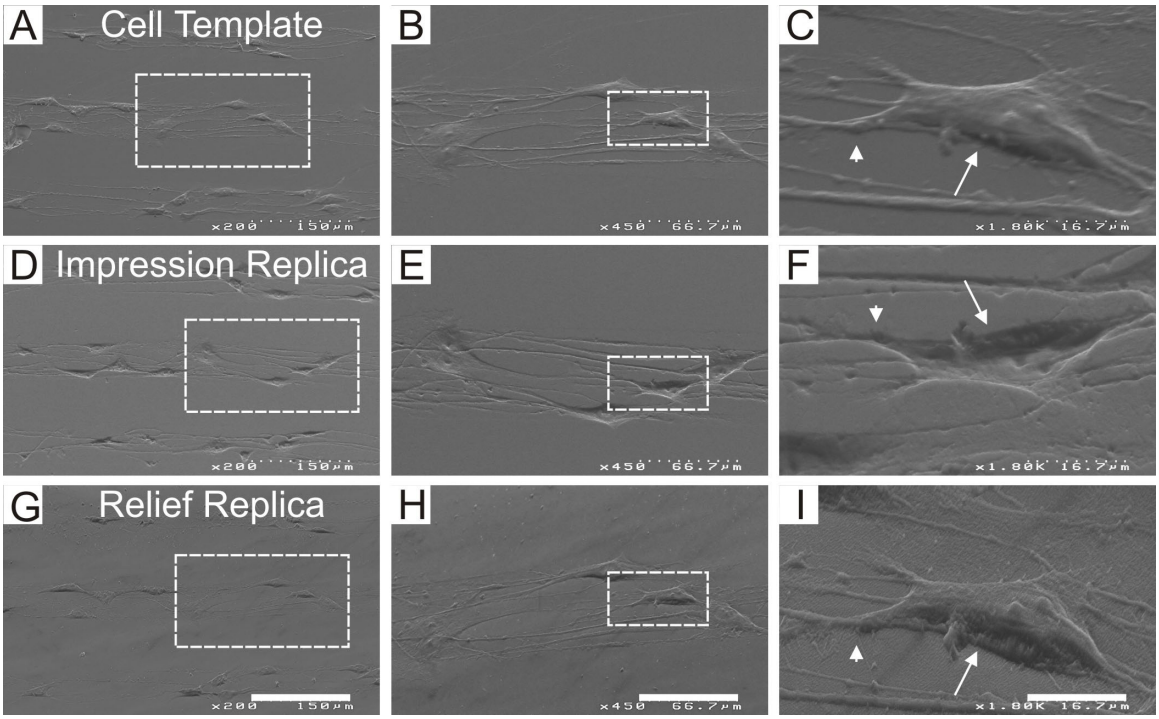

Figure 2. Biomimetic materials replicate cellular features, as visible under SEM.

SC were cultured at 30,000 cells/ml on stripes of LN for 24h, fixed, and used as cellular templates to prepare the impression replica and the relief replica from PDMS. Corresponding regions of the impression replica and the relief replica show replication of cellular topographical features in the original template. SEM micrographs of SC template (A-C), the impression replica (D-F), and the relief replica (G-I). Rectangle outlines the borders of the region that is magnified in the image to the right. Note that inherent to the process, features in the impression replica are inverted relative to those of the template and the relief replica. Arrows, cell somata; arrowheads, cellular extensions. Scale bars, 2G = 150μm, 2H = 66.7μm, 2I = 16.7μm.

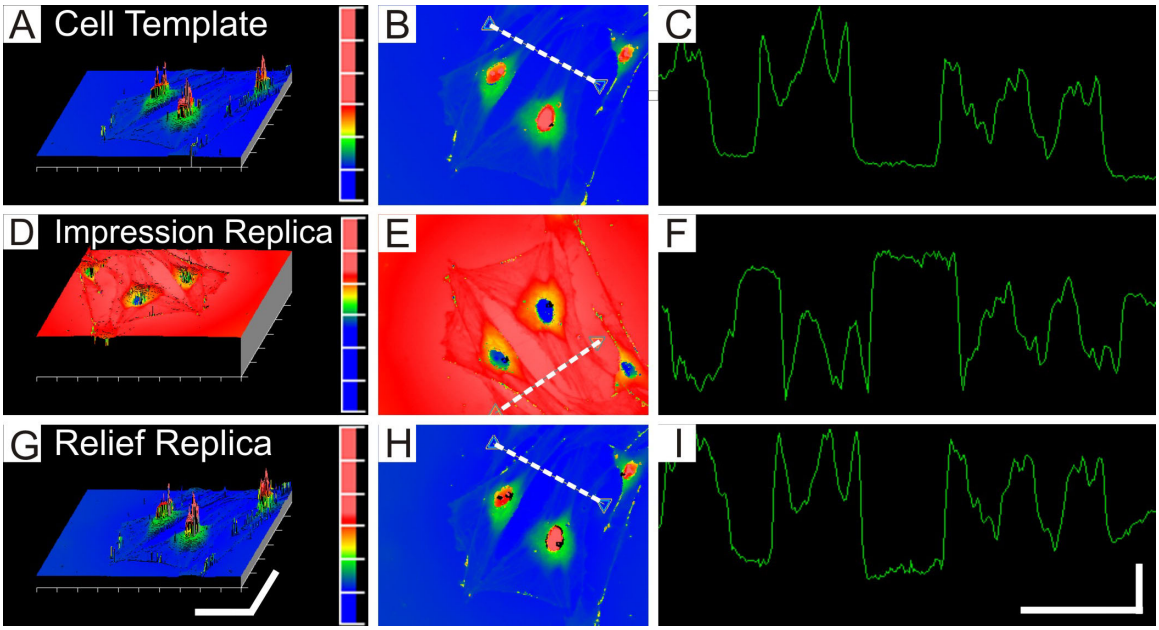

Figure 3. Biomimetic materials replicate cellular features, as quantified by WIM.

SC were cultured at 30,000 cells/ml on stripes of LN for 24h, fixed, and used as cellular templates to prepare the impression replica and the relief replica from PDMS. Corresponding regions of the impression replica (D-F) and the relief replica (G-I) replicate the sizes and shapes of cellular topographical features in the original template (A-C). Oblique images (A, D, G) provide a three-dimensional view of cellular topographical features on each substrate; corresponding overhead images (B, E, H) provide a top view of each surface; and corresponding surface profile plots (C, F, I) provide measurements of a cross-section along the line superimposed on each overhead image. Note that inherent to the process, features in the impression replica are inverted relative to those of the template and the relief replica. Color bars in A, D, and G show pseudocolor scales where the range of each entire color bar represents a z-axis difference of 2.25μm (A), 2.55μm (D), and 2.03μm (G). Scale bars in G: x-axis = 50μm, y-axis = 70μm; scale bars in I: x-axis = 20μm, z-axis = 20nm.

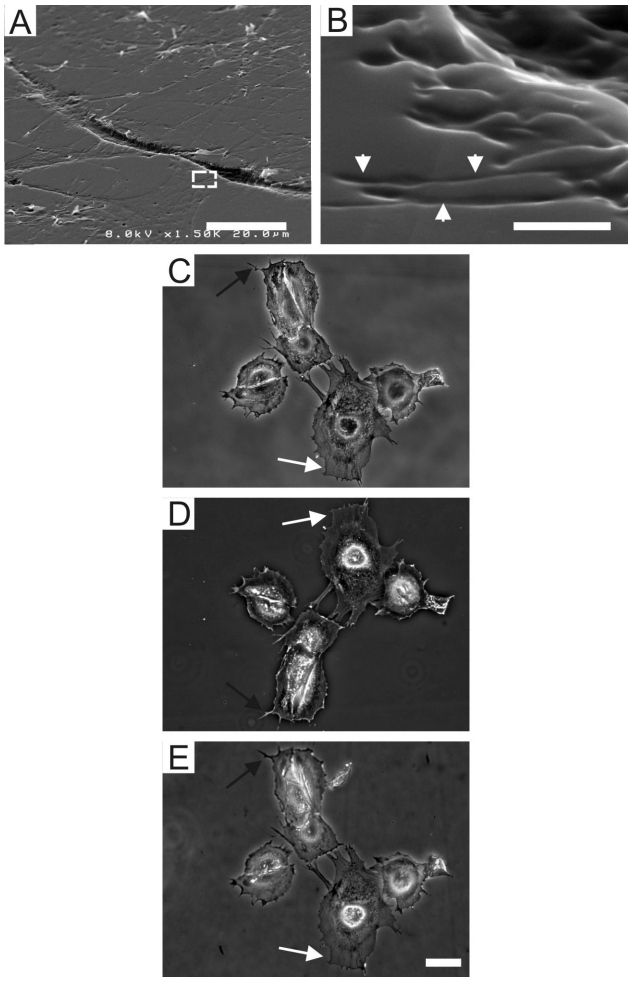

Figure 4. Various polymers and cell types can be utilized.

A, B. SC were cultured at 30,000 cells/ml on stripes of LN for 24h, fixed, and used as cellular templates to prepare the impression replica from PU. SEM micrographs of the impression replica film of PU containing indented topographical features of aligned SC. This region corresponds to cellular extensions (white arrowheads). Rectangle in A outlines the region that is magnified in B, in which nanoscale features are visible. C-E. SMC were cultured at 30,000 cells/ml on PLL-coated coverslips for 24h, fixed, and used as cellular templates to prepare impression and relief replicas from PDMS. Phase-contrast micrographs of corresponding regions of the impression replica (D), and the relief replica (E) show replication of cellular features in the original SMC template (C). Note that inherent to the process, features in the impression replica are inverted relative to those of the template and the relief replica. Arrows, lamellipodia; black arrowheads, filopodia. Scale bars, 4A = 20μm, 4B = 1μm, 4E = 50μm.

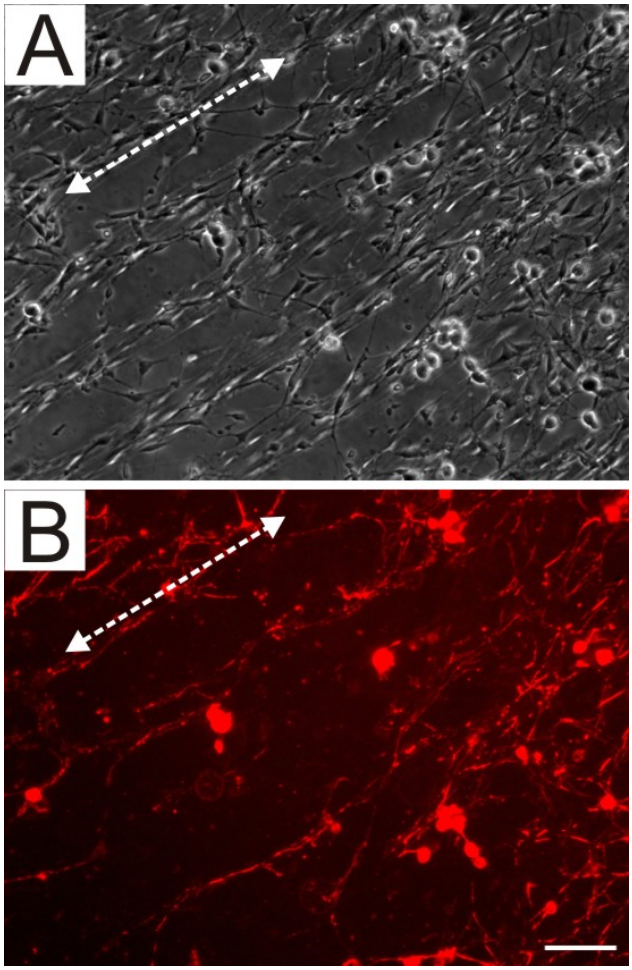

Figure 5. DRG neurons extend neurites on impression replica of SC.

SC were cultured at 30,000 cells/ml on stripes of LN for 3 days, fixed, and used as cellular templates to prepare the impression replica from PDMS. Dissociated DRG neurons were cultured on LN-coated impression replica for 3d and stained for anti-neurofilament immunocytochemistry. In the phase contrast micrograph (A), both the patterned replica and the neurons are visible, whereas in the corresponding fluorescence micrograph (B), only the neurites are labeled. Dotted arrows indicate the direction of the cellular pattern indented in the replica surface. Many neurites are aligned to the pattern. Scale bar, 100μm.

Supporting Information Available

Two supplemental figures containing (1) superimposed surface profile plots of a corresponding cell template, impression replica, and relief replica; and (2) AFM images of the surfaces of a cell template, an impression replica, and a relief replica. *This material is available free of charge via the Internet at http://pubs.acs.org.*

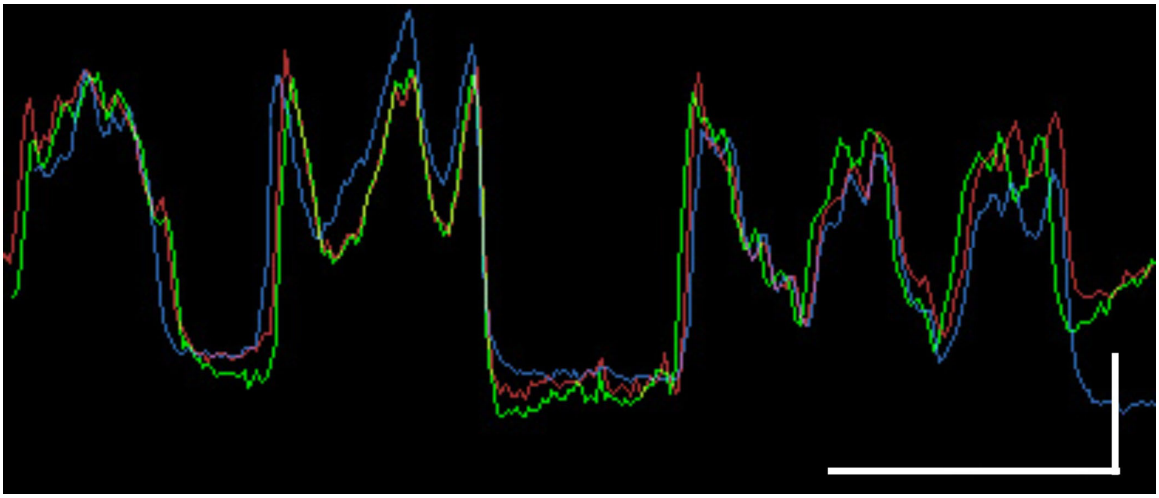

Supplemental Figure 1. Biomimetic materials replicate cellular features, as quantified by WIM.

SC were cultured at 30,000 cells/ml on stripes of LN for 24h, fixed, and used as cellular templates to prepare the impression replica and the relief replica from PDMS. Surface profile plots of corresponding regions of the template (blue), impression replica (red), and relief replica (green) demonstrate that each replica contains features of the same sizes and shapes as the cellular topographical features in the original template. To overlay multiple surface profiles, the original images from the Zygo Profiler were opened in Adobe Photoshop CS and stacked, with the line graph of the impression replica mirrored to match the orientation of the line graphs of the template and relief replica. Scale bars: x-axis = 20μm, y-axis = 20nm.

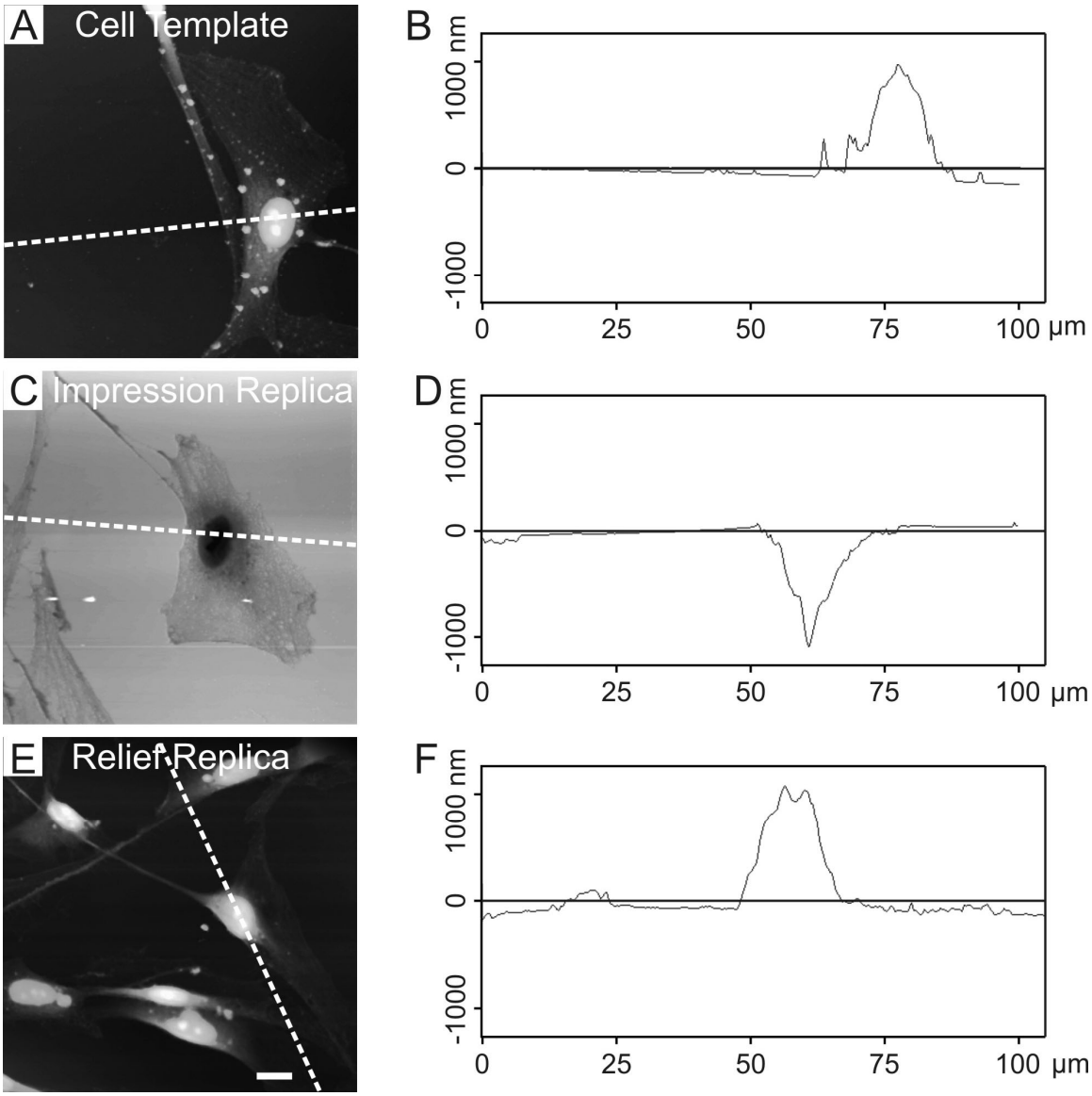

Supplemental Figure 2. Biomimetic materials replicate cellular features, as analyzed by atomic force microscopy (AFM)

AFM scans (A, C, E) and surface profile plots (B, D, F) along the dotted lines of a cell template (A, B), an impression replica (C, D), and a relief replica (E, F) illustrate reproduction of cellular morphology of SC, including the nuclear, peri-nuclear, and peripheral regions. The respective regions of the template and replicas are distinct and non-matching, and each was generated from SC cultured at 30,000 cells/ml on stripes of LN for 24h. AFM scan of the cell template following >15 uses as a template demonstrates good preservation of cellular features through multiple cycles of replication. Scale bar: 10µm.

References

(1) Langer, R.; Vacanti, J. P. *Science* 1993, 260, 5110, 920-6.

(2) Berry, C. C.; Dalby, M. J.; McCloy, D.; Affrossman, S. *Biomaterials* 2005, 26, 24, 4985-4992.

(3) Yu, X.; Dillon, G. P.; Bellamkonda, R. V. *Tissue Engineering* 1999, 5, 4, 291-304.

(4) Thapa, A.; Miller, D. C.; Webster, T. J.; Haberstroh, K. M. *Biomaterials* 2003, 24, 17, 2915-26.

(5) Shin, M.; Matsuda, K.; Ishii, O.; Terai, H.; Kaazempur-Mofrad, M.; Borenstein, J.; Detmar, M.; Vacanti, J. P. *Biomedical Microdevices* 2004, 6, 4, 269-278.

(6) Chehroudi, B.; McDonnell, D.; Brunette, D. M. *J Biomed Mater Res* 1997, 34, 3, 279-90.

(7) Miller, D. C.; Thapa, A.; Haberstroh, K. M.; Webster, T. J. *Biomaterials* 2004, 25, 1, 53-61.

(8) Yu, T. T.; Shoichet Molly, S. *Biomaterials* 2005, 26, 13, 1507-14.

(9) Belkas, J. S.; Munro, C. A.; Shoichet, M. S.; Midha, R. *Restorative Neurology and Neuroscience* 2005, 23, 1, 19-29.

(10) Ito, Y. *Biomaterials* 1999, 20, 23-24, 2333-42.

(11) Curtis, A.; Wilkinson, C. *Biomaterials* 1997, 18, 24, 1573-83.

(12) Johansson, F.; Carlberg, P.; Danielsen, N.; Montelius, L.; Kanje, M. *Biomaterials* 2006, 27, 8, 1251-8.

(13) Clark, P.; Connolly, P.; Curtis, A. S. G.; Dow, J. A. T.; Wilkinson, C. D. W. *J Cell Sci* 1991, 99, 73-77.

(14) Miller, C. A.; Shanks, H.; Witt, A.; Rutkowski, G.; Mallapragada, S. K. *Biomaterials* 2001, 22, 1263-1269.

(15) Yim, E. K. F.; Leong, K. W. *Nanomedicine* 2005, 1, 1, 10-21.

(16) Uttayarat, P.; Toworfe, G. K.; Dietrich, F.; Lelkes, P. I.; Composto, R. J. *J Biomed Mater Res A* 2005.

(17) Yim, E. K.; Reano, R. M.; Pang, S. W.; Yee, A. F.; Chen, C. S.; Leong, K. W. *Biomaterials* 2005, 26, 26, 5405-13.

(18) Clark, P.; Connolly, P.; Curtis, A. S. G.; Dow, J. A. T.; Wilkinson, C. D. W. *Development* 1990, 108, 635-644.

(19) Goldner, J. S.; Bruder, J. M.; Li, G.; Gazzola, D.; Hoffman-Kim, D. *Biomaterials* 2006, 27, 3, 460-72.

(20) Anselme, K.; Noel, B.; Hardouin, P. *Journal of Materials Science: Materials in Medicine* 1999, 10, 12, 815-819.

(21) Savaiano, J. K.; Webster, T. J. *Biomaterials* 2004, 25, 7-8, 1205-13.

(22) Goodman, S. L.; Sims, P. A.; Albrecht, R. M. *Biomaterials* 1996, 17, 21, 2087-95.

(23) Sims, P. A.; Albrecht, R. M. *Microscopy And Microanalysis* 1999, 5, 2, 99-105.

(24) Gadegaard, N.; Mosler, S.; Larsen, N. B. *Macromolecular Materials and Engineering* 2003, 288, 76.

(25) Flemming, R. G.; Murphy, C. J.; Abrams, G. A.; Goodman, S. L.; Nealy, P. F. *Biomaterials* 1999, 20, 573-588.

(26) Gates, B. D.; Xu, Q.; Stewart, M.; Ryan, D.; Willson, C. G.; Whitesides, G. M. *Chemical Reviews (Washington, DC, United States)* 2005, 105, 4, 1171-1196.

(27) Muys, J.; Alkaisi, M.; Melville, D.; Nagase, J.; Sykes, P.; Parguez, G.; Evans, J. *J Nanobiotechnology* 2006, 4, 1.

(28) Morrissey, T. K.; Kleitman, N.; Bunge, R. P. *J Neurosci* 1991, 11, 8, 2433-42.

(29) Thompson, D. M.; Buettner, H. M. *Ann Biomed Eng* 2004, 32, 8, 1120-30.

(30) Desai, T. A. *Med Eng Phys* 2000, 22, 9, 595-606.

(31) Dalby, M. J.; Pasqui, D.; Affrossman, S. *IEE Proc Nanobiotechnol* 2004, 151, 2, 53-61.

Chapter 4

Biomimetic Materials Replicating Schwann Cell Topography Enhance Neuronal Adhesion and Neurite Alignment In Vitro

Jan M. Bruder, Andrea Lee, and Diane Hoffman-Kim PhD

The following chapter was published in *Journal of Biomaterials Science, Polymer Edition* 18 (8), 967-982, 2007.

Abstract

It is well established that Schwann cells (SCs) promote and enhance axon guidance and nerve regeneration by providing multiple cues, including extracellular matrix, cell surface molecules, neurotrophic factors, and cellular topography. Which of the elements of the complex environment associated with SCs provides the essential information for directed nerve growth is unclear, because until now, it has been impossible to investigate their contributions individually. Our development of biomimetic materials that replicate the micro- and nanoscale topography of SCs has allowed us to investigate for the first time the role of cellular topography in directing nerve growth. Dorsal root ganglion (DRG) neurons were cultured on flat poly(dimethyl siloxane) (PDMS) and on PDMS replicas with protruding SC topography. Image analysis showed that more neurons adhered to the replicas than to the flat substrates, and that neurite growth on the replicas followed the underlying SC pattern. Neuronal alignment was dependent on cell density. Live SCs derived from the DRG also grew along the replica SC pattern. These results suggest that the combination of micro- and nanoscale topographical cues provided by SCs can influence nerve growth, and point toward design parameters for future nerve guidance channels.

Introduction

Successful nerve regeneration requires directed nerve growth. When peripheral nerve regeneration is achieved *in vivo*, it is largely due to the endogenous growth-promoting environment provided by Schwann cells (SCs) that includes extracellular matrix molecules that function as permissive substrates, cell adhesion molecules that promote adhesion and growth of axons, and neurotrophic factors that attract and support axons.[1],[2]; for review, [3] The ability of SCs to promote nerve regeneration in the peripheral nervous system (PNS) has been exploited to stimulate regeneration of nerves in the central nervous system (CNS) when SCs are transplanted to the site of injury.[4]

In addition to the rich molecular environment provided by SCs, the directional influence of SC orientation in the post-injury environment has been demonstrated to play an important role in promoting axon growth. After injury, SCs in the PNS align longitudinally in columns to promote the regrowth of injured axons.[5] Transplantation of oriented SCs leads to enhanced peripheral nerve regeneration with axonal alignment parallel to the SCs.[6] Thompson and Buettner recently demonstrated neurite alignment to SC monolayers that were oriented longitudinally without presenting other directional cues.[7] Studies showing neurite growth along aligned SCs incorporated into materials such as fibronectin[8], collagen[9], and micropatterned polymers[10], [11] have also suggested important roles for SC physical orientation and topography in guiding axons.

In the study of axon guidance, some cues, such as diffusible factors, are easily isolated and have been systematically altered and presented to neurons in culture. Other factors,

including the topography introduced by SCs and presented to neurons in co-culture, are difficult to introduce without inherently changing a multitude of biochemical variables that SCs contribute. Until now, the difficulty in reproducing the complex shapes of cells without including a mixture of molecular components has left the influence of cellular topography largely unexplored. We have recently developed transparent, biocompatible polymeric substrates with biomimetic, cell-shaped surfaces that have nanoscale resolution of topographical features.[12] As a result, the contribution of cellular topography as an independent factor in co-cultures, and in particular, the role of SC topography in axon guidance can be studied for the first time.

In this study, we evaluated the response of postnatal rat dorsal root ganglion (DRG) neurons to biomimetic PDMS substrates whose surfaces contained protruding features of aligned SCs. Here we show that biomimetic substrates with SC topography enhanced neuronal adhesion and alignment, that neurites aligned strongly in the direction of the SC topographical features, and that the alignment was cell density-dependent.

Materials and Methods

Cell Culture

Cell culture reagents were from Invitrogen Life Technologies (Carlsbad, CA) unless otherwise indicated. Cultures were incubated at 37 degrees C with 5% CO_2 in a humidified environment. SCs from rat sciatic nerve, a generous gift of Dr. Mary Bunge (University of Miami, FL), were cultured on tissue culture plastic dishes coated with 100

μg/mL poly-L-lysine (PLL; Sigma, St. Louis, MO) in Dulbecco's modified eagle's medium (DMEM) with 10% fetal bovine serum (FBS), 4 mM L-glutamine, 100 U/ml penicillin, and 100 μg/ml streptomycin (base media) supplemented with 2 μM forskolin (Sigma), 10 μg/ml bovine pituitary extract (Sigma), and 2 μM heregulin (generous gift from Genentech) (SC media).

Dorsal root ganglia (DRG) were dissected from the spinal columns of postnatal (P0-P5) rat pups and cleaned of axons, blood, and connective tissue. DRG were incubated in 0.05% trypsin-EDTA in Hanks' Balanced Salt Solution without calcium or magnesium at 37 degrees C for 60 min and dissociated by trituration. Cells were plated at varying densities onto substrates in base media with 50 ng/ml nerve growth factor (NGF) (neuronal media). NIH guidelines for the care and use of laboratory animals were observed throughout this study.

Substrate Preparation

Reagents for cell template preparation were from Electron Microscopy Sciences (Hatfield, PA) unless stated otherwise. Substrates were prepared as outlined in Figure 1 and described by Bruder et al.[12] For preparation of the cell template, laminin (LN) stripes of 10 mm length and 50 μm width were stamped onto glass coverslips via soft-lithographic micro-contact printing techniques in a modification of the method of Thompson et al.[13] SCs were plated on the LN-striped coverslips at 30,000 cells/ml, incubated for 3-7 days to reach near-confluence, and fixed with 2% paraformaldehyde (Sigma) and 4% sucrose (CalBiochem, La Jolla, CA) in 0.1 M phosphate buffered saline

(PBS). Cells were then stained with 4',6-diamidino-2-phenylindole (DAPI, Sigma) and analyzed for alignment as described below. Samples were post-fixed in Karnovsky's fixative overnight, rinsed with 0.1 M cacodylate buffer, incubated in 1% OsO_4 in 0.1 M cacodylate buffer for 1 h, rinsed with dH_2O, incubated in 1% thiocarbohydrazide in dH_2O for 30 min, incubated in 0.5% OsO_4 in dH_2O for 30 min, dehydrated with graded ethanols to 100% ethanol, air-dried, and sputter-coated with gold-palladium. The fixed cells were used as a template to generate a PDMS (Dow Corning, Midland, MI) substrate with indented cell impressions, and this substrate was subsequently used as a template to generate the replica with protruding cell-shaped features. In each case, for replica molding with PDMS, Sylgard 184 elastomer base was mixed with Sylgard 184 curing agent (10:1 wt/wt) and applied to the template to form a layer of 1-3mm thickness. The solution was heated to 95 degrees C for 2 h, and the resulting polymer film was removed.

White Light Interferometry

To measure integrated surface area, 10 fields of view of replicas with biomimetic surface topography were acquired at 400x magnification with a Zygo New View 6000 3D profiler (Middlefield, CT) using white light interferometry (WIM). The resulting integrated surface areas, taking into account the surface area increase introduced by the topographic peaks and valleys, were averaged and compared to non-integrated surface areas.

Study Parameters

LN Adsorption Study

Circular substrates of flat PDMS and replicas (10 mm diameter, n=4 per condition) were coated with 100 µg/ml PLL and 50 µg/ml LN for 1 h each, then blocked for 1 h at room temperature with 10% goat serum (Jackson Immuno Research Laboratories, West Grove, PA), 1% bovine serum albumin (Sigma), in 0.1M phosphate buffered saline (PBS) (blocking buffer) with the addition of 0.1% Triton X-100 (VWR, West Chester, PA) for permeabilization. Samples were incubated overnight at 4 degrees C with a rabbit polyclonal anti-LN primary antibody, diluted 1:200 in blocking buffer. Samples were rinsed in PBS, incubated for 1 h at room temperature with Cy2-conjugated goat anti-rabbit secondary antibody (Jackson Immuno Research Laboratories) diluted 1:200 in blocking buffer, rinsed in PBS, and viewed under fluorescence microscopy. 12-bit fluorescent images were obtained at 100x magnification with a 100msec exposure, and analyzed as described below.

Adhesion Study

Circular substrates of flat PDMS and replicas (10 mm diameter, n=6 per condition) were coated with PLL and LN as described above, placed in a 12 well tissue culture dish. Samples were incubated with 30,000 DRG cells per well (equivalent of 7900 cells/cm^2) in neuronal media for 3 h, then in Neurobasal media with 2% B27 supplement (Sigma), 2% 200mM L-glutamine, 100U/ml penicillin, and 100 µg/ml streptomycin for 21 h. Samples were fixed, stained with DAPI, and analyzed as described below.

Alignment Study

Circular substrates of flat PDMS and replicas of 10 mm diameter were coated with PLL and LN as described above, placed into a 12 well tissue culture plate, and incubated with 16,000; 30,000; 50,000; 100,000; or 200,000 cells/well in neuronal media (n=4 biomimetic substrate and n=4 flat substrate per condition; equivalent of 4,210; 7,890; 13,160; 26,320; or 52,640 cells/cm^2). After 5 days, the samples were fixed, stained with DAPI, stained for anti-neurofilament immunocytochemistry, and analyzed as described below.

Cell Processing and Immunocytochemistry

Samples were fixed with 2% paraformaldehyde (Sigma, St Louis, MD) and 4% sucrose (CalBiochem, La Jolla, CA) in PBS for 7 min at room temperature, rinsed with PBS, and stained with 1 μg/ml DAPI for 5 min. For samples of the alignment study, nonspecific staining was blocked by incubating for 1 h at room temperature with 10% goat serum, 1% bovine serum albumin (Sigma), and 0.1% Triton X-100 (VWR, West Chester, PA) in PBS (blocking buffer). Samples were incubated either with a rabbit polyclonal anti-S100 antibody (1:300; DAKO, Carpinteria, CA) for three days at 4 degrees C or with a mouse monoclonal antibody RT97 (1:200) overnight at 4 degrees C. RT97 was directed against the phosphorylated epitopes of neurofilament, developed by Dr. John Wood, and obtained from the Developmental Studies Hybridoma Bank (developed under the auspices of NICHD and maintained by the University of Iowa). Samples were rinsed in PBS, incubated for 1 h at room temperature with Cy3-conjugated goat anti-mouse secondary antibody or Cy2-conjugated goat anti-rabbit secondary antibody (Jackson

Laboratories) diluted 1:200 in blocking buffer, rinsed in PBS, and viewed under fluorescence microscopy. For double-immunostaining, samples were incubated sequentially with both primary antibodies, rinsed, then incubated sequentially with both secondary antibodies. For controls, samples were processed without incubation with primary antibodies.

Microscopy

For examination under scanning electron microscopy (SEM), samples were sputter-coated with gold-palladium and examined with a Hitachi S-2700 SEM using an acceleration voltage of 8 kV, at an angle of incidence of 60 degrees. To visualize the cell templates, ten 669 μm x 878 μm fields of view (FOVs) of DAPI-stained aligned SCs were acquired at 200x magnification on an Axiovert 200M inverted microscope with an appropriate filter cube, outputting to a Zeiss AxioCam MRc5. To visualize the DAPI-stained nuclei for the adhesion studies, ten FOVs per sample were acquired at 100x magnification on an Olympus IX70 inverted microscope with an appropriate filter cube, outputting to a Zeiss AxioCam MRC. To visualize the corresponding images of the substrate, DAPI-stained nuclei, and neurofilament-stained neurites for the alignment studies, ten FOVs were acquired at 100x magnification with a Nikon Eclipse TE2000-S phase-contrast and epifluorescence microscope, equipped with a software-controlled motorized stage. Patterned samples were oriented so that substrate pattern direction was uniform between samples. Images were captured using a Hamamatsu Orca-ER camera, an Orbit shutter controller, and a Ludl stage controller, outputting to OpenLab v4.0.4 (Improvision, Lexington, MA).

For confocal microscopy, samples were examined on a Leica spectral confocal microscope (TCS SP2 AOBX) with sequential laser illumination for each fluorescent channel. 100 z-slices of 0.35µm thickness were acquired per channel and assembled into image stacks using Voxx 2.0 software (University of Indiana).

Image Analysis

LN-immunostained images were analyzed with ImageJ v1.38f and the average fluorescence intensity for the entire field of view was recorded with the "measure" tool.

DAPI images for adhesion analysis were converted to 8-bit greyscale with Adobe Photoshop CS2, inverted, and the contrast was adjusted using the level and curve functions. Nuclei number and orientation were assessed with ImageJ v1.36, using the Otsu function of the multithresholder plugin and the particle analyzer plugin with size filter set to 50-850 pixels to exclude image artifacts and cell clusters. Data was analyzed with Oriana v2.02c (Kovach Computing Services, Anglesey, Wales, UK).

Neurofilament-immunostained images obtained with a 10x objective lens were cropped in Adobe Photoshop CS2 to generate circular-shaped images with the direction of the pattern on replica images oriented horizontally. Contrast was adjusted equally across the batches of images using level and curve functions and images were thresholded to optimize visualization of neurite networks. Images were analyzed with Matlab R2006a v7.2.0.232 using custom-written software. In order to analyze the angular distribution of neurofilament-positive neurite segments, each image was rotated 90 degrees clockwise and counterclockwise in 10 degree increments. Each resulting image (original image and 18 rotated images) was divided into a series of horizontal rows one pixel wide. The

number of instances of 50 consecutively bright pixels within the image rows was counted during an iterative analysis per row and summed separately for all rows. The value of 50 pixels (= 32 μm) was chosen to minimize incorrect counting of somata as neurite segments.

Statistical Analysis

LN adsorption results were analyzed using a Student's t-test assuming equal variances, and adhesion results were analyzed using a Student's t-test assuming unequal variances. Circular analysis was used to analyze the angular distributions of the major axes of the nuclei and of the neurite segments. Circular mean vectors and standard errors of the mean were calculated, where the length of the mean vector corresponds to the degree of clustering of the data, and the direction of the mean vector corresponds to the mean direction of the data. Uniformity of the distribution of nuclei was assessed using a Rao's spacing test[14], uniformity of the distribution of the angles of neurite segments was assessed using a chi-squared test, and alignment of nuclei or neurite segments in the direction of the substrate pattern was assessed via a V-test[14], that allowed for comparison of the distributions to the pattern direction, which was set to 90 degrees. Oriana 2.02c software was used for circular analysis. For all cases, a p value of 0.05 was taken to be significant.

Results

We recently reported the development of novel biomimetic materials whose surfaces contain protruding cellular features. Here we have utilized these materials to present

growing neurons with topographical cues from aligned SCs. Materials containing aligned SC topography were prepared by a replica molding procedure as described previously (Figure 1 [12]). In the cell template, SC were well aligned ($p < 0.001$), with 73% of SC aligned to within 20 degrees of the direction of the LN stripes, and the replicas reflected this alignment. The resulting replicas contained SC protrusions (Figure 2B) that were similar in appearance and dimension to the fixed SC templates (Figure 2A), including replication of the topography of SC somata and processes. WIM analysis demonstrated that the replicas contained an increase in surface area of $4.1 \pm 0.19\%$ over flat substrates. However, quantitative densitometry of anti-LN immunostaining showed no differences in the amounts of LN adsorbed to the surfaces of flat and replica materials (Figure 3).

After 24 hours in culture, DRG exhibited significantly higher levels of adhesion to biomimetic materials than to flat substrates (Figure 4). On average, 11.2 ± 0.8 cells/FOV adhered to flat substrates and 21.8 ± 1.2 cells/FOV adhered to the replicas, corresponding to an increase of 95% over the flat substrates.

Phase contrast microscopy showed both the DRG and the underlying SC patterns, where present (Figure 5A, D), DAPI fluorescence showed the DRG nuclei (Figure 5C, F) and anti-neurofilament immunofluorescence showed the neurons and neurites (Figure 5B, E). When DRG were cultured on flat materials, they exhibited no qualitative directional preference in their neurite extension (Figure 5A-C). In contrast, on biomimetic materials, DRG growth appeared aligned to the underlying pattern (Figure 5D-F).

Alignment was quantified using circular analysis.[14] When DRG were cultured for 5 days, Rao's spacing test demonstrated that the distribution of the angles of DRG nuclei was uniform on flat substrates and nonuniform on biomimetic substrates (Figure 6). A V-test confirmed that cells showed alignment of their nuclei to the biomimetic patterns when plated at densities > 50,000 cells/well (Figure 6A). On the replicas, DRG exhibited stronger alignment at higher seeding densities. The length of the mean vector increased with seeding density for replicas, and this increase followed a logarithmic relationship, with all points lying within the 95% confidence interval of their best-fit line (Figure 6B; $r^2 = 0.95$).

DRG neurite segment orientation was also aligned to the underlying pattern on biomimetic materials and distributed randomly on flat materials (Figure 5B, E; Figure 7). A chi-squared test showed that when DRG were cultured at 100,000 cells/well, the angles of neurite segments displayed a uniform distribution on flat PDMS and a nonuniform distribution on replicas. A V-test confirmed that neurite segments were aligned in the direction of the SC patterns on the replicas (90 degrees), with a mean vector direction of 91 ± 1.6 degrees.

Confocal microscopy of double-immunostained samples revealed the growth of live SCs as well as neurons derived from the DRG (Figure 8). On the replicas the SCs and neurons grew in close spatial proximity to each other, with SC processes and neurites closely

aligned with each other and with the underlying replica pattern. In some cases neurites could be observed extending on top of the SC processes (Figure 8F).

Discussion

The main objective of this work was to determine whether SC topography influenced neuronal growth. Toward this end, we employed new biomimetic substrates with protruding surface features that replicated SC morphology at the nanoscale.[12] The major finding of this study was that materials containing the topography of SC enhanced DRG adhesion and alignment as compared to control flat substrates.

Biomimetic replicas significantly enhanced adhesion, with nearly twice as many cells adhered to replicas as compared to flat substrates. We have shown previously with quantitative interferometric analysis that the cellular features present on the replica surfaces present a complex range of surface heights that vary from tens of nanometers to single microns.[12] Here we have demonstrated higher levels of DRG adhesion on these replicas that provided higher surface areas. These results agree with those of Curtis et al., who showed that surfaces containing nanotopography promoted cell adhesion.[15], [16] The replicas in this study contained multiple surface discontinuities and local variations in material height, features which have been shown previously to increase cell adhesion. [15]

DRG alignment was also significantly affected by replicas containing protruding SC topography. As cells aligned longitudinally, their nuclei became elongated and elliptical

in shape, and the length of the major axis of the ellipse provided an effective measure of the cellular orientation.[13], [17] Cell density was correlated with alignment. Rao's spacing test indicated that on the replicas, the angles of the nuclei were unequally spaced around 360 degrees for densities > 50,000 cells/well. As the cell density increased, the direction of the mean vector of the nuclear angles approached the direction of the original aligned SC, which was designated as 90 degrees. The mean vector direction was 81 $\pm$ 3 degrees for 50,000 cells/well; 89 $\pm$ 4 degrees for 100,000 cells/well; and 88 $\pm$ 0.5 degrees for 200,000 cells/well ($p < 0.001$ by V-test for all three cell densities). Since the length of the mean vector corresponds to the clustering of the angles of the nuclei, the logarithmic relationship between the length of the mean vector and the seeding density provided further evidence of the strong correlation between density and nuclear alignment. In addition, neurite segment alignment reflected nuclear alignment. Quantitative analysis of the distribution of the angles of neurofilament-positive neurite segments from DRG plated at 100,000 cells/well confirmed the alignment of neurite segments to the SC topographical patterns.

These results suggest important roles for SC topography in mediating neuronal function. Both the replicas and flat substrates were coated homogeneously with PLL-LN to promote adhesion. Of note, the relative increase in surface area on the replicas did not result in a detectable increase in LN adsorption. The presence of similar amounts of molecular coatings on both substrates, taken together with results from previous studies showing that molecular coating did not mask the ability of the topography to influence cellular behavior, suggests that coating was not a contributing variable in these

experiments. The observations by Yim et al. that nanopatterned PDMS influenced smooth muscle cell function regardless of collagen coating[17] lends further support to the idea that topography, and in particular cellular topography, exerts a strong effect on cellular function. The variations in DRG alignment at different seeding densities observed in this study likely reflect the complexity of cell-material and cell-cell interactions, where a single cell interacts both with underlying material cues and surrounding cellular cues. DRG contain multiple cell types, including glial cells and fibroblasts, as well as neurons. This study has demonstrated that live SC grow together with neurons on the SC topography presented by the replica materials. It will be of interest in future studies to elucidate the complex dynamics and mechanisms of cellular alignment.

Neuronal capacity to respond to topographical features in their microenvironments has been demonstrated previously as neurons have adhered, migrated, and oriented their neurites to navigate surface features such as grooves in substrates.[18], [19], [11], [20], [21] Neurons have also been shown to orient to other cells[22], [23], [24], [25], which provide a more complex array of signals. DRG alignment has been enhanced by culture on meningeal cell monolayers that were pre-aligned on nanoscale grooved substrates.[26] DRG neurites have been found to align to SCs that were oriented on micropatterned LN and presented so as to minimize access to underlying biochemical cues.[7]

To our knowledge, this study is the first demonstration of neuronal guidance by cellular topography. These findings facilitate the deconstruction of the local cellular environment

in the nervous system, and by separating out cellular topography as a key parameter for study, pave the way for investigations of the fundamental cell biology of cell adhesion, cell alignment, and cell-cell interactions. Finally, preliminary studies have shown that these materials can be utilized to form nerve guidance channels (Bruder et al., unpublished observations), and thus this work suggests exciting potential directions for biomimetic biomaterial-based strategies for nerve repair technologies.

Acknowledgements

The authors thank Michael Sherback for assistance with software development and Grace Li for helpful discussion of the manuscript. This work was funded by the Whitaker Foundation and the Brown University Seed Fund Program.

Figures

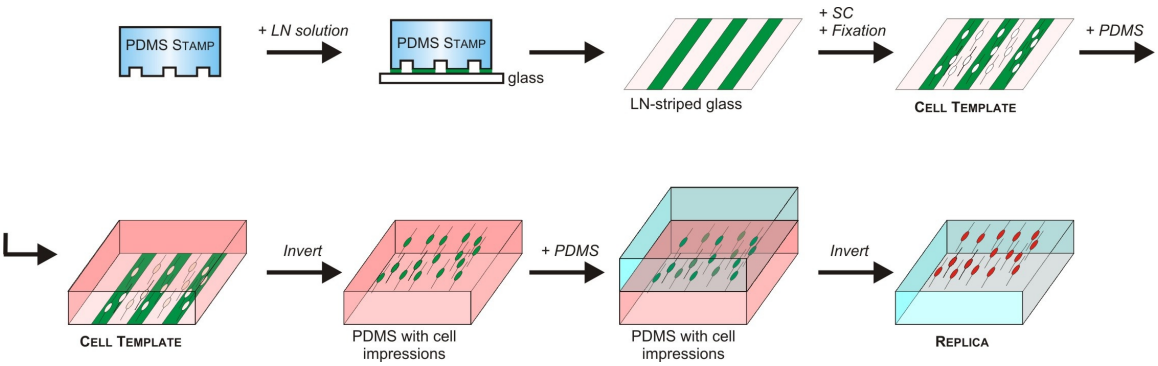

Figure 1. Overview of the technique.

A PDMS stamp, prepared by soft lithography, was used for microcontact printing to generate a glass substrate with 50µm LN stripes. Cultured SCs aligned in the direction of the LN stripes, generating the cell template. The replica was generated via two sequential casting and replica molding steps.

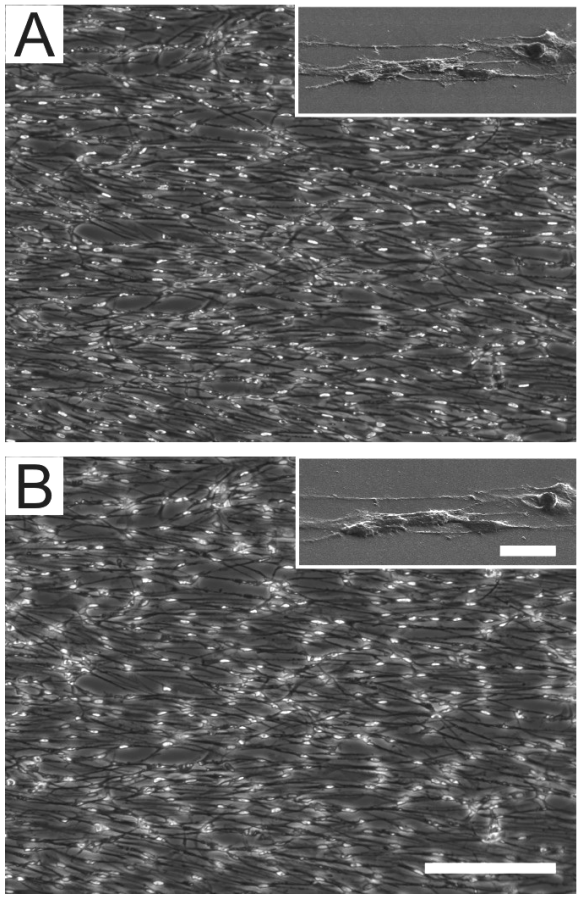

Figure 2. Biomimetic materials replicate SC features, as visible under phase contrast microscopy and SEM.

SCs were cultured at 120,000 cells/ml on 50μm wide stripes of LN on glass for 24 h, fixed, and used as cell templates to generate replicas from PDMS. Phase contrast and SEM micrographs of corresponding regions of the replica (B) show the replication of SC topographical features in the original template (A). Scale bars, 200 μm for phase contrast micrographs and 20 μm for SEM micrographs.

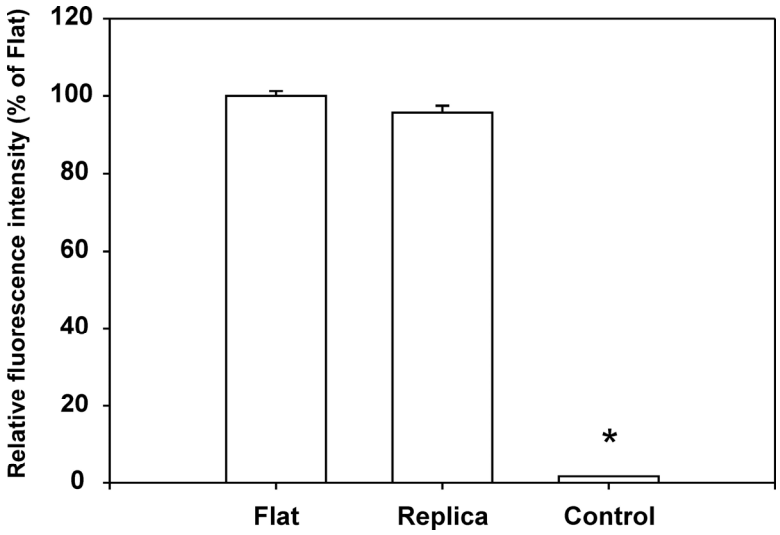

Figure 3. Similar LN adsorption on flat and biomimetic materials.

Similar LN adsorption on flat and biomimetic materials. Relative anti-LN immunofluorescence intensity (normalized to LN-coated flat materials) on LN-coated flat materials, LN-coated replica materials, and LN-coated replica material with no primary antibody (control). Immunofluorescence of flat and replica materials were significantly different from immunofluorescence for control conditions (*$p < 0.005$ by two-tailed student's t-test assuming equal variances), but were not significantly different from each other. ($n = 4$ for flat and replica materials; $n = 1$ for control; Error bars are SEM.)

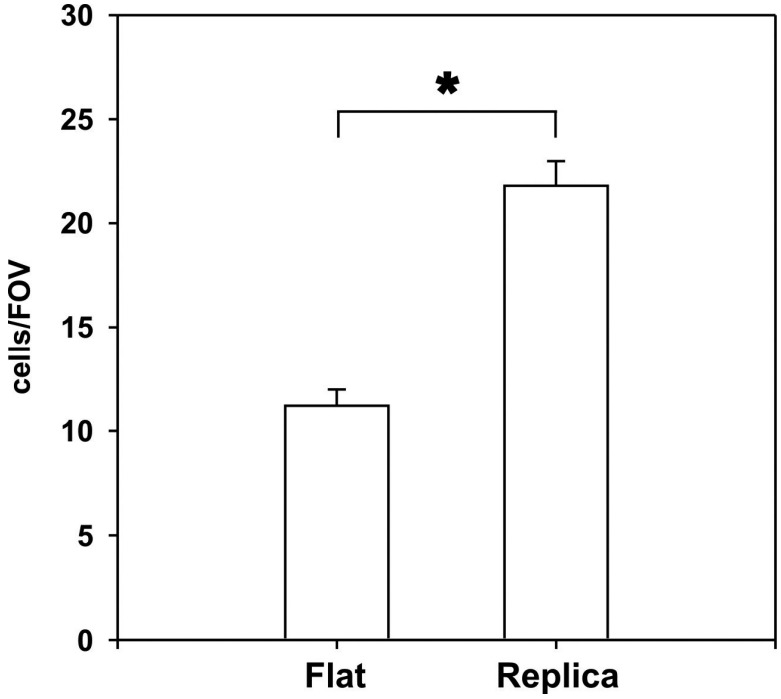

Figure 4. Enhanced DRG adhesion on biomimetic materials.

DRG adhesion after 24 h in culture was significantly enhanced on PDMS replicas with SC features versus on flat PDMS ($p < 0.001$). Error bars are SEM, n = 8 samples.

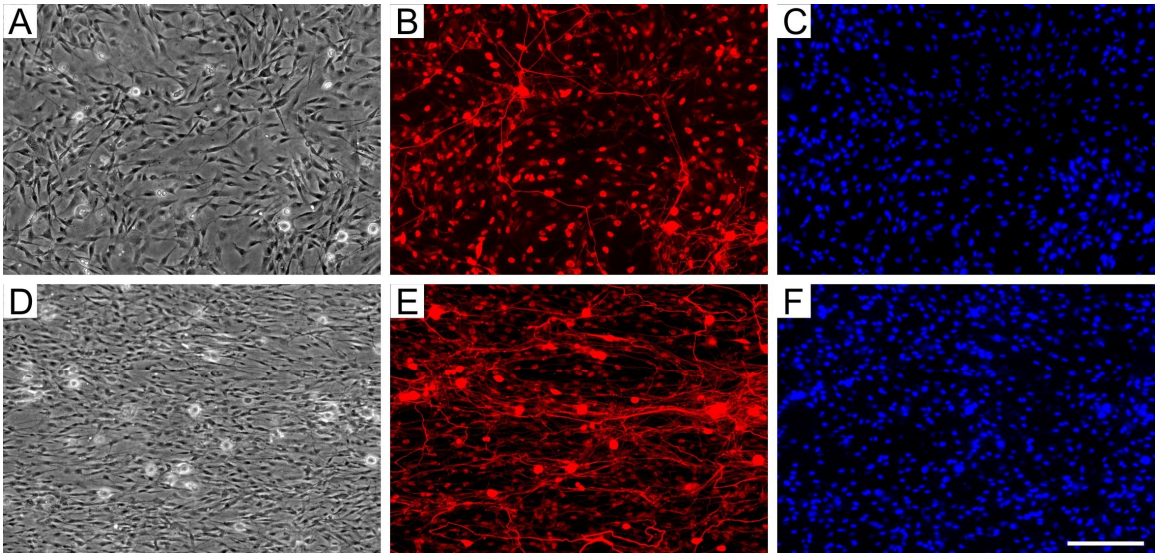

Figure 5. DRG morphology on biomimetic materials.

Phase contrast (A, D) and fluorescent micrographs (B, C, E, F) of dissociated DRG cultured for 5 d on flat PDMS (A-C) or replicas (D-F) and stained with neurofilament immunocytochemistry (B, E) and DAPI nuclear stain (C, F). Scale bar, 200 μm.

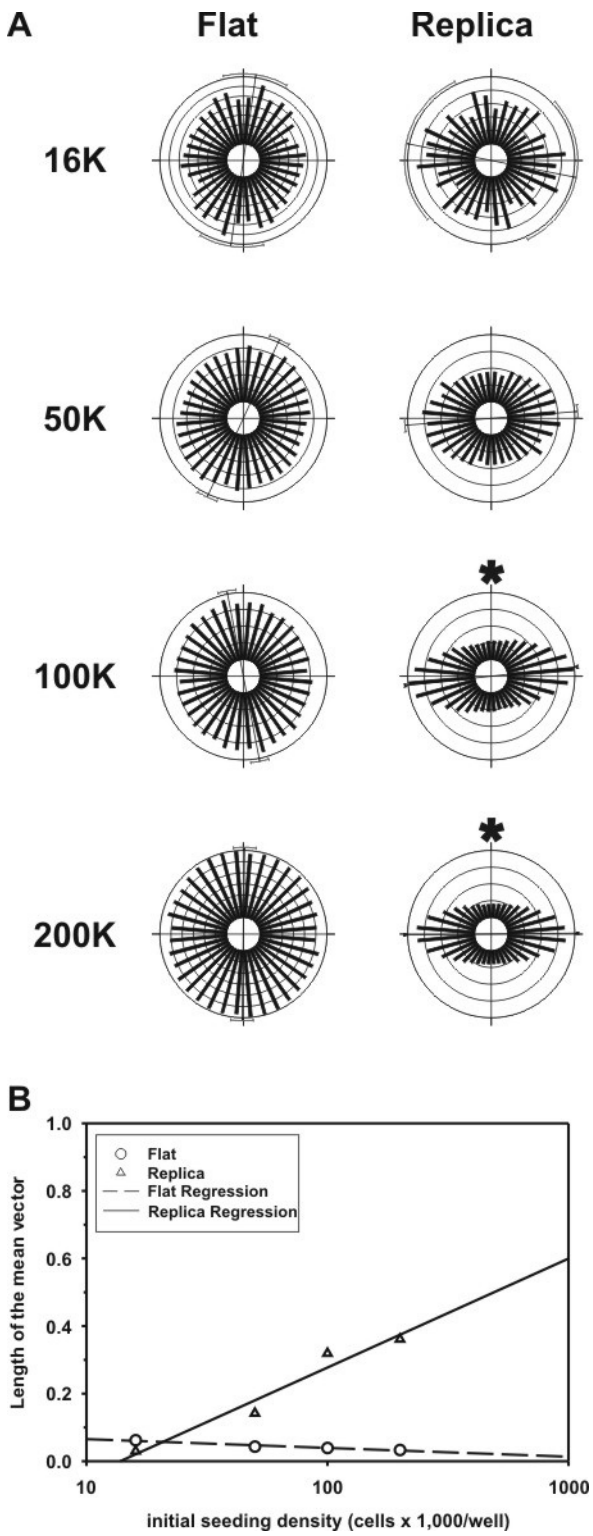

Figure 6. Enhanced nuclear alignment on biomimetic materials.

(A) Circular histograms show the distributions of the angles of the long nuclear axes of dissociated DRG plated at varying cell densities, cultured for 5 d on flat PDMS or replicas, and stained with DAPI. The length of each bar represents the number of nuclei oriented at the corresponding angle, and the arcs indicate the 95% confidence interval. The horizontal axis corresponds to the direction of the SC pattern in the replicas. For plating densities > 50,000 cells/well, Rao's spacing test confirmed a non-uniform distribution of nuclear angles (*$p < 0.01$ for 100,000 and 200,000 cells/well) and a V-test confirmed nuclear alignment in the direction of the SC pattern (*$p < 0.001$). Number of cells measured for each condition are: 16K seeding: 588 replica, 860 flat; 50K seeding: 4,117 replica, 17,142 flat; 100K seeding: 4,216 replica, 28,870 flat; 200k seeding: 44,117 replica, 25,035 flat.(B) Graph of the relationship between plating density and nuclear alignment, as represented by the lengths of the mean vectors in (A). Plating density showed a logarithmic correlation with mean vector length for both replicas and flat substrates (r^2 = 0.95 for both).

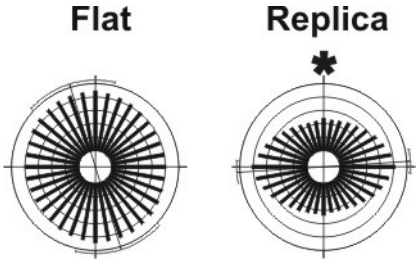

Figure 7. Enhanced alignment of neurite segments on biomimetic materials.

Circular histograms show the distributions of the angles of neurofilament-positive DRG neurite segments cultured at 100,000 cells/well for 5 d on flat PDMS and replicas. For replicas, the direction of the underlying pattern was defined as 90 degrees. *$p < 0.001$ by chi-squared test and *$p < 0.001$ by V-test. N = 4 samples per material type; n = 4 images per sample.

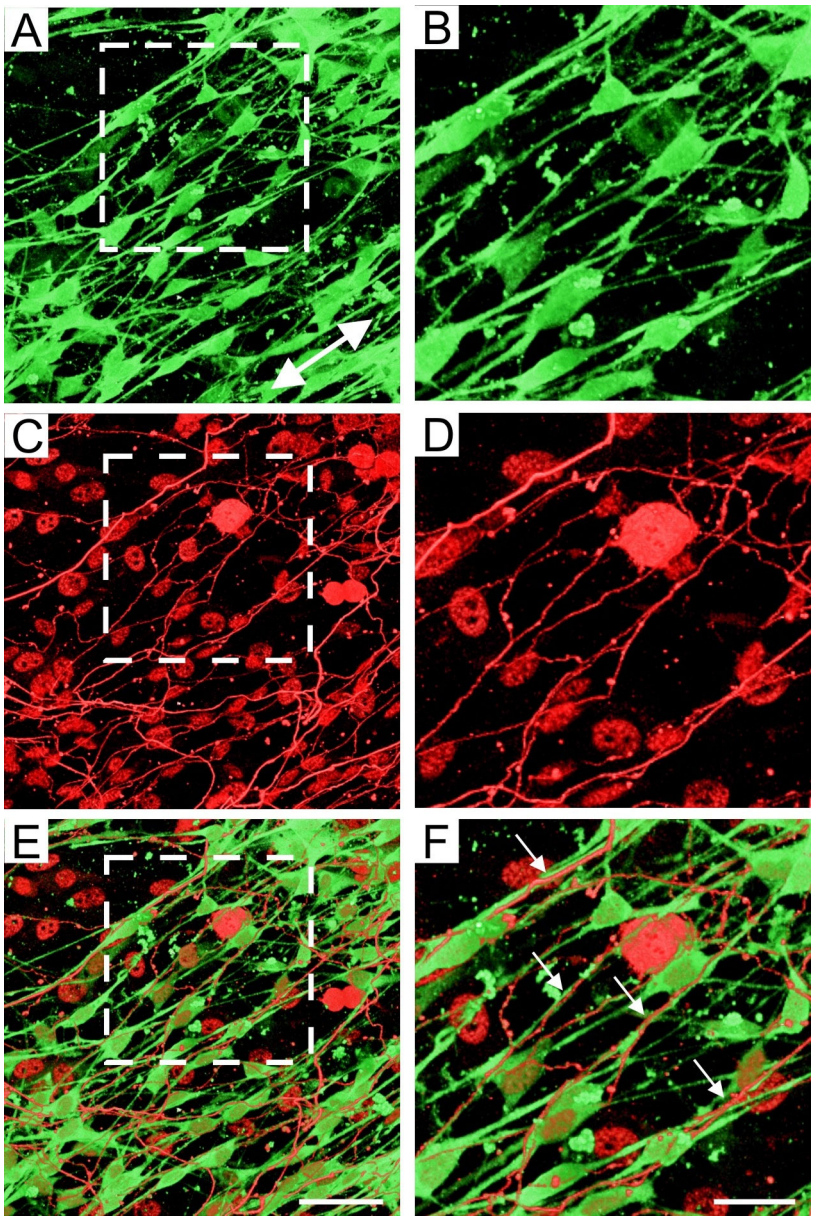

Figure 8. Neurons and SC from DRG extend neurites and processes on biomimetic materials in the direction of the underlying pattern.

Neurons and SC from DRG extend neurites and processes on biomimetic materials in the direction of the underlying pattern. Confocal micrographs of cells dissociated from DRG explants, cultured at 100,000 cells/well for 5d on replica material, and stained by immunocytochemistry for S100 (A, B) and neurofilament (C, D). E is a merged image of A and C, and F is a merged image of B and D. A, C, and E are images of the same field of view; scale bar, 50μm. B, D, and F are higher magnification images of the regions within the rectangles in A, C, and E, respectively; scale bar, 25 μm. The double arrow in A indicates the direction of the pattern of the biomimetic material. Arrows in F show neurites growing on top of SC.

References

1. M. B. Bunge, M. I. Johnson, M. D. Ard and N. Kleitman. *Prog Brain Res* 71, (1987).

2. R. P. Bunge. *J Neurol* 242, 1 Suppl 1 (1994).

3. J. W. Fawcett and R. J. Keynes. *Annu Rev Neurosci* 13, (1990).

4. M. B. Bunge. *Neuroscientist* 7, 4 (2001).

5. R. P. Bunge and C. Fernandez-Valle, in: *Neuroglia*, Ketternmann H, Ransom BR, (Eds.) pp 44-57. Oxford University Press, New York (1995).

6. V. Guenard, N. Kleitman, T. K. Morrissey, R. P. Bunge and P. Aebischer. *J Neurosci* 12, 9 (1992).

7. D. M. Thompson and H. M. Buettner. *Ann Biomed Eng* 34, 1 (2006).

8. I. H. Whitworth, R. A. Brown, C. Dore, C. J. Green and G. Terenghi. *J Hand Surg [Br]* 20, 4 (1995).

9. N. Dubey, P. C. Letourneau and R. T. Tranquillo. *Exp Neurol* 158, 2 (1999).

10. C. Miller, S. Jeftinija and S. Mallapragada. *Tissue Eng* 7, 6 (2001).

11. C. Miller, H. Shanks, A. Witt, G. Rutkowski and S. Mallapragada. *Biomaterials* 22, 11 (2001).

12. J. M. Bruder, N. C. Monu, M. W. Harrison and D. Hoffman-Kim. *Langmuir* 22, 20 (2006).

13. D. M. Thompson and H. M. Buettner. *Ann Biomed Eng* 32, 8 (2004).

14. N. I. Fisher. *Statistical Analysis of Circular Data*. Cambridge University Press, Cambridge, United Kingdom (1995).

15. A. S. Curtis, B. Casey, J. O. Gallagher, D. Pasqui, M. A. Wood and C. D. Wilkinson. *Biophys Chem* 94, 3 (2001).

16. A. S. Curtis, N. Gadegaard, M. J. Dalby, M. O. Riehle, C. D. Wilkinson and G. Aitchison. *IEEE Trans Nanobioscience* 3, 1 (2004).

17. E. K. Yim, R. M. Reano, S. W. Pang, A. F. Yee, C. S. Chen and K. W. Leong. *Biomaterials* 26, 26 (2005).

18. P. Clark, P. Connolly, A. S. Curtis, J. A. Dow and C. D. Wilkinson. *Development* 99, 3 (1987).

19. A. Rajnicek, S. Britland and C. McCaig. *J Cell Sci* 110 (Pt 23), (1997).

20. C. Miller, S. Jeftinija and S. Mallapragada. *Tissue Eng* 8, 3 (2002).

21. P. Weiss. *Journal of Experimental Zoology* 100, 3 (1945).

22. E. Stepien, J. Stanisz and W. Korohoda. *Cell Biol Int* 23, 2 (1999).

23. R. Biran, M. D. Noble and P. A. Tresco. *Exp Neurol* 184, 1 (2003).

24. Y. Li, Y. Sauve, D. Li, R. D. Lund and G. Raisman. *J Neurosci* 23, 21 (2003).

25. G. A. Brook, J. M. Lawrence, B. Shah and G. Raisman. *Exp Neurol* 126, 1 (1994).

26. J. F. Walsh, M. E. Manwaring and P. A. Tresco. *Tissue Eng* 11, 7-8 (2005).

Chapter 5

Cellular Alignment on Substrates Combining Biochemical and Biomimetic Cell-shaped Cues

Jan M. Bruder, Andrea P. Lee, and Diane Hoffman-Kim

The following chapter is a manuscript in preparation.

Abstract

In vivo, cells are surrounded by a multitude of directional cues including substrate-bound protein cues, topography in the form of extracellular matrix and other cells, soluble protein gradients, and electrical stimuli. While the influence of many individual cues on cell behavior has been researched for several decades, little is known about the combined effects of multiple cues or how to optimally blend them for implant and tissue engineering applications. Combining micro-contact printed laminin stripes and recently developed poly(dimethyl-siloxane) materials with Schwann-cell shaped surface topography allows independent and simultaneous presentation of these two cues in arbitrary and unrelated directions. Under the conditions tested, neuronal and glial cells aligned preferentially and more strongly to protein cues than to topographical cues when both were presented simultaneously and orthogonally. These findings inform efforts to aid the design of implants that can bridge sites of injury or dysfunctional areas in the central and peripheral nervous system. The results of this study also aid understanding of cellular integration of biochemical and topographical cues.

Introduction

It is well established that the extracellular environment exerts a profound influence on cellular behavior through a variety of pathways and mechanisms[1-4]. Over the past decades, several types of environmental interactions with neuronal cells have been characterized and their individual contributions in terms of adhesion, alignment, proliferation, differentiation, or motility have been quantified. Such cues are often grouped into classes including substrate-bound cues[5-8], soluble cues[9-11], electrical gradients[12-14], and topography[3, 15-20] . Only more recently have researchers attempted to assess the combined effects of extracellular cues, establish hierarchies, and search for synergistic interactions[21-26]. Deconstructing the interplay of different classes of cues is important to fully understand the in vivo processes occurring during development, stasis, and after injury. A quantitative knowledge of the effects and interactions of extracellular control of neuronal cells aids the optimization of materials used in regenerative approaches[27-33], neural-machine interfaces[34-36], and the construction of artificial neural networks.

Recent work indicates that the surface chemistry of biomaterial implants may play a much less important role than the micro- and nanotopography[37]. Previous work has combined geometrical topography on quartz substrates with orthogonal protein cues and quantified the direction of cellular alignment with respect to each cue[24-26]. Britland et al.[26] presented neonatal rat dorsal root ganglia (DRGs) with rectangular grooves with widths varying from 12 um to 100 um and depths ranging from 5 nm to 6 um. They overlaid

these grooves with laminin stripes of varying widths between 5 um and 100 um either in parallel or orthogonally oriented to the grooves. The results indicated that the strength of cellular alignment to topographical cues was a function of groove depth, with a groove depth of 0.75 microns or more resulting in cells aligning predominantly to topographical cues. The maximum cell alignment was reached when the cells encountered 6 um deep grooves with parallel protein tracks of 25 um width. Another study has examined embryonic rat hippocampal cell polarization and axogenesis and recorded substrate preference for substrate-bound or topographical cues[23]. With the experimental conditions employed, a cell placed between the border of areas featuring grooved topography and/or substrate-bound cues directed axonal growth predominantly towards the area featuring grooved topography. Studies with osteoblast-like cells[22] indicated that geometrical topography exerted a stronger net influence over substrate-bound cues on cells of non-neuronal origin. While these studies address the effects of geometrical topography on cellular behavior, they do not take into the account the much more complex topography that cells encounter in vivo.

During development or after injury in the peripheral nervous system, regenerating axonal tips are guided by biochemical as well as topographical cues, and SCs are the primary mediators of this process. After injury, SCs migrate along any remaining fragments of basal lamina and align to their environment and to each other. Together with macrophages, SC are the “first responders”, providing positive guidance cues in the form of laminin, substrate-bound and soluble neurotrophins, and topography[38]. It is thus desirable to attract and align SCs to span across an area of injury, to promote, guide, and

accelerate neuronal regeneration processes. While previous experiments have shown that aligned Schwann cells are capable of directing neurite outgrowth in vitro[39, 40], it remains unclear whether this process is mediated by substrate-bound biochemical cues, such as laminin, and/or by topographical mechanisms such as contact guidance.

We have recently described a replica molding approach for fabricating transparent, biocompatible substrates that mimic the surface shape of aligned Schwann-cells at the macro-, micro-, and nano-scale, while maintaining a homogeneous biochemical surface[41]. Utilizing these substrates, we can systematically vary the relative orientations of aligned SC topography with micro-contact printed protein stripes. This biomimetic setup approximates the rich gamut of topographies that axonal tips encounter in vivo and, for the first time, allows the assessment of hierarchies and synergies between cellular topography and protein cues. Here we assess the ability of these substrates to align both SCs and DRGs and quantify the relative impacts of conflicting cellular topography and biochemical cues.

Methods

Cell Culture

Cell culture materials were from Invitrogen Life Technologies (Carlsbad, CA) unless indicated otherwise. Primary P1-5 postnatal rat dorsal root ganglion cells (DRGs) were harvested as described previously.[42] DRGs were seeded at 180,000 cells/cm^2 in Dulbecco's modified eagle's medium (DMEM) with 10% fetal bovine serum (FBS), 4

mM L-glutamine, 100 U/ml penicillin, and 100 μg/ml streptomycin (base media) supplemented by 50 ng/ml nerve growth factor (NGF) (neuronal media) and grown to confluence over 5 days.

Primary P18-22 rat sciatic nerve Schwann cells (SCs) were obtained from sciatic nerves from adult rats according to a procedure adapted from Morrissey et al.[43]. SCs were cultured in Schwann cell media (base media supplemented with 2 μM forskolin (Sigma), 10 μg/ml bovine pituitary extract (Sigma)) and grown to confluence over 5 days.

Substrate Preparation

Reagents for substrate preparation were from Electron Microscopy Sciences (Hatfield, PA) unless stated otherwise. Biomimetic substrates were fabricated as previously described (Figure 1)[41]. Briefly, glass slides were micro-contact-printed (uCP) with laminin stripes of 60 um width and pitch and 1 cm length. Elastomeric poly-dimethylsiloxane (PDMS) stamps (Sylgard Elastomer 184, Dow Corning) with repeating grooves of 60 um pitch and width were "inked" with 50 ug/ml laminin in Hanks's Balanced Salt Solution (HBSS) for 10 minutes and rinsed in dH_2O. Glass coverslips (VWR, West Chester, PA) were plasma-activated in a Plasma-Cleaner/Sterilizer (PDC – 32 G, High RF level) for 30 s. The inked stamps were then inverted onto the activated glass surface and left in contact for at least 5 minutes. After removal, the glass slides were ready for cell seeding. Primary P18-22 rat SCs were cultured at 30,000 cells/cm^2 on the uCP glass slides and grown to confluence in SC media over 3-7 days at 37 C, 5% CO_2 in a humidified environment. Cells were then fixed using 2% paraformaldehyde (Sigma, St Louis) and 4% sucrose (CalBiochem, La Jolla, CA) and postfixed in Karnovsky's

fixative overnight. Samples then underwent a standard osmium-tetraoxide fixation protocol[41] followed by a dehydration step using graded ethanol washes from 50-100% ethanol in dH_2O. Dried samples were sputter-coated with a layer of gold-palladium and formed the "cell template". Biomimetic replicas were generated using a simple replica-molding approach: Sylgard 184 PDMS solution (Dow Corning, Midland, MI) was mixed with the appropriate curing agent in a 10:1 ratio (w/w), degassed, and poured over the cell template to form a layer of 3 mm thickness. After curing at 95° C for 1 hour, the elastomer was peeled off the template to form the "impression replica" with indented cellular shapes. The molding process was repeated with the impression replica serving as a master mold, yielding the "relief replica" after separation, with protruding aligned SC-shaped cellular shapes.

Protein Coating

Laminin stripes of 60 um width and 60 um pitch were micro-contact-printed onto relief replicas following the same uCP steps as described above. Control samples were fully coated with laminin by plasma activation of the substrate followed by exposure of the substrate surface to 50 ug/ml laminin in HBSS for 10 minutes. All protein coating steps were followed by two rinses with 0.1 M sodium phosphate with 0.9% sodium chloride, pH 7.4 (PBS) to remove unbound laminin.

Experimental Setup

Alignment Study:

Five groups of n=3 samples were prepared as indicated in Figure 1: 2 experimental conditions and 3 controls. For the experimental conditions, micropatterned protein stripes were stamped either in parallel or perpendicular to aligned SC topography on biomimetic substrates. As controls, fully laminin-coated SC-shaped replicas were used, along with flat (no-topography) PDMS samples with and without protein stripes. Dissociated DRG cells were seeded at 188,000 cells/well and grown to confluence over 3-5 days.

Densitometry Study:

The integrity of uCP protein coats over time was assessed using fluorescence densitometry following immunostaining against laminin. Four groups of n=3 samples were prepared: the first group underwent laminin immunostaining immediately following uCP according to the protocol described below; the second group was covered in PBS following uCP and was stored at 4 C for 5 days, followed by laminin immunostaining; the third group was incubated with base media for 5 days at 37 C, then immunostained for laminin.

Fixing and Immunostaining

Before immunostaining, all samples were fixed at the appropriate times by rinsing with PBS followed by incubation with 2% paraformaldehyde and 4% sucrose in PBS for 10 minutes. Cell nuclei were visualized with 4',6-diamidino-2-phenylindole (DAPI, Sigma) and analyzed as described below. Nonspecific staining was blocked by incubating for 1 h

at room temperature with 10% goat serum, 1% bovine serum albumin (Sigma), in PBS (blocking buffer) with the addition of 0.1% Triton X-100 (VWR) for permeabilization.

Samples immunostained for laminin were incubated overnight with 1:250 primary polyclonal rabbit antibody directed against laminin in working solution and 1:200 secondary antibody Cy3-conjugated goat anti-rabbit antibody (Biomedical Technologies) in working solution for 1 h.

DRG samples were stained with 1:200 RT97 mouse monoclonal primary antibody (developed by Dr. John Wood, and obtained from the Developmental Studies Hybridoma Bank (developed under the auspices of NICHD and maintained by the University of Iowa)) against neurofilament (NF) overnight, followed by a secondary Cy3-conjugated antibody (Jackson Laboratories). In each case one sample without primary antibody served as a control.

Microscopy

All samples were imaged on a Nikon TE 2000 microscope equipped for phase contrast acquisition and epi-fluorescent light source with appropriate filter cubes. Images were outputted to Openlab 4.0.4 (Improvision) using a Hamamatsu Orca-ER camera.

For confocal microscopy analysis, immunostained samples were mounted on thin glass cover slides and imaged on a spectral confocal microscope (Leica TCS SP2 AOBS). Fifty

image slices were acquired per field of view on a 63x water-immersion lens, with the vertical z-distance between slices ranging from 0.5 – 1 um between samples, depending on sample morphology. Stacks of multiple z-planes were assembled using ImageJ 1.39o (NIH).

Image Analysis

Fluorescence was assessed using a Nikon TE 2000 inverted microscope equipped with a Hamamatsu Orca-ER camera and appropriate fluorescent light source and filter sets. For densitometry analysis, three fluorescent stripes and three dark regions were selected per sample and the brightness averaged in Openlab 4.0.4. For cell alignment analysis, images of DAPI stained nuclei were imported into ImageJ, inverted, converted to 8-bit, manually threshholded, and measured using the ellipse-fitting function of the particle analyzer plugin. Size threshold was set to measure particles between 50-1000 pixels to exclude artifacts. This outputted the angle of the long axis of the fitted ellipses for each nucleus.

Statistical Analysis

Circular histograms were generated using Oriana 2.02c (Kovach Computing Services), based on data from nuclear alignment exported from ImageJ. Rao's spacing test was used to assess uniformity, and V-test, a variant of Rayleigh's uniformity test, was used to confirm non-uniform population mean directions with a specified mean orientation. In all cases, samples with a $p < 0.05$ were taken to vary significantly from a uniform distribution or deviate from putative alignment, respectively. Other statistical comparisons were carried out using a student's t-test, with $p < 0.05$ taken to be significant.

Results

Generation of Substrates

To generate biomimetic replicas, aligned SCs served as a template in a double-replica molding process. Laminin stripes of 60 um width and pitch were adsorbed to the PDMS surface using micro-contact printing to generate the parallel and orthogonal experimental conditions (Figure 1). Fully laminin coated flat PDMS substrates, uCP flat substrates with laminin stripes of 60 um width and pitch, and fully coated "topography-only" substrates served as experimental controls.

Examination of the substrates with phase and fluorescent microscopy confirmed the presence of biomimetic SC-shaped topography as well as the integrity and appropriate orientation of the micro-contact printed laminin stripes (Figure 2). The underlying SC pattern was confluent and highly aligned. Corresponding views of phase and fluorescence images illustrate the combined presence and independent orientation of biochemical and topographical cues. Fluorescence microscopy confirmed that laminin stripes had 60um width and pitch and were continuous and uninterrupted by the topography.

DRG Alignment: Orientation

Primary neonatal rat DRG were harvested, dissociated, and plated on the experimental and control samples at 188,000 cells/well on a 12 well plate. After 5 days of incubation in 37 C, 5% CO_2, cells were fixed and stained with DAPI to visualize nuclei and stained for NF to assess overall neuronal alignment and morphology.

DRG alignment to either biochemical or topographical cues was assessed via measuring nuclear alignment of DAPI-stained nuclei and summarized in the form of circular histograms (Figure 4). It has been previously demonstrated that nuclear alignment correlates strongly with cellular alignment[22, 40, 44]. Nuclear data are bi-axial, and thus data sets are mirrored between 0-180 degrees and 180-360 degrees. Circular histograms summarize population orientation as follows: the direction of the long axes of the nuclei are grouped into bins of 10 degrees and plotted on a circular diagram. The direction of each bar in the diagram corresponds to the binned direction of nuclei, and the length of the bar represents the number of nuclei for that particular bin.

As summarized in Figure 4 and Table 1, oriented single cue control conditions resulted in significant DRG alignment parallel to the cue (V-test, $p<0.001$). When cells encountered protein stripes on a flat substrate, the mean vector deviated from the direction of the stripes by 1.4 degrees (99% confidence interval (CI) = 0.9 to 1.9 degrees, 26,744 cells measured). Presenting cells with aligned cellular topography resulted in a mean vector that deviated from the direction of the topography by 2.1 degrees (99% CI = 0.9 to 3.4 degrees, 25,487 cells measured). Both single-cue conditions resulted in highly aligned distributions (Rao's spacing test $p < 0.01$). As expected, cellular alignment on flat control samples with homogeneous laminin coating was not significantly different from a uniform distribution (Rao's spacing test; $p > 0.10$, 35,179 cells measured).

Experimental conditions with combined biochemical and topographical directional cues generated the following results: parallel presentation of laminin and SC pattern resulted

in a significantly non-uniform cell population (Rao's spacing test; $p < 0.01$) that was aligned (V-test $p < 0.001$) to the parallel cues within 0.1 degrees (99% CI = -0.3 to 0.5 degrees, 35,289 cells measured). When laminin and topography were orthogonal, cells aligned (Rao's spacing test; $p < 0.01$, 30,177 cells measured) in the direction of the protein cue (V-test $p < 0.001$).

DRG Alignment: Strength

To assess the relative strength of cellular alignment, we computed the mean vector for each cell population per experimental condition (Figure 5). Pertaining to circular analysis, the mean vector represents the normalized vector sum of the individual vectors as represented by the length and direction of the individual bins. A mean vector length of 1 represents total alignment, and a mean vector length of 0 represents no alignment.

As expected, the flat control sample with homogeneous laminin coating displayed the lowest degree of alignment with a mean vector length of 0.027. The other single cue controls displayed cell alignment with mean vector lengths 0.58 and 0.26, for laminin stripes on flat substrates and "topography only" substrates, respectively. The highest alignment was obtained when the biochemical and topographical cues were arranged in parallel, with a mean vector length of 0.60. When the orientation of the two cues was changed to be orthogonal, the resulting alignment was the second-lowest alignment with a mean vector length of 0.50, only surpassing the flat homogeneously coated control sample. Combining cues did not result in additive or synergistic alignment strengths under the conditions tested.

SC-Alignment: Orientation

To assess the ability of cellular topography to affect the behavior of SCs, we have seeded SCs onto biomimetic substrates and analyzed nuclear alignment in daily intervals for a period of 5 days. Experimental design closely followed the setup described for DRGs above; however, the experiment provides an overview of how alignment develops and changes over time in addition to the data gathered for DRGs. Alignment results are summarized in Figure 7 and Table 2.

As expected, SCs on flat control substrates were randomly oriented, and the directions of their nuclei were uniformly distributed over the entire period of 5 days (Rao's spacing test $p > 0.1$). Single cue substrates, both flat substrates with laminin stripes as well as "topography only" substrates, resulted in populations of aligned SC nuclei (Rao's spacing test $p < 0.01$). The direction of the mean vector in each case was within 13 degrees of the cue over the entire course of the experiment. Substrates with combined topographical and directional protein cue also resulted in aligned SC nuclei (Rao's spacing test, $p < 0.01$); however, the direction of the mean vector depended on the relative direction of the cues presented. When both physical and chemical cues were parallel, the resulting mean vector of SC nuclei aligned with the cues and stayed within 12 degrees over the course of the experiment. When the cues were arranged orthogonally, the mean vector initially lined up with the protein cue within 1.2 degrees on day 1. Over the course of the experiment, however, the direction of the mean vector diverged from the direction of the protein cue, reaching its maximum on day 3 with 42 degrees discrepancy between cell orientation and

protein stripe orientation. During day 4 and day 5, the directions of the mean vector of SC nuclei re-aligned, but the discrepancy never dropped below 9.8 degrees.

SC-Alignment: Strength

The mean vector lengths for the nuclear alignment of SCs on biomimetic substrates with varying protein cues are summarized in Figure 8. Homogenously laminin coated flat substrates showed the lowest alignment, with a mean vector maximum length of 0.069 on day 4. As with the DRG alignment studies, highest alignment at all time points was achieved with a combination of topography and protein cues presented in parallel, with a maximum mean vector of 0.689 on day 3. The second highest alignment was consistently observed on flat substrates with laminin stripes, with a maximum mean vector of 0.673 on day 3. The third highest alignment on day 2-5 was measured on "topography only" substrates with homogeneous laminin coating, with a maximum mean vector of 0.592 on day 3. After day 1, alignment on substrates with orthogonal cues was consistently lower than on any other substrates with the exception of the flat homogeneously coated controls. SC nuclei on orthogonal cues reached a maximum alignment on day 1, with a mean vector length of 0.545. The general hierarchy of alignment according to mean vector length after day one presents itself as follows (highest to lowest): parallel cues, protein cue, topographical cue, orthogonal cues, no directional cue. The alignment strength of combined cues was neither additive nor synergistic.

Discussion

This study is the first to characterize the combined effects of cellular topography and molecular guidance cues. By combining biomimetic SC-shaped topography with uCP laminin stripes that are oriented independently of the morphology of the substrates, we established that, under the conditions tested, protein cues dominate over topographical cues. The novelty over existing literature lies in the biomimetic nature of the topography, which closely mimics the natural shape of SCs down to the nanoscale. The findings of this study explore both neural and glial behavior and are relevant to optimize biological responses to implant materials after nerve injury.

In contrast to other conflicting cue studies[22, 23], the uCP laminin stripes are continuous and uninterrupted by the topographic undulations of the substrate surface and are presented overlaid onto the topography. The technology used to fabricate these substrates is easily scalable to larger surfaces and could be readily transferred to metal surfaces via a recently developed method of explosive embossing[45].

Circular statistics provide a high degree of accuracy in displaying and analyzing the alignment results. Where previous studies [25, 26, 39] have presented alignment in terms of number of cells oriented within 10 or 20 degrees of the cue, circular statistics take into account the *entire* cellular population per analyzed area and can integrate the results to form a mean vector. Thus, circular statistics provide a more complete picture of the orientation of a cellular population in response to various cues. The use of circular statistics was facilitated by utilizing nuclear orientation as a marker for cellular

orientation. At the cell densities employed in these studies, neurite (neurofilament-positive) morphology is too dense and too complex to appropriately measure cellular orientation on a per cell basis. However, even at high densities, nuclei remained discrete, easily imaged and threshholded entities of near homogeneous size, which makes them suitable for automated analysis. Previous studies have established that nuclear orientation correlates strongly with cellular orientation[40]. Thus, results of the present studies are based on quantitative assessment of nuclear orientation and backed up by qualitative immunofluorescence analysis where appropriate.

DRG Alignment

The single-cue DRG substrates confirmed previous findings: both cell-shaped topography[44] and protein stripes[40] were capable of strongly aligning DRG outgrowth when presented singly. Comparing the mean vectors of the protein stripe and the topography only condition indicated that the protein cue conferred stronger alignment than the topographic cue. Discrepancies of cellular alignment with the underlying cue corresponded well with values cited in the literature, which were on the order of 10 degrees[22] and may result from stochastic noise in cellular behavior[46] and/or from artifacts stemming from manual alignment of substrates to the vertical imaging direction of the microscope.

Results from parallel cue setups indicated that parallel cues enhanced the resulting alignment, but did not act additively or synergistically, in contrast to previous reports[25, 26]. Britland et al. observed that the combined effects on cellular alignment of parallel

protein tracks and grooved topography exceeded those of the sum of each cue alone. Specifically, they found that almost 100% of all DRGs aligned to parallel cues when the groove dimensions were 2 um wide, 6 um deep, and overlaid with 25 um wide protein stripes. While we could not detect any synergism in our study, the non-additive nature does confirm earlier reports that the integration of these cues is interdependent[22]. While the exact mechanism underlying this result cannot be determined with the data at hand, these results support several possibilities. First, each cue could function via an independent pathway from the other cue, and each cue alone is strong enough to confer a near-maximum alignment. Hence, adding two cues in parallel would not enhance the net alignment in an additive fashion, since a summation of the alignment caused by each cue would exceed the maximum alignment possible. Second, the cues could work through a common pathway, and one cue alone is sufficient for large scale activation of the pathway. In this case, adding a second cue would just marginally saturate the already activated pathway, and thus not confer a significant increase in overall alignment. In both cases, alignment strengths with a mean vector below "1" could result from stochastic noise inherent to all cellular systems.

The fact that these experiments did not match previous findings can have a number of reasons. It is very likely, that the cellular behavior is sensitive to small alterations of the experimental conditions[25]. Britland et al. utilized geometric rectangular grooves with orthogonal protein cues and thus had a different setup than was examined in this study. Biomimetic topography differs significantly from geometric topography employed in previous studies in a variety of factors: surface roughness, edge sharpness, number of

discontinuities, homogeneity of feature sizes, and size of surface features. In addition, previous studies showed that DRG alignment is cell-density dependent[44], and thus Britland's lower density (5,000 cells/cm^2 compared to 50,000 cells/cm^2 used in this study) may have contributed to differential findings. This study strived to assess alignment responses at or near confluence on biomimetic substrates in order to best approximate in-vivo conditions.

Exposing DRGs to orthogonal cues resulted in an aligned distribution with a mean vector parallel to the protein cue and a magnitude smaller than in a protein-only condition. This result indicates that the protein cue exerted a dominant effect over the topographical cue and that DRGs were capable of integrating both classes of cues at the same time. These findings correspond to previous reports and extend the findings to biologically relevant topography.

Qualitative observations of cellular behavior on orthogonal cues showed that cells initially adhered to the protein stripes and preferentially aligned to them during the first hours of culture. Subsequently, cellular alignment to protein cues weakened, yet remained predominantly aligned in parallel with the protein stripe orientation. This trend does not result from a loss of laminin from the substrate surface. Immunofluorescent densitometry directed against laminin confirmed that the strength of the protein cue did not diminish over time under culture conditions (Figure S1).

SC Alignment

In vivo, SCs mediate regenerative responses in the peripheral nervous system. Initially, SCs and macrophages migrate into the site of an injury and clear any remaining cellular debris. As time progresses, the macrophages retreat, and SCs begin to align to each other and environmental stimuli. Subsequent topographical and biochemical guidance conducted by SCs promotes axonal outgrowth of adjacent neurites and directs re-generating growth cones. Therefore, we think it is valuable to not only characterize neuronal responses to biomimetic guidance cues, but it is equally important to analyze SC response to these factors. A successful implant should be optimized to direct SC and neuronal growth after injury. Thus, we assessed the alignment response of SCs to biomimetic substrates over 5 days.

In general, the results for SCs mirrored those obtained for DRGs. Single cues aligned cellular populations along their orientation. In multiple cue scenarios, parallel presentation of cues resulted in non-additive, non-synergistic enhancement of the alignment response over single cues. Orthogonal cues diminished alignment and broadened the distribution of nuclear directions, with the exception of day 1. During days 2-5 of the experiment, there was a clear hierarchy of cues as determined by the magnitude of the mean vector of SC populations cultured on each cue / combination of cues. Flat striped and parallel cues resulted in maximum alignment, closely followed by topography only. Orthogonal cues resulted in mean vector magnitudes of about two-thirds of the maximum alignment conditions. This stands in contrast to day 1, where the topography-only and the orthogonal cues' hierarchy was switched: orthogonal cues rank second after

parallel and flat striped conditions, and topography-only substrates showed about half of the alignment of the other conditions measured.

These results support a theory of delayed sensitivity to topographic guidance cues. Cues involving protein stripes (parallel, flat stripe, and orthogonal) displayed high alignment on day 1 of the study (Figure 8), in that the corresponding direction of nuclear alignment correlated with the direction of the protein stripes. In other words, the SCs were sensitive to the direction of the protein stripes early on. However, alignment to the topography only substrate was low on day 1, possibly indicating a diminished sensitivity to topographical cues following plating. This notion is reinforced by the alignment data collected on day 2: mean vector magnitude in response to topography-only was high, and the SCs were responding to the aligned biomimetic topography. In the case of orthogonal cues, where topography confounds alignment to protein cues, we recorded a 50% diminished magnitude of the mean vector, indicating that the SCs did integrate both conflicting cues on day 2. Further experiments will have to be conducted to confirm this theory. If ascertained, this could indicate a complex interplay for long and short term guidance in vivo. Topographical cues could give a slow-acting, long-term directional bias for cell and cell-process locomotion, and substrate-bound or cell-cell cues could be the dominant, short-acting guidance cues that are amenable to quick regulation. Together, these two mechanisms could provide long- and short-range guidance, ensuring that cellular processes reach large target areas without close, high-dose biochemical guidance, while keeping cells more responsive to quicker, temporally and spatially succinct biochemical cues that can enforce, supplement, or override topographical guidance.

These findings could influence the design of biomaterial implants to fine-tune cellular behavior at different size- and time-ranges. Topography could function as a director of overall alignment bias, which could be supplemented by local protein drug delivery clusters to temporally and spatially alter general cellular growth. For example, branching of smaller nerves from a main nerve may be achievable in this manner.

In this study, cellular alignment directions followed underlying directional cues as expected, with one exception. On substrates with orthogonal cues, SCs aligned initially with the direction of the protein cue on day 1. On subsequent days, the alignment deviated from the direction of the protein cue until the cellular alignment reached the half-angle between protein and topographical cues on day 3. During day 4 and 5, the alignment re-oriented towards the direction of the protein cue. While the exact mechanism remains unclear, there are some theories that could explain this behavior. It has previously been established that cells exposed to conflicting directional cues can have two spatially separated levels of cytoskeletal organization. Britland et al. found that actin stress fibers in BHK cells can be aligned to topographical features on the cell side in contact with the substrate, while the actin cytoskeleton on the top surface above are aligned with the protein cue[25]. Several publications have shown that neuronal extensions are steered by a delicate dynamic balance of retracting and extending cytoskeletal elements, most notably actin filaments in the filopodia[46-48]. Filopodia have been shown to react to topography[49-51] and biochemical cues[52, 53]. It is thus conceivable that a cytoskeleton that integrates two distinct levels of orientation within the same cell would exert a steering impulse on the cell as a whole. The theoretical direction would depend on

the relative strength of the cues and the cell's sensitivity to these cues. In this view, the transient misalignment with the protein cue in this experiment could indicate a transient heightened sensitivity to topographical cues. However, further experiments to verify this notion are necessary.

Conclusion

In this paper we present a novel method to assess the hierarchies of cellular topography and biochemical patterning on cellular alignment. Under the conditions tested, protein cues dominated over cellular topographical cues, and both DRGs and Schwann cells integrated both classes of cues simultaneously. Observations suggest but do not conclusively prove a delayed sensitivity to cellular topography compared to substrate-bound protein cues as well as a directional integration of orthogonal cues. Further work is necessary to confirm and elucidate these theories.

Acknowledgement

The authors thank the Brown Seed Fund Program, The Whitaker Foundation, the Susan and Robert Kaplan Fellowship, and NIBIB for funding, and Jennifer Mitchel for help with manuscript preparation.

Figures

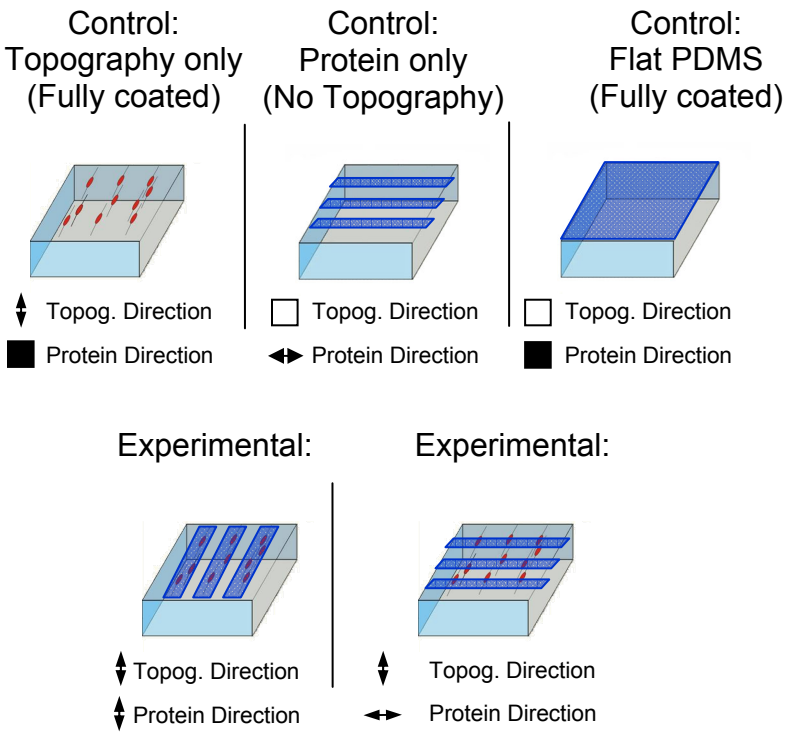

Figure 1. Cartoon overview of experimental setup conditions.

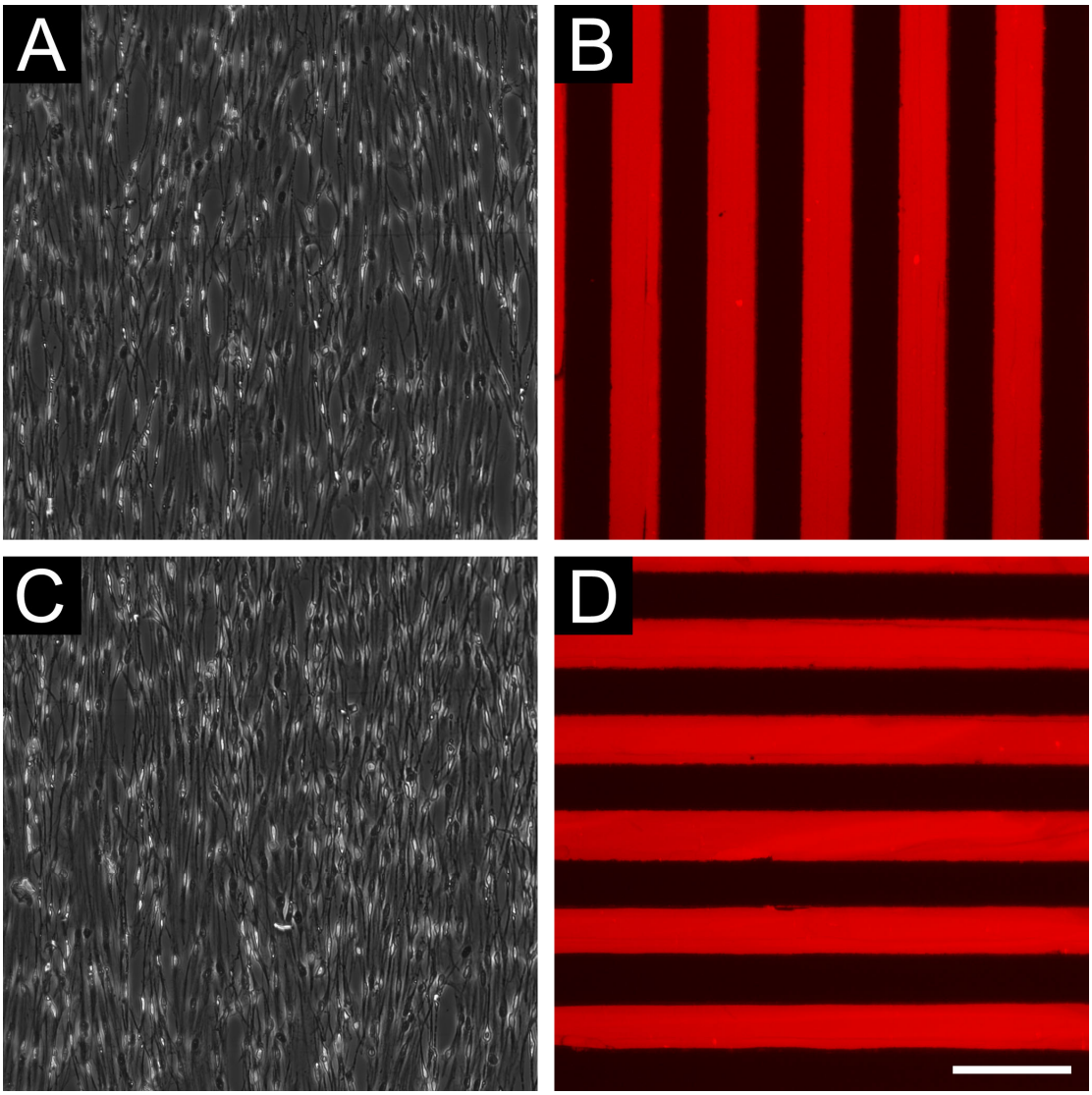

Figure 2.Independence of topographical and biochemical pattern via optical microscopy

Phase (A, C) and fluorescence (B, D) micrographs of corresponding fields of view of parallel cue (A, B) and orthogonal cue (C, D) samples showing independence of orientation of topographical (A, C) and biochemical cues (B, D). A and C display confluent biomimetic vertically aligned SC-shaped surface morphology under phase illumination. B and D show corresponding fields of view with vertical (B) and horizontal (D) immunofluorescently labeled laminin stripes under fluorescence illumination. Scale bar, 100 um.

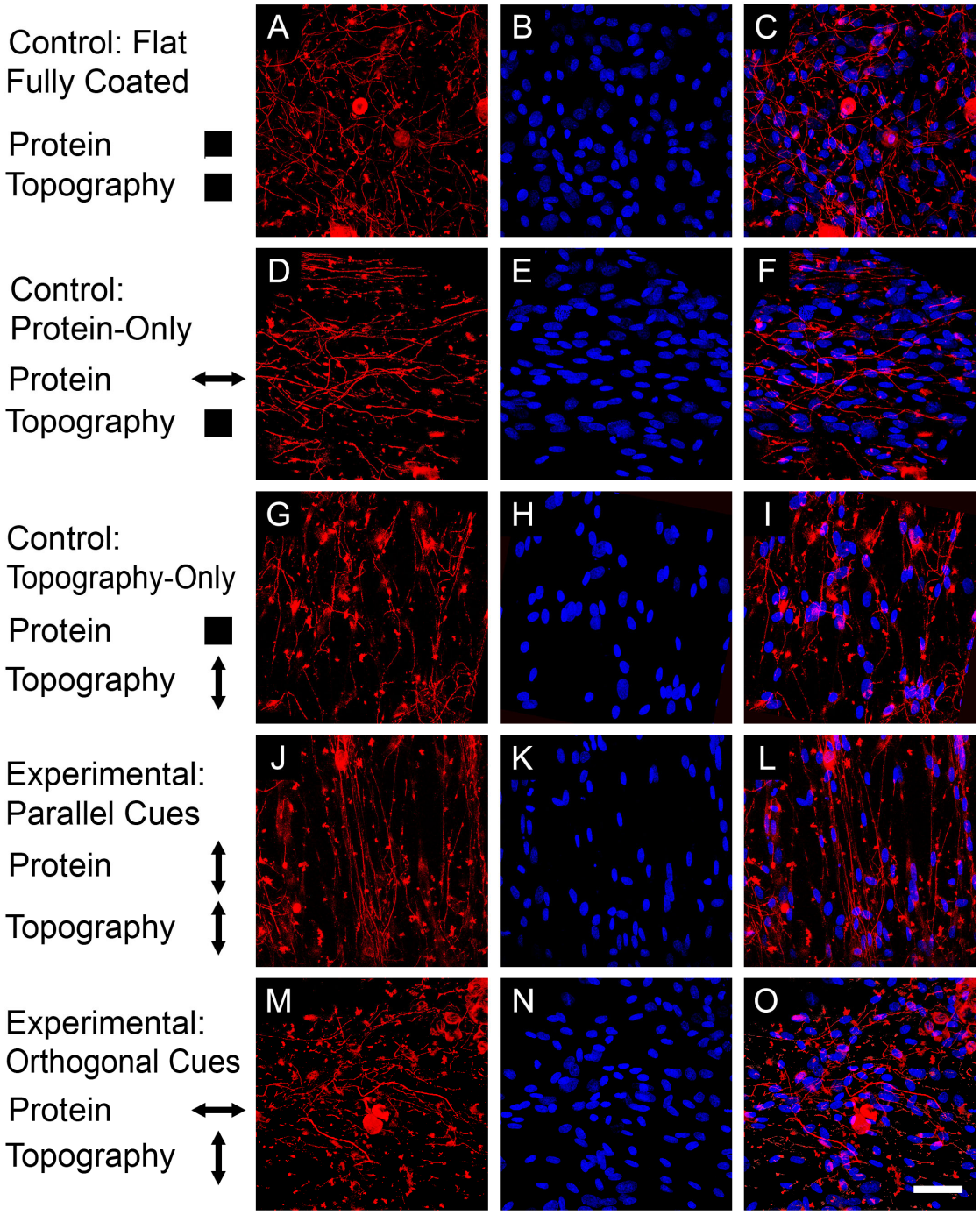

Figure 3. Confocal fluorescent micrographs showing DRG morphology.

Staining and immunolabeled are grouped by column, and substrate type is grouped by row. A, D, G, J, and M are labeled for neurofilament. B, E, H, K, and M are corresponding fields of view stained with DAPI to visualize nuclei location and orientation. C, F, I, L, and O are corresponding overlays of the two images in the same row. The nature and direction of laminin patterning and topography for each row is indicated to the left of each row. Scale bar, 50 um.

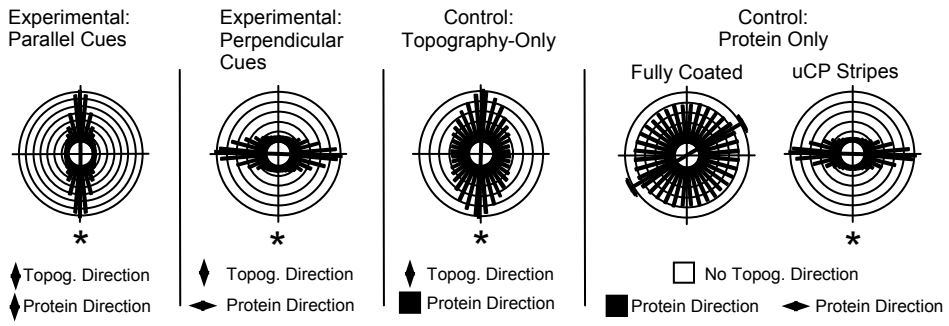

Figure 4. Circular histograms summarizing nuclear alignment of DRG cells on various substrates after 5 days of culture.

* = significantly different from a random distribution by Rao's spacing test, where $p < 0.05$ is taken to be significant. "Stripe" refers to a topographically flat PDMS surface with micro-stamped laminin stripes. N = 3 samples per condition for all samples except flat stripe (n=2) with a minimum of 25,487 analyzed cells each.

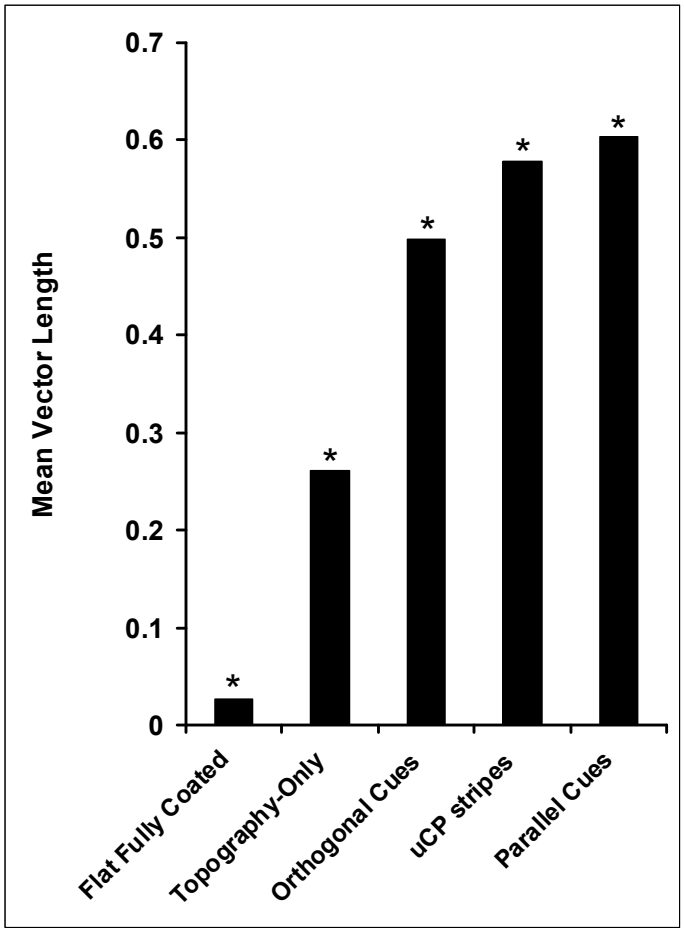

Figure 5. Bar graph depicting length of the mean vector of DRG nuclei alignment per substrate type after 5 days of culture.

Strongest alignment has a mean vector length of 1, no alignment a mean vector length of 0. * = distributions giving rise to mean vector lengths were significantly different at the $p < 0.05$ level using the Mardia-Watson-Wheeler test.

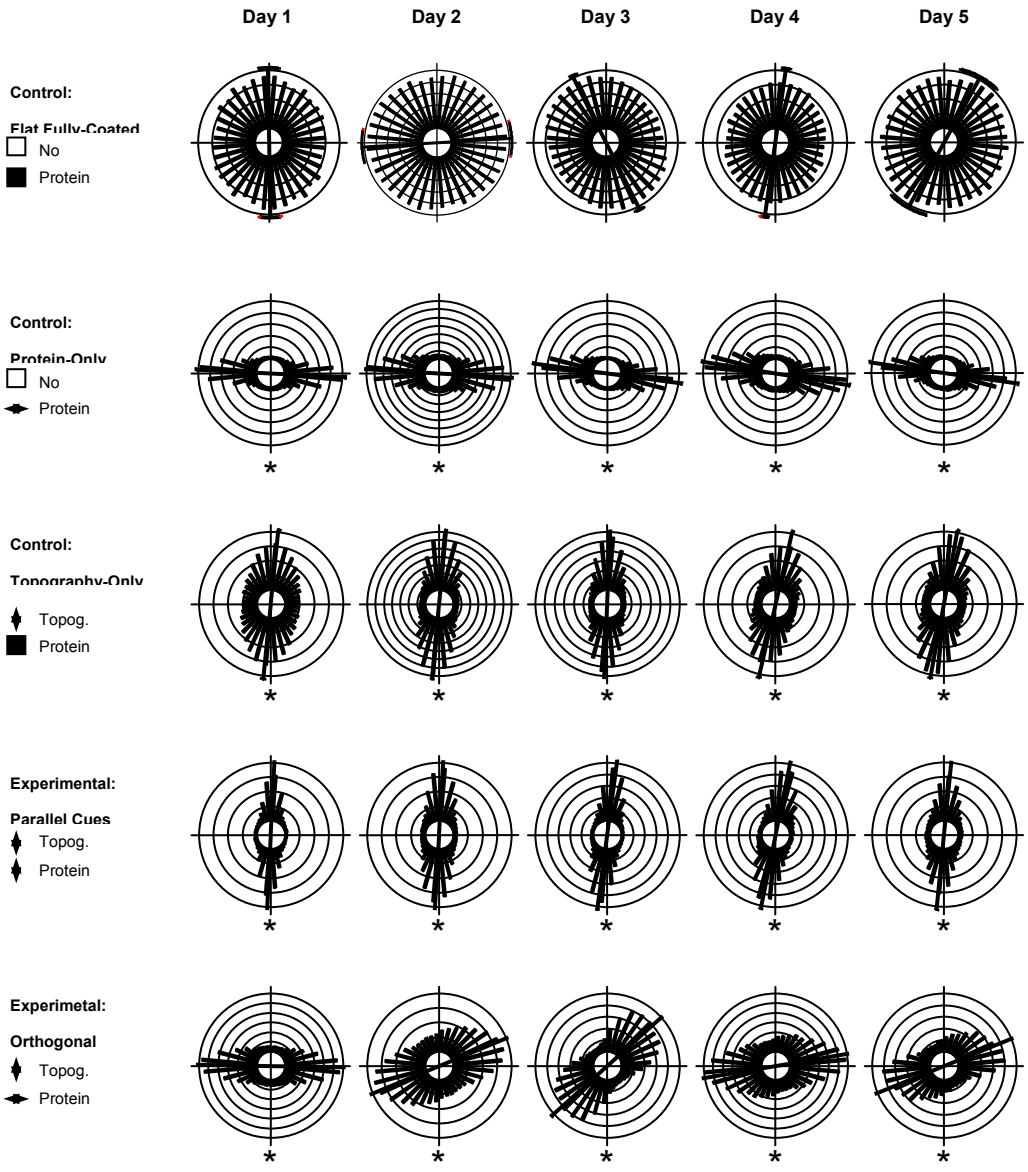

Figure 6. Circular Histograms showing orientation of SC nuclei over 5 days of culture.

* = significantly different from a random distribution by Rao's spacing test, where $p < 0.05$ is taken to be significant. N = 3 samples per condition for all samples except day 4 topography-only and day 5 fully-coated (n=2) with a minimum of 11,533 analyzed cells each.

	Day 1	Day 2	Day 3	Day 4	Day 5
Flat Fully-Coated	11,533	39,099	36,544	24,645	12,237
Protein-Only	21,024	37,211	40,611	25,617	19,390
Topography-Only	15,705	42,463	31,043	11,970	13,485
Parallel Cues	13,266	39,675	40,005	23,049	17,132
Orthogonal Cues	16,695	36,528	37,947	24,259	17,785

Table 1. Number of cells measured for each condition in figures 6 and 7.

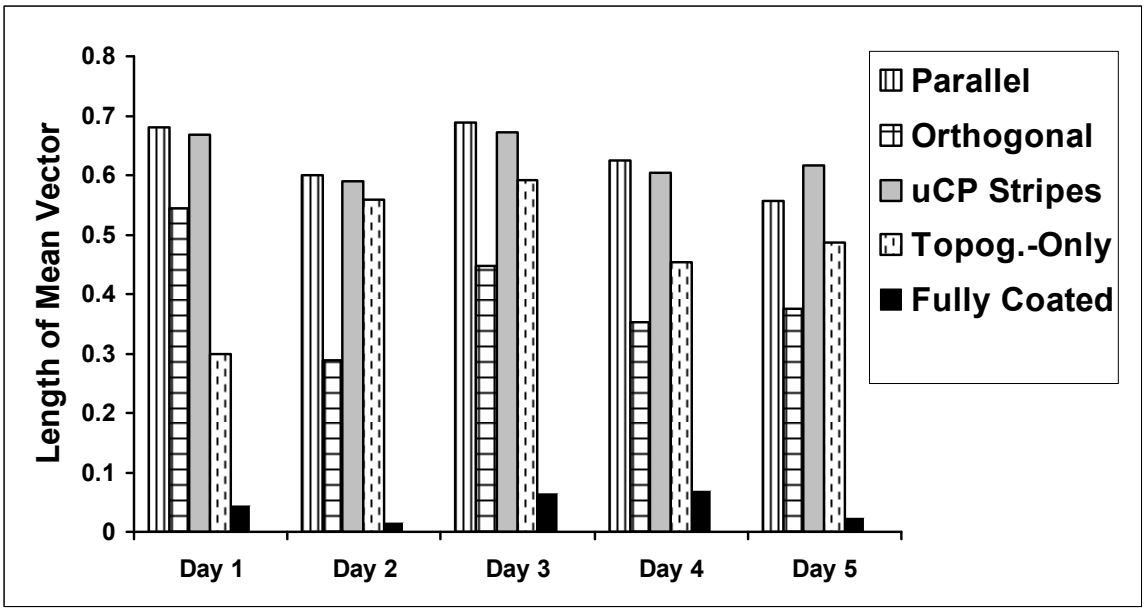

Figure 8. Bar graph of mean vector lengths of SC nuclei populations over 5 days of culture on various substrates.

SCs were seeded at 180,000 cells per well on n = 3 samples per condition for all samples except day 4 topography-only and day 5 fully-coated (n=2) with a minimum of 11,533 analyzed cells each.

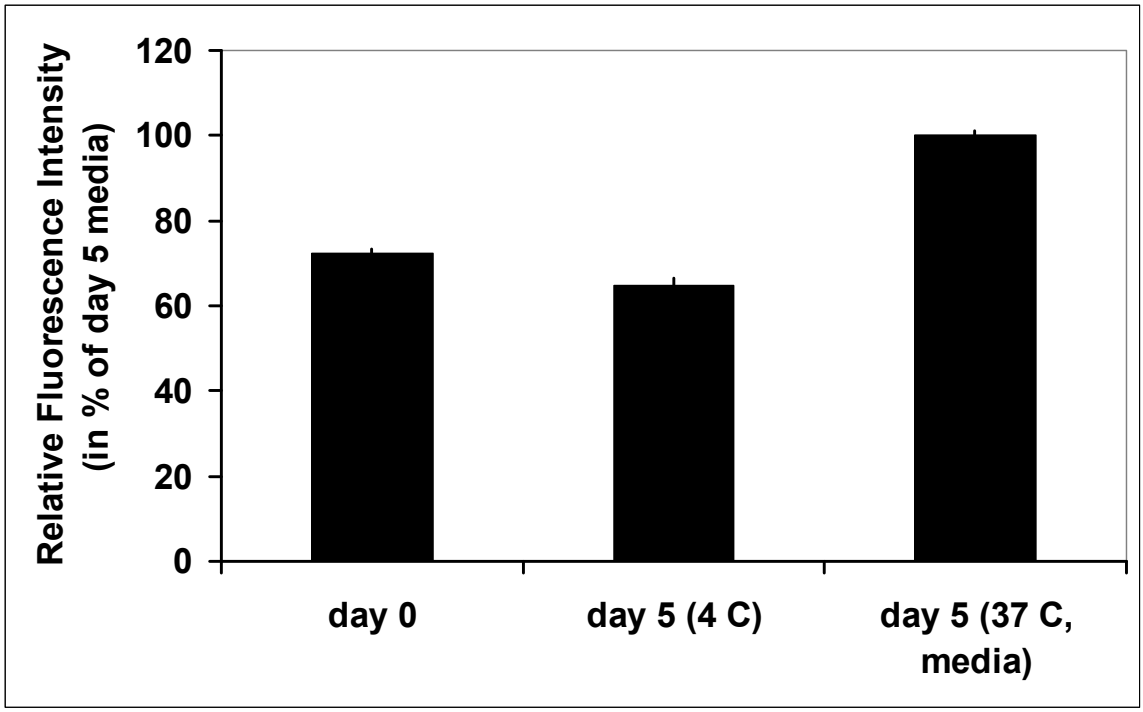

Figure S1. Bar graph representing fluorescence intensity of micro-contact printed laminin stripes at 0 and 5 days post-stamping, stored under different conditions.

Day 0 samples were fluorescently labeled and analyzed immediately after stamping. Day 5 (4C) samples were stored in PBS at 4 C for 5 days before analysis. Day 5 (37 C, media) were stored in neuronal cell culture media at 37 C, 5% CO_2. Error bars = SEM.

	Experimental Conditions		Control Conditions		
	Parallel	**Orthogonal**	**Flat Fully Coated**	**Topography Only**	**Protein Stripes Only**
number of nuclei measured	35289	30177	35179	25487	26074
Discrepancy between mean vector and direction of cue (degrees)	0.01	1.79 (with respect to protein)	n/a	2.1	1.4
Rao's Spacing test	non-uniform $p < 0.01$	non-uniform $p < 0.01$	uniform $p > 0.10$	non-uniform $p < 0.01$	non-uniform $p < 0.01$
V-Test	aligned with cues $p < 0.001$	aligned with protein cue $p < 0.001$	n/a	aligned with cue $p < 0.001$	aligned with cue $p < 0.001$

Table 2. Statistical data for DRG nuclei cultured on various substrates for 5 days.

		Experimental Conditions		Control Conditions		
		Parallel	Orthogonal (relative to protein)	Flat Fully Coated	Topography Only	Protein Stripes Only
Discrepancy between mean vector and direction of cue (degrees)	**Day 1**	2.8	1.2	n/a	5.8	2.8
	Day 2	3.2	22.4	n/a	5.2	3.3
	Day 3	7.4	42	n/a	2.6	7.6
	Day 4	11.4	9.8	n/a	12.8	8.9
	Day 5	5.5	22	n/a	10.6	8.3

Table 3. Discrepancy mean vector of orientation between SC nuclei and underlying cue.

References

1. Lutolf, M.P. & Hubbell, J.A. Synthetic biomaterials as instructive extracellular microenvironments for morphogenesis in tissue engineering. Nature biotechnology 23, 47-55 (2005).

2. Raivich, G. & Makwana, M. The making of successful axonal regeneration: Genes, molecules and signal transduction pathways. Brain research reviews 53, 287-311 (2007).

3. Clark, P., Connolly, P., Curtis, A.S., Dow, J.A. & Wilkinson, C.D. Topographical control of cell behaviour. I. Simple step cues. Development 99, 439-448 (1987).

4. Flemming, R.G., Murphy, C.J., Abrams, G.A., Goodman, S.L. & Nealey, P.F. Effects of synthetic micro- and nano-structured surfaces on cell behavior. Biomaterials 20, 573-588 (1999).

5. Song, H. & Poo, M. The cell biology of neuronal navigation. Nature cell biology 3, E81-88 (2001).

6. Suter, D.M. & Forscher, P. Substrate-cytoskeletal coupling as a mechanism for the regulation of growth cone motility and guidance. Journal of neurobiology 44, 97-113 (2000).

7. Dertinger, S.K., Jiang, X., Li, Z., Murthy, V.N. & Whitesides, G.M. Gradients of substrate-bound laminin orient axonal specification of neurons. Proceedings of the National Academy of Sciences of the United States of America 99, 12542-12547 (2002).

8. Thompson, D.M. & Buettner, H.M. Schwann cell response to micropatterned laminin surfaces. Tissue engineering 7, 247-265 (2001).

9. David, S. & Lacroix, S. Molecular approaches to spinal cord repair. Annual review of neuroscience 26, 411-440 (2003).

10. Chilton, J.K. Molecular mechanisms of axon guidance. Dev Biol 292, 13-24 (2006).

11. Mueller, B.K. Growth cone guidance: first steps towards a deeper understanding. Annual review of neuroscience 22, 351-388 (1999).

12. McCaig, C.D., Rajnicek, A.M., Song, B. & Zhao, M. Has electrical growth cone guidance found its potential? Trends in neurosciences 25, 354-359 (2002).

13. Patel, N. & Poo, M.M. Orientation of neurite growth by extracellular electric fields. J Neurosci 2, 483-496 (1982).

14. Schmidt, C.E., Shastri, V.R., Vacanti, J.P. & Langer, R. Stimulation of neurite outgrowth using an electrically conducting polymer. Proceedings of the National Academy of Sciences of the United States of America 94, 8948-8953 (1997).

15. Lofberg, J. & Ebendal, T. Substrate topography and shape of motile cells. Experientia 36, 508-510 (1980).

16. Curtis, A. & Wilkinson, C. Topographical control of cells. Biomaterials 18, 1573-1583 (1997).

17. Curtis, A.S. & Wilkinson, C.D. Reactions of cells to topography. Journal of biomaterials science 9, 1313-1329 (1998).

18. Clark, P., Connolly, P., Curtis, A.S., Dow, J.A. & Wilkinson, C.D. Topographical control of cell behaviour: II. Multiple grooved substrata. Development 108, 635-644 (1990).

19. Dalby, M.J., Riehle, M.O., Johnstone, H.J., Affrossman, S. & Curtis, A.S. Polymer-demixed nanotopography: control of fibroblast spreading and proliferation. Tissue engineering 8, 1099-1108 (2002).

20. Gallant, N.D., Charest, J.L., King, W.P. & Garcia, A.J. Micro- and nano-patterned substrates to manipulate cell adhesion. Journal of nanoscience and nanotechnology 7, 803-807 (2007).

21. Li, N. & Folch, A. Integration of topographical and biochemical cues by axons during growth on microfabricated 3-D substrates. Exp Cell Res 311, 307-316 (2005).

22. Charest, J.L., Eliason, M.T., Garcia, A.J. & King, W.P. Combined microscale mechanical topography and chemical patterns on polymer cell culture substrates. Biomaterials 27, 2487-2494 (2006).

23. Gomez, N., Chen, S. & Schmidt, C.E. Polarization of hippocampal neurons with competitive surface stimuli: contact guidance cues are preferred over chemical ligands. Journal of the Royal Society, Interface / the Royal Society 4, 223-233 (2007).

24. Britland, S. & McCaig, C. Embryonic Xenopus neurites integrate and respond to simultaneous electrical and adhesive guidance cues. Exp Cell Res 226, 31-38 (1996).

25. Britland, S. et al. Synergistic and hierarchical adhesive and topographic guidance of BHK cells. Exp Cell Res 228, 313-325 (1996).

26. Britland, S. et al. Morphogenetic guidance cues can interact synergistically and hierarchically in steering nerve cell growth. Exp Biol Online 1 (1996).

27. Berry, C.C., Dalby, M.J., McCloy, D. & Affrossman, S. The fibroblast response to tubes exhibiting internal nanotopography. Biomaterials 26, 4985-4992 (2005).

28. Eisenbarth, E., Meyle, J., Nachtigall, W. & Breme, J. Influence of the surface structure of titanium materials on the adhesion of fibroblasts. Biomaterials 17, 1399-1403 (1996).

29. Eriksson, C., Lausmaa, J. & Nygren, H. Interactions between human whole blood and modified TiO2-surfaces: influence of surface topography and oxide thickness on leukocyte adhesion and activation. Biomaterials 22, 1987-1996 (2001).

30. Dalby, M.J., Marshall, G.E., Johnstone, H.J., Affrossman, S. & Riehle, M.O. Interactions of human blood and tissue cell types with 95-nm-high nanotopography. IEEE transactions on nanobioscience 1, 18-23 (2002).

31. Dalby, M.J. et al. Increasing fibroblast response to materials using nanotopography: morphological and genetic measurements of cell response to 13-nm-high polymer demixed islands. Exp Cell Res 276, 1-9 (2002).

32. Rompen, E., Domken, O., Degidi, M., Farias Pontes, A.E. & Piattelli, A. The effect of material characteristics, of surface topography and of implant components and connections on soft tissue integration: a literature review. Clinical oral implants research 17 Suppl 2, 55-67 (2006).

33. Curtis, A.S., Dalby, M. & Gadegaard, N. Cell signaling arising from nanotopography: implications for nanomedical devices. Nanomedicine (London, England) 1, 67-72 (2006).

34. Donoghue, J.P. Connecting cortex to machines: recent advances in brain interfaces. Nat Neurosci 5 Suppl, 1085-1088 (2002).

35. Lebedev, M.A. & Nicolelis, M.A. Brain-machine interfaces: past, present and future. Trends in neurosciences 29, 536-546 (2006).

36. Patil, P.G. & Turner, D.A. The development of brain-machine interface neuroprosthetic devices. Neurotherapeutics 5, 137-146 (2008).

37. Meredith, D.O., Riehle, M.O., Curtis, A.S. & Richards, R.G. Is surface chemical composition important for orthopaedic implant materials? Journal of materials science 18, 405-413 (2007).

38. Chen, Z.L., Yu, W.M. & Strickland, S. Peripheral regeneration. Annual review of neuroscience 30, 209-233 (2007).

39. Thompson, D.M. & Buettner, H.M. Neurite outgrowth is directed by schwann cell alignment in the absence of other guidance cues. Annals of biomedical engineering 34, 161-168 (2006).

40. Thompson, D.M. & Buettner, H.M. Oriented Schwann cell monolayers for directed neurite outgrowth. Annals of biomedical engineering 32, 1120-1130 (2004).

41. Bruder, J.M., Monu, N.C., Harrison, M.W. & Hoffman-Kim, D. Fabrication of polymeric replicas of cell surfaces with nanoscale resolution. Langmuir 22, 8266-8270 (2006).

42. Goldner, J.S., Bruder, J.M., Li, G., Gazzola, D. & Hoffman-Kim, D. Neurite bridging across micropatterned grooves. Biomaterials 27, 460-472 (2006).

43. Morrissey, T., Kleitman, N. & Bunge, R.P. Isolation and functional characterization of Schwann cells derived from adult peripheral nerve. Journal of Neuroscience 11, 2433-2442 (1991).

44. Bruder, J.M., Lee, A.P. & Hoffman-Kim, D. Biomimetic materials replicating Schwann cell topography enhance neuronal adhesion and neurite alignment in vitro. Journal of biomaterials science 18, 967-982 (2007).

45. Scholz, T., Kraft, A., Reithmeier, E. & Helferich, G. in Experimental Analysis of Nano and Engineering Materials and Structures, Vol. C. (ed. E.E. Gdoutos) 587-588 (Springer Netherlands, 2007).

46. Maskery, S.M., Buettner, H.M. & Shinbrot, T. Growth cone pathfinding: a competition between deterministic and stochastic events. BMC Neurosci 5, 22 (2004).

47. Gallo, G. & Letourneau, P.C. Regulation of growth cone actin filaments by guidance cues. Journal of neurobiology 58, 92-102 (2004).

48. Gallo, G. & Letourneau, P.C. Axon guidance: A balance of signals sets axons on the right track. Curr Biol 9, R490-492 (1999).

49. Dalby, M.J., Gadegaard, N., Riehle, M.O., Wilkinson, C.D. & Curtis, A.S. Investigating filopodia sensing using arrays of defined nano-pits down to 35 nm diameter in size. The international journal of biochemistry & cell biology 36, 2005-2015 (2004).

50. Dalby, M.J., Riehle, M.O., Johnstone, H., Affrossman, S. & Curtis, A.S. Investigating the limits of filopodial sensing: a brief report using SEM to image the interaction between 10 nm high nano-topography and fibroblast filopodia. Cell biology international 28, 229-236 (2004).

51. Rajnicek, A. & McCaig, C. Guidance of CNS growth cones by substratum grooves and ridges: effects of inhibitors of the cytoskeleton, calcium channels and signal transduction pathways. Journal of cell science 110 (Pt 23), 2915-2924 (1997).

52. Grabham, P.W., Reznik, B. & Goldberg, D.J. Microtubule and Rac 1-dependent F-actin in growth cones. J Cell Sci 116, 3739-3748 (2003).

53. Gomez, T.M., Robles, E., Poo, M. & Spitzer, N.C. Filopodial calcium transients promote substrate-dependent growth cone turning. Science (New York, N.Y 291, 1983-1987 (2001).

Chapter 6

Conclusions and Future Directions

Neurite Bridging (Chapter 2)

A subset of neuronal (chapter 2) and non-neuronal cells (Appendix A) are capable of detaching from their substrate and forming cellular bridges across grooves of up to 300 um width and 50 um depth. While the exact cellular mechanism remains to be determined, tension generation within a bridging cell clearly plays an important role in this process. We have conducted pilot studies using cytoskeletal inhibitors against actin and tubulin dynamics, such as phalloidin and taxol, but found that we could not titrate their levels low enough to maintain bridge formation over 24 h of culture. Clearly, uninhibited actin and tubulin dynamics are essential for bridge formation. Our lab is currently investigating the dynamics of bridging to gain insight into the forces generated during these processes. Modelling speeds, geometries, elasticity, and weight of substrate and cell components may help quantify the magnitude of forces involved in cellular bridging. Without a doubt, these forces are considerable, as anecdotal evidence suggests substrate deformation in the area of cellular bridges. (See appendix B).

Bridging has a number of potential long term implications that merit a brief mentioning in this text. First, studies have indicated that neurites under tension display a density in calcium channels that is more than twice that of neurites at rest [1-3] (and personal communication with Dr. B. Pfister). The finding that the shape of the external cell

environment can promote tension generation in a subset of cells could indicate that the geometry of the extracellular environment can feed back into the biochemical base levels of calcium, a very potent regulator of neural behavior[4, 5]. It is also conceivable that cytoskeletal mechanisms such as the contractility machinery involving actin/myosin can be utilized to bias calcium levels as part of a feedback loop involving the external cell environment, including tension generated by physically connected cells. This agrees well with findings on haptotactic and durotactic cell guidance by substrate strains amassed in the recent decade[6-8]. Carefully tailored biomaterials could benefit from knowledge that links internal cellular chemistry to easily-controlled environmental factors such as pore size and material stiffness.

Second, the mechanical interaction between ECM and cellular behavior is clearly a bilateral relationship. Some reports indicate that cortex shape is a logical result of cell-cell interactions in the form of tension[9]. Understanding and ultimately controlling factors governing tension generation of neuronal cells could help to understand and repair brain tissue at the organ level. If we understand how mechanics and biochemistry at a cellular level affect whole organ dynamics, we can influence wound healing processes at a cellular and organ scale using localized mechanical or pharmaceutical interventions.

Third, the course of discovery points towards a potential theory, in which tension is a mediator of long term potentiation and memory reinforcement[10]. More and more studies link the mechanical interactions of scaffolding proteins to changes in their activity via changing relative conformations and positions of proteins anchored on the same scaffold

protein[11-13] or alter the strength and duration of interactions via "catch-bonds"[14]. Thus, increased tension could mediate a change in enzyme activities for example, which in turn could reduce the activation threshold for a nerve impulse. Thus, tension could directly and dynamically influence the functionality of neurons through their mechanical interactions with each other and their extracellular environment[15]. Regulation of these dynamics would depend equally on intracellular regulation of biochemical dynamics, such as ion channel expression, or tension generation via the cytoskeleton, but it would also depend on substrate stiffness, on tension generated by adjacent cells, and on tension propagated through the tissue as a whole. Thus, cellular behavior is not only dependent on the local and global *biochemical* environment in an organ system, but is also intricately linked to the local and global *mechanical* milieu in a tissue.

More immediate future directions are the following:

1) One could re-visit the use of cytoskeletal inhibitors to identify cellular components involved in bridge formation. A good strategy would be to identify protein targets starting with the extracellular cell surface and then follow known mechanical transduction pathways[16] towards the intracellular space: for example, one could inhibit components of the focal adhesion complex (integrins, talin, vinculin, FAK) and check whether bridging still occurs. Working inwards, one could then target actin and tubulin and spend more time titrating the dosage. Also, short pulses of inhibitors followed by observation of existing bridges may prove to be more feasible than low dose long term experiments. Next candidates would be the cytoskeletal associated proteins such as filamin, to see whether the organization of the cytoskeletal fringe is important for bridge formation. This

could be followed by inhibiting the upstream regulators such as ROCK, Rho, or Cdc42 or their effector proteins such as myosin. The expected results would be that inhibition of any of these cytoskeletal mediators disable bridge formation; however, if one component fails to de-activate bridging, one could reverse-engineer the cytoskeletal machinery that is involved in bridging by a process of exclusion. Other avenues of inhibition of particular cellular elements could be explored via RNAi as a means of selectively reducing activity.

2) One could consider bridging dynamics as a stochastic phenomenon. Most cells align to grooved substrates in accordance with the principle of contact guidance. Only 2-3% of a given cell population will form bridges. If one assesses the migration and orientation of a population of cells over time, one could attempt to prove that bridge formation is the result of stochastic misalignment to underlying substrate patterns, in other words “noise” in a system of general alignment. These studies could go hand in hand with a gradual variation of substrate parameters, such as groove depth and groove width, but also less obvious parameters such as edge radius. It is conceivable that the cytoskeletal assembly/disassembly rates underlying cellular dynamics are mechanically biased to extend faster on flat substrates than over substrate discontinuities, thus evoking a steering response during multiple encounters with a discontinuity. A systematic change of edge sharpness could provoke a “dose response” phenomenon between bridging frequency and edge radius in this case.

3) To explore the biochemical details in cells under tension, one could artificially stretch neurons and perform measurements on their physiology, morphology, and biochemistry on several levels. Surface stains could identify changes in surface protein densities, such as the aforementioned change in calcium channel density. This could lead to further insight into the physiological relevance of neuronal tension generation. One could also run gene expression profiles, comparing stretched and un-stretched neurons to identify cellular pathways that are activated when neurons are mechanically challenged. These findings could feed back into the biochemical identification of molecular changes in stretched neurons. Potential targets here would be the abundance of scaffolding proteins that function as mechanical linkers for proteins that are functionally relevant for membrane potential maintenance and neurotransmitter vesicle dynamics. Findings of these studies would also be directly applicable to understanding the processes that affect nerve cells during and immediately after mechanical trauma.

Overall, I believe that bridging opens up avenues of research into different directions beyond the realm of neuronal cells, some of which may have potential to unravel fundamental mechanisms of mechanical cellular interactions with each other and their ECM on a per cell level and as part of a tissue and organ system.

Fabrication of Biomimetic Materials (Chapter 3)

We have demonstrated the fabrication of topographically biomimetic replicas of cell surfaces with nanoscale resolution. The technique is applicable to all adherent cell types and a wide variety of polymers. We demonstrated replication of Schwann cells and

smooth muscle cells using poly-(dimethyl siloxane) and poly-urethane. Polymers suitable for this approach need to be flowable and slightly elastic to facilitate release from the template. With these novel materials, for the first time, we can explore the impact of cellular topography on cellular behavior in the absence of any anisotropic biochemical cues.

Future directions for this technique include the following points:

1) Adapt and explore the use of double-replica molding on a greater variety of polymers, particularly biodegradable polymers such as PLA, PLGA, or PVA. These materials could form the basis of novel implant designs.

2) Design and fabricate suitable control materials that mimic the surface parameters of biomimetic substrates (root mean square surface roughness (RMS), average surface roughness (Ra), surface anisotropy, etc) without replicating cellular shapes. These materials could help to identify the particulars mediating cellular responses to biomimetic topography by step-wise elimination and/or modification of surface parameters. Possible candidates include micro- and nano-aggregated metal or ceramic surfaces, controlled polymer-demixed and phase-separated surfaces, and mechanically stressed (sandblasted) surfaces.

3) The fabrication of replicas mimicking ECM and cellular topography in one process and on the same substrate. This will predominantly require careful fixation of fragile tissue-like samples. Combination with flash-freezing and/or metal casting are conceivable

for this purpose. Replicas of whole tissue or organ surfaces are imaginable (see appendix D). These platforms could be used to assess cellular responses to complex cell-ECM mixtures.

Cellular Response to Biomimetic Substrates (Chapter 4)

We have demonstrated that aligned biomimetic SC-shaped relief replicas are capable of enhancing neuronal adhesion, motility, and alignment. Unpublished results extend these findings to impression replicas (appendix E).

Future directions for this technique include:

1) The assessment of cellular behavior to biomimetic substrates that are replicating cell types other than Schwann cells. Two of my colleagues have already begun this work and are underway to determine neuronal cell behavior on astrocyte and fibroblast shapes, and human umbilical vein endothelial cell response to smooth muscle cells.

2) The assessment of the effect of biomimetic topography on cellular differentiation, particularly focusing on stem cells. Since recent findings indicate that topography can alter gene expression[17], the notion that topography can influence differentiation appears plausible and first attempts towards this direction have been made[18]. Stem cells are commonly induced by biochemical factors[18]; however, topography could pose an alternative or supplemental strategy that could open avenues to new treatment strategies governed by topographical control of differentiation behavior.

3) Exploration of commonalities and differences between cellular behavior on indented and protruding topography. Since impression replica and relief replica differ only in z-orientation but are identical at a micro- and nanoscale in terms of their relative dimensions, roughness, and angularity, findings of differential cellular reactions to these substrates could aid understanding of the cytoskeletal mechanisms involved in translating topographical information into behavioral outcomes.

4) One can use the fabrication of biomimetic replicas to separate out effects of topography and surface chemistry on a variety of substrates. For example, one could fabricate replicas of metal or ceramic surfaces with nano-resolution and test cellular response to these surface shapes in the absence of the original surface chemistry. In general, this technique could serve as a control in a wide variety of experiments.

5) Exploration of the effect of sub-cellular topography on cellular behavior. For example, one could immobilize immune-reactive substances (i.e. bacterial or viral cell wall components) on a surface and fabricate a relief replica of this surface. Subsequently, one could test the response of immune mediators to this topography. If feasible, this approach could potentially breach the barrier between surface chemistry and topography and allow the design of an entirely novel class of biomaterial surfaces.

6) Impression surfaces could potentially promote adhesion of cells/species whose impression is replicated and thus serve as a selective adhesion promoter (similar to findings from nanoimprint materials).

7) Exploration of biomimetic surface designs as part of implant technology. We have demonstrated the potential for biomimetic materials to enhance cellular outgrowth and migration in nerve guidance channels with biomimetic patterns that are oriented in parallel to the long axis of a nerve guidance channel (appendix F). Biomimetic surface engineering could also enhance vascular grafts, heart valves, bone implants, and permanent transdermal devices by streamlining cellular interactions with the material surface. All of these options need to be explored in vitro and in vivo to assess their feasibility.

Overall, the potential of biomimetic materials is just starting to emerge. I am sure that with time, new and surprising ways will be found to use this simple technology.

Conflicting Cues (Chapter 5)

We have shown that, under the conditions tested, DRGs and SCs preferentially align to substrate-bound protein cues, when these are presented orthogonally and simultaneously with aligned cell-shaped topography. We also found evidence for a delayed sensitivity of SCs to topographical cues. SC were responsive to substrate-bound laminin cues but not topographical cues at day 1. At day 2, SCs integrated both topographical and biochemical cues. Overall, no sign of additive or synergistic interactions of both types of cues was detected.

Future directions for this project include:

1) Variation of protein type. Laminin was chosen due to its strong effect on neuronal adhesion and outgrowth, and because it is a major constituent of the basil lamina and present on the surface of SCs. However, neurons encounter a large variety of proteins in vivo, and the alignment effects of other proteins, such as vitronectin or fibronectin, may help establish a hierarchy of influence of protein cues in experimental setups that more closely mimic in vivo conditions.

2) Variation of protein strength. Under the conditions tested, protein cues were dominant over topographical cues. If one lowered the concentration of protein per substrate area, one may be able to titrate the balancing point of topography and protein cues. This may grant further quantitative insight into the signal cascades involved in cellular integration of directional signals.

3) Variation of protein stripe dimensions. Previous studies have shown that the dimensions of protein stripes can have a profound influence on how well cells align to them. In order to develop an optimum alignment regime, one may want to vary the width and pitch of protein stripes.

4) Variation of cell types. We have explored SC and DRG behavior on substrates with conflicting cues, but it would be interesting to test cell types from the CNS, such as hippocampal neurons or astrocytes in these conditions. Differential behaviors could point towards biomaterial designs that prevent ingrowth of glial scar tissue while promoting neural regeneration.

5) Variation of culture times. We explored cell behavior on conflicting cues over a period of 5 days. However, implants are likely to dwell longer in their target locations, and thus an examination of cells to these surfaces over longer time spans is warranted.

Omissions. This thesis does not contain the results of my entire body of work in the Hoffman-Kim lab. During the first 2 years in the DHK lab, I rotated through all active projects at the time and contributed to gradient design, setup and analysis of gene expression data comparing neuronal growth in 2 and 3 dimensions, and initial stages of laser-guided direct writing and laser-assisted chromophore inactivation. This thesis also does not contain preliminary results obtained through collaboration with Dr. Elke-Bremus Koebberling from the Fraunhofer Institute Fuer Lasertechnik in Aachen, Germany; work which attempted to address neuronal bridging behavior in response to complex geometric substrates that were generated using laser ablation. Lastly, this thesis does not detail the preliminary results obtained in collaboration with Dr. David Laidlaw and Trevor O'Brien from the computer science department of Brown University which focuses on developing new computational 3D analysis methods to better quantitatively assess cellular orientation and volume comparisons of cells grown on non-planar surfaces. The reason for these omissions is that the preliminary nature or fragmentary mode of contribution of and to this work precludes it from a coherent write-up. Thus, in order to keep this thesis coherent as a whole, I chose to focus on the parts of my research that form a more solid narrative. If you have any questions regarding the work omitted in this document, please do not hesitate to contact me.

References

1. Jacques-Fricke, B.T., Seow, Y., Gottlieb, P.A., Sachs, F. & Gomez, T.M. Ca2+ influx through mechanosensitive channels inhibits neurite outgrowth in opposition to other influx pathways and release from intracellular stores. *J Neurosci* **26**, 5656-5664 (2006).

2. Pfister, B.J., Weihs, T.P., Betenbaugh, M. & Bao, G. An in vitro uniaxial stretch model for axonal injury. *Annals of biomedical engineering* **31**, 589-598 (2003).

3. Pfister, B.J., Bonislawski, D.P., Smith, D.H. & Cohen, A.S. Stretch-grown axons retain the ability to transmit active electrical signals. *FEBS letters* **580**, 3525-3531 (2006).

4. Gomez, T.M. & Zheng, J.Q. The molecular basis for calcium-dependent axon pathfinding. *Nature reviews* **7**, 115-125 (2006).

5. Zheng, J.Q. & Poo, M.M. Calcium signaling in neuronal motility. *Annual review of cell and developmental biology* **23**, 375-404 (2007).

6. Guo, W.H., Frey, M.T., Burnham, N.A. & Wang, Y.L. Substrate rigidity regulates the formation and maintenance of tissues. *Biophysical journal* **90**, 2213-2220 (2006).

7. Lo, C.M., Wang, H.B., Dembo, M. & Wang, Y.L. Cell movement is guided by the rigidity of the substrate. *Biophysical journal* **79**, 144-152 (2000).

8. Discher, D.E., Janmey, P. & Wang, Y.L. Tissue cells feel and respond to the stiffness of their substrate. *Science (New York, N.Y* **310**, 1139-1143 (2005).

9. Van Essen, D.C. A tension-based theory of morphogenesis and compact wiring in the central nervous system. *Nature* **385**, 313-318 (1997).

10. Peyton, S.R., Ghajar, C.M., Khatiwala, C.B. & Putnam, A.J. The emergence of ECM mechanics and cytoskeletal tension as important regulators of cell function. *Cell biochemistry and biophysics* **47**, 300-320 (2007).

11. Pawson, T. & Nash, P. Assembly of cell regulatory systems through protein interaction domains. *Science (New York, N.Y* **300**, 445-452 (2003).

12. Han, B., Lodyga, M. & Liu, M. Ventilator-induced lung injury: role of protein-protein interaction in mechanosensation. *Proceedings of the American Thoracic Society* **2**, 181-187 (2005).

13. Vollrath, M.A., Kwan, K.Y. & Corey, D.P. The micromachinery of mechanotransduction in hair cells. *Annual review of neuroscience* **30**, 339-365 (2007).

14. Thomas, W. For catch bonds, it all hinges on the interdomain region. *The Journal of cell biology* **174**, 911-913 (2006).

15. Dalva, M.B., McClelland, A.C. & Kayser, M.S. Cell adhesion molecules: signalling functions at the synapse. *Nature reviews* **8**, 206-220 (2007).

16. Zaidel-Bar, R., Itzkovitz, S., Ma'ayan, A., Iyengar, R. & Geiger, B. Functional atlas of the integrin adhesome. *Nature cell biology* **9**, 858-867 (2007).

17. Dalby, M.J. et al. Nanomechanotransduction and Interphase Nuclear Organization influence on genomic control. *J Cell Biochem* (2007).

18. Lutolf, M.P. & Hubbell, J.A. Synthetic biomaterials as instructive extracellular microenvironments for morphogenesis in tissue engineering. *Nature biotechnology* **23**, 47-55 (2005).

Final Thoughts

Over the course of my graduate education, I have tackled nerve regeneration from a basic and an applied science level. I have characterized novel cell behaviors and developed new materials. Both findings apply directly to implant optimization but also lend themselves to be used as tools to address further questions about cellular behavior in response to their environment. I do not feel that my work is done, and I think that this is as it should be. As a scientist, I stand in the beginning of my career, a career in which I hope to never run out of questions. It would be unproductive to be "done" at the end of graduate school...

Thank you to all those who supported and encouraged me over the years (you know who you are!). Your feedback, insight, and corrections have often shaped my understanding of matters big and small. It is the moments in which I stand corrected that I cherish most. Thank you!

Appendix

Appendix A

Neurite Bridging Beyond Dorsal Root Ganglia

Introduction

Topographical features in cellular environments can direct cellular functions such as activation, orientation, and migration. The observation that fibroblasts modulate their orientation in response to surface topographies gave rise to the principle of contact guidance, the phenomenon where a cell encounters a geometrical feature and is both inhibited from crossing over it and polarized along its length axis. Contact guidance has been described in regard to the response of cells to repeating grooved topographies.

We have previously reported an unusual capability of a subpopulation of DRG neurons to extend neurites that spanned across grooves of 30-300 um width and 50 um depth, with no underlying support. Here we examined the effects of topographically micropatterned substrates on process extension from a variety of cell types. Micropatterned grooved substrates were cultured with embryonic rat hippocampal neurons, rat B104 neuroblastoma cells, neonatal human fibroblasts, J2 mouse fibroblasts, A7r5 rat smooth muscle cells, or adult rat Schwann cells.

Methods

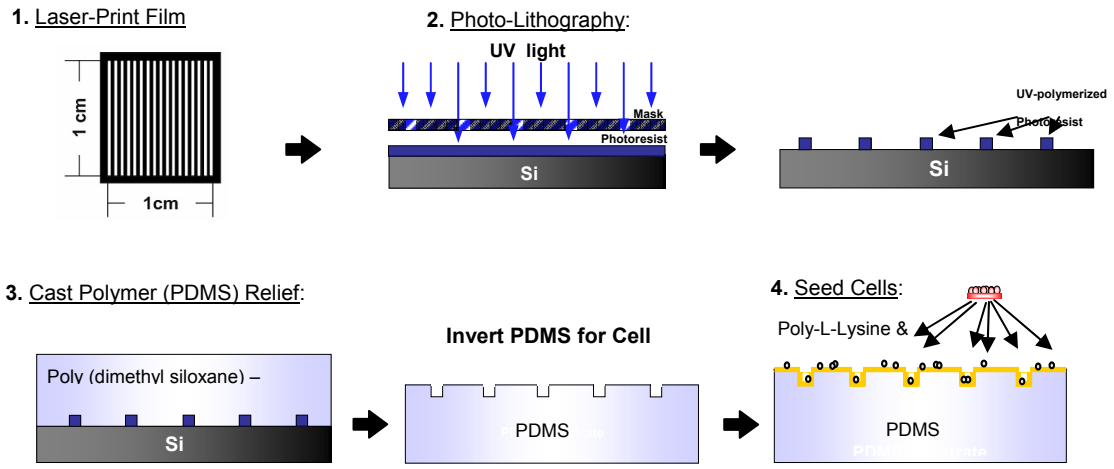

Figure 1 – Schematic of substrate production steps 1-4

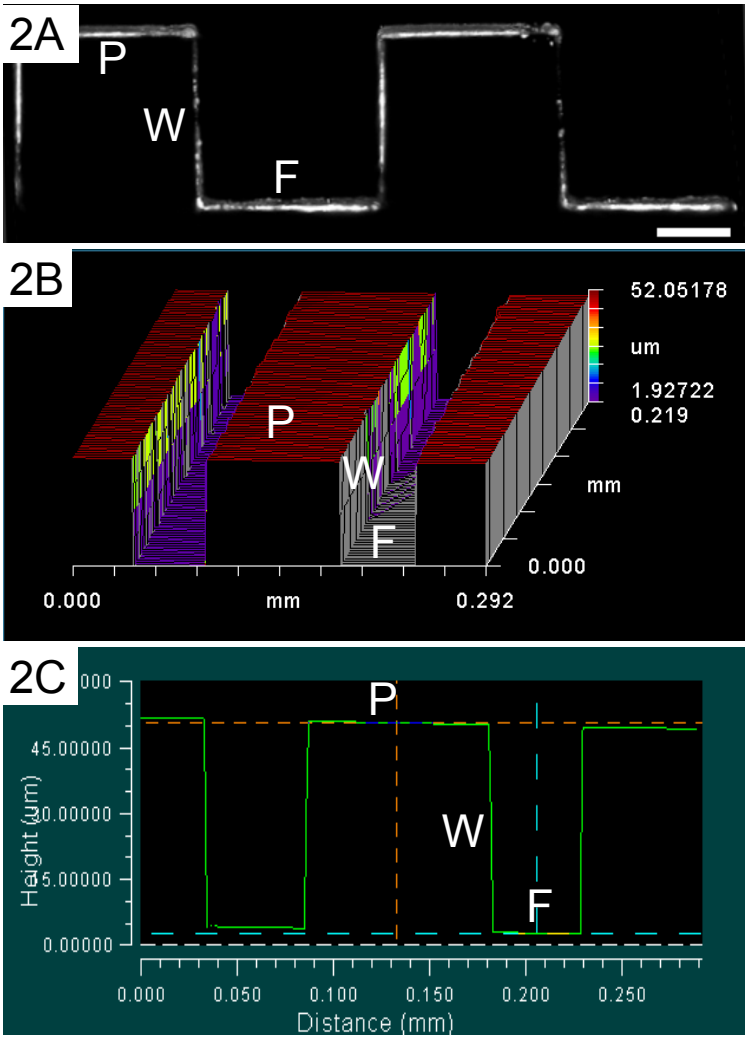

Figure 2A – (above) Confocal Z-stack of a 30 um thick cross section coated with poly-L-lysine and laminin, immunostained for laminin. Scale bar, 25um.

Figure 2B – (above) White-light-interference microscopy (WIM) image of uncoated substrate for in-depth analysis of substrate dimensions. (Provided by Dr. Elke Bremus-Koebberling, Fraunhofer Institute for Laser Technology in Aachen, Germany)

Figure 2C – (above) Cross-sectional measurements acquired from WIM data showing substrate dimensions.
P – Plateau; W – Groove Wall; F – Groove Floor

Cell Culture

Cells were seeded at varying densities onto grooved substrates and cultured for 24hrs at 37C and 5% CO2 with appropriate cell media specific for each cell type. In some cases, cell growth was followed by time-lapse microscopy during the first 24 hrs. All cells were viewed under phase contrast, epifluorescence, and scanning electron microscopy (SEM) following fixation at 24hrs.

Cell Type	**Primary Antibody / Stain**
Rat dorsal root ganglion (DRG)	Anti-neurofilament
Rat hippocampal neurons (E18)	Anti-neurofilament
Rat schwann cells (P15 -36)	Anti-S100
Rat A7R5 smooth muscle cells	Phalloidin (actin)
Rat B104 neuroblastoma cells	Anti-neurofilament
Mouse J2 fibroblasts	Phalloidin (actin)
Normal human neonatal fibroblasts	Phalloidin (actin)

Table A1 – Overview over cell types and immunolabeling.

Results

All cell types employed in this experiment showed bridging behavior on substrates with 50 um width, pitch, and depth, as illustrated in the following figures.

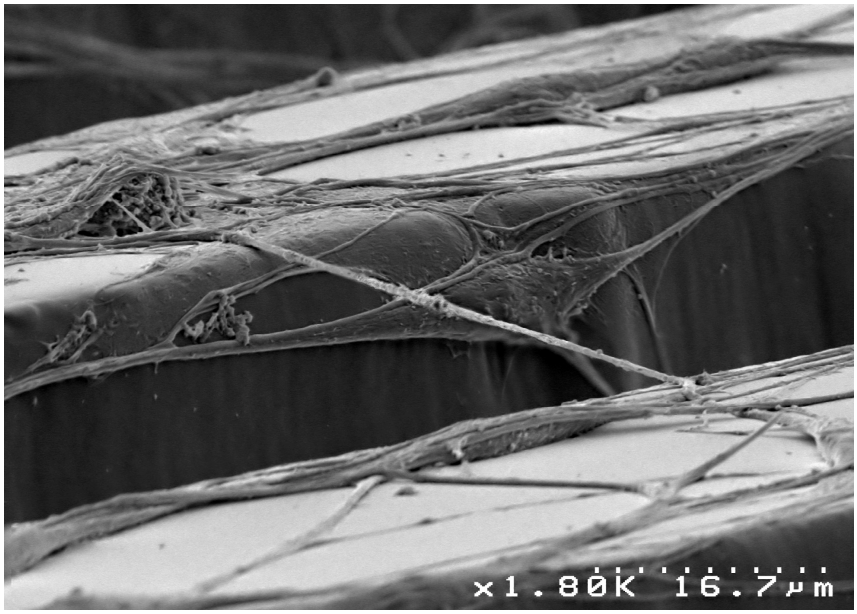

Figure 3A – (top) Scanning Elecrton Microscopy (SEM) image of a B104 mouse cell extending from one plateau to an adjacent plateau. Seeding density was 100K cells/cm2.

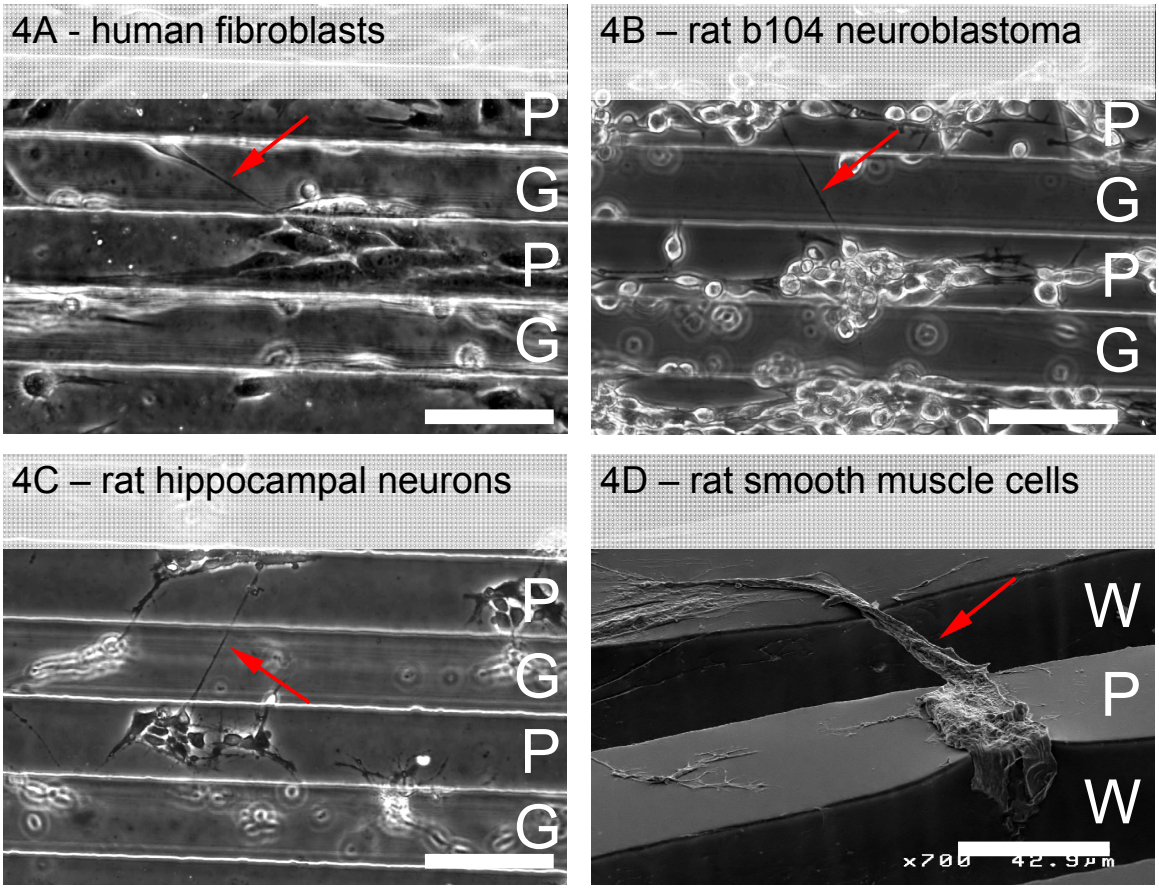

Figure 4 – (right) Bridging of multiple cell types: All images taken of fixed samples seeded with 100K cells/cm2 after 24hrs of culture focused on the plateaus.
A: Phase contrast micrograph of normal neonatal human fibroblasts in a culture. Bridge extends from a soma clinging to a groove wall (arrow).
B: Phase contrast micrograph of b104 rat neuroblastoma cells. Bridge extends between two cell clusters on adjacent plateaus (arrow).
C: Phase contrast micrograph of neonatal rat hippocampal neurons. Bridge extends from a soma clinging to a groove wall (arrow).
D: SEM image of A7r5 rat smooth muscle cells. One Smooth muscle cell extends from one plateau in the foreground to an adjacent plateau further in the background. It is unclear whether the PDMS deformation at the attachment point of the SMC in the foreground is due to processing or due to force generation of the cell.
Scale bar, 100 um (A-C), 42.9 um (D)
P – Plateau; G – Groove; W – Groove Wall

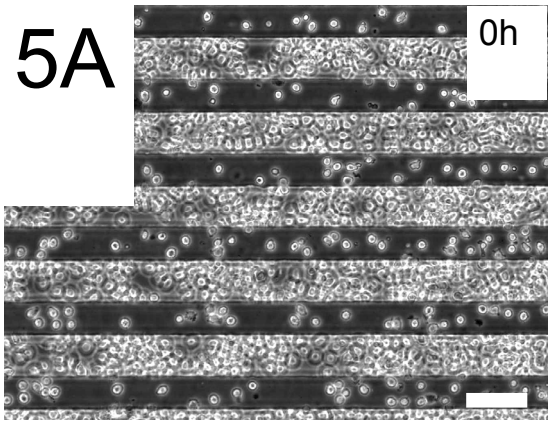
5A
0h

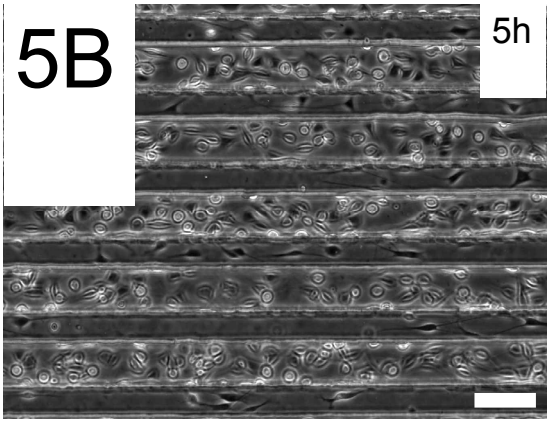
5B
5h

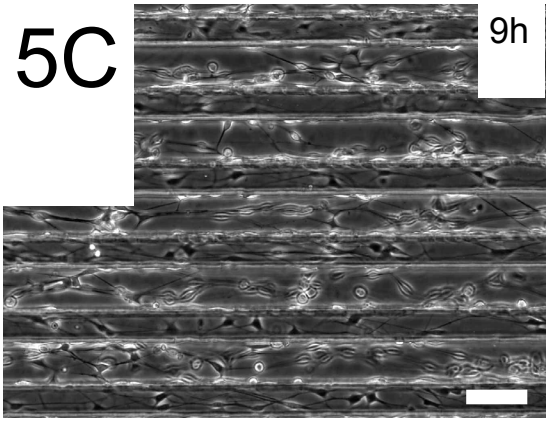
5C
9h

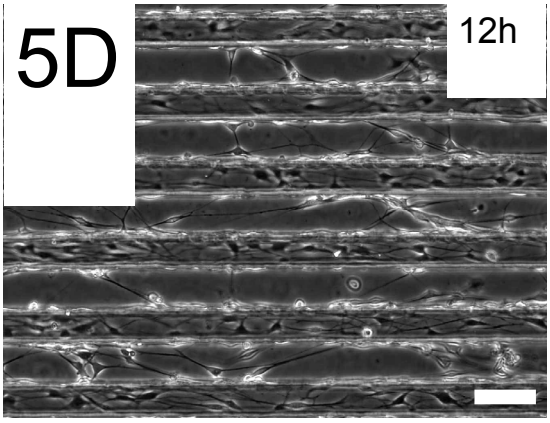
5D
12h

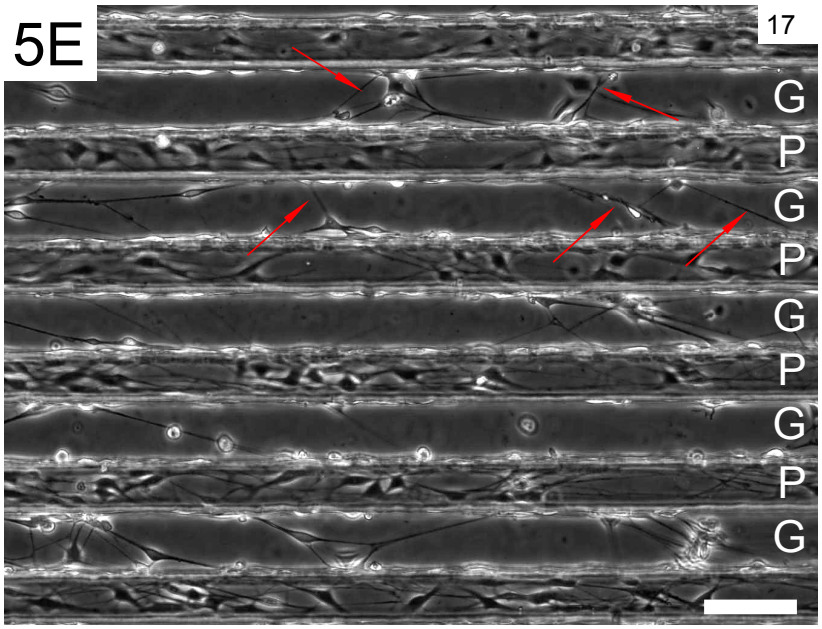
5E
17
G
P
G
P
G
P
G
P
G

Figure 5A-E – (above) Timelapse phase contrast micrographs taken a plateau level showing Schwann Cells (SCs) seeded at 150K cells/cm2. A: 0h, after initial seeding. Cells are round and mostly concentrated in grooves due to gravity. B: 5h, SCs have adhered and spread, many migrate towards the groove walls. C: 9h, first bridges are visible, cell number in grooves is similar to that seen on plateaus. D: 12h, more bridges form, cell migration from groove to plateau continues. E: 17h, long bridges are visible (arrows), hardly any cells are left on the groove floor. Cells on plateaus are mostly aligned parallel to the grooves. Scale bar, 100um. P – Plateau; G – Groove

Conclusion

With all cell types, examination under phase contrast and scanning electron microscopy revealed typical contact guidance, with multiple cellular extensions adhered to the groove and plateau features and aligned along the longitudinal axis of the features. Interestingly, in all cultures, a subset of the cellular extensions also bridged across the substrate grooves between adjacent plateaus. These studies are of interest to understanding cytoskeletal dynamics and designing biomaterials for three-dimensional cell and tissue engineering.

Appendix B

Neuronal Bridging Exerts Tension

Introduction and Rationale

The following SEMs show DRG cells that bridged across grooved substrates. Bridge generation clearly involved intracellular tension. These images provide anecdotal evidence of this tension. The underlying PDMS substrate was deformed around the attachment points of the cellular bridge.

Methods

General methods follow procedures outlined in chapter 2. 100,000 DRGs were seeded onto PDMS substrates with 60 um groove width and pitch, and 50 um groove depth and cultured for 24 h. After osmium tetraoxide fixation, cells were imaged under SEM. For detailed methods, please consult chapter 2.

Results

PDMS in the vicinity of cellular bridging was deformed, possibly indicating tension generation. Results are anecdotal because 1) not all cellular bridges showed evidence of substrate deformation, and 2) deformation could theoretically have occurred during SEM fixation.

Figures

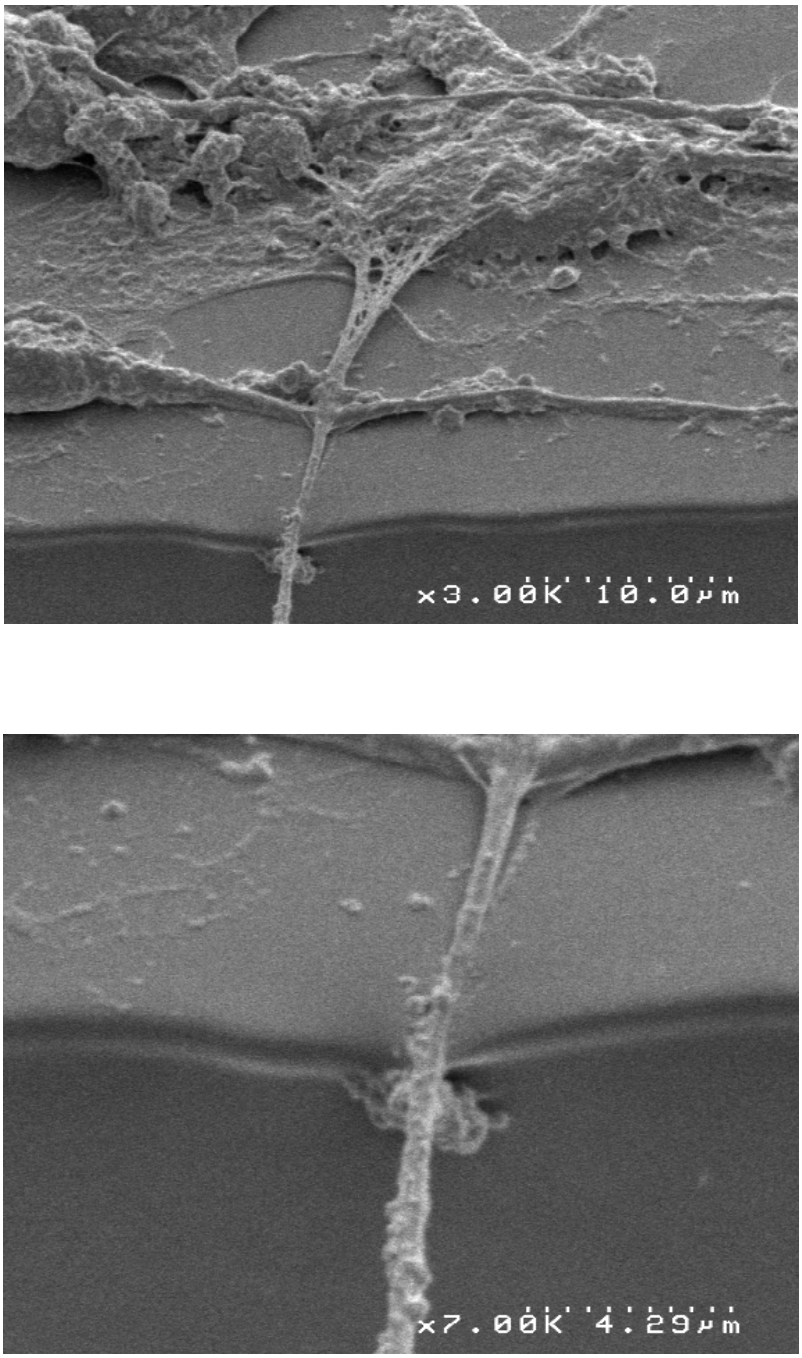

Figure 1. Top image. Scanning electron micrograph of a DRG neuron located on a plateau, extending a neurite directed to the bottom of the image. Substrate is deformed and the neurite is embedded in the substrate, possibly due to tension. Scale bar: 10 um. Bottom image: enlargement of portion of the top image. Scale bar: 4.29 um.

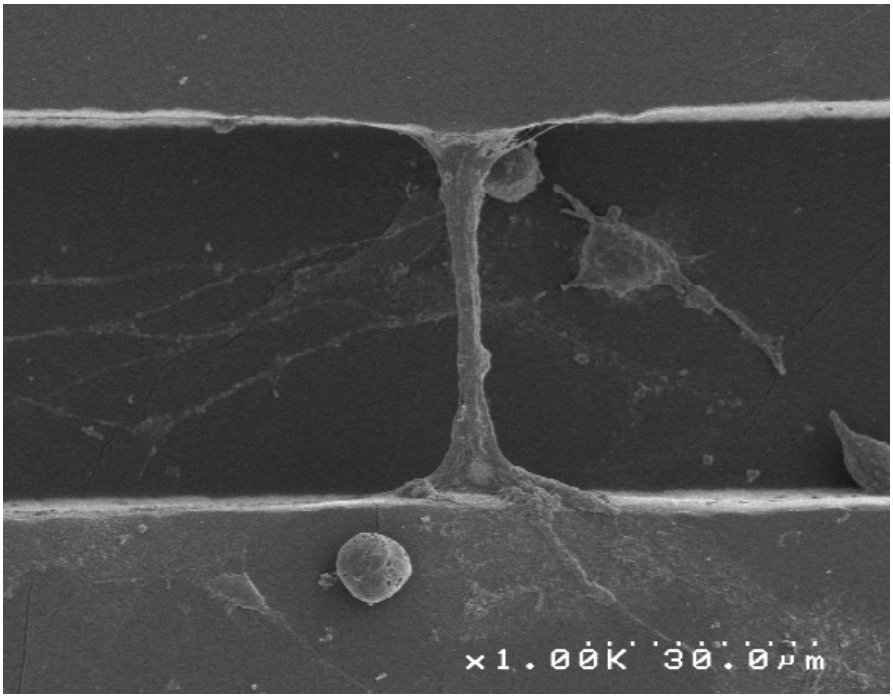

Figure 2. Scanning electron micrograph of a DRG neuron extending between two adjacent plateaus (top view). Substrate edge on the upper portion of the image shows signs of deformation towards the direction of the bridge.

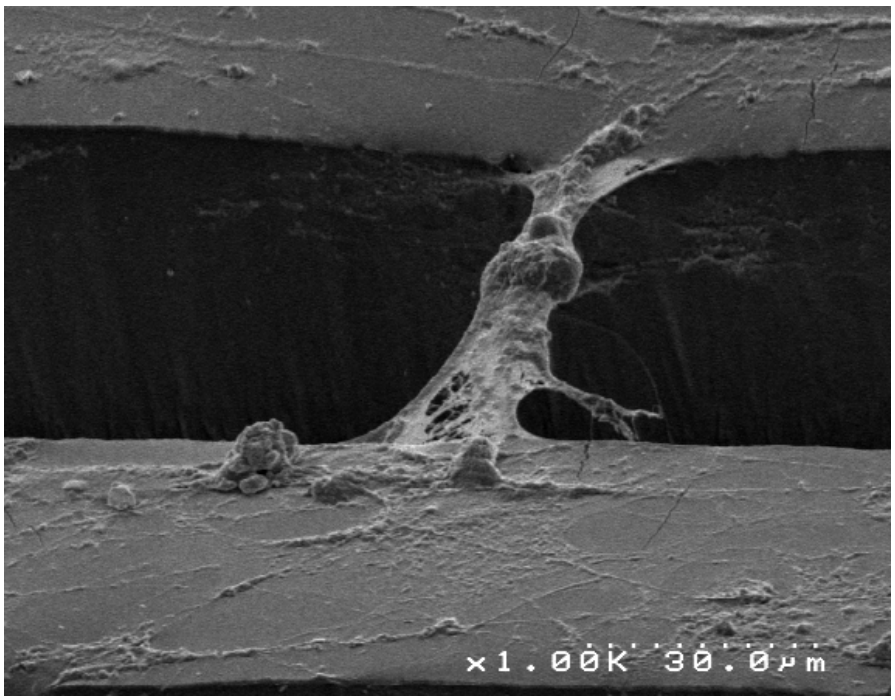

Figure 3. Scanning electron micrograph of a DRG neuron extending between two adjacent plateaus (angled view). Substrate edge on the upper portion of the image shows signs of deformation towards the direction of the bridge.

Appendix C

Extracellular Protein Patterns Influence Frequency of Neurite Bridge Formation

Introduction and Rationale

Many cellular behaviors such as adhesion, migration, and differentiation are influenced by extracellular cues. Our lab has recently characterized the phenomenon of cellular bridging where cells cultured on grooved substrates extend cellular processes from one plateau across one or multiple grooves without underlying support. The hypothesis behind this current study is that we can control the frequency of cellular bridges by altering the cellular environment not only in terms of its topography but also biochemically by altering the configuration of substrate-bound cues. Here, we have designed novel 3-dimensional micropatterns of laminin cues on substrates with multiple grooves of 60 um width, pitch, and 50 um depth. Bridging frequency correlates positively with the configuration of laminin patterns and the overall amount of laminin deposited.

Methods

Substrate with repeating grooves were fabricated as described previously in chapter 2[1].

Selective coating methods were adapted from DeSilva and Chang[2, 3]. All PDMS and glass control substrates were sterilized by immersion in 70% ethanol and rinsed with sterile dH2O before protein patterning. All substrates were rinsed with Hanks Balanced Salt Solution without calcium or magnesium (HBSS-CMF, Invitrogen Life Technologies) after patterning and before plating.

Uniform Coating.

Substrates were exposed to plasma at 10.5W for 1 min (PDC-32G, Md F level, Harrick) and rinsed with dH_2O. A 100µL droplet of 50µg/mL mouse laminin (LN, Invitrogen Life Technologies) in HBSS-CMF was suspended on the substrate for 1 hour. The droplet was blown off with high velocity air.

Plateau Coating.

Glass coverslips were immersed in 10% sodium dodecyl sulfate (SDS, Shelton Scientific). They were sonicated for 5 mins and remained immersed for an additional 5 mins. The substrates were rinsed gently in sterile dH2O for 4s and dried with high velocity air. The glass was coated with 100 µL LN for one hour, the solution was blown off with high velocity air, the coverslips were adhered to

PDMS substrates that had recently been plasma etched, and left to transfer proteins overnight.

Checkerboard Coating.

Checkerboard coating followed the same procedure as plateau coating except patterned PDMS substrates were used as the stamps in the place of glass coverslips. After coating with LN, the stamps were placed on different plasma-etched PDMS substrates so that the grooves of the respective substrates were orthogonal, and left in contact overnight.

Groove Coating.

PDMS substrates, cut so the edges of grooves are exposed, were plasma etched and then adhered to glass coverslips. A bead of LN was placed along the exposed edge of the substrates and allowed to fill the grooves through capillary action. After one hour, the substrates were blown completely dry with high velocity air and peeled of the coverslip.

Checkerboard and Groove Coating.

Checkerboard and groove coating was simply a combination of the above procedures. Groove coated substrates were used as the template onto which the PDMS stamps were placed orthogonally, without being plasma etched again.

Cell Culture, Microscopy, and Immunostaining

Conditions for the procedures above were as previously described in chapter 2[1]. Cell seeding density for these experiments was 100,000 cells/cm^2.

Results

SEM (Figure 1) and phase contrast observations confirmed that DRG cells seeded on substrates with grooved topography of 60 um width, pitch, and 50 um depth could grown on all surfaces: plateau, groove walls, and groove floor. Epifluorescent and confocal microscopy on uCP lamin-patterned substrates confirmed presence of 6 distinct laminin configurations as depicted in Figure 2. Comparing the amount of laminin-covered area per substrate (Figure 3A) with number of bridges per substrate (Figure 3B) showed a correlative trend between bridging and amount of laminin plated.

Conclusion

Bridging frequency is not only dependent on substrate dimensions, but also correlates with the amount of laminin present on substrates. Further details and a more extensive discussion of the results of this project can be found in the honors thesis of Caitlin Elgarten, available from Diane Hoffman-Kim upon request.

Figures

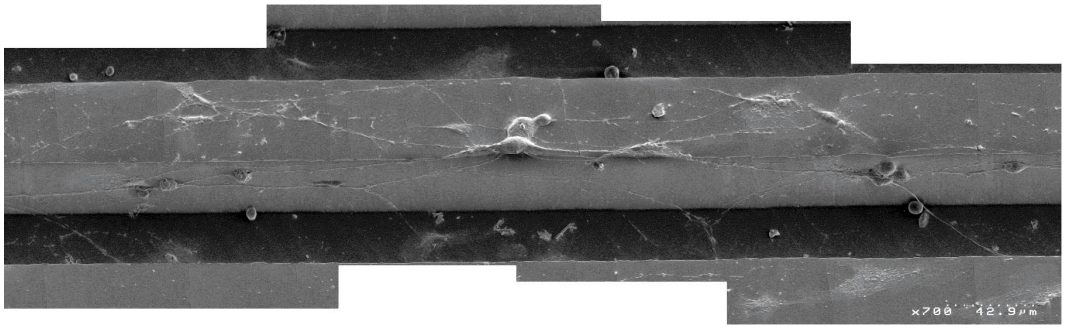

Figure 1: Scanning electron micrograph showing DRGs growing on all surfaces of a laminin-coated grooved substrate after 24 h of culture. Magnification: 700 x, scale bar = 42.9 um.

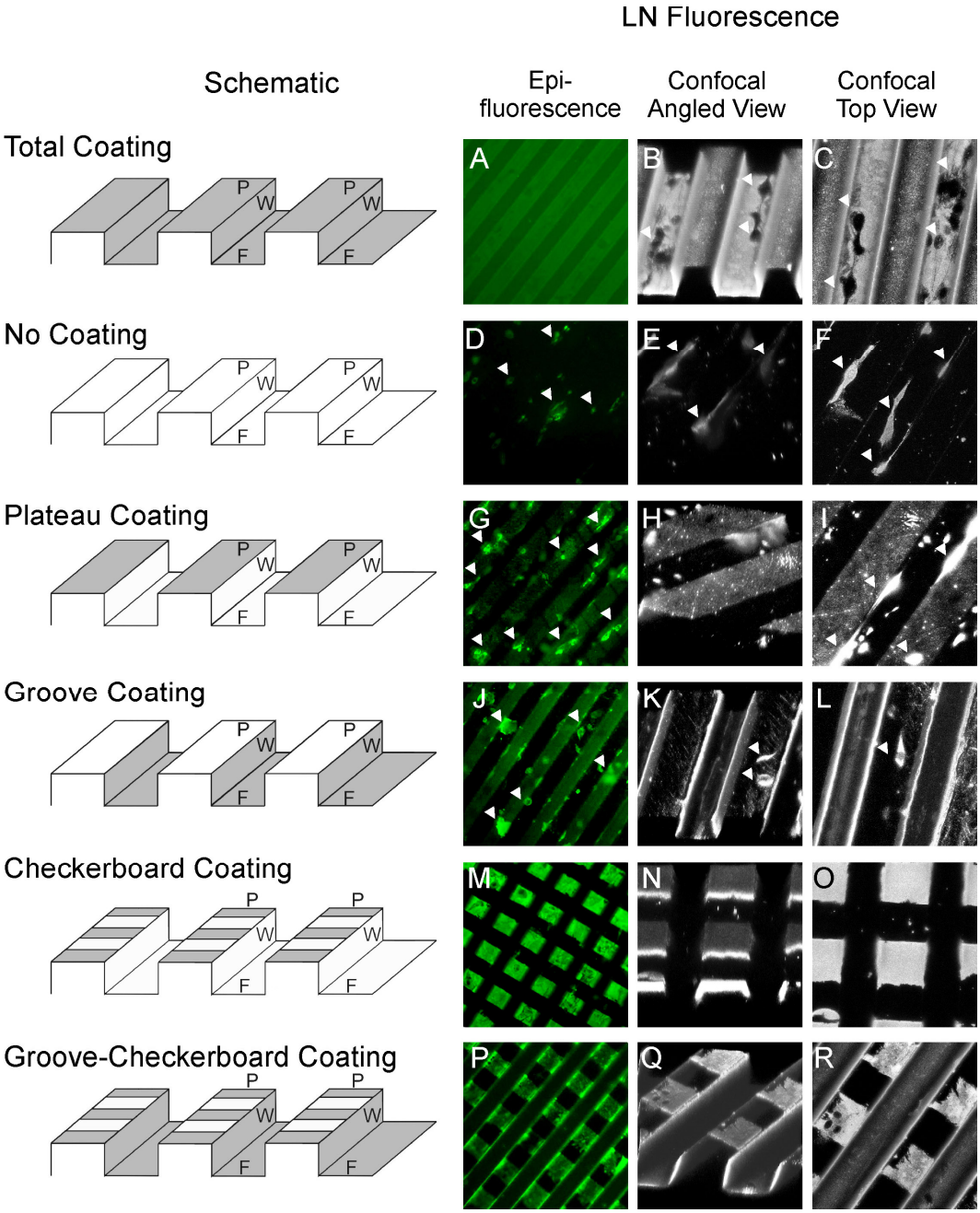

Figure 2. Laminin can be coated in distinct geometrical arrangements on substrates with repeating grooves with 60 um width and 60 um pitch.

Left column shows cartoon schematics of coating where dark grey areas represent areas coated with laminin and white areas represent areas without protein coating. Images A, D, G, J, M, and P in the second column labeled “LN Fluorescence” show samples seeded with DRGs after 24 h of culture and after immunostaining for laminin as acquired on an inverted fluorescence microscope. Scale bar = 50 um. Images in the next two columns labeled “Angled view” and “Top view” show views of the same samples as in the previous row, this time as acquired on an inverted confocal microscope and with different angles of view. Bright spots (arrow heads) in the images represent DRG cells, which can secrete laminin on their surface. Scale bars = 50 um.

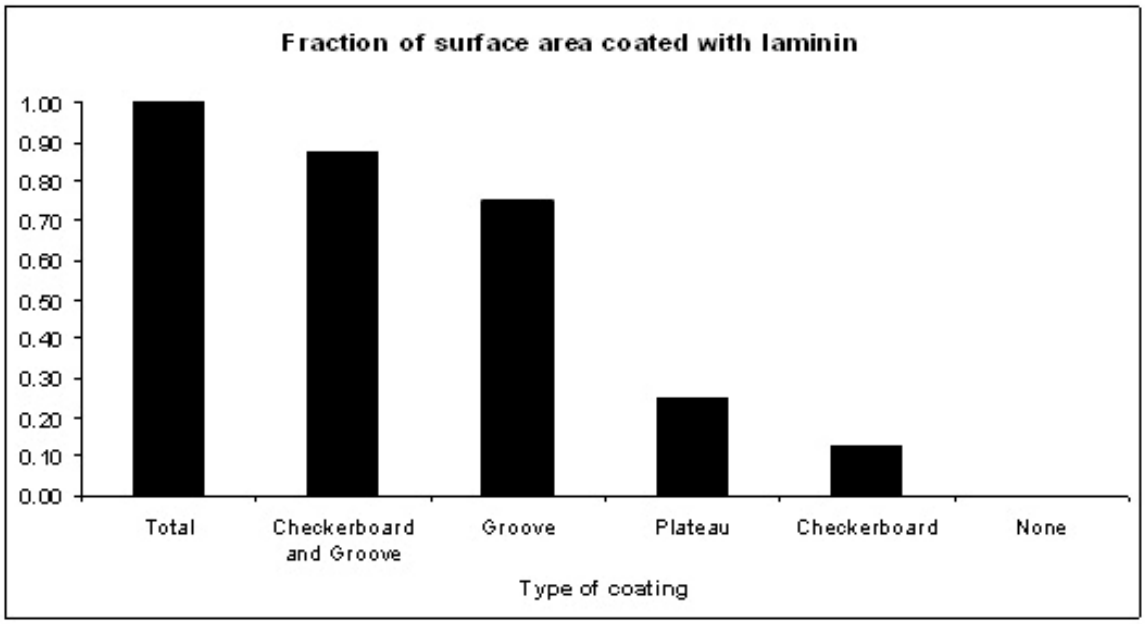

Figure 3A. Theoretical fraction of surface area coated with laminin per coating type relative to full coating.

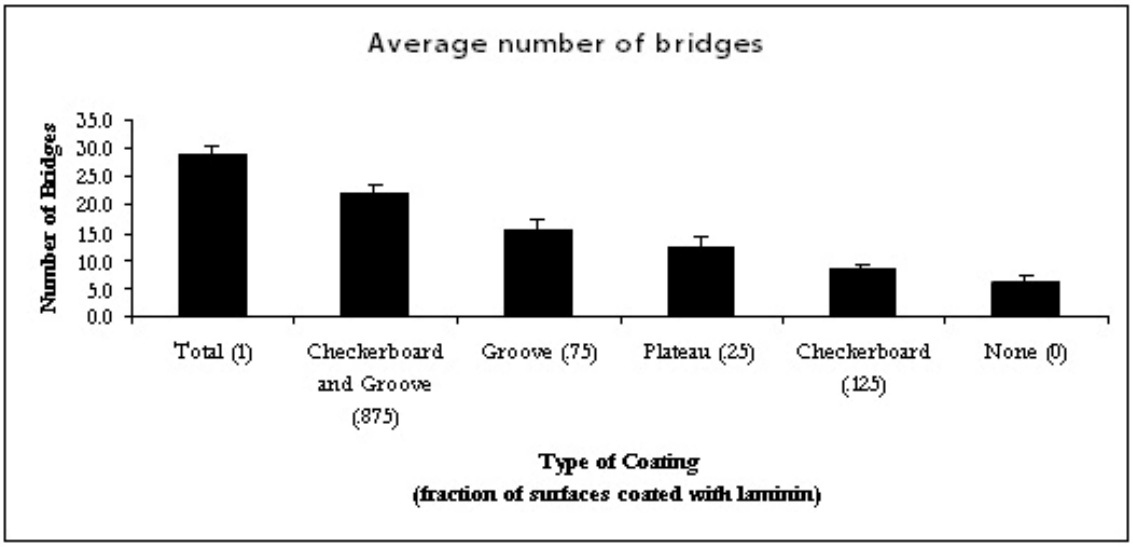

Figure 3B. Average number of bridges per 10 grooves corresponds to amount of surface area covered with laminin. N=2 samples per condition (10 grooves each) and error bars = std deviation.

References

1. Goldner, J.S., Bruder, J.M., Li, G., Gazzola, D. & Hoffman-Kim, D. Neurite bridging across micropatterned grooves. *Biomaterials* **27**, 460-472 (2006).

2. Chang, J.C., Brewer, G.J. & Wheeler, B.C. A modified microstamping technique enhances polylysine transfer and neuronal cell patterning. *Biomaterials* **24**, 2863-2870 (2003).

3. De Silva, M.N., Desai, R. & Odde, D.J. Micro-patterning of animal cells on PDMS substrates in the presence of serum without use of adhesion inhibitors. *Biomed Microdevices* **6**, 219-222 (2004).

Appendix D

Biomimetic Materials Replicating Schwann Cell Topography Enhance Neuronal Adhesion and Neurite Alignment In Vitro - Addendum

Introduction and Rationale

Chapter 4 was published containing only results for relief replicas. We have also gathered the equivalent data for impression replicas, which are included here.

Methods

Please refer to chapter 4 for complete methods.

Results

Please refer to figures and figure captions for results.

Conclusion

While statistically significant differences exist between DRG response to impression and relief replica, both replicas significantly enhance adhesion, alignment, and motility over flat controls. The implications of the differences between these two nearly identical substrates are discussed in more detail in future directions in chapter 6.

Figures

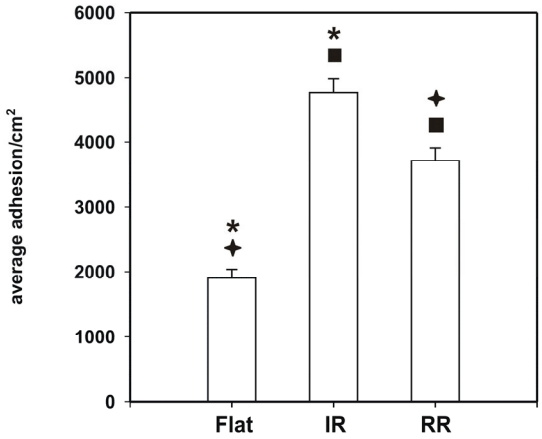

Figure 1. Enhanced DRG adhesion on biomimetic materials. Compared to flat PDMS, DRG adhesion on biomimetic micro- and nanostructured PDMS was significantly enhanced on IRs (*p < 0.001), and RRs ($^{a}p < 0.001$) after 24 h in culture. DRG adhesion on RRs was significantly lower than on IRs (np < 0.001). Values are mean +/- SEM; n=8 samples, 80 FOV per condition. IRs could possibly retain more cells due to a “settling” effect mediated by gravity in the indented features.

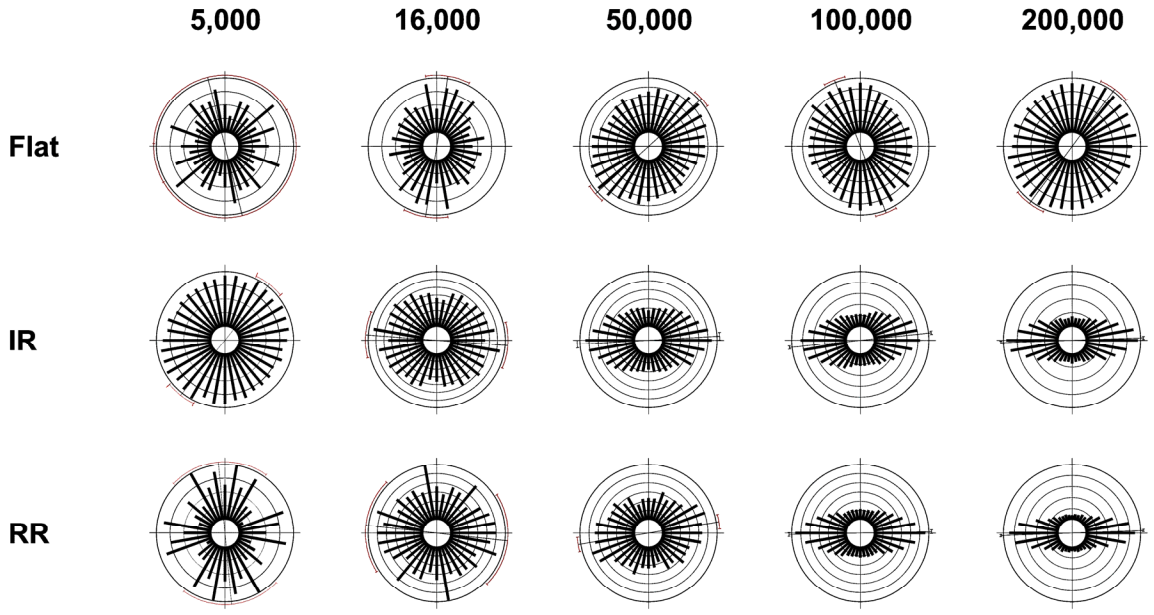

Figure 2. Quantification of enhanced nuclear alignment on biomimetic materials. Circular histograms show the distributions of the angles of the long nuclear axes of dissociated DRG plated at varying cell densities, cultured for 5 d on flat PDMS, IRs or RRs, and stained with DAPI. The length of each bar represents the number of nuclei oriented at the corresponding angle, and the arcs indicate the 95% confidence interval. The horizontal axis corresponds to the direction of the SC pattern in the replicas. For plating densities > 50,000 cells/well, Rao's spacing test confirmed a non-uniform distribution of nuclear angles ($p < 0.05$ for 50,000 cells/well; $p < 0.01$ for 100,000 and 200,000 cells/well) and a V-test confirmed nuclear alignment in the direction of the SC pattern ($p < 0.001$).

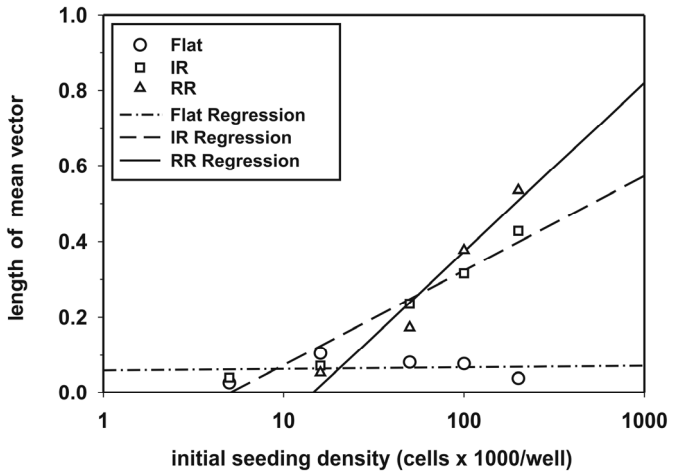

Figure 3. Graph of the relationship between plating density and nuclear alignment, as represented by the lengths of the mean vectors in Figure 2. Plating density showed a logarithmic correlation with mean vector length for RRs and IRs (r^2 = 0.95 in either case) and but not for flat substrates (r2 = 0.067).

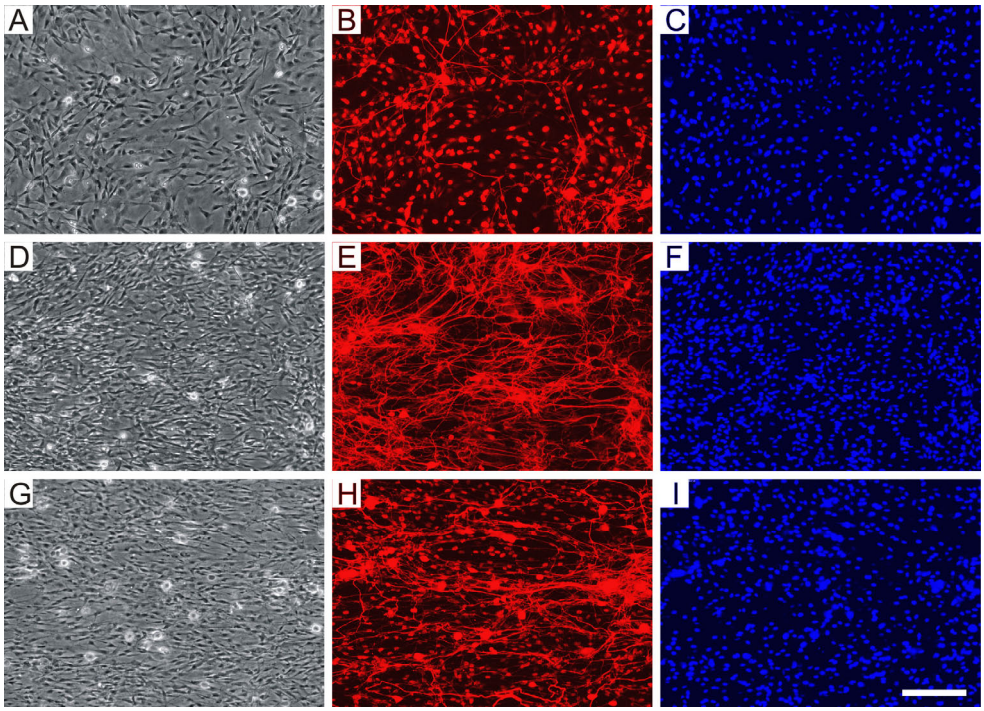

Figure 4. DRG morphology on biomimetic materials. Phase contrast (A, D, G) and fluorescent micrographs (B, C, E, F, H, I) of dissociated DRG cultured for 24 h on flat PDMS (A-C), IRs (D-F), or RRs (G-I) and stained with neurofilament immunocytochemistry (B, E, H) and DAPI nuclear stain (C, F, I). Scale bar, 200 μm.

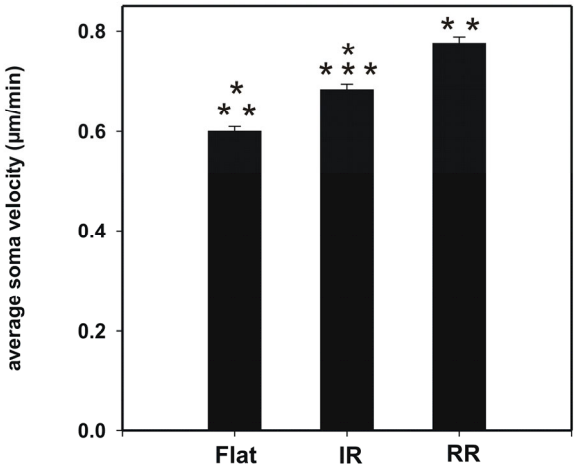

Figure 5. Increased DRG velocity on Biomimetic materials. Results indicated that compared to flat PDMS, DRG velocity on biomimetic micro- and nanostructured PDMS was significantly enhanced on IRs (*p < 1E-08, student's t-test), and RRs (**p < 1E-28, student's t-test) 2-14 h post plating, with measurements taken every 10 min. DRG velocity on RRs was significantly higher than on IRs (***p < 4E-08, student's t-test). Values are mean +/- SEM; n=3 samples with 4 FOV each, or >56 cells per condition.

Appendix E

Nerve guidance channels featuring cellular topography on their luminal surfaces enhance nerve regeneration in vitro

Introduction and Rationale

For peripheral nerve repair, autografts have been the gold standard for the past few decades. However, sourcing of these tissues creates additional morbidity and secondary impairment to patients already dealing with neurological damage. Artificial grafts could obliterate the need for graft sourcing and allow for greater control of mechanical properties, such as length, diameter, wall thickness, permeability, degradability, and interior surface morphology [1-3]. In addition, artificial grafts can be tailored from the onset on to incorporate drug delivery systems for temporally and spatially succinct delivery of diffusible as well as substrate-bound cues [4]. Before building a graft that incorporates a variety of different cues, it is important to understand the contribution of single guidance cues, in this case topography. A number of studies have shown that macro-topography, such as the bending of a surface at the sub-millimeter and millimeter level can have profound effects on cellular behavior [5]. It is thus important to test the effect of cellular topography in combination with the macro-topography presented in the inside of a nerve guidance channel and compare the results to flat (non-bent/rolled) control samples. The findings of this approach work towards untangling the combined effects of biomimetic macro-, micro-, and nanotopography on cells in culture.

Once deciphered, topography as a regenerative enhancement becomes one part in a modular approach to artificial nerve graft design. Other “modules” such as surface chemistry treatments or drug delivery can then be easily combined to form an “ideal” nerve graft.

Poly-dimethyl-siloxane (PDMS) is flexible, elastic, gas-permeable, transparent, biocompatible, and non-degrading, making it a good material for in vitro evaluation of cell fitness in an artificial guidance nerve guidance channel (NGC) with SC-shaped topography. Poly-lactic-acid (PLA) is an FDA-approved biodegradable biocompatible polymer for the fabrication of nerve guidance channels that can be utilized to study the effects of material degradation on regenerative processes in vitro.

Here we have fabricated thin (~100 um) membranes of PDMS with indented cellular SC shapes by spin-coating PDMS onto cellular templates. The fabrication process is summarized in Figure 1. These membranes can be assembled into nerve guidance channels by wrapping them around a cylindrical mandrel of controllable diameter. The primary experimental condition with SC-shaped patterns aligned longitudinally with respect to the lumen of the NGC have been tested against the following controls: A) NGCs with flat lumen, B) NGCs with SC-shapes aligned perpendicularly to the lumen, C) NGCs with SC shapes that have no alignment. The experimental conditions are summarized in Figure 2).

Methods

The fabrication methods of the NGCs are an extension of the fabrication methods of biomimetic substrates as outlined in chapter 2. Instead of producing polymeric replicas of 3-5 mm thickness, the polymers are spin-coated (2000 rpm for 1 minute) onto their templates and form thin (50-100 um) membranes with biomimetic surface topography. Varying spin coating speed and duration results in precise control of the resulting biomimetic polymer membranes.

These thin membranes then are assembled into NGC's by rolling them around glass mandrels of 1 mm diameter. (for an overview of the process, see figure 1), resulting in NGCs with SC-shaped indentations on the luminal surfaces.

Subsequent SEM analysis of NGCs shows the presence of SC-shaped indentations on the luminal surface (Figure 2). The development of production techniques of relief-replica (RR) NGCs is ongoing at the moment. RR-NGCs pose a greater challenge since the separation of thin polymer RRs from polymer IRs is much more intricate than the separation of thin IRs from cellular templates.

As an in vitro model of nerve regeneration we employed neonatal rat DRG explants cultured for 5 days at the end of nerve guidance channels with varying topographies summarized in Figure 3:

A) no pattern – containing no biomimetic features but a smooth surface

B) parallel pattern – containing aligned SC-impression replicas parallel to the length of the channel

C) perpendicular pattern - containing aligned SC-impression replicas perpendicular to the length of the channel, in other words: circumferential patterning

D) random pattern -- containing non-aligned SC-impression replicas that showed no alignment.

To quantify outgrowth, explants positioned at the end of a NGC and cultured for 5 days in neuronal media. After resulting cell growth was fixed and stained with alexafluor phalloidin, the distance of cellular outgrowth and migration was measured from the edge of the channel parallel to the lumen of the channel (Figures 4 and 5).

Results

We are capable of fabricating nerve guidance channels with aligned and unaligned biomimetic SC-shaped impressions on their luminal surface (Figure 2). Aligned biomimetic SC-shaped patterns affect DRG outgrowth from explants in NGCs (Figure 5). The direction of alignment of the pattern significantly alters the extent of explant outgrowth and cellular migration after 5 days in culture. Patterns aligned in parallel with the lumen result in maximum outgrowth and alignment.

Further experiments need to be carried out to fully elucidate the effects of biomimetic patterns on explant growth in NGCs.

Figures

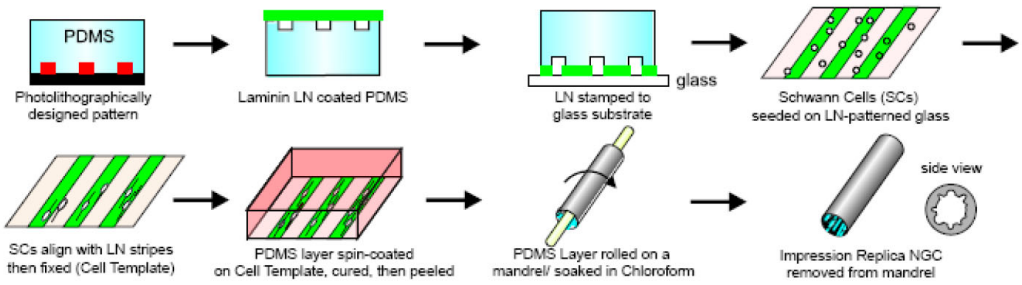

Figure 1: Cartoon overview of NGC fabrication.
Photolithographic methods are employed to produce an elastomeric PDMS stamp. This stamp generates a striped laminin pattern on glass substrates with 60 um stripe width and 60 um pitch. Schwann cells cultured to confluence on these substrates align with the direction of the protein pattern and form an aligned, confluent monolayer. After osmium-tetraoxide fixation, these cells serve as a template for a replica molding process, resulting in thin (~50-100 um) sheets of PDMS with indented SC features. These features are then rolled around a glass mandrel of 1 mm diameter and form a NGC of 1 cm length, featuring indented SC shapes in their lumen.

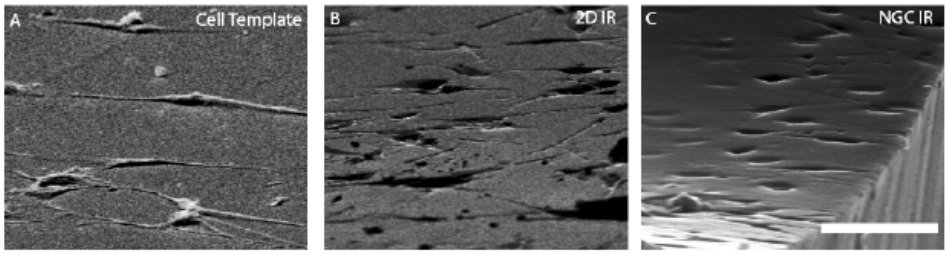

Figure 2: SC-morphology can be successfully incorporated into NGCs as an impression replica. Scanning electron micrographs showing cell template (A), SC-shaped impressions in 2D substrate (B), and aligned SC-shaped impressions at the edge of the lumen of the NGC (C). Scale bar, 43 um.

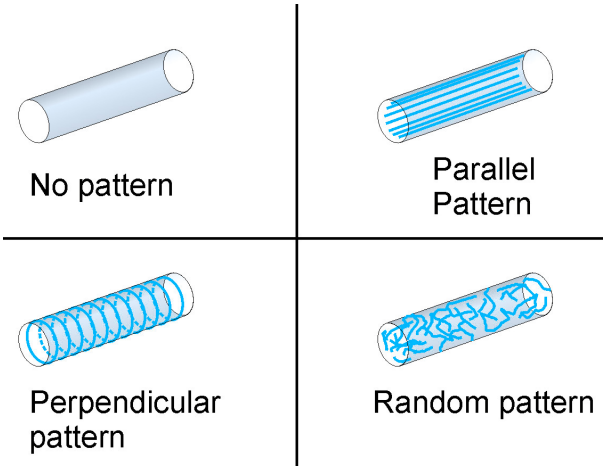

Figure 3: Cartoon drawing of various biomimetic pattern configurations used in this pilot trial.

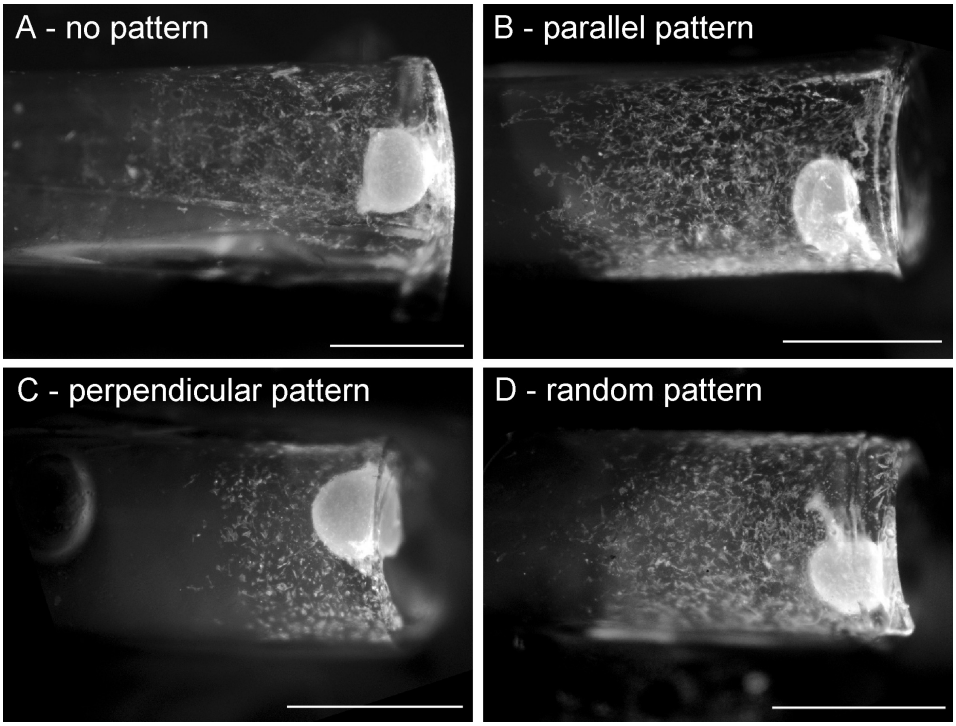

Figure 4: DRG explants show qualitatively different growth patterns on SC-patterned versus flat control substrates as observed via phalloidin staining.
DRG outgrowth and migration from explants after 5 days of culture in NGCs with no pattern (A), biomimetic aligned SC-shaped patterns in luminal direction (B), biomimetic SC-shaped patterns aligned perpendicular to the lumen (C), and NGC featuring random / non-aligned biomimetic SC-shaped pattern. N=6, scale bar, 1mm.

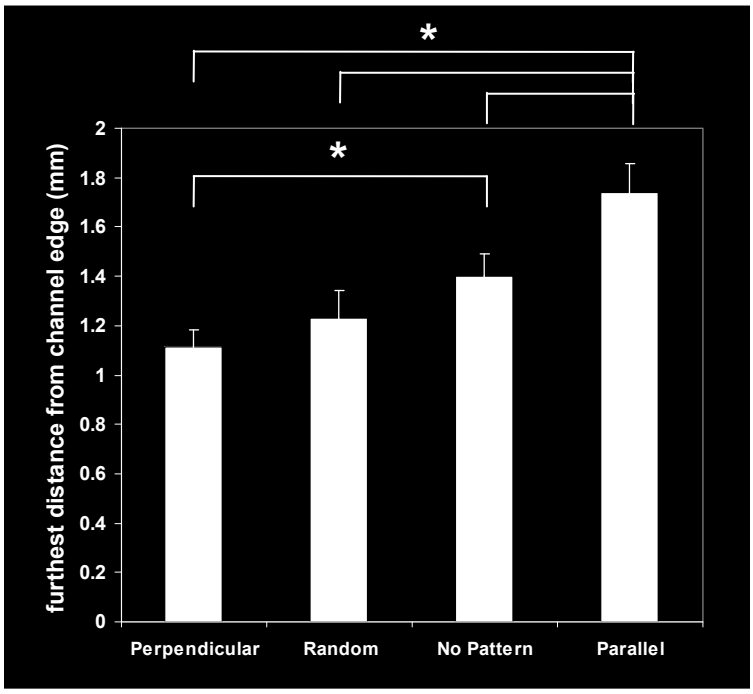

Figure 5: DRG explants show quantitatively different growth patterns on SC-patterned versus flat control substrates.

References

1. Huang, Y.C. & Huang, Y.Y. Biomaterials and strategies for nerve regeneration. *Artificial organs* **30**, 514-522 (2006).

2. Belkas, J.S., Shoichet, M.S. & Midha, R. Peripheral nerve regeneration through guidance tubes. *Neurological research* **26**, 151-160 (2004).

3. Kim, S.M., Lee, S.K. & Lee, J.H. Peripheral nerve regeneration using a three dimensionally cultured schwann cell conduit. *The Journal of craniofacial surgery* **18**, 475-488 (2007).

4. Pfister, L.A., Papaloizos, M., Merkle, H.P. & Gander, B. Nerve conduits and growth factor delivery in peripheral nerve repair. *J Peripher Nerv Syst* **12**, 65-82 (2007).

5. Smeal, R.M., Rabbitt, R., Biran, R. & Tresco, P.A. Substrate curvature influences the direction of nerve outgrowth. *Annals of biomedical engineering* **33**, 376-382 (2005).

Appendix F

Schwann Cells and Dorsal Root Ganglia on Polycarbonate Urethane-Carbon-Nanotube Composites

Introduction and Rationale

Carbon nanotubes (CNTs) are novel materials that are biocompatible, electrically conducting, and present size features to cells at a nanoscale. They have been shown to alter and enhance cellular functions on many different levels for a variety of cell types. One example is the increased formation of bone matrix in osteoblast cell lines when grown on CNT materials compared to non-CNT controls. The electrical conductivity of CNTs coupled with the positive effects recorded in conjunction with a variety of cell types makes CNT materials an interesting candidate as material for nerve regeneration.

The work in this pilot study is a collaboration between the Hoffman-Kim lab and the Webster lab at Brown, with Dongwoo Kang and Jan Bruder responsible for substrate production and bio-assay, respectively.

Overall, 4 experimental runs were conducted, and an overview is given in table 1. Since these experiments had “pilot” status, conditions were optimized between runs, and a direct comparison between runs is not feasible.

Methods

Detailed substrate fabrication parameters are available from our collaborators. Generally, commercially available CNTs were suspended in polycarbonate urethane (PCU) in different w/w ratios. One pure PCU sample and one glass cover slip coated with pure CNT served as controls. Further preparation for cell seeding included exposure to UV light in the tissue culture hood and rinsing with 70% EtOH for sterilization and plasma etching (times as indicated in table 1) and protein coating with poly-L-lysine or laminin (as indicated in table 1). Some CNT samples were assembled as “grids” by flowing PCU-CNT mixtures over TEM grids that have fine gratings. Removal of these grids resulted in sample surfaces with alternating stripes of pure CNT and PCU.

For assessment of adhesion of SCs and DRGs to substrates, cells were seeded suspended in media in varying concentrations (see table 1) and allowed to adhere for 4 hours at 37 C, 5% CO2. Following incubation, non-bound cells were washed away with PBS and the remaining cells fixed with 2% paraformaldehyde and 4% sucrose in PBS, as detailed in chapter 2. Adhesion was quantified by DAPI-staining nuclei and recording at least 10 random fields of view per sample, followed by manual or automated counting of nuclei as outlined in chapter 4.

For visualization of cellular morphology, select samples were stained for actin with alexafluor phalloidin and viewed under epifluorescence. This did not enable us to view the cells’ relation to the CNTs, as CNTs absorb nearly all incoming

excitation wavelengths and thus their morphology remains indeterminable under epifluorescence. To further visualize cellular morphology, select samples underwent osmium tetraoxide fixation (chapter 2) and were imaged under SEM.

Results

Please refer to figures for results.

Conclusions

Both SCs and DRGs showed low adhesion on pure CNTs. Pure CNTs appeared to damage cells as observed via SEM and epifluorescence. DRGs adhered more to CNT-PCU composites than control samples. However, SCs adhered better to control samples. Further experiments that build on the parameters established in these pilot experiments are necessary to ascertain these trends.

Figures

Jan Bruder	Overview over CNT experiment conditions			
Experiment	**I**	**II**	**III**	**IV**
Sample age:	> 2 years	> 2 years	> 2 years	recently fabricated
Date	7/14/2006	10/29/2006	11/9/2006	3/14/2007
cell type	SC	SC and DRG	SC and DRG	SC
protein	none and PLL	none	PLL and PLL-LN	PLL plasma-etched, and PLL non-plasma-etched
substrate	grid	homogeneous and grid	homogeneous and grid	homogeneous and grid
seeding density	aimed for 3000 cells/cm^2, but over-shot, exact density unknown	3000 cells/cm^2	9000 cells/cm^2 for SC 4500 cells/cm^2 for DRG	15000 cells/cm^2
UV time	5min per side EtOH	7 minutes per side EtOH	7min per side EtOH	2 mins - NO contact with EtOH
Incubation time	4 hrs	4 hrs	4 hrs	4 hrs
plasma etching	none or 1 minute	none	1 minute	1 minute
analysis	dapi phalloidin SEM	dapi phalloidin	dapi anti-LN after 48 hr incubation SEM	dapi CNT area fraction on grid samples
substrate types	8 CNT grid samples	12 CNT/PCU samples r_1 12 CNT/PCU samples r_2 12 CNT/PCU samples r_3 12 glass controls 12 PLGA samples 12 PCU samples 18 CNT grid samples	16 CNT/PCU samples r_1 16 CNT/PCU samples r_2 19 CNT/PCU samples r_3 6 glass controls 15 PLGA samples 21 PCU samples 12 CNT grid samples	11 1/2 CNT/PCU samples 11 1/4 CNT/PCU samples 11 1/6 CNT/PCU samples 12 glass controls 7 pure CNT samples 6 "200" CNT grids 5 "300" CNT grids

Table 1. Overview over experimental conditions.

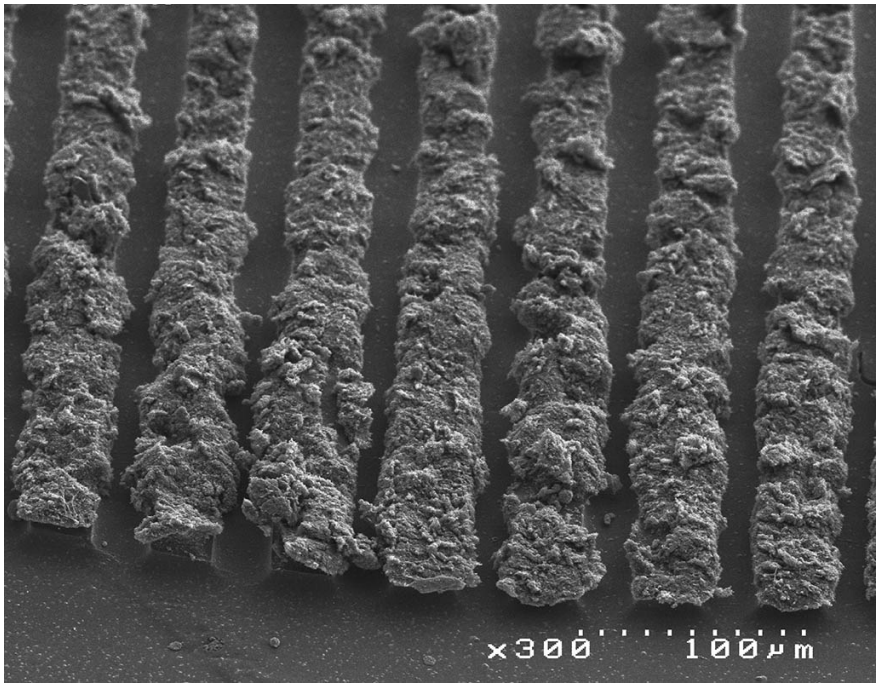

Figure 2. Scanning electron micrograph of a grid sample showing variable coverage of CNT, resulting in unpredicatable ratios of CNT/PCU areas. CNTs also introduce a considerable topography to the samples, protruding from the sample surface.

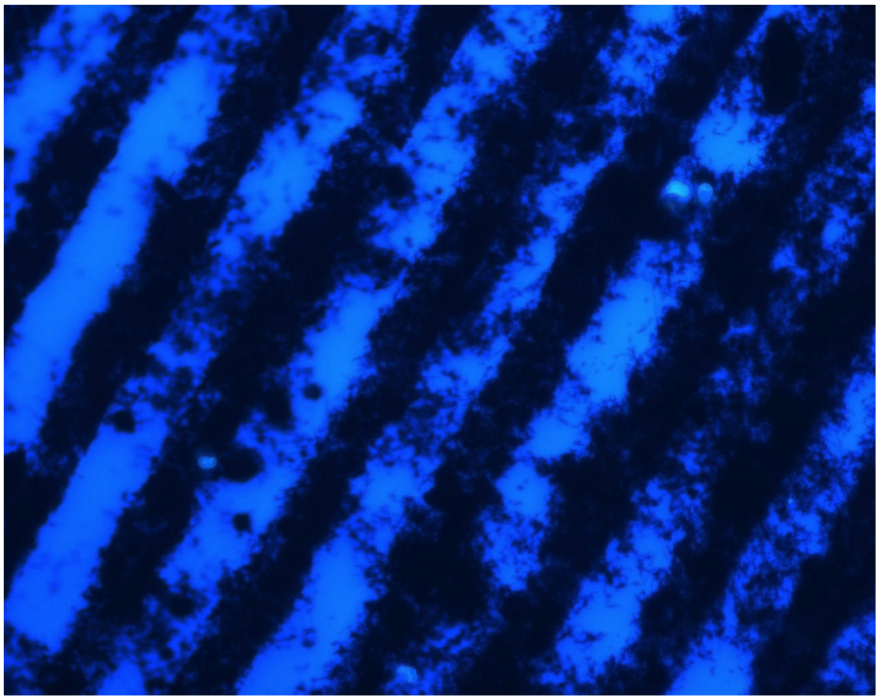

Figure 3. Epifluorescent micrograph of a grid sample showing variable coverage of CNT. CNTs clearly contaminate areas of adjacent “pure” PCU.

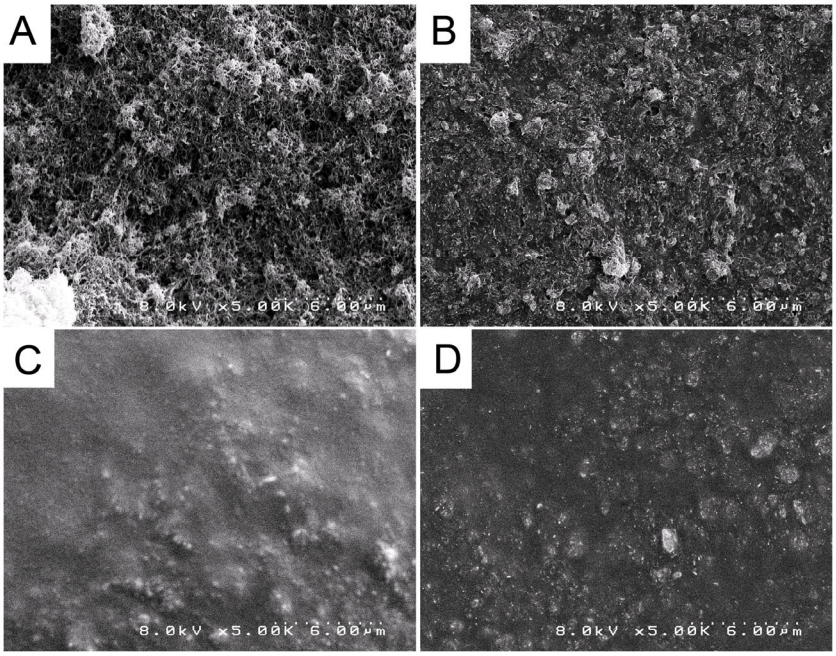

Figure 4. Scanning electron micrographs of CNT-PCU composites with varying CNT-PCU w/w ratios: A) pure CNTs, B) CNT/PCU = 0.5, C) CNT/PCU = 0.25, D) CNT/PCU = 0.16. Surface roughness decreases with decreasing CNT fraction in samples.

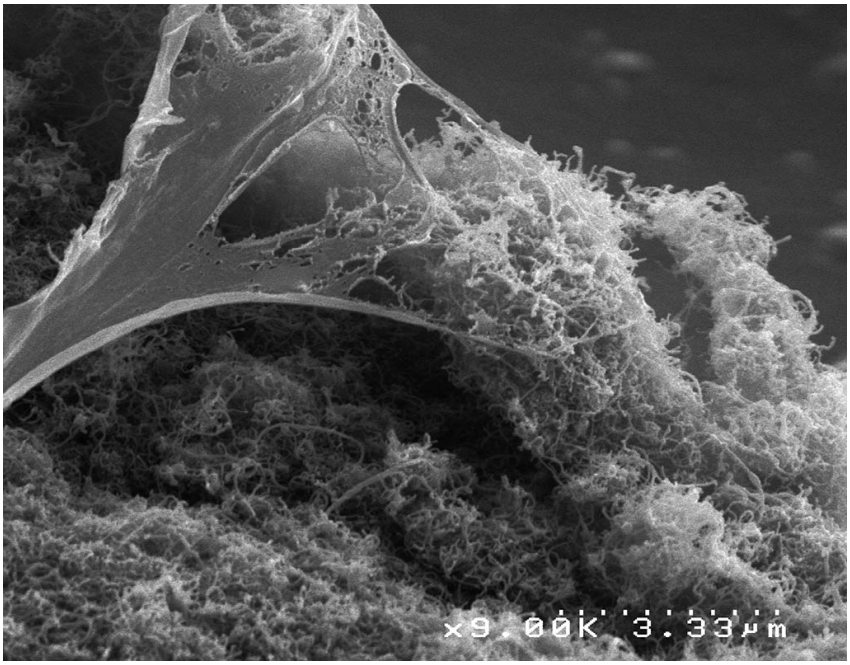

Figure 4. Scanning electron micrograph of a SC on pure CNTs. Cell appears to be damaged by interaction with the substrate. This morphology was not an isolated incident and could be observed on more than half of all SCs imaged via SEM in this experiment.

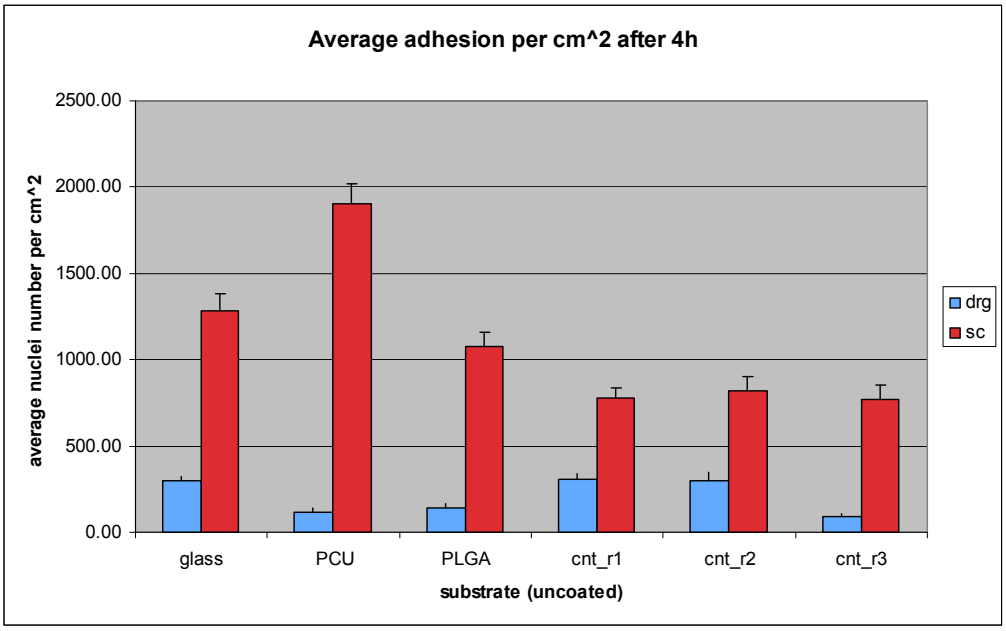

Figure 5. Bar graph showing SC and DRG adhesion to various substrates after 4 h. Substrates were not coated with protein prior to seeding. Cell seeding density was 3,000 cells/cm^2.

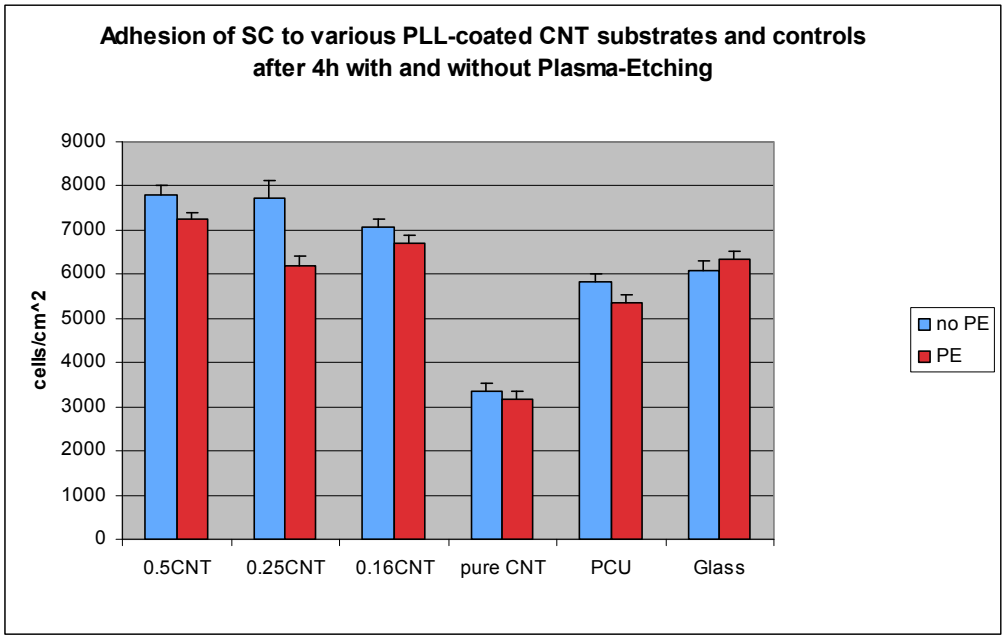

Figure 6. Bar graph showing SC adhesion to various substrates after 4 h. Substrates were coated with PLL prior to seeding. Seeding density was 15,000 SC/cm^2. PE = plasma etched.

Appendix G

Protocols and Designs

In the following section I have appended a selection of the most essential protocols for my work. Having worked in the very beginning phase of the Hoffman-Kim lab, I often had to find, invent, discover, or design my own tools and techniques as I went along. Often, small tweaks have made a large difference, and I have spent a great deal of my time and efforts working out the details contained in the next few pages. While I have not created everything you will find in the following section from scratch, I have invented some, adapted, refined, and modified many of the procedures listed here. I am happy to know that these protocols will continue to be used and developed by future DHK lab members.

Protocols for Cell Media

Base Media (B104 Neuroblastoma cells, A5r7-type Smooth Muscle Cells)

For 200 ml of media:

174ml DMEM (Gibco #10313-021)

20ml FBS

4ml L-glutamine

2ml pen/strep

Neuronal Media

For 200 ml of media:

Neuronal Media (Dorsal Root Ganglia)

For 200 ml of media:

174 ml of MEM

20 ml FBS

4 ml L-Glutamine

2 ml Penicillin-Streptomycin

Add NGF (100 μL aliquots) to base media at 1:100 dilution of stock.

SHSY5y Media (SHSY5Y neuroblastoma cells)

For 200 ml of media:

89 ml MEM

89 ml F-12

20 ml FBS (fetal bovine serum)

2 ml P/S (pen-strep antibiotic)

Schwann Cell Media (Bunge lab)

360mL DMEM without L-glutamine (in fridge)

40mL FBS (in -20)

heregulin (-80)

forskylln (fridge)

4mL penn/strep (-20)

332uL bovine pituitary extract (BPE)

Schwann cell proliferation media (DHK Primary Rat Sciatic SCs)

174ml DMEM (Gibco #10313-021)

20ml FBS

4ml L-glutamine

2ml pen/strep

140ul bovine pituitary extract

32ul forskolin

Protocol for Cell Thawing

Materials

- Cryo-gloves
- Appropriate cell media
- Pipette man (1ml or larger)
- Water bath at 37 C
- T75
- 15 ml falcon tube
- centrifuge

Procedure

Select cells:

1. Obtain cryo log from the lab shelf (above Celinda's desk)

Select cell type

2. note location and remaining vials (don't go under 3 vials!)
3. mark off the vials you are thawing

Prepare:

4. fill a 15 ml falcon tube with pre-warmed cell media
5. fill a T75 with 11 ml of media, store in hood in the TCR

Thaw cells:

6. Location: cryopreservation tank on the Morgan side of the lab.
7. Use cryo-gloves
8. Locate appropriate box on the legend on the lid of the cryo-tank
9. Open lid, pull up row of boxes slowly, let liquid nitrogen drain, remove box, re-immerse row of boxes for the duration of the next steps
10. Open the appropriate (retained) box. Make sure there are more vials of the same type still present in the cryo-tank (sometimes the cryo-log is incorrect)
11. Remove appropriate vial, close box, replace in row of boxes, close cryo-tank
12. thaw the cells in the water bath in the TCR very quickly to prevent partial re-freezing, otherwise large ice crystals may form in the vicinity of cellular membranes and destroy them.
13. Shake vial in the water bath vigorously so the entire contents melt as quickly as possible
14. Prevent water from flowing into the crack between lid and body of the vial, this is a possible source of contamination.

Plate cells

15. Once you have thawed the vial, remove contents and place in 15 ml falcon tube with 5-10 ml pre-warmed media.

16. Centrifuge at 1000 rpm for 10 minutes (this gets rid of thawing media additives such as DMSO)
17. Resuspend cells in 1-2 ml of fresh media and transfer to T75 with media from above

Place the T75 in the upper incubator.

You'll probably need to change media and split the cells 1:10 once a week.

Protocol For Cell Splitting

Materials

- HBSS
- Appropriate cell media
- T75 flask
- Coating protein solution if needed (depends on cell type)
- 10 ml pipette tips
- Cell media waste container

Procedure

1. Warm your media and HBSS-CMF in the water bath
2. Remove media and put it in waste container
3. Add 5mL HBSS to wash cells and remove (2x)
4. Add 5mL 1x trypsin to digest ECM and free cells from flask
5. 5 min with trypsin in incubator
6. Add 5mL media to stop the reaction of trypsin
7. Triturate and remove cells in 10mL solution to a large tube and centrifuge to bring cells to a pellet (1000rpm for 10min)
8. Remove supernatant, and resuspend.
9. Count cells if needed

10. Pipet desired amount of cell solution and reseed it in a new T75 flask, add media to 12mL.
11. Throw away the rest of the cells. (add bleach, dispose in cell waste container under the sink)

Cleanup

- Place all solids that have been in contact with animal cells into the grey bin
- Place all solids that have been in contact with human cells into the red bin
- Place all non-hazardous trash (wrappers etc) in the steel can under the TC hood
- Dispose of needles, other sharps in the sharps container

Protocol for Paraformaldehyde Fixation

paraformaldehyde is very toxic, wear gloves at all times

Materials

- 2% paraformaldehyde, 4% sucrose solution
- PBS
- Haz trash cell waste container

Procedure

1. Take your samples out of the incubator to the green hood in the lab
2. Remove media and rinse with PBS 2x, each time letting the sample sit under PBS for 5 minutes
3. Replace PBS with 2% para, 4% sucrose solution, let sit 10 minutes
4. Remove para solution to appropriate haz trash container
5. Rinse samples 2x with PBS (discard into haz trash

Cleanup

- All materials that have come into contact with paraformaldehyde must be discarded in haz trash or triple rinsed (rinsate is haz trash).
- Para is very toxic, wear gloves at all times.

Protocol for Dissection and Culture of Dorsal Root Ganglia (DRG) Neurons

Materials

- Dissection instruments
- ~10 Gauze Pads
- ~ 3 Q-tips
- Scalpel blades – can use #11, 12, or 15, 11 preferred
- 1 0.5 ml Eppendorf tube per rat pup
- Two pairs of clean No. 5 fine tipped dissection forceps
- One pair angled forceps
- One ice bucket full of ice
- Two small 3.5 cm Petri dishes with HBSS
- 400 uL of 1 x trypsin
- Incubator
- Black trash bag
- Scissors
- 200 uL pipet-man with tips
- Dissection scope
- Base media
- Neuronal media

Prepare

- 1 buckets of ice
- 2 sterile 35 mm dishes with HBSS
- 1 empty 100 mm dish
- Base media (with 10% FBS, 4mM L-glutamine, 1% pen-strep, + insulin)
- Neuronal media
- Add NGF (100 μL aliquots) to base media at 1:100 dilution of stock.

Dissection

1. Get P0-P5 pups from ACF and cover in ice. Be sure to document the number of pups in the rat log.
2. Each pup can yield ~30-40 DRGs (up to 2 million cells).
3. Prepare working area
4. 2 paper towels soaked in EtOH serves as “sterile field”
5. Fill 10 cm Petri dish with ice and fill two small 3.5 cm Petri dishes with HBSS. Keep these two small Petri dishes on top of the 10 cm, making sure they remain cold throughout the procedure.
6. After pup is well-iced (not moving, min 5 minutes under ice), ethanol the head and neck area.
7. Cut off the head into the black bag using large scissors.
8. Hold skin back, use apex of scissors, and cut in one swift motion. Clean scissors under tap immediately, dried blood is very difficult to remove.

9. Blot excess blood against sterile (EtOH soaked) gauze, squeeze pup slightly with headwound facing down for 30 s (removes most of the blood from the body)
10. Use two pieces of sterile gauze to hold pup body in your left (non-dominant) hand.
11. Keep the dorsal side up and the tail pointing down
12. Hold the body in such a way as to pinch the belly skin and make the dorsal skin taut.
13. The midline/spinal column should be somewhat visible, extending from the top of the body down the center back to the tail.
14. Holding the scalpel in your right (dominant) hand, make a midline incision through the skin from the top to the tail. Avoid multiple cuts, one slow, deliberate cut will keep things simple.
15. Reflect skin back away from midline using blade held flat.
16. Cutting a small “T” on tail-side of incision makes it easier to push skin away from midline
17. Cut through top of spinal column with blade.
18. Try to use a single cut for the entire length.
19. Exert enough force to cut through top of vertebrae, but not so much as to sever entire spinal column.
20. Should feel like tracing the blade down a zipper
21. Use Q-tip to pry open column and remove spinal cord.

22. The spinal cord is a white, glossy, cylindrical piece of tissue laying in the exposed spinal column.
23. Wipe the open wound thoroughly with sterile Q-tips (pre-wet with saline and/or dry) to remove excess blood and connective tissue.
24. Use angled forceps to pick out the DRGs; place them in the dish with HBSS.
25. The DRGs are the soft spheres alternating in between the harder vertebrae. Do not grab DRGs directly, rather lever them our and handle them by their dorsal and ventral roots. Place in one of the cold, small Petri dishes with HBSS.
26. After the DRGs have been removed from the pup, place the body in the black bag.
27. When all the DRGs have been collected in the HBSS, use two forceps to clean off the blood, axons, and connective tissue from the DRGs. As DRGs are cleaned, transfer to second dish of HBSS. Carefully clean forceps with saline or other sterile liquid and wipe with gauze as needed.
28. It is helpful to hold the DRGs to the bottom of the dish with one forceps and manipulate the tissue with the other.
29. Preferences for this procedure vary by user: two fine forceps, a fine forceps and an angled forceps, an angled forceps and a scalpel
30. Retrieve an eppendorf with 0.5ml 1x Trypsin from the freezer and thaw.

31. Use angled forceps to gently transfer each DRG explants into the eppendorf, making sure that the DRGs are immersed in the 1x Trypsin solution.
32. Incubate eppendorf tube with DRGs at 37°C for 60 minutes – do not exceed 60 mins.
33. Flick the tube every 15 minutes to dislodge the DRGs from the bottom and mix them with “fresh” trypsin solution.
34. After incubation, remove as much of the 1x Trypsin as possible using a P200 Pipetman. Be careful not to suck up the DRGs. If this is too difficult, try spinning the cells in the mini-cycler at 1000 RPM for 2-3 minutes – this should pellet the DRGs to the bottom of the eppendorf and facilitate Trypsin removal.
35. Add 200 μL of Base Media (or Neuronal Media) to tube (astrocyte or dissection; must have >10% FBS) to further stop digestion the reaction.
36. Set the P200 Pipetman to 150 μl with a yellow tip. This volume is used to minimize bubbles. Triturate 50-70x.
37. To further break up the tissue, you can shoot the suspension against the side of the tube as you triturate.
38. Trituration should continue until there are no more observable DRG explants or tissue debris. Fluid should look relatively homogenous and slightly cloudy.
39. Trituration harms cells, so it is best to minimize the amount of strokes.

40. Depending on the quality of the DRG cleaning step, a small sticky ball of fibrous tissue may form on the tip of the pipette – remove this tissue from further processing.
41. Bring the cell solution in the tube to 1 mL using neuronal media – mix for an even suspension.
42. Count cells on a hemocytometer.
43. Using neuronal media, plate your cell suspension into well-labeled plates.

Cleanup

- Discard any tissue waste into the black bag. Bag can have paper but not plastic dishes. Therefore, clean dishes with paper towels or Kimwipes, discard paper and gloves in black bag and cleaned dish in regular trash. Take the bag to the morgue (need elevator/morgue key).
- Clean work area and instruments.
- Remove scalpel blade using hemostat NOT hands.
- Discard blade into red sharps container.
- Take care when cleaning the fine-tipped instruments and do not place new tweezers into metal box. ALWAYS cover fine tipped forceps with protective caps, and NEVER store them in the metal dissection box.

M. Shah 6/26/02

D. Hoffman-Kim edited 6/28/02

V. Fong edited 06/19/06

J. Bruder – Spring 2008

Protocol for Hoechst 33342 Live DNA staining

Materials

- Hoechst 33342 stock solution (-20 C freezer)
- Fetal Bovine Serum
- PBS
- Incubator

Procedure

The following outlines the procedure for staining and analysis of cells using Hoechst 33342. Modifications may be required depending on the application and with variable response of individual cell types.

H33342 is a "vital" DNA stain that binds preferentially to A-T base-pairs. The cells require no permeabilization for labeling, but do require physiologic conditions since the dye internalization is an active transport process. This condition typically varies among cell types, but the following procedure will give good results in most cases.

1. Stock H33342 solution: H33342 should be originally suspended in dH2O at a 1mM concentration (H33342 will precipitate in PBS).
2. Cell suspension: This procedure is very sensitive to cell concentration and pH of the media. Cells should be approximately 1-2x106/ml, in buffered

media, pH 7.2. It is also helpful to include 2% fetal bovine serum to maintain the cells.

3. Add H33342 dye from the stock solution to cell suspension to 10μM final concentration.
4. Cells are then incubated at 37 C for 1 hour. Time is a critical factor due to the transport of the dye. Typically, 30 minutes is a minimum, but it is important to remember that the signal may begin to degrade after ~120 minutes. It is recommended that the staining kinetics be empirically defined.
5. Analyze immediately after incubation. Washing is not recommended (see step 4). H33342 stained cells will be illuminated DAPI optics.

H33342 will also work with Paraformaldehyde-fixed cells, with modification to the above protocol, usually calling for a reduction of H33342 concentration (to ~1μM). Dye incubation time is drastically reduced (to ~15 minutes) since the cells are permeabilized while fixing.

Jan Bruder – Spring 2008

Protocol for Alexa Fluor 488 Phalloidin (Actin Stain)

Materials

- Triton X
- Alexa Fluor Phalloidin
- PBS
- Pipette
- Cell waste haz trash container

Procedure

1. Cover para-fixed cell sample in 0.1% Triton-X in PBS solution, let sit for ~3-5 min
2. Rinse twice with PBS
3. For 1 “unit” of staining solution, dissolve 10 uL methanolic phalloidin stock into 200 uL PBS. (In my experience, using 2 “units” per coverlsip -- 20 uL stock solution into 400 uL PBS -- yields the most aesthetic result.)
4. Place Phalloidin solution on sample, and let incubate at room temperature for 20
   minutes.
5. Rinse twice with PBS; view immediately for best results
6. Coverslips will retain fluorescence for ~3 days.

Cleanup

Place all materials that have been in contact with phalloidin stain or the cells into the cell waste container.

Jan Bruder – Spring 2008

Protocol for Dapi Staining

Materials

- 100x (100ug/ml) stock solution of Sigma D9542-1MG 4',6-Diamidino-2-phenylindoldihydrchloride (DAPI)
- PBS
- Fixed cell sample

Of note

- DAPI is soluable in dH2O up to 20mg/ml, not very soluable in PBS at all. Thus, stock is frozen in dH2O, but can be diluted in PBS for final use.
- DAPI only fluoresces when in contact with DNA, thus rinsing samples after application for DAPI is optional.
- DAPI can enter through cell membranes, permeabilization is not necessary but may enhance results.
- PDMS appears to be slightly autofluorescent for the excitation wavelengths used for DAPI. Good DAPI staining still provides a sufficient S/N ratio to result in clear DAPI images despite low PDMS autofluorecence.

Procedure

1. Obtain 100x DAPI stock in box 48 in the -20C freezer.
2. Dilute stock 100x with PBS
3. Apply DAPI solution to para-fixed sample.
4. View sample immediately or rinse and resuspend in PBS
5. addition of 0.01% triton x can aid visualization if problems arise.

Cleanup

Dispose of DAPI containing solutions in a hazardous waste bottle clearly labeled with contents.

Jan Bruder – Spring 2008

Protocol for Immunostaining

Materials

- Goat serum
- PBS
- Aluminum foil
- 50 ml falcon tubes
- Pipette-aid
- 10 ml pipette tips
- Appropriate primary antibody
- Appropriate secondary antibody
- Triton-X

Working Solution

(5% goat serum + 1% BSA in PBS)

to make 40mL Working Solution:

2 mL 100% normal goat serum (NGS) (freezer)

38 mL PBS

0.4 g BSA (fridge door)

Block Solution

(Working (5% goat serum + 1% BSA) + 0.1% Triton in PBS)

to make 40 mL Block

39.6 mL Working Solution

0.4 mL 10% Triton in PBS

Procedure

Overview

1. Block nonspecific binding
2. Apply primary antibody
3. Rinse
4. Apply secondary antibody
5. Rinse

1. Block nonspecific binding. (1 h)

- Remove and discard PBS used for storage of cells.
- Cover each sample with blocking solution
- Shake at speed = 30 rpm on shaker for 60 minutes.

- While this step is incubating, prepare primary antibody in Working Solution. Save working solution (good for at least one week).

2. Apply Primary Antibody (overnight)

- Once the block incubation is over, remove Block from wells.
- Cover sample in working solution with primary antibody. Put working solution without primary antibody in control (no primary) wells.
- Parafilm plate and refrigerate overnight.

The next day…

3. Rinse (~1 h)

- Take plates from fridge, shake at 30 rpm for 30 minutes at room temperature.
- Dilute stock secondary antibody in fresh Working Solution.
- *Note: Keep secondary antibody in the dark as much as possible using aluminum foil wrap for both test tubes and 6-well plates.
- Remove solution (primary Abs) from wells.
- Label and Save this solution in Ab-box: 4°C fridge. It can be reused for up to a year.
- Wash all wells with PBS for 5 minutes on shaker. Repeat 2 additional times.
- Wash all wells once with Working Solution for 5-10 minutes on shaker.

4) Apply Secondary Antibody

- Cover each sample with secondary antibody in working solution.
- Shake at speed = 30 on shaker for 60 minutes or longer if signal is weak.

5) Rinse

- Once the incubation is over, rinse 3 times with PBS for 5-10 minutes. Done.

The concentration and incubation times for primary and secondary antibodies varies from antibody to antibody and should be explored with a few pilot samples before important experiments. Primary incubation times can be as high as 3 days (S100) and secondary as high as 3 h (S100).

Cleanup

- When dealing with Para, use gloves, work on a large kimwipe in the green hood. For the purpose of easy disposal, use two 10ml pipets, one clean & one dirty (para).
- Dispose of contaminated plastics, papers, and fluids in the ParaHazWaste container.

- Contaminated pipets should be rinsed 3 times with normal water and thrown in the trash. (Dispose of wash water in the waste container.)
- Gloves should be wiped (with kimwipe – dispose of in waste container) removed inside-out before disposal in the regular trash.

Mathu Subramanian (2/28/02)

Modified: Meera Shah 4/15/02

Modified: Pearl Yu 6/25/02

Modified: Joshua Goldner 10/10/03, 6/19/04

Modified: Jan M. Bruder, Spring 2008

Procedure for Microstamping

Materials

- __ PDMS stamp fresh off the wafer (cured for 2h at 95C)
- __ coating protein
- __ pipettes
- __ sonicator
- __ dH2O
- __ air gun

Optional

- __MeOH
- __EtOH

Procedure

Throughout this procedure, DO NOT touch the patterned side of the samples with your hands, and try to minimize handling with tweezers. If you have to move substrates, use tweezers and grab only the edges of the samples. We are trying to produce a very thin, very homogeneous protein coat, use common sense to avoid any disturbances. No steps in this procedure are sterile, but avoid exposure to dust.

1. prepare PDMS stamps, remove from wafers

   ------optional substrate cleaning ----------

2. Fill a 50 ml eppendorf tube with 10% SDS in dH2O and drop substrates into it
3. Close lid and sonicate in a bath sonicator for 5 mins
4. Rinse in large quantity (~1L) of dH2O
5. Blow dry
6. Submerse in MeOH (works well in 50ml eppendorf tube)
7. Without rinsing transfer to 100% EtOH (again 50ml eppendorf works well)
8. Blow dry with air gun

   ------- end optional substrate cleaning ---------

9. To prepare for laminin removal, take a 2ml pipette-aid pipette, break off the first 3 inches and firmly jam this tip into the front of the air gun.

44. *We want to create a strong laminar air flow that quickly and homogeneously removes any liquids from our stamps in the following steps. The plastic tip focuses the air flow and accelerates it, making it very easy to remove liquids out of the microfluidic grooves of the samples.*

10. Place droplet of desired protein solution on stamp surface, let sit 10 min or more (if fluorescent, protect from light)

45. *The substrates are very hydrophobic, and thus this task is tricky. One way around this is suspending a very large droplet on a substrate initially and "dragging" it out with the tip of the pipette (without touching the surface), then moving on to other samples and later coming back and removing some of the excess liquid. Often, the droplets are more stably suspended after a minute or two and one can remove 50-70% of the volume without contraction.*

11. Pipette protein solution off, carefully avoiding contact with stamp surface
    a. *One thing to watch out for is the possibility of drying the droplets out. Leave a sufficient volume per sample (~100-300 ul) and cover the Petri dish with a lid during incubation.*

12. Immediately submerse in dH2O, 2 rinses

13. plasma-etch substrates at "high" for 30s
14. Place substrates face up into a 100 mm petri dish

15. Remove/dry remaining dH2O from stamps with air gun immediately before stamping

16. Without delay, invert stamps onto stamping substrates, let then adhere by surface interaction. Do not let them slide/move in X-Y direction, this will destroy pattern fidelity. Let sit for a minimum of 10 seconds (if fluorescent, protect from light). Apply light pressure (~20-50g) if desired).

17. Carefully remove stamps from stamping substrates, patterns should be done.

Safety Concerns

Refer to MSDS of materials used.

Jan Bruder – Spring 2008

Procedure for Schwann Cell Seeding And Alignment

Protocol makes 9 samples, 1cm^2 each, on one glass slide

Materials

- __ SC media (20 ml, +15 ml for resuspending)
- __ Confluent Flask of SCs
- __ 10x trypsin
- __ ample HBSS and tissue culture water
- __ PLL
- __ 1 new, PLL coated T75 flask

Procedure

- This procedure is sterile, so be sure to use sterile technique in the TC hood.
- This protocol describes how to seed the SCs while replating them into a new flask to continue the cell line.

1. Start by carefully removing the stamping substrates from the glass slide with forceps. Rinse gently with TC water.

2. Prepare the SCs: Retrieve a confluent T75 from the incubator, remove the media, rinse with 5ml HBSS, and add 5 ml 1x Trypsin. Replace into incubator for ~5 min.
3. Retrieve the flask and firmly tap it with your fingernails on the side. Holding it up against the light you can see whether the cellular film dislodges from the plastic. If not, place the flask back into the incubator for another ~2 minutes.
4. If the film does come off the plastic surface, take a 10ml pipette, fill the new (unused PLL-coated) T75 flask with 11 ml of SC media, and add 5 ml of media to the flask containing trypsin, vigorously pipetting up and down a couple of times to break up cell aggregates. Take 0.5 ml of the resulting solution and transfer it sterilely to the new T75 flask containing 11 ml of media. Label this flask and place it into the incubator.
5. Pipette the remaining trypsin/cell/media solution into a 10ml falcon tube and spin the cells down at 1K rpm for 5 mins. Remove supernatant and resuspend in 10 ml of media.
6. Place a drop of solution onto a hemocytometer and determine the cell concentration. Dilute with SC media so that you have 20 ml of solution with 30K cells/ml in SC media. To be on the safe side, prepare 40 ml.
7. Pipette the mixture into a 10 cm Petri dish, put on a rotary shaker at 30 rpm for 3 min to evenly disperse the cells
8. Place the petri dish into the incubator and monitor cell density until SC become confluent (usually 5-7 days). Do not replace media, since SCs

produce factors that promote their own growth. At our low cell density, they will not starve in 5-7 days.

Cleanup

- Place all solids that have been in contact with animal cells into the grey bin
- Place all solids that have been in contact with human cells into the red bin
- Place all non-hazardous trash (wrappers etc) in the steel can under the TC hood
- Dispose of needles, other sharps in the sharps container

Procedure for Cell Fixation of Cell Templates

Materials

__ 2% paraformaldehyde / 4% sucrose solution

__ ample amounts of PBS

__ SEM preparation chemicals (listed on a separate sheet)

Procedure

Work in the green hood in the back of the lab for this procedure. Wear gloves. Avoid spillage and clean up meticulously after yourself. Paraformaldehyde (even its vapor) is VERY toxic.

1. When the SCs are confluent and aligned, remove them from the incubator, pipette off the media, and rinse twice with PBS for 5 min each.
    a. This rinsing step is crucial, since the paraformaldehyde will crosslink all proteins present. The SC media contains lots of proteins that will cling to the cell prep and give it a “beer-battered” appearance if not removed by thorough PBS rinses. Since these samples will be used to study the influence of topography, the proper surface identity of the SCs is essential.

2. Add the formaldehyde solution and let it sit at room temperature for 15-20 min. Remove the solution, and rinse twice with PBS. All discarded liquids after the addition of Para should be discarded into the para waste bottle to the right of the hood in the main lab.
3. Discard the PBS covering the samples and replace it with Karnovsky's fixative. Place the samples in the fridge overnight.
4. Follow steps for SEM prep outlined on a separate sheet ("O-T-O Fixation" from the EM facility). Plan 1 full day for this. There is no need to HMDS dry. Gold sputter coat for 2-3 minutes rather than 4.

Cleanup

- All materials that have come into contact with paraformaldehyde must be discarded in haz trash or triple rinsed (rinsate is haz trash).
- Para is very toxic, wear gloves at all times.

Protocol for Osmium-thiocarbohydrazide-Osmium SEM Preparation

** Almost all chemicals (including vapors) involved in this procedure are extremely toxic. Wear gloves at all times!**

Materials

- Karnovsky's fixative
- 4% Osmium Solution in dH2O
- Thiocarbohydrazide in powder form
- Ethanol
- Cacodylate buffer solution

Procedure

1. Only work under a flow hood. Vapors are toxic.
2. Fix specimens in Karnovsky's fixative for 3 hours ----> months. Rinse well with cacodylate buffer and postfix in buffered Osmium tetroxide (1 part 1% OsO4 : 1 part 0.1M NaCacod. buffer) for 1 hour under the hood.
3. Rinse well in distilled H2O - 3 x 10 minutes. (Mixing 0s04 and TCH will result in a metallic ppt. that can ruin surface morphology.)

4. While samples are rinsing, dissolve 1% Thiocarbohydrazide (TCH) in distilled H2O. Filter solution with medium speed filter paper. (Solution may turn slightly pink in color.) Immerse specimens in TCH for 30 min. - 1 hour.
5. Rinse well as before.
6. Immerse in 1 part 1% 0s04 1 part distilled H2O for 30 minutes.
7. Dehydrate in ETOH: 50, 70, 90, 100% (2x) 10 minutes each.
8. Air dry on filter paper. When properly dried, samples should have a matte black appearance and be very brittle. (Handle carefully.)

Tips

**Place TCH waste in designated waste container in the hood. Do not pour down the sink!

**While samples are drying, be sure to cover them to prevent debris on the viewing Surface.

Cleanup

All chemicals in contact with samples become hazardous waste. Dispose accordingly.

Protocol for Preparing PDMS Polymer

Materials

- Sylgard 184 Elastomer Kit from Dow Corning
- Glass rod
- 50 ml Falcon tube
- centrifuge

Procedure

Mix & Degas Elastomer

1. Tare a 50-mL Falcon Tube on the Mettler open-air analytical balance.
2. Pour elastomer base into the beaker. (~4g/mm of thickness on a 3in Si-wafer)
3. Note the mass of elastomer base.
4. Tare the balance.
5. Dropwise, add curing agent (10% of the elastomer base weight) to the beaker.
6. Example: 4.00 g of curing agent for 40.00 g of elastomer base.
7. Mix thoroughly by hand using a glass stirring rod until the mixture turns extremely bubbly; it appears almost white in color.
8. WHIPE OFF the glass rod and the edge of the elastomer container with a paper towel. PDMS residues either remain greasy and slime up all surfaces, or it turns lumpy and becomes very difficult to remove. Residue

on the glass rod can dislodge during the next use and will create artifacts in future samples.

9. Centrifuge beaker for 1 minute at 2000 rpm to remove bubbles.

Prepare Mold/Wafer and Cure

10. Be sure your mold is free of dust etc. (spray with air gun on bench)
11. If this is the first time you're using a Si-mold, be sure you have Silaned first.
12. Pour de-gassed PDMS onto the mold to reach desired thickness. Pour slowly and try to minimize the distance between pouring vessel and mold as this minimizes the chance of bubble formation.
13. Let the mold and PDMS sit on the bench top for 10-20 mins during which the PDMS will degas itself. Once no bubbles are visible, move on.
14. Do not place the sample into a vacuum. If tiny bubbles are trapped underneath the silicon wafer, the sample can "explode".
15. Place the dish with the mold and PDMS on a hotplate at 95°C for 2 h to cure.
16. After 2 h, remove the dish from the hotplate, cut out the PDMS with a razor blade
17. CAREFUL not to chip or crack the wafer or any of the features!
18. Do not cut out individual parts from one wafer. Either cut out the whole molded area (leaving a slight rim to hold the wafer in place) or don't cut

out anything at all. Partial cutouts create menisci during refilling, and samples will be useless for phase microscopy.

19. Once cooled, place the PDMS pattern up in new Petri dish and refill the wafer with more PDMS, repeat curing procedure. Store wafers with cured PDMS on top as a protective layer.

Cured PDMS Storage

- Store in Petri dish, protect from dust. PDMS attracts dust.

Millie Ford (2002)

Modified - Joshua Goldner (August, 17, 2004)

Modified – Caitlin Elgarten (August 5, 2005)

Modified – Jan Bruder (October 18th, 2006)

Protocol For Replica Molding

Materials

- __ Dow Corning Sylgard 185 PDMS and curing agent
- __ 10 cm dishes
- __ availability of the hotplate
- __ glass rod
- __ 50 ml falcon tube
- __ centrifuge

Procedure

This protocol walks you through the fabrication process of an impression and relief replica.

1. Prepare PDMS: Mix elastomer and curing agent in a 10:1 ratio (w/w) in a 50 ml flacon tube. 5 ml per used cell template should suffice. 20 ml are needed to embed a new template into a solid layer of PDMS in a 10 cm Petri dish. When mixing, use a glass rod and make sure to trace the rod along the inside surface of the falcon tube, mixing PDMS that is adherent to the plastic walls. Incompletely mixed PDMS will not cure properly and destroy your cell template or wafer. Properly mixed PDMS appears milky

white to entrapped bubbles.

2. Degas PDMS mixture by placing it into a centrifuge at 2000 rpm for 15 s.

3. Pour degassed mixture over cell template. Keep the distance between falcon tube and wafer under 1 inch, this will help avoid bubbles.

4. DO NOT place your cell template into the vacuum chamber to remove bubbles, should they occur. The vacuum chamber can cause entrapped air under the cell template to generate enough pressure to “detonate” your cell template.

   DO let the sample sit on a flat table top while covered with a lit for ~30 minutes. PDMS is self-degassing, and this is the easiest and gentlest way to get rid of air inclusions. If you are preparing a new template and are embedding it in PDMS, it is best to let the sample sit and cure in PDMS overnight on a plane surface without the use of a hotplate.

5. Once all bubbles have disappeared, cure PDMS at 95 C for 1 h (if you don’t want to culture cells on the sample the same day) or 2 h (if you do want to culture cells on the sample the same day). PDMS appears to negatively affect cell growth when only cured for 1 h and used on the

same day.

6. After curing, remove impression replica from cell template by cutting around the perimeter of the glass slide with a razor blade. Leave a small rim of PDMS overlapping the glass slide; this will make subsequent casting and handling easier. Remove impression replica with No. 5 tweezers, surfaces should separate relatively easily.

7. To generate a relief replica. Place the impression replica pattern side up in a 10 ml Petri dish and use a small metal strip (10 by 0.5 inches) bent in a square shape as a removable cast “wall”. Place this wall around the desired pattern on your impression replica and pour freshly mixed, uncured PDMS into this molding form. Use a 1 L water bottle filled with water as a weight to minimize PDMS leaking through the “wall”.

8. Cure at 95 C for 1 or 2 h as before.

9. Remove the “wall”/molding form and use No. 5 coarse forceps to separate impression and relief replica. Force the tip of the forceps between any obvious spot demarking the boundary between IR and RR and trace the forceps around the perimeter of the sample. This loosens the edge of the RR and greatly facilitates separation. Once the whole perimeter is separated, take gloved fingers and pull IR and RR apart.

Procedure for Timelapse Microscopy

This tutorial explains the process of setting up samples for timelapse microscopy, Koehler illumination, operating Openlab with automation, shutting down the automation, and optimizing the liff image workflow for handling and archival.

Days before time-lapse

- Sign up for the microscope time right next to the white-out board in the lab.

About one hour before microscope use, make sure to

- Attach your samples with vacuum grease to prevent drifting during timelapse.
- Turn on the heater (it should heat up to 37C within 30min-1h)
- Fill all Petri dishes in the incubator with water to moisturize the chamber.
- Check the CO_2 tank, making sure there is enough CO_2 for the duration of your run (you need ~100psi per 24h).

Timelapse microscopy procedure

1. Check that the heat has stabilized at 37C

2. Turn on the four power supplies next to the microscope. They are the halogen lamp, Hamamatsu camera, Orbit box, Halogen light source, and LudlMac5000 box.
3. Place your sample onto the stage.
4. Focus on your sample and go through the steps of Koehler illumination:
5. Making sure the port is switched over to “eye,” peer through the eyepiece and focus on the surface of your sample
    a. *Never use the fine focus as this will damage the z-motor!!*
6. Turn on the light (on the bottom left side) and use the light adjustment knob to adjust appropriately.
7. On the Orbit keypad, make sure the shutter is set to S1 (transmitted light).
8. Manually turn the filter turrets so that all transmitted light passes through the filter wheel. (No visible color cast from a fluorescent filter is visible)
9. optimizing light dispersion for maximum contrast:
10. Close the field diaphragm (at the top, above the plastic incubator).
11. Focus the condenser assembly (inside the incubator, above the stage) up or down until the light beam has an octagonal shape
12. While peering through the eyepiece, open the diaphragm just enough to bring the edges of the octgon outside the field of view.
13. Aligning the phase ring:
14. Switch the Bertrand lens counterclockwise (wheel mechanism directly under the eyepiece) to focus onto the plane of the phase ring assembly.

You will see a bright circle with a hoop disconnected in three parts around it.

15. Align the circle toward the center of the hoop by inserting a small allen wrench into either hole angled at 45 degrees from the axis between you and the microscope on the front side of the condenser assembly
16. Switch the phase ring lens back to the normal view.
17. Turn the main valve of the CO_2 tank ccw about one full turn, and regulate the air flow to 10 psi by turning the middle black increase/decrease regulator valve accordingly.
18. Switch on gas flow controller (controller is on “purge” mode for 10-20s, flow normalizes after this)
19. Submerge the CO2 outlet into a dish with water, making sure that bubbles come out to test adequate gas flow
20. Heat up the needle syringe CO2 outlet tip with a lighter. Quickly insert then pull the syringe tip out of side of the sample container lid, effectively poking a hole through the container.
    a. *If you do not pull the syringe tip out fast enough, the plastic container will cool and solidify around it and make it very hard to pull back out. Be careful about deciding where to place the gas input on your sample: keep in mind that the stage can move around freely if you do multi-position timelapse.*
21. Heat the syringe tip again and let it cool before re-inserting it.

   a. *This is to melt off any plastic that may have clogged the tip during insertion.*

22. Insert the tip into the hole that you just made in the container lid.
23. Tape the sample container down to the part of the stage that will not dislodge the tape (usually the right side, taping over the metal part of the syringe).
    a. *This ensures that no extra movement occurs while moving the stage around with the joystick.*
24. Restart the computer.
25. Change energy setting to “never sleep.”
26. Start OpenLab 4.0.4.
27. Operating Openlab:
28. Switch the microscope view to camera (button on right side of scope).
29. Calibrate the stage by clicking control → calibrate in the xy-stage menu (open it under windows/xy-stage)
30. Press “V” on the keyboard for the video preview window.
31. To make the window larger, drag the bottom right corner, then click zoom → fit to window.
32. Click Focus Drive → Servo off.
33. Click window → X-Y Stage. In that window, select all points and delete them.
34. In the xy-stage palette (not the xy-stage window) tab, manually set points using the joystick to move the lens over each desired point. Click on the

icon (a little red cross) at the bottom right of the window to save the current position as a point.

35. Start the automator by clicking Automation → the desired automation and follow the steps presented to you on the screen.

Shut down check-list

1. Turn off the CO2 tank and the heater. Keep the CO2 flow monitor switched on until all remaining gas has been drained from the gas tubes (pressure on the manometers on the gas flask = 0)
2. Turn off all the power supplies.

Handling the TL files

1. In Openlab, determine how many images (layers) each liff file contains.
2. Transfer all liff files from eeyore to either Britney or the Lab PC
3. Create a new volocity library on the ImageData HD. Note: if you are using the lab PC, you need to rename the files by using the File Renamer program on the desktop. Search for the desired files, then change the extension by clicking change to custom extension and type in “liff.”
4. Take these liff files and drag them into the Volocity window – do not exceed 3000 images per session (Britneys ram runs out around ~3000 images and things slow down significantly if you add more images).

5. Each folder contains both folder thumbnails and “empty” files. To highlight only the image files, press Apple F and enter a phrase common to only image files (In most cases, it is the letter “z”).
6. In Volocity, click file → export. A window will appear asking where to export these files into. Check jpg, and click naming → check only the “append the file name” option.
7. Quit Volocity to purge the RAM. In finder, highlight the liff files that you have turned into jpg’s and press Apple Delete to send them to trash. Repeat previous steps until all liff files are processed into jpgs.
8. Sort and assemble jpgs with your favorite batch program, good choices are imageJ and Openlab (for quicktime movies).

Common Pitfalls

There may be focus drift due to lack of moisturization of the chamber and/or the gas input, focus drift due to bubbles that form underneath the samples, XY drift due to badly attached samples, and dead cells due to clogged needle/inadequate gas input.

Andrea Lee with Jan Bruder – Fall 07

Jan Bruder – revised and extended Spring 08

Protocol for Image Analysis of Nuclear Cell Alignment

Materials

Sample with cells stained for DAPI

Microscope with DAPI imaging capability

Computer with Photoshop and ImageJ

Image Acquisition

1. Follow microscope protocol to turn on fluorescence microscope, making sure all equipment is off before turning the mercury bulb on. Focus on your sample in phase contrast mode (F1) and Koehler illuminate. Rotate filter wheel for DAPI filter, dull blue light shining onto substrate. (Cells should appear blue with black background if correct filter is in place.) Use F6 on the computer to change settings to DAPI mode.
2. Exposure setting for F6 is 15ms, however, it is helpful to decrease the exposure time to make the images darker so that only the nuclei appear, (~10ms). Keep it consistent for images of all substrates of a particular experiment. Alternatively, go to the camera tab in Openlab and select “auto-contrast” checkbox.

3. In phase contrast mode, align the substrate as desired (ie substrate pattern is horizontal in FOV).
4. Take desired number of FOVs per substrate, with phase and DAPI for each FOV, adjusting the fine focus each time, but keeping exposure time consistent.
5. Save all OpenLabLiff files as “tiffs for presentation” onto Britney and then turn off microscope.
6. Dispose DAPI solution into hazardous waste container. If needed, re-submerge substrates with PBS.

Image Analysis

1. Create a new automation in Adobe Photoshop.
    a. Under ‘Window’ make sure ‘Actions’ window is checked off and visible.
    b. Open one of the tiff images in Adobe (File>Open). Press ‘begin recording’ (circle at the bottom of the Actions window).
    c. Invert the image (Image> Adjustments> Invert)
    d. change the image to 8-bit greyscale (Image> Mode> check Greyscale and 8-bit)
    e. apply levels or curves command until nuclei are as close to black as possible on a white background
    f. DO NOT save the image (File> Save).

g. press ‘stop recording’ (square at the bottom of the Actions window).

2. Batch automation:
    a. Select File> Automate> Batch.
    b. Chose the action you have just created from the drop-down menu.
    c. Select the source and destination files of your images.
    d. If your automation has a ‘save as’ command, check the box ‘override save as commands.’

3. Open ImageJ. Analysis can be done individually or with all pictures as a batch.
    a. Batch analysis:
        i. Select File> Import> Image Sequence and choose an image from the source folder of your adjusted images.
        ii. A window will appear where you will enter the number of images from the folder to be analyzed.
        iii. Check the box ‘Convert to 8-bit grayscale.’

    b. Select Plugins> MultiThresholder.
        i. Change the function (pull down menu) to Otsu.
        ii. Cell bodies should appear red, the background white. If so, click ‘apply;’

iii. if the background appears red you may have to go back to Photoshop and make the nuclei darker and the background lighter.

iv. On the next screen that appears, make sure all boxes are checked and click ‘Ok.’

c. select Analyze> Analyze Particles.

i. Enter 50-850 in Size (this is the size range accepted by the analyzer; you want to include all of the individual nuclei, but disregard stray pixels and nuclei that are clumped together).

ii. Make sure Circularity is 0.00-1.00.

iii. Under the Show menu, select ‘Outlines’ to see the particle accepted by the analyzer (to check your work). Make sure all the boxes are checked, and click ‘Ok.’

iv. Check the Drawing to see if most of the nuclei were selected individually

v. copy all of the data in Results into an Excel file, and enter the information in Summary in the same Excel file.

vi. Then close the Results, Summary, and Drawing windows and repeat the process for each batch of pictures.

4. Circular Statistics

a. Open Oriana circular statistics software on a PC (sorry, no Mac version available)

b. click on the icon to make a new file, select the ‘Axial (bi-directional angles)’ option, and click ‘Next.’
c. Make sure ‘Circular Data Only’ is selected, then click ‘Next.’
d. Depending on how much data you have, select the appropriate number of columns. If all substrates are the same (including the angle of the orientation) then only one column is needed.
e. If you would like to group samples that had the same substrates, but different angles (i.e. you didn’t rotate them before you took pictures), you have to measure the angle in Open Lab and make adjustments in Excel.
f. Enter a title for your data and click ‘Finish.’
g. Copy the columns of angular data from the Excel file, and paste them into the table in Oriana (it will automatically add enough rows for your data as long as the columns match).
h. To make a circular histogram: Select ‘Graphs>Histograms’. Make sure ‘Circular’ is selected on the ‘Main’ tab, and otherwise edit the graph as you would like. Click ‘Okay’ and copy the resulting graph into your Excel file.
i. To get statistics: Select ‘Analyses> Stats’. Make sure the statistics you want reported are checked off and click ‘Okay.’ Copy the statistics return into your Excel file.

Jan Bruder (recorded by Jennifer Pallay and Christina Johnson) Fall 2007

Revised and extended – Jan Bruder Spring 2008

Protocol for Handling and Compiling Confocal Images

1. Save acquired confocal images to desktop (these are in the form of .tif files; 1 file per channel and slice).
2. Search (in folder) for particular channel you desire (i.e. channel 1 is red, channel 2 is phase etc). Select images in that channel for one substrate and copy to a new temp folder.
3. Open Irfanview and go to VIEW- Multipage images- Create Multipage TIFF – Add Images. Select your images from the temp folder.
4. Create the file and open the program VOXX 2.0 (freeware from Indiana Center for Biological Microscopy)
5. Drag your newly created multi-tiff file onto the Voxx view screen and voila!
6. Note : make sure that the x-y-z ratios are as desired. To view ratios from confocal data, open the accompanying text file from your raw Tiffs and find your data set. Look for “voxel width/height/depth” and compare ratios. Divide Z/X and input that number in Voxx -VIEW-Scale – Z value
7. Voxx can save snapshots of your image. You can zoom, do cut-aways, and even animate movies.

Protocol for Use of Matlab Program to Measure Pixel Alignment

Purpose

The matlab program is designed to achieve two separate goals:

1. to take a source image and create 18 distinct images from it, each one rotated 10 degrees from the previous one.
2. To iteratively evaluate every pixel in each image and return counts for segments of 50 consecutively bright pixels in separate horizontal and vertical counts.

The numbers generated can be plotted against rotational angle and indicate the main direction of pixel alignment to the nearest 10 degrees, and can be used to quantitatively compare the extent of alignment between separate images, no matter what content the images contain.

Preliminary Image Preparation

1. Assemble images into 2x2 image arrays without seams (ImageJ works well for this)

2. Convert images to 8-bit greyscale images and threshold them to yield maximum visibility of the features you are trying to analyze (i.e. neurites). Avoid creating excessively large white areas, as these tend to “water down” the final counts.
3. Save images as .tif or .tiff
4. Import images in photoshop and create a black region on the outside of the square image with a circular hole showing the original data (use the marquee tool and the invert selection functions). It is imperative to create a perfectly circular window with a black outline, as the matlab code will otherwise generate biased data during rotation, which will lead to false counts.
5. save this file as “image_0.tif” and place it into the matlab/{version number}/work folder. This folder should already contain the rotate.m and original.m matlab editor files containing the program.

Running the Matlab Program

1. In the first step, open the rotate.m file and execute it by pressing f5. The program should generate rotated versions of the original image_0.tif file and name them image_10.tif, image_20.tif, and so on.
2. Once finished, re-import all rotated images into photoshop and crop away as much of the black area as possible without truncating the circular central region containing the actual data. This is to minimize memory

needs in matlab, which tends to crash if the images are not cropped. Save the cropped images over the originals located in the “work” folder.

3. Return to Matlab and doubleclick on original.m . The “rotate” function should be preceded by a “%”, effectively turning it off. Run original.m by pressing f5. Depending on the size of data, this can take up to 30 minutes.
4. Once the program has completed, it will generate three kinds of data in the main matlab window:
   - Horizontal Line count: number of segments with 50 pixels in pixel rows for each image
   - Vertical Line count: number of segments with 50 pixels in pixel rows for each image
   - Anisotropy: vert line count/(vert+horz line count)*100
5. Copy the desired data into an excel spreadsheet for further analysis.
6. Repeat procedure for more images if necessary.

I developed this Matlab program by an inspiration from Liane and wrote the code with help from Michael Sherback.

Matlab code

Program 1:

```
% image loading
clear all; % clear all variables
close all; % close all figure

rotate;
clear all;

% parameters of method
threshhold = 50
lineLength = 50
highLevel = 255
maxAngle = 190
numFiles = 20% should be maxAngle/10+1


for(imageNum = 1:numFiles)

   degreeList = linspace(0,maxAngle,numFiles);

   filename = sprintf('image_%i.tiff',degreeList(imageNum))
   a= imread(filename,'TIFF');
   %figure(100+imageNum)
   %image(a)

   [nrows,ncols] = size(a);
   b = zeros(size(a));

   % thresholding
   for ii = 1:nrows
      for jj = 1:ncols
         if(a(ii,jj)>threshhold)
            b(ii,jj) = highLevel;
         end
      end
   end
   figure(200+imageNum)
   image(b)

   %%%%%%%%%%%%%%%%%%%%%%%%%%%%%%%5
   %line counting part

   %initializations
```

```
    horizLineCount(imageNum) = 0;
    vertLineCount(imageNum) = 0;

    for ii = 1:nrows
        for jj = 1:ncols-lineLength
            if(min(b(ii,jj:jj+lineLength))>0)
                horizLineCount(imageNum) = horizLineCount(imageNum) + 1;
                jj = jj+lineLength;
            end

        end
    end

    for ii = 1:ncols
        for jj = 1:nrows-lineLength
            if(min(b(jj:jj+lineLength,ii))>0)
                vertLineCount(imageNum) = vertLineCount(imageNum) + 1;
                jj = jj+lineLength;
            end
        end
    end

end
horizLineCount
vertLineCount

anisotropy = (vertLineCount./(horizLineCount+vertLineCount))*100;

anisotropy
figure(1)
plot(degreeList,vertLineCount); hold on;
```

Program 2

```
% image loading
clear all; % clear all variables
close all; % close all figure

% parameters of method
threshhold = 50
lineLength = 50
highLevel = 255
maxAngle = 18
numFiles = 19% should be maxAngle/10+1
rotation = 10 %increment in degrees the image should be rotated by clockwise
```

```
%generation of rotated versions of the base image
for(imageNum = 1:numFiles)
   degreeList = linspace(0,maxAngle+1,numFiles+1);
   filename = sprintf('image_%i.tiff',degreeList(imageNum))
   a= imread('image_0','TIFF');
   b= imrotate(a, -10*degreeList(imageNum+1));
   newfilename = sprintf('image_%i0.tiff',degreeList((imageNum+1)));
   imwrite(b, newfilename, 'TIFF');
end
```

Automations for Improvision Openlab Software

This automation captures time lapse series in three channels. I extended it from the original version supplied by the vendor to allow more fields of view and the acquisition of a 2nd and 3rd channel.

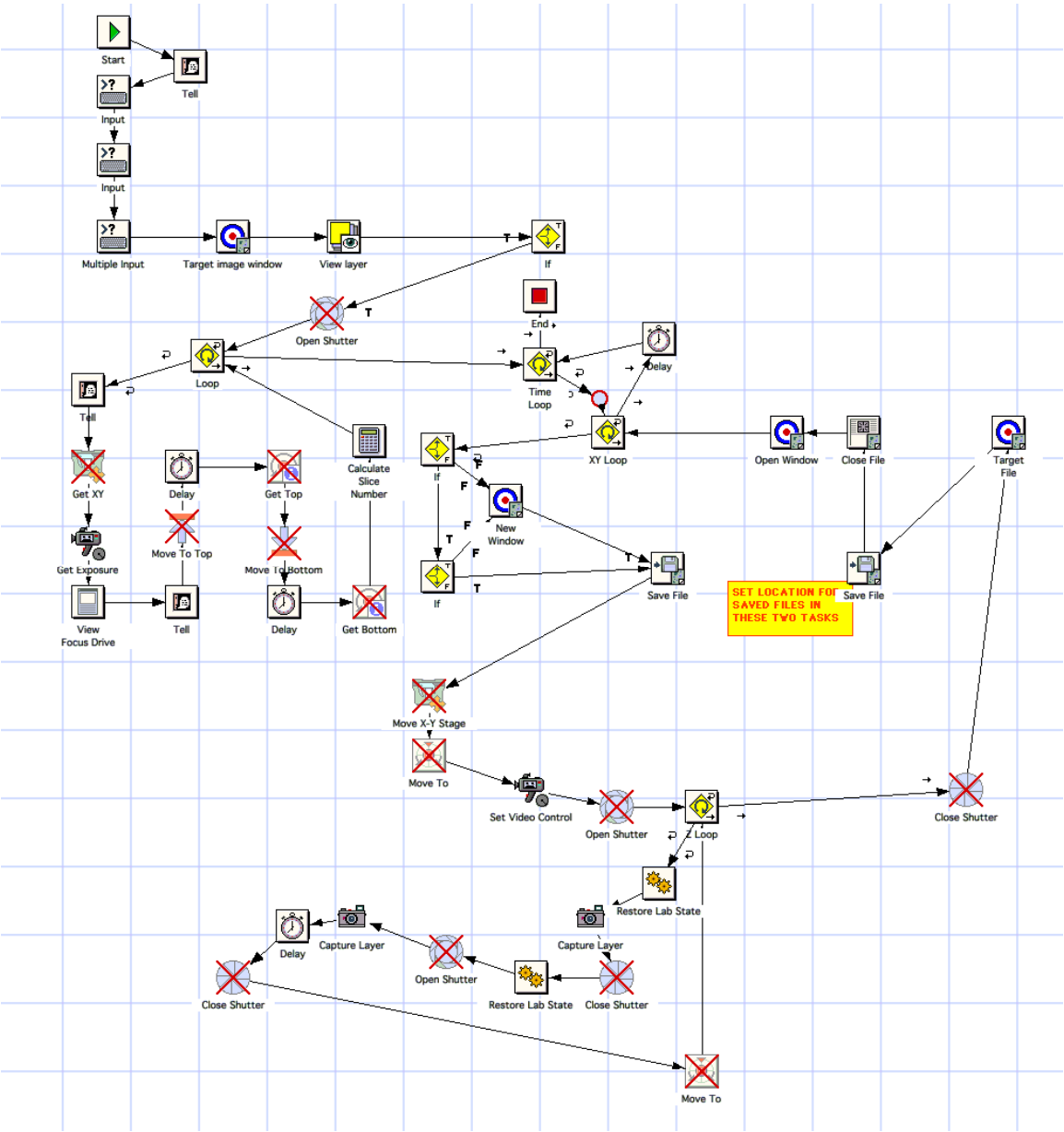

This automation is a multichannel timelapse automation that can record up to 24 distinct xy positions and allows for user adjustment of positioning during acquisition. This automation was initially supplied by the vendor (Improvision), but was malfunctional. The author repaired this automation.

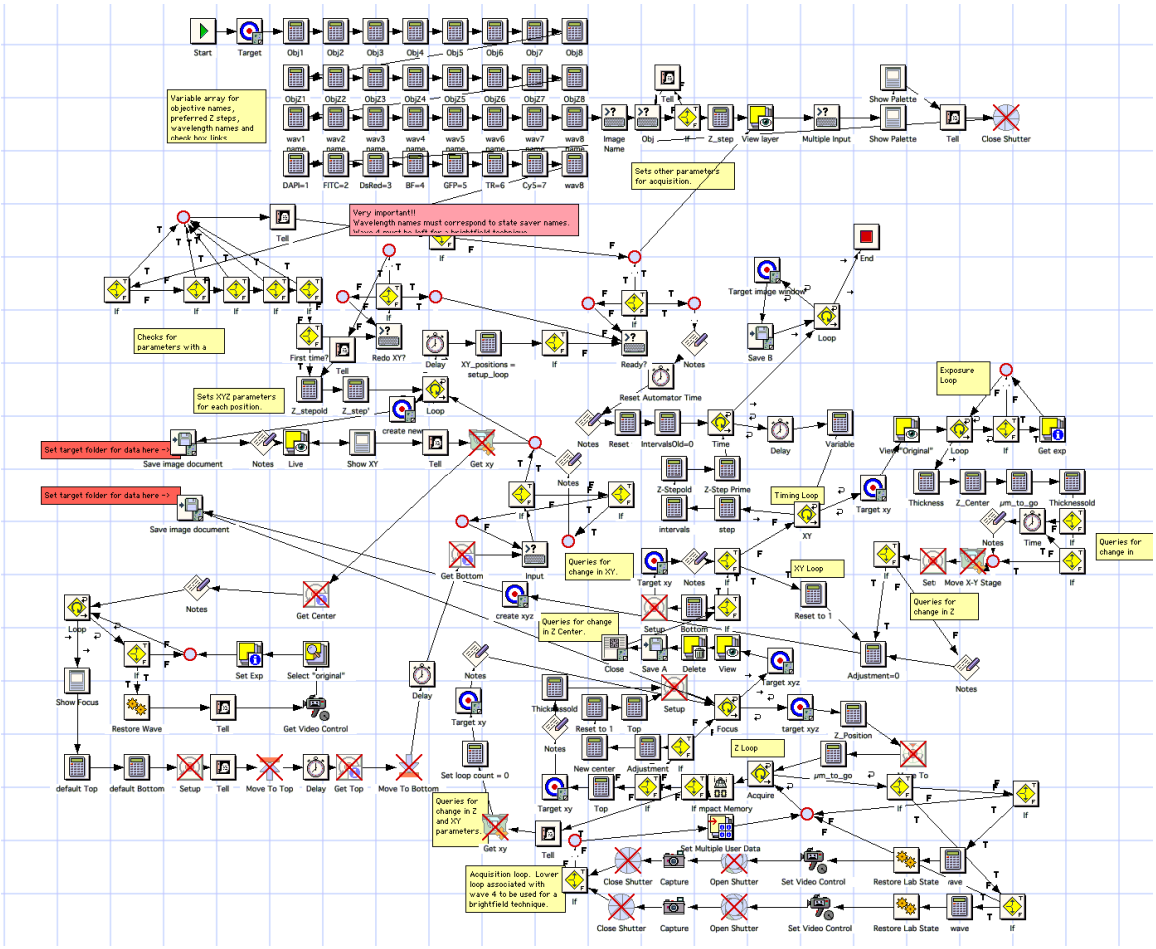

The following automation takes adjacent non-overlapping fields of view in blocks of three. The author designed it to accelerate random sampling for cell counts.

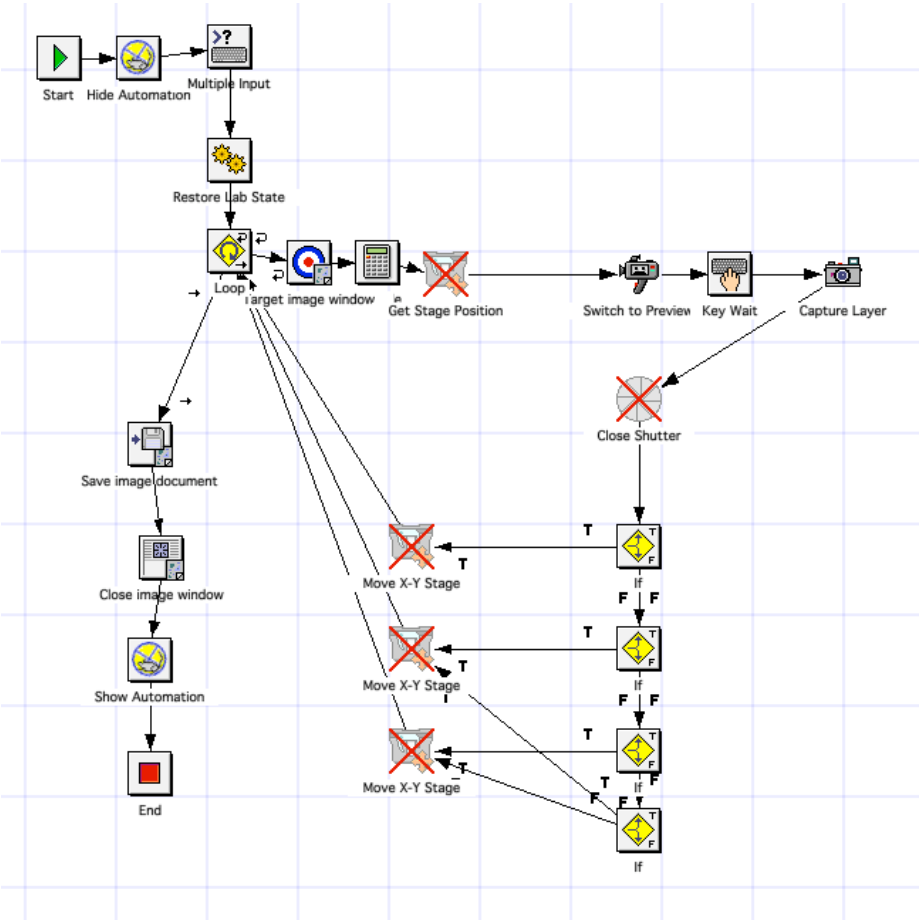

The following automation was designed by the author to minimize switching of filter wheels during manual multi-channel acquisitions.

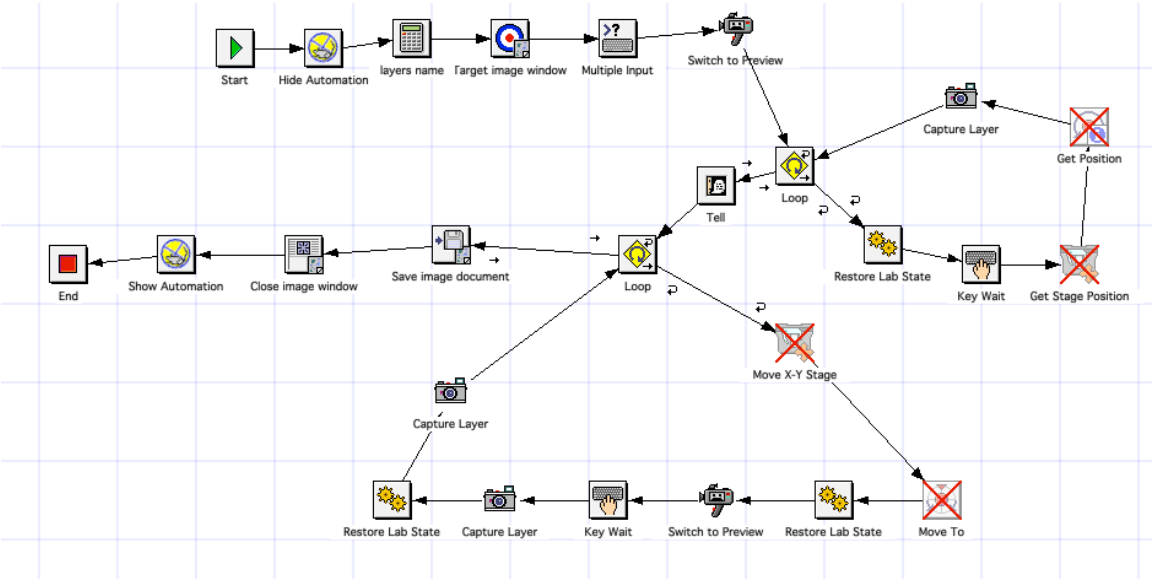

Protocol for Microfabrication/Soft Lithography

Quicksheet for 50 um deep wafers

Cleaning (optional)

Coat in acetone

Rinse with IPA

Blow-dry the wafer with N2 gun

Spin coat

Bake at 100-150 C (remove moisture)

SU-8: ramp at 100 r/s for 10 sec at 500 rpm

ramp at 300 r/s for 30 sec at 2000 rpm

KEEP WAFERS COVERED !

Soft bake

ramp temp

DO NOT COVER ENTIRELY (solvent needs to evaporate)

65 degr 6 min

95 degr 20 min

let cool down (5 mins)

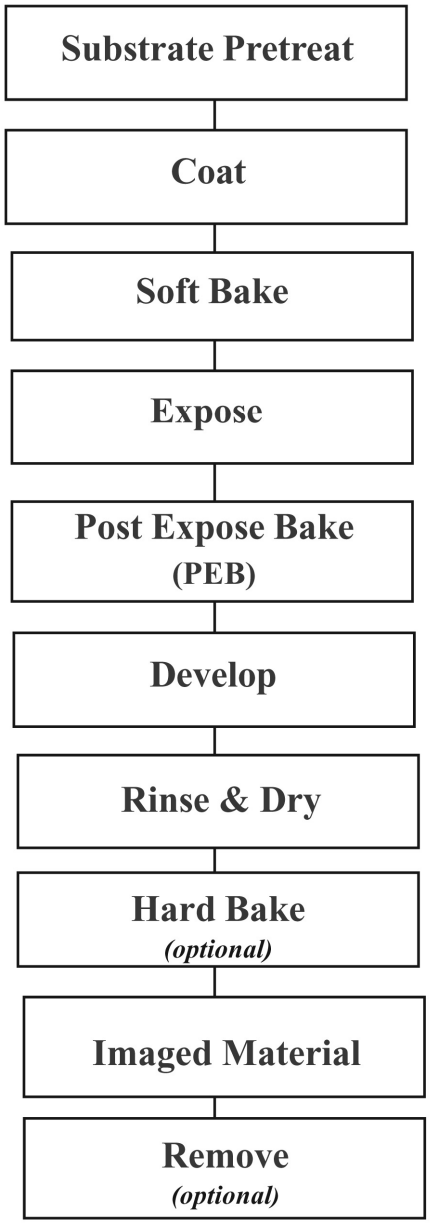

check to make sure the SU-8 is hard, if not,

re-bake for 5-10 mins.

Exposure

1.1 min 275 W CI1 (~300 mJ/cm^2)

TYPE SHOULD NOT BE READALE (facing down/printed side down)

press mask firmly between wafer and glass slide –

too much pressure is as bad is too little

Post bake

ramp to

2 min 65 degr, then ramp to

5 min at 95 degr

RAMP DOWN by turning off plate

COVER WAFERS!

Develop

60-90 sec strong agitation - suspending wafer (face-down) in developer, check

QC patterns

Rinse with IPA, if no white precipitate,

Dry with nitrogen

Post expose (1 min at CI 1)

remove glass plate before loading finished wafer

Hard bake at 100 C (optional)

For questions: Michael Jibitsky (3-1402).

Detailed Protocol for Microfabrication/Soft Lithography

Materials

(found in clean room or in Rubbermaid toolkit container):

- Rubbermaid container to store equipment
- Test grade silicon wafers
- 1 600 ml beaker
- 1 80 ml beaker to hold instruments
- 1 100 ml beaker for pouring acetone or developer
- SU-8 50 Photoresist (in flammable cabinet in cleanroom)
- SU-8 Developer (in flammable cabinet in cleanroom)
- HMDS (HP MicroPrimer) (in flammable cabinet & on spinner in cleanroom)
- spatula
- 2 tweezers (one for dirty and one for clean wafers)

- shallow beakers (at least one for each wafer – to cover during bakes and to develop)
- template(s)/masks
- scissors (if template not cut)
- aluminum foil (for covering spinner bowl - should be present in cleanroom)

- stop watch
- large glass plate (to support mask against wafer in the aligning process)
- Materials to be gathered:
- wafer timing sheet and pen
- one 100mm Petri dish for every wafer you plan to make
- notebooks not necessary (unless for reference) – use clean room towels for note paper
- Nitrile (probably purple or green) gloves (solvent resistant)

Procedure

(upon entering the cleanroom)

1. Check that the toggle for the blower of the hotplate/spinner bench (top right hand side above bench) is switched on – otherwise the particle count in the room is much higher and you get inclusions on the soft wafers.
2. Turn on the switch for the vacuum for the spinner. It's resting above the top left-hand side of the hotplate/spinner bench.

3. Turn on the nitrogen for the UV aligner: Flip up the Purge N2 switch on the right leg of the table where the aligner is located. Loosen part-way the nitrogen twist-valve (also near the floor). Flip up the N2 switch and the vacuum switch on the aligner controls box (top right).
4. Make sure to hit power on the actual aligner. It's a red button that's also on the aligner controls box.
5. Now you have to change the filter and the objective lens of the Suss Aligner.

   - filter: open the hatch held down by 4 screws at the top-middle of the aligner. (it is labeled with wavelength specifications. – you want 365nm.) Exchange (by sliding) the clear glass filter for the reflective filter (you want the clear filter in place for SU-8). They both have aluminum frames. (Find in small box on bench opposite Suss)

   - objective lens: Install the cobalt blue lens in place of the clear one. This piece is stored under the table in the mini-trunk or is to the left of the aligner. Also change both vacuum plates (of the pink sliding arm and of the removable mask holder) to the 3" diameter holders.
6. Turn on the fat switch of the black UV control box to the left of the aligner. The screen should read 'rdy' (ready). Hit START so that it can begin to warm up. It will take about 10 minutes.
7. Once the lamp is hot, press to select 'CI1' on the UV control box CI (constant intensity) 1 – and adjust the exposure time to 1.1 minutes with the knob on the aligner controls box.

8. Be sure to sign in at the binder near the door..

Coat

general notes:

the goal is to spread a film of SU-8 of known thickness on the wafer

keep the wafers CLEAN – the clean room is NOT as clean as you think. Cover wafers with glass dishes when they sit in the open air

SU-8 has a high viscosity – softbake it soon after spinning, otherwise it may retract (by surface tension) from the edge of the wafer and contribute to edge bead formation, which makes proper exposure difficult.

1. At the spinner, remove the chuck. (monkey wrenches can be found on the right)
2. Line the plastic spinner bowl with tin foil (found to the right of the hotplate hood).
3. Load the 3” diameter chuck from the selection of chucks to the right of the spinner. Tighten the screw firmly, to insure proper vacuum.
4. Open the wafer container IN THE HOOD ONLY and transport one wafer to the spinner using tweezers. Keep the wafer container closed as much as possible. Minimize exposure to room dust. Place wafer in the spinner shiny side up.
5. Precoat wafers with HMDS – this is supposed to increase bonding strength of the photoresist with the silicon surface.

- check and run program 3 on the spinner centering wafer carefully (for high RPMs)

6. work quickly: put a two inch diameter puddle of HDMS in the center of the wafer, spin (HDMS evaporates very easily - can lead to uneven coating)
   - bake wafer at 100-150 C for 2 mins (trust the thermometer, not the hotplate reading).
7. keep wafer covered with a glass dish (allow for solvent venting – see diagram p6)
8. Coat with SU-8: Program the spinner. Set for Program 0.
9. Ramp to 500rpm at 100rpm/sec and spin for 10sec
10. Ramp to Xrpm at 300rpm/sec and spin for 30sec
11. Spin Conditions:

Viscosity @25C	Thickness (um)	X = Spin Speed (rpm)
12250	40	3000
	50	2000
	100	1000

12. Hit RUN-> PROGRAM # -> ENTER -> START to do a test run.
13. Take the photoresist from the left-hand cabinet on the floor. (Labeled DHK) Pour roughly 3ml (quarter-sized dallop) of SU-8 50 onto the wafer. Pour with the lip of the bottle as close the wafer as possible. Photoresist will pour thickly. When approaching enough, quickly lift the bottle and twist (like pouring wine) to cut off the flow. Try to catch any drippings with the spatula spoon. Pouring carefully will help you avoid bubbles. Bubbles are detrimental and may necessitate cleaning the botched wafer in acetone

and starting fresh. You can remove a few small bubbles by scooping them out with the spatula while a wafer is in the spinner.

14. Hit START a second time to begin the actual spin cycle. Handle wafers with soft photoresist with dirty tweezers only.
15. Cleanup: When finished, remove the chuck and plastic bowl from the spinner. Throw the tin lining out and clean bowl & chuck with acetone (found on left side of sink). Collect waste acetone in a beaker. DO NOT FLUSH DOWN SINK. A few washes may be necessary. Leave solvent-soaked paper towels in hood until dry, or dispose of them in the 5 gallon acetone-soaked-towel-bucket. (under hotplate bench) Dispose of liquid waste in appropriately labeled hazardous waste containers found in the cabinet opposite the hood.

Troubleshooting

- If you have bubbles on your wafer after pouring, try to remove them by scooping them out with the spatula.
- If you didn't have bubbles when pouring, but it appears you have features on the wafer that look like bubbles, you probably have dust from the room air on the wafer – you have to clean the wafer and start over. Always cover your wafers with glass bowls when possible.
- to clean wafers that are not acceptable: submerse them in acetone and leave them for 15-20 mins, gently swirling occasionally. Finally, rinse with fresh acetone from the spray bottle, followed by a rinse with IPA (2-

propanol / isopropyl acohol). Without letting the acetone dry onto the wafer, quickly spray with IPA, then put the wafer horizontally on a paper towel and dry with N2.

Soft bake

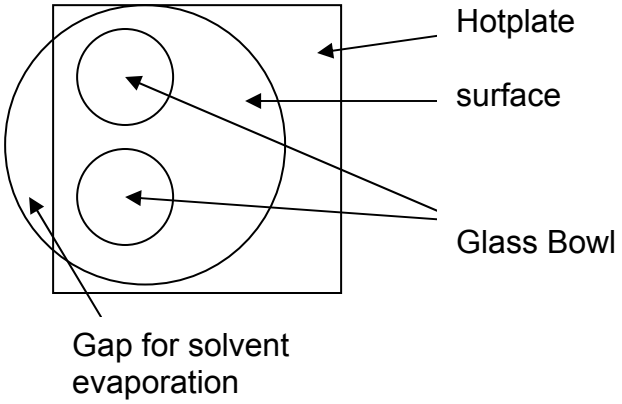

general notes:

soft baking removes solvent from the SU-8, hardening it for the exposure step.

covering the wafers completely in this step is not desirable because it interferes with the solvent evaporation.

wafers are sticky during this step until they are cooled down – they need to be protected from dust.

1. Remove unnecessary aluminum foil and place wafers on hotplate using dirty tweezers. Bake for recommended times on hotplates.
2. During bake, cover wafers with large glass bowl (from the communal glass cabinet next door – to left of hood) to minimize dust deposition and still allow for solvent evaporation in the following manner (top view):

Thickness (um)	Step 1 @65C	Step 2 @95C
40	5	15
50	6	20
100	10	30

3. After bake times remove from hotplate and set on counter. (IMPORTANT) Turn 95C hotplate off and leave wafer on hotplate so that it cools slowly. Cooling too quickly can crack the photoresist. When the temperature gets to 75-70C remove from hotplate and continue to cool on clean room towels on the counter.

Troubleshooting

- bubbles and imperfections can not be removed at this stage. see same section above for wafer-cleaning and re-use instructions.

Exposing

1. After the wafer has dried on the counter for ~3 min, tap wafer on the edge with the back of tweezers to make sure the photoresist is hard. If hard, proceed.
2. Secure glass slide to the mask holder by pressing “mask vacuum” on the aligner control box. Install metal holder and glass slide in the light path by tightening the two metal knobs at the front of the aligner.
3. Center the wafer on the vacuum plate of the pink pullout. IMPORTANT: Put the mask on top with the printed side facing DOWN (type should not be readable). (If you are not sure, scratch both sides of the mask to see which one holds ink) – This simplifies the light’s path, by reducing distance

and reflections between the wafer and the mask pattern, resulting in clean, crisp lines on the wafer. Make sure the mask is centered.

4. Carefully, push in the pink slide with wafer. Flip over the metal piece on the left-hand side near the table. This will raise the wafer up to the mask. Use the front adjustments so that the mask is pressed against the glass slide with a maximum amount of pressure.
5. Push the horizontal arm back until the “contact” button on the aligner control box lights.
6. Set the exposure timer to 1.1 minutes. (double check that the light source is ready and set to CI 1).
7. When everything is ready hit Expose on the aligner conrol box and face away from the aligner. DO NOT look back until the exposure is finished. You can tell when the UV turns on and off by the loud click of the lamp shutter.
8. When exposure is done, flip the left metal switch to lower the sample. Press the DS button on the UV power box to read the number. Record the number in the logbooks as the number of lamp hours. When finished turn off power. Leave the nitrogen purge on for another 15 minutes to cool the lamp. Record final time in binder.
9. **For further info refer to the manual in the clean room, or call Michael Jibitsky (3-1402).

Post expose bake

general idea:

post baking completes the process of crosslinking the photoresist – it is a chemical process that needs a certain reaction time and is driven by heating. It shouldn't be shortened in any way.

ramping (gradually changing the temperature) is important for proper post-baking. According to the manufacturer of SU-8, rapid temperature changes are used to REMOVE patterns from the wafers, so this is NOT desirable.

Thickness (um)	Step 1 @ 65C (min)	Step 2 @ 95C (min)
40	2	4
50	2	5
100	3	10

1. Expose all wafers and transfer them onto a cold hotplate (three at a time is ideal because of uneven hotplate heating). Keep them covered. Turn on the hotplate and ramp the temperatures according to the following scheme:
2. after step 2, turn the hotplate off and let it cool down until the surface reaches 50 C (thermometer, not hotplate reading). Then take the wafers off, set them on a paper towel on the bench, cover them and let them cool down for another 10-15 minutes before developing.

Develop

general idea:

the developer dissolves both the crosslinked as well as the non-crosslinked photoresist. The keys is that it dissolves the non-crosslinked photoresist at a faster rate. Thus it is desirable to minimize developing time while maximizing the mechanical exposure of the developer to the photoresist. Especially narrow grooves and crevices benefit from higher developer turnover. In other words, developing works best if the wafer is shaken as vigorously as possible. :-)

1. Get SU-8 Developer from the left-hand side cabinet. Pour enough to cover wafer into a 2” tall glass dish. Pour a smaller amount of developer into a second shallow glass dish for rinsing.
2. Add wafer to container facing upside down, and shake as vigorously as possible without splattering for 1 minute to 90 seconds. (Violent circular and percussive motions in the horizontal plane are recommended.) Check for remaining photoresist ‘shadows’ on wafer and transfer into second, cleaner rinse dish. Wafer is developed when no photoresist is visible apart from the desired features. (If a 10um pilliar grid pattern is on the wafer, this will probably be coming off as the wafer approaches maturity.)
3. Once the wafer is developed, quickly rinse with isopropyl alcohol (smallest unlabeled, clear squirt container on left-hand side of sink) Rinse and spray dry with nitrogen gas. If a white streaking is produced during rinsing then

the wafer is underdeveloped. Briefly immerse in cleaner developer again and continue with rinse and dry.

Clean-up

- Dispose of isopropyl alchohol, developer, and acetone waste in appropriate waste containers. Put developer and photoresist back in cabinet. Make sure that the UV machine has the original 2” diameter plates in place. Shut off the nitrogen valve under the aligner table. Turn off the vacuum switches on the aligner control box, and the vacuum for the spinner. Clean up materials and leave room the way it was found.

Recommended Post Expose& Hard Bake

- In order to ensure full crosslinking, expose developed wafers to UV for 1 min each. Before loading the developed wafer, be sure to remove the mask support plate (glass) from the vacuum mask holder of the aligner. (the wafer can stick to it, and be ruined)
- In order to fully dry and crosslink the wafers, ramp them up to 100 C on a hotplate for ~10 mins.

Millie Ford 11/10/02

Revised 12/3/02

Revised 7/1/04 Jan Bruder & Josh Goldner

AutoCAD Designs for Photolithography

Bridging Designs

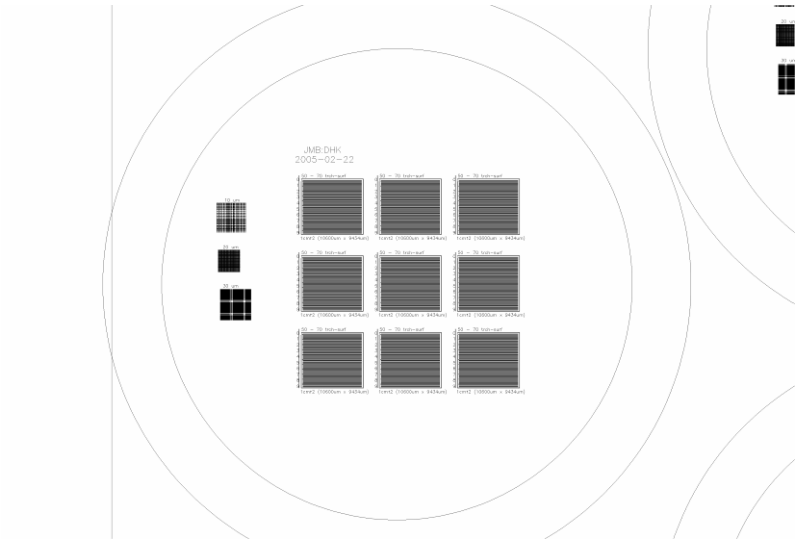

Figure A1 – Whole wafer layout for bridging substrates. Wafer contains 9 square regions of 1 cm^2 area with repeating grooves and trenches (grooves 70 um wide, trenches 50 um wide) and 3 quality control patterns with small square features (10, 20, and 30 um edge length). I have designed a number of different variations of this type of wafer with varying groove and trench dimensions; the design depicted here is representative.

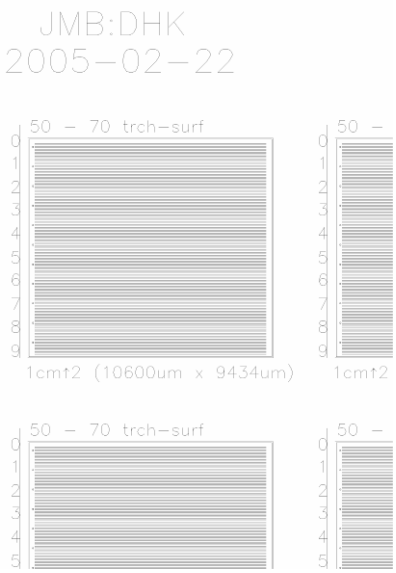

Figure A2 – Detail of bridging wafer, showing individual 1 cm^2 regions with grooves and trenches.

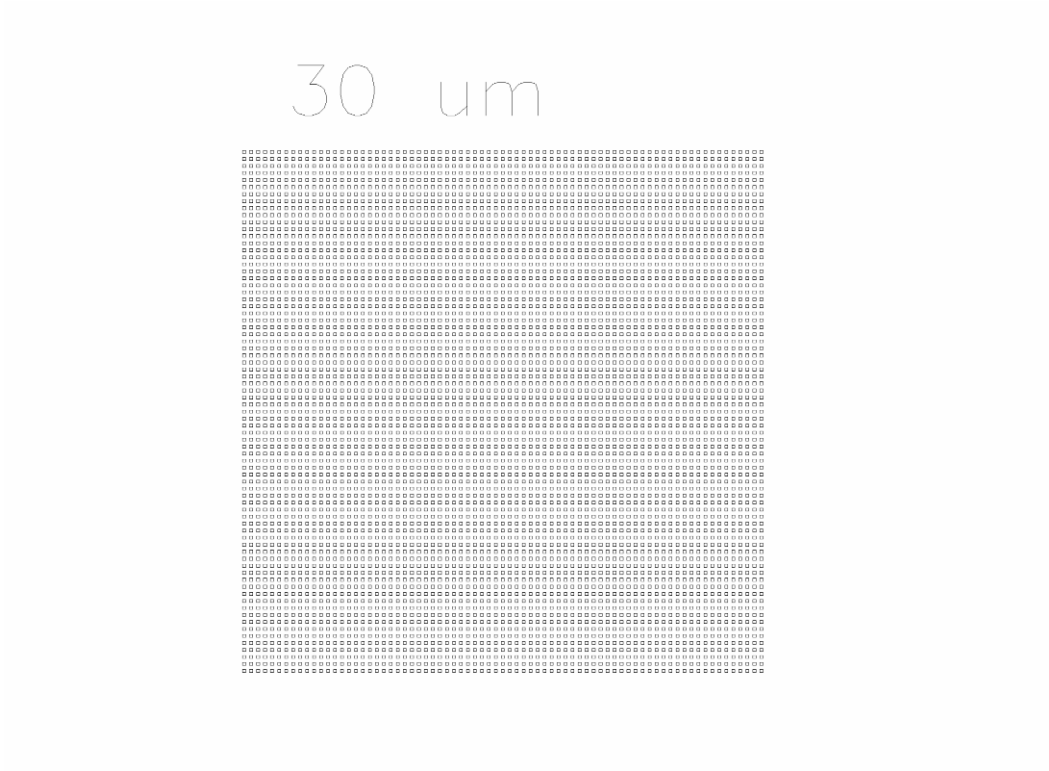

Figure A3 – Detail view of quality control pattern on bridging wafer. Each square has 30 um edge length. I introduced this pattern, along with two adjacent patterns with 10 um and 20 um square features as a means to judge correct developing time wafers during production. Once the thinnest features wash off, one has to conduct further developing with caution.

Gradient Designs

The gradient designs were drawn by Pearl Yu and Shaily Kapur according to my design parameters and sketches. These gradients represented a further development on the previous designs in several factors:

- Curved mixing portions instead of sharp “zig-zag” patterns prevent air bubbles from getting trapped in the gradients during filling
- Widened portions at the inlets and outlets facilitate attachement of in- and outflow tubes
- Two gradients per wafer increase production efficiency

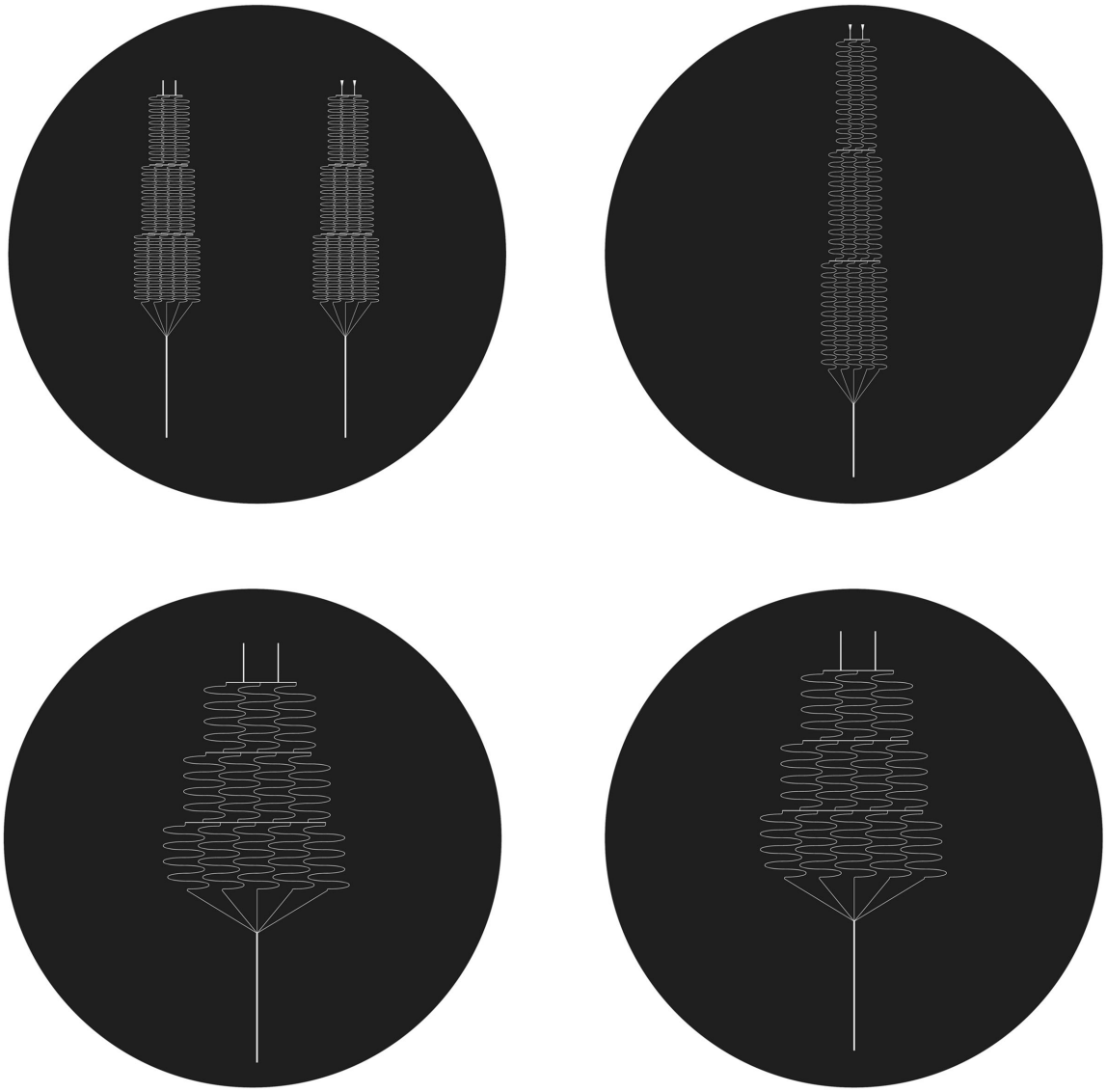

Figure A4 – Four different designs for gradient wafers showing different inlet and outlet configurations, varying mixing channel length, and altered main channel feeding angles.